University of Nottingham
UK | CHINA | MALAYSIA

Methodology for Selection of Optimal Satellite Constellation for Precise GNSS Positioning

By:

Abdulaziz Alluhaybi

Supervisors:

Panagiotis Psimoulis

Rasa Remenyte-Prescott

Thesis submitted to the University of Nottingham

for the degree of Doctor of Philosophy

Nottingham Geospatial Institute, Department of Civil Engineering

University of Nottingham, UK

28/01/2025

Abstract

Continuous advancements in GNSS systems, apart from the broadly used GPS, have led to the development of other satellite systems (Galileo, BeiDou, GLONASS), which have significantly increased the number of available satellites for GNSS positioning applications. However, GNSS satellites' redundancy and potential poor GNSS satellite signals can negatively affect the GNSS's positioning speed and accuracy. On the other hand, selecting high-quality GNSS satellite signals by retaining a sufficient number of GNSS satellites can enhance the GNSS's positioning performance. Various methods have been applied for satellite selection. However, the selected satellites via these methods could be insufficient for precise positioning. These methods were designed to select satellites for Single Point Positioning (SPP) solution with meters level accuracy. This is because these satellite selection methods only consider SPP factors. To choose satellites for precise positioning, new satellite selection method was developed considering Precise Point Positioning (PPP) factors. Various satellite selection methods were investigated and assessed to developed new satellite selection method that fit PPP- satellite selection. To test the performance of the new satellite selection method, several experiments have been conducted. Satellites were selected for various PPP applications: i) static open-sky, ii) kinematic open-sky, and iii) static at multipath conditions. In addition, satellites were selected in all possible subset sizes, i.e., they were selected in subsets with all possible numbers of satellites. According to experiment results, the efficiency of the new satellite selection method was excellent at low multipath environment regardless of PPP modes: static or kinematic. The positioning accuracy of original PPP, using all satellites, was achieved by multiple sizes of selected satellite subsets by the selection method. It was also obtained by selected satellites with different subset sizes. In terms of high multipath environments, the performance of the satellite selection method was less effective. The positioning accuracy of the original PPP was not achieved by the selected satellite subsets although they provided positioning accuracy close to the original PPP with a few satellites. This achievement is quite promising although the new satellite selection method needs further improvement.

Keywords

GNSS, GPS, Satellite Selection, GDOP, WGDOP, SNR, Elevation Angle, RAIM

Acknowledgment

This research was carried at Nottingham Geospatial Institute (NGI), a research group at the University of Nottingham. The research was funded by Taibah University. Many thanks to my sponsors for providing me such a great chance to live and study in the UK for four years.

I would like to especially thank my academic supervisors: Dr. Panos Psimolis and Dr. Rasa Reminette-Prescott, for their guidance and support throughout my PhD journey. Their suggestions helped me in the design of the experiment, data processing and analysis. I am also grateful to my internal examiner, Dr. Paul Blunt. He provided me with very valuable feedback that helped me gain a comprehensive understanding of the problem. Many thanks to Mr. Sean Ince and Dr. Chenyu Xue who helped me collect GNSS data and use GNSS software such as Leica infinity and RTKLIB.

Last but not least, I would like to express my deep gratitude and respect to my parents, brother, and wife for their continuous support and encouragement throughout my years of study.

Table of Contents

List of Figures

List of Tables

List of Abbreviations

ABC	Artificial Bee Colony
AC	Autonomous Car
ACO	Ant Colony Optimization
AI	Artificial Intelligence
ANN	Artificial Neural Network
BDS	BeiDou Navigation Satellite System
BIGF	British Isles continuous GNSS Facility
BNG	British National Grid
CEA	Cut-off Elevation Angle
CNR	Carrier-to-Noise Ratio
CODE	Centre for Orbit Determination in Europe
CPU	Central Processing Unit
CRAIM	Carrier RAIM
DCB	Differential Code Bias
DGNSS	Differential Positioning
DMS	Degree-Minute-Seconds
DOP	Dilution of Precision
ENH	Easting, Northing, and Height directions
ETRF89	European Terrestrial Reference Frame 1989
EU	European Union
GA	Genetic Algorithm
GB	Gigabyte
GDOP	Geometric Dilution of Precision
GEO	Geostationary Earth Orbit
GHz	Gigahertz

GLONASS	Globalnaya Navigazionnaya Sputnikovaya Sistema
GNSS	Global Navigation Satellite System
GOT	Ocean Tides Loading
GPS	Global Positioning System
HDOP	Horizontal Dilution of Precision
HPC	High Performance Computing
HWNs	Heterogeneous Wireless Networks
IGSO	Inclined Geo-Synchronous Orbit
IRNSS	Indian Regional Navigation Satellite System
ITRF	International Terrestrial Reference Frame
KF	Kalman Filter
KFITH	Kalman Filter Innovation Threshold
LOS	Line-of-Sight
LS	Least Squares
MEO	Medium Earth Orbit
MGV	Minimum GDOP Value
MHz	Megahertz
MOLA	Multi-Objective Land Allocation
MPPT	Maximum Power Point Tracking
NGI	Nottingham Geospatial Institute
NSAT	Number of satellites
OPAva	Optimal Positioning Availability
OSGB36	Ordnance Survey of Great Britain 1936
PAva	Positioning Availability
PCV	Phase Centre Variation
PDOP	Position (3D) Dilution of Precision

PF	Polarized Feedback
PNT	Positioning, Navigation, and Timing
PPP	Precise point positioning
PRN	Pseudorandom Noise
PSO	Particle Swarm Optimization
QZO	Quasi-Zenith Orbit
QZSS	Quasi-Zenith Satellite System
RAIM	Receiver Autonomous Integrity Monitoring
RAM	Random-Access Memory
RINEX	Receiver Independent Exchange
RMS	Root Mean Square
RTK	Real-Time Kinematic
SA	Simulated Annealing
SBAS	Satellite Based Augmentation System
SEAva	Selection Epochs Availability
SHM	Structural Health Monitoring
SN	Solution Number
SNR	Signal-to-Noise Ratio
SPP	Single Point Positioning
TB	Terabyte
TDOP	Time Dilution of Precision
TEC	Total Electronic Content
TM	Traditional Method
TSABC	Tabu Search Artificial Bee Colony
UERE	User Equivalent Range Error
USA	United States of America

VDOP	Vertical Dilution of Precision
WGDOP	Weighted Geometric Dilution of Precision
WGS84	World Geodetic System 1984
XYZ	X, Y, and Z directions
ZTD	Zenith Total Delay

List of Publications

Based on Chapter 4, Section 5.1, and Chapter 6, we published a Journal paper in Remote Sensing.

Alluhaybi A, Psimoulis P, Remenyte-Prescott R. An Evaluation of Optimization Algorithms for the Optimal Selection of GNSS Satellite Subsets. Remote Sensing. 2024; 16(10):1794. https://doi.org/10.3390/rs16101794

Chapter 1 Introduction

1.1 Introduction

The Global Navigation Satellite System (GNSS) is a system of satellites, including GPS (Global Positioning System, USA), GLONASS (Global Navigation Satellite System, Russian), Galileo (European Union), BDS (BeiDou Navigation Satellite System, China), and other regional navigation satellite systems. Essentially, GNSS provides positioning, navigation, and timing (PNT) services. Nowadays, it becomes an important part of human life as it supports a large number of applications. GNSS has been used in transportation. It supports road navigation, as well as tracking and controlling the trips of trains, ships, and planes. In farming, it supports precision agriculture by determining the right location for soil sampling, seed spreading, and guiding harvesting machines. In engineering, it is utilized for applications like mapping, construction, and structural health monitoring (SHM). Furthermore, it has been used in emergency response services, social networking, and even gaming.

Reliable and continuous GNSS results are necessary for many applications, as aviation and autonomous car (AC). Due to the recent development in GNSS satellite systems, the number of satellites available in space has reached 126; 31 GPS [1], 24 GLONASS [2], 25 Galileo [3], 35 BeiDou [4], 4 QZSS [5], and 7 IRNSS satellites [6]. As a result, the number of satellites simultaneously visible from a single location, depending on geographic location, can reach or exceed 30 [7]. The potential of using such a diverse and large number of GNSS satellites can improve the accuracy and availability of the GNSS solution in positioning, navigation and timing (PNT) services.

1.2 Problem Background

However, using large number of GNSS satellites also has limitations. The number of computations required for GNSS positioning grows as the number of the used GNSS satellites increases. Compared to 10 GNSS satellites the required time for processing the position based on 20 and 30 GNSS satellites increases by a factor of 3 and 6, respectively [8]. In addition, GNSS positioning accuracy generally increases with the number of available satellites, but practically no further enhancement is achieved after a certain number of satellites [9,10]. This was also revealed by Msaewe et al., [11], using zero-baseline GNSS measurements. The accuracy of GNSS positioning did not improve with the decrease of geometric dilution of precision (GDOP). Moreover, increasing the number of GNSS satellites cannot always guarantee a higher quality of the sustained position. The positioning derived from multi-satellite system (multi-GNSS) integration is not of the highest possible accuracy due to introduced errors of various error sources. For example, multipath is one of the main error sources [12], even under relative positioning [13]. As the number of positioning

satellites decreases, the efficiency of positioning processing increases in terms of time cost and power consumption.

This improvement can be sensitive for low-cost receivers [14], which are used for more than 91% of GNSS applications [15]. Recently, low-cost receivers have been tested in SHM [16–19], which is a critical application [16]. One of the main requirements in many GNSS monitoring applications is to limit as much as possible the GNSS data size for more sustainable and reliable transmission of the GNSS data, which makes important to choose only the optimal satellites which will lead to accurate and reliable GNSS solution. Therefore, the GNSS satellite selection is required not only to improve the GNSS performance but also to make the application of GNSS technology more sustainable.

1.3 Motivation and Significance of The Study

GNSS satellite selection is the process of choosing the right GNSS satellite combination from the available GNSS satellites, aiming for better positioning quality with lower computation load [20]. Various methods were used for satellite selection and have applied in multiple studies for the three positioning techniques. However, most of these studies were implemented for single point positioning (SPP) [21]. In addition, satellites for differential positioning (DGNSS) and precise point positioning (PPP) were chosen using SPP satellite selection methods, which ignored DGNSS and PPP factors such as satellite precise orbit. Except for Martini et al. [22], who considered satellite precise orbit and clock in satellite selection for PPP. However, achieving precise outcomes using PPP requires further correction, such as solid earth tide and ocean loading corrections [23]. Thus, satellite selection for DGNSS and PPP needs more investigation.

DGNSS is a positioning technique that determine the location of receiver (rover) with respect to another (station) with known coordinates. Receiver difference measurements are used to eliminate or mitigate common errors, as the errors of satellite orbit, clock and atmospheric biases. It also eliminates the delay due to satellite and receiver hardware, which increases carrier phase ambiguity resolution. Hence, DGNSS provides fast and high accurate positioning. However, the distance between the receivers (rover and station) is critical because the greater it is, less common errors there are, consequently, corrections become less accurate [24]. Therefore, a network of GNSS station-receivers is required to obtain precise results of DGNSS. This makes DGNSS expensive and not suitable in remote areas and undeveloped countries with no GNSS reference stations or benchmarks.

On the other hand, PPP is an absolute/ standalone positioning technique. It provides centimetres to millimetres positioning accuracy by using precise products of satellite orbit and clock and correction models to mitigate other types of GNSS errors, as atmospheric biases. PPP takes tens of minutes to reach centimetre level of accuracy when using signal

satellite system [24]. Recently, centimetre of PPP accuracy can be reached in few minutes by using multiple satellite systems [25–27]. Compared to DGNSS, PPP is more flexible, less expensive and provides comparable positioning accuracy.

1.4 Aims and Objectives

The aim of this thesis is to develop a method for the selection of an optimal subset of GNSS satellites for precise PPP solution, considering all the corrections for PPP solution. The project aim can be achieved through the following objectives:

1.4.1 Investigate different satellites selection methods and define the most suitable one.

Various methods were used to select satellites. Each satellite selection method consists of two components: criterion and technique. The criterion is a factor based on which satellites are selected, as satellite selection elevation angle, satellite signal quality, and geometry (GDOP). The technique is an approach for selecting satellites based on the criterion, such as cut-off elevation angle. Thus, the quality of the selected satellites is affected by the satellite selection method (criterion and technique), revealing the importance of defining appropriate one of them. In order to find them, various types of them were investigated based on literature. This is to determine the most suitable satellite selection method for PPP.

1.4.2 Evaluating the performance of the chosen technique for satellite selection

After determining the suitable satellite selection criterion and technique, their reliability, integrity and efficiency should be evaluated. As mentioned earlier, the criterion is a factor based on which satellites are selected, and the technique is an approach for selecting satellites based on the criterion. Hence, the performance of the selection technique affecting the efficiency of the selection criterion. As a result, the performance of selection technique was proven first before criterion.

The technique was evaluated based on selection accuracy and speed. The selection accuracy is how closely the WGDOP value of the optimal satellite subset selected by optimization algorithms matches that of the actual optimal subset. Regarding the evaluation of the selection speed is defined as the time required to determine the optimal subset of GNSS satellites.

1.4.3 Define the criteria and process for satellite selection

The most suitable selection criterion was chosen from previous satellite selection methods that were design to consider SPP factors. Therefore, more positioning factors (PPP factors) were considered along with chosen in different combinations. Their efficiency was

evaluated to determine their fitness for PPP-satellite selection. They were evaluated based on the positioning quality of the selected satellites, including positioning accuracy, precision, and continuity.

1.4.4 Experimental evaluation of satellite selection method

As mentioned in section 1.4.3, new criterion for selecting satellites was developed by considering more positioning factors. However, it was only evaluated in static open-sky environment. To have comprehensive evaluation, the new satellite selection method was used for satellite selection in different scenarios, including kinematic mode and multipath environments. The performance of satellite selection method (criterion) was assessed based on the positioning quality of its selected satellites.

1.5 Innovation of The Work

This work contributes by providing a new satellite selection method suitable for PPP solution (i.e., precise positioning solution). It considers all PPP's corrections like orbit, clock, ocean loading, and Earth rotation. In addition, it also takes into account carrier phase ambiguity resolution by considering the continuity of the selected satellites. Furthermore, the work defines the most suitable number of satellites and the environment for the fixed satellite selection. To do so, various techniques and criteria for selecting satellites, as well as order of selection, were investigated.

1.6 Thesis Outline

In addition to this Introduction chapter (Chapter 1), the thesis has nine main chapters, which are listed below. Chapter 2 describes the GNSS principle, covering GNSS overview, observation types, and error sources. Chapter 3 investigates various satellite selection methods, including their criteria and techniques. Chapter 4 presents an overview of five types of optimization algorithms, covering their principle, advantages, limitations, and applications. Chapter 5 presents the methodology of the project. Chapter 6 evaluates the efficiency of the five optimization algorithms in satellite selection. Chapter 7 define new criteria for PPP-satellite selection and evaluates their quality to determine the most suitable one. Chapter 8 assesses the performance of the new satellite selection method (criterion) in kinematic and multipath scenarios. Finally, Chapter 9 concludes the thesis by presenting findings and recommendations.

Chapter 2 Overview of GNSS

2.1 GNSS Background

GNSS consists of three main segments: i) the space segment, ii) control segment, and iii) user segment. The space segment is the GNSS satellites orbiting Earth at different elevations and continuously broadcasting their signals. The control segment is ground stations monitoring the health of GNSS satellites and providing necessary corrections, as updating their orbits and clocks. The user segment is GNSS receivers on Earth controlled by users for various applications of positioning, navigation and timing.

126 GNSS satellites are currently in operation. They are controlled by different operators and transmitting signals in different frequency bands. In addition, they are orbiting Earth at different altitudes, including: i) Medium Earth Orbit (MEO), ii) Geostationary Earth Orbit (GEO), iii) Inclined Geo-Synchronous Orbit (IGSO) and iv) Quasi-Zenith Orbit (QZO). They are classified into six constellations as shown below:

Table 2.1 Characteristic of six GNSS satellite systems

System	Operator	NSAT	Orbital	Frequency MHz	References
GPS	USA	31	MEO (20,200 km)	L1 (1575.42), L2 (1227.60), L5 (1176.45)	[1,28]
GLONASS	Russia	24	MEO (19,100 km)	G1 (1598.063 – 1608.75), G1a (1600.995), G2 (1242.938 – 1251.25), G2a (1248.06), G3 (1202.025)	[2,28]
Galileo	EU	25	MEO (23,222 km)	E1 (1575.42), E5(1191.795), E5a (1176.45), E5b (1207.14), E6 (1278.75)	[3,28]
BeiDou	China	35	MEO, GEO, IGSO	B1 (1575.42), B1-2 (1561.098), B2 (1191.795), B2a (1176.45), B2b (1207.14), B3 (1268.52)	[4,28,29]
QZSS	Japan	4	QZO, GEO	L1 (1575.42), L2 (1227.60), L5 (1176.45), L6 (1278.75)	[5,28]
IRNSS	India	7	GEO, IGSO	L5 (1176.45), S-band (2492.028)	[6,28]

The location of user's receiver is basically defined via triangulation, where unknown location (user) is determined by measuring the distance to several known locations (satellites). At least 4 satellites are required to obtain the user's location in three coordinates. GNSS satellites are continuously broadcasting their signals. Each GNSS satellite signal has three main components: i) code, ii) carrier, and iii) navigation message. The navigation message contains satellite information, including its location. By collecting satellite signals, their location can be known. The distance between the satellite and receiver can also be found from satellite signal using its code and carrier. The code-based distance is called pseudo-range, and the carrier-based distance is called carrier phase.

Once GNSS receiver receives a satellite signal, it creates a replica of its code to determine the signal travel time by measuring the delay between the incoming code and its replica. Hence, the distance between a satellite and receiver is the signal travel time multiplied by light speed (i.e., signal speed) [30]. This distance is code-based distance and known as the pseudo-range. In contrast, the carrier-based distance is the sum of the carrier cycles including the fractional cycle multiplied by the carrier wavelength [30]. Both pseudo-range and carrier phase measurements are negatively affected by error source. Common sources of error are explained below.

2.2 GNSS Common Error Sources

2.2.1 Satellite Orbit and Clock Errors

Satellites fly in well-defined orbits although sometimes satellites deviate from their orbits. As a result, the error in satellite orbit is the difference between actual and the predicted orbit [31]. On the other hand, the satellites are equipped with highly accurate atomic clocks. However, they are not perfectly synchronised with the GNSS reference time, resulting in clock error [24]. If the orbit and clock errors are not corrected, the pseudo-range and carrier phase measurements will be significantly inaccurate [24].

2.2.2 Ionospheric Delay

The ionosphere is a layer of the atmosphere that extends from about 50 to 1,000 kilometres above the Earth's surface [32]. According to [24], ultraviolet radiation from the Sun ionizes some of the gas molecules in the ionospheric layer. This creating free electrons that affect GNSS signals. They delay the code while advancing the carrier phase measurement [24]. The amount of delay or advance is affected by the satellite elevation angle, signal frequency, and total electronic content (TEC). The ionospheric bias can be expressed as follows:

$$dion_u^e = \frac{1}{\sin(elev_u^e)} * \frac{40.3}{f^2} * TEC \tag{2.1}$$

Where:

- $dion^{e}_{u}$ is the ionosphere bias in meter between the satellite e and receiver u.
- $elev^{e}_{u}$ is the elevation between the satellite e and receiver u.
- $1/sin(elev^{e}_{u})$ is the mapping function (MF^{e}_{u}), which is affected by the elevation angle of the satellite e with respect to receiver u ($elev^{e}_{u}$).
- f is the frequency of the satellite signal.
- TEC is the quantity of free electronic per square meter, and $1TEC$ equals 10^{16} electrons/m^2.

2.2.3 Tropospheric Delay

According to [32], the troposphere is the atmospheric layer closest to the Earth's surface. it is spread approximately 50 kilometres above the earth surface. It is a nondispersive medium for GNSS frequencies less than 30 GHz. As a result, it has an equal effect on L-band GNSS frequencies (L1, L2, and L5) [32], and S-band GNSS frequencies [24]. According to [24], It delays both code and carrier phase measurements equally. The troposphere delays are classified into two types: hydrostatic (dry) and nonhydrostatic (wet). More than 90% of the total delay in the troposphere is due to dry delay, which is caused by dry air. It can by estimated accurately. In contrast, less than 10% of the total tropospheric delay is due to wet delay caused by water vapor. Because of the uncertainty in the distribution of water vapor in the atmosphere, the wet delay is more difficult to predict. Overall, tropospheric delay is affected by atmospheric pressure, temperature, humidity, and satellite elevation angle. The tropospheric delay expressed as follows:

$$dtrop^{e}_{u} = m_{dry} Z_{dry} + m_{wet} Z_{wet} \tag{2.2}$$

Where:

- $dtrop^{e}_{u}$ is the tropospheric delay between the satellite e and receiver u.
- m_{dry} and m_{wet} are the dry and wet mapping function.
- Z_{dry} and Z_{wet} are the dry and wet zenith (90°) delay.

2.2.4 Receiver Clock Error and Noise

To reduce the size, cost and complexity of GNSS receivers, cheap crystal clocks are utilized [24]. Thus, these clocks are roughly set to the GPS time and can drift over time, causing an offset between the receiver clock and the GNSS reference time, which is known as receiver clock error. On the other hand, receiver noise is caused by receiver thermal noise and dynamic stress [32]. Receiver clock errors and noise have an impact on both pseudo-range and carrier phase measurements [24].

2.2.5 Multipath

According to [24], multipath is a major source of positioning errors in GNSS, which occurs when the signal reaches the receiver via multiple paths due to signal refraction by buildings, the ground, and other objects. Multipath affects both pseudo-range and carrier phase measurements, but it causes more errors in pseudo-range measurements than in carrier phase measurements [32]. The size of multipath error depends on the receiver environment, satellite elevation angle, signal characteristics, antenna gain pattern and polarization, and receiver signal processing. Multipath error is difficult to eliminate as it cannot be entirely removed using models and it cannot be rejected by relative positioning technique if both receivers (rover and station) do have different environment. However, it can be mitigated by using special antennas (e.g., choke ring antenna) and applying satellite elevation mask [32]. In addition, it could be reduced by processing wide bandwidth signals and using narrow correlators.

2.2.6 Cycle Slip

Cycle slip is a discontinuity of the cumulative count of cycles due to the temporary loss of satellite signal (loss of lock) [33,34]. Losing satellite signal can be happened because of obstacles (e.g., buildings, and trees), dynamic motion, and ionospheric anomalies [34]. Due to this losing, receiver incorrectly calculates the total number of cycles (carrier phase measurement), consequently, the positioning accuracy is negatively affected [35,36]. To maintain high positioning accuracy, cycle slip should be detected and repaired. Satellite signal with cycle slip can easily be ignored for a period until it becomes stable again. [24], or it can be corrected based on difference between code and phase measurements (code-phase), and doppler measurements [37].

2.3 Equations of Pseudo-Range and Carrier Phase

To improve GNSS positioning, several positioning techniques were developed, including SPP, DGNSS, and PPP. In SPP, the location of a user receiver is determined using pseudo-range measurement. Either pseudo-range or carrier phase measurements is used for positioning in DGNSS. Whereas both pseudo-range measurements and carrier phase measurements are used to locate user receiver in PPP. The observation equation of pseudo-range and carrier phase are presented in equations (2.3) and (2.4), respectively.

$$PR_u^e = \rho_u^e + c(\delta t_u - \delta t^e) + dion_u^e + dtrop_u^e + \varepsilon_u^e \tag{2.3}$$

where,

- PR_u^e is observed code distance (pseudo-range) between a satellite (*e*) and user receiver (*u*) in unite of meters.

- ρ_u^e is geometric range (true distance) between satellite (*e*) and receiver (*u*). It is equals $\rho_u^e(T^e + T_u) = \sqrt{(X^e - X_u)^2 + (Y^e - Y_u)^2 + (Z^e - Z_u)^2}$. (X^e, Y^e, Z^e) are satellite (e) coordinates, while (X_u, Y_u, Z_u) are receiver (u) coordinates.
- c is the speed of the light in the vacuum, which equals 299,792,458 metres/second.
- δt^e and δt_u are the clock offset of satellite (*e*) and receiver (*u*) from GPS time.
- $dion_u^e$ is ionospheric delay between satellite (*e*) and receiver (*u*) in meters.
- $dtrop_u^e$ is tropospheric delay between satellite (*e*) and receiver (*u*) in meters.
- ε_u^e is general error source, including multipath, thermal noise, dynamic stress, and receiver clock error in meters [24].

$$\lambda\varphi_u^e = \rho_u^e + c(\delta t_u - \delta t^e) + \lambda N_u^e - dion_u^e + dtrop_u^e + \varepsilon_u^e \quad (2.4)$$

where,

- φ_u^e is observed carrier phase measurement between a satellite (*e*) and user receiver (*u*) in unite of cycle.
- λ is carrier wavelength, which equals $\lambda = c/f$. c is the speed of the light m/sec, and *f* is satellite signal frequency Hz.
- N_u^e is the correction of initial phase ambiguity in unite of cycle.

Chapter 3 Satellite Selection Methods

Various methods have been used for selecting satellites, and these methods have relied on selection criteria. Based on these criteria, the satellites selection methods can be divided into five categories: 1) satellite angles, 2) satellite signal power, 3) Geometric Dilution of Precision (GDOP), 4) Weighted GDOP (WGDOP), and 5) positioning residuals.

3.1 Satellite Angles

Satellite elevation and azimuth angles as well as the angles between the satellites have been an approach to improve positioning by removing poor and redundant satellite signals. The satellite's location relative to the earth's GNSS receiver is critical for positioning accuracy. Satellite signals at low elevation angles are more vulnerable to multipath [38,39], and ionospheric and tropospheric biases [38,40]. As a result, these defective satellite signals can negatively impact positioning accuracy. In addition, satellites' geometric distribution is important for positioning accuracy. Tracking crowded satellites in one part of the receiver sky increases the uncertainty zone of the receiver position (Figure 3.1). As the uncertainty zone expands, the error in receiver position increases [24]. Satellites are considered redundant when they contribute little to improving the geometric distribution; removing them reduces the positioning processing time [41]. As a result, satellites were chosen based on their angles to achieve two goals: 1) to avoid defective satellite signals and 2) to remove redundant satellite signals.

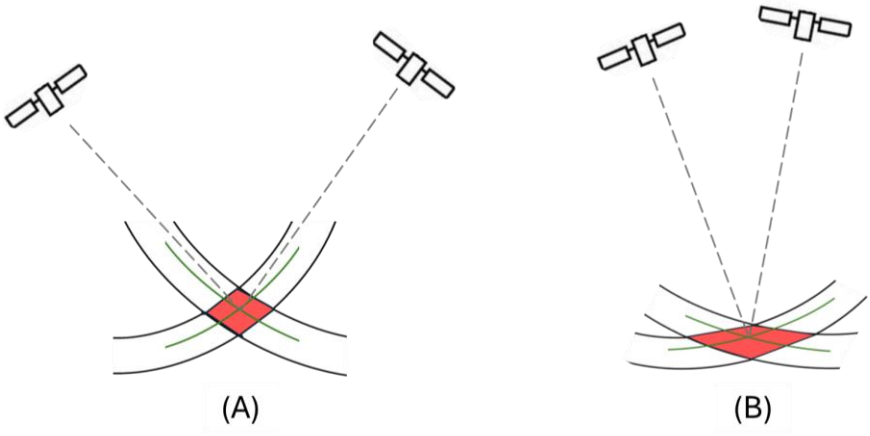

Figure 3.1 Positioning error due to satellites distribution (geometry): A) good satellite geometry and B) bad satellite geometry. The green centred circles are the real distance from satellites to receiver. The black side circles are the error measurements between satellites and receiver obtained by the receiver. The red area is the area of uncertainty.

3.1.1 Avoiding Defective Satellite Signals

As mentioned before, satellite signals at low elevation angles are more vulnerable to errors due to multipath, ionospheric, and tropospheric. To reduce the impact of these errors on positioning accuracy, it is necessary to ignore low-elevation satellite signals using Cut-off Elevation Angle (CEA) [38]. The common elevation angles applied for CEA are 10 and 15 degrees [42]. However, multipaths can exist at higher elevation angles depending on the surrounding environment, such as urban areas due to tall buildings [43].

Therefore, several studies [42,44–48] have investigated satellite selection using CEA with an elevation angle greater than 15 degrees. In these studies, elevation masks up to 40 degrees were tested using single and dual frequencies, as well as single and multiple satellite systems (multi-GNSS). Despite the positioning modes they used (real-time kinematic (RTK) [42,45–47], kinematic-DGNSS [48] and static-PPP [44]), all agreed that high elevation mask (i.e., CEA) is achievable and can provide better GNSS results using multiple satellite system as more satellites are available.

According to [49], satellite selection method based on CEA is the simplest and the least time-consuming, but it has two limitations. First, high elevation mask angles reduce the availability of GNSS satellites, which can affect positioning continuity. Second, no clear standard defines the appropriate height for the elevation mask under different conditions to achieve a high positioning accuracy. In addition, the satellites at low elevation angles can improve satellite geometric distribution [50]. However, CEA-based satellite selection prevents the use of high-quality satellite signals at low elevation angles.

3.1.2 Eliminating Redundant Satellite Signals

Redundant satellites contribute little to the geometric distribution of visible satellites; removing them reduces the number of computations required for positioning [41]. As a result, several methods for removing these redundant satellites were applied. According to [41,51], redundant satellites can be removed based on the satellites' Line-of-Sight (LOS) vectors, which represent the straight path between the satellites and the receiver (Figure 3.2). Based on the similarity of the satellites' LOS, the redundant satellites defined. The satellites' LOS similarity was judged by a cost function determined based on the angle between two satellites' LOS using Equation (3.1).

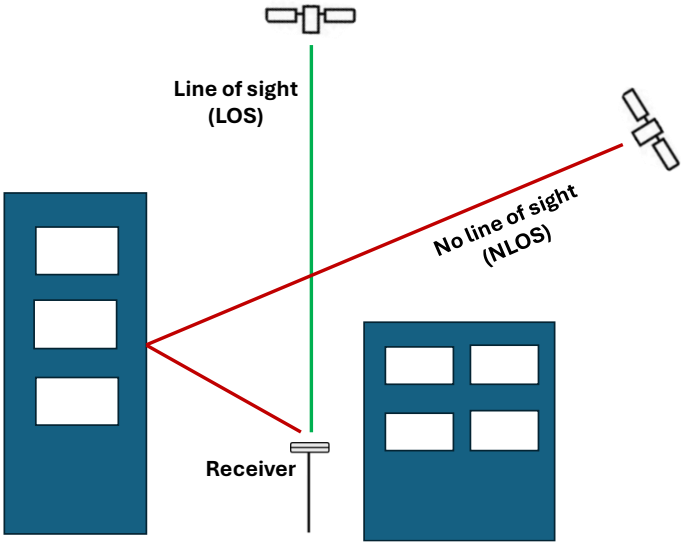

Figure 3.2 satellite line-of-sight vector

$$J_{ij} = cos2\theta_{ij} \tag{3.1}$$

where, J_{ij} is the cost function and θ_{ij} is the angle between i^{th} and j^{th} satellites. The cost function has the maximum value when $\theta_{ij} \approx 0$ or 180 degrees, while it has the minim value when $\theta_{ij} \approx 90$ degrees. The fitness of i^{th} satellites is the sum of its cost function with all visible satellites (N) using Equation (3.2).

$$J_i = \sum_{j=1}^{N} cos2\theta_{ij} \tag{3.2}$$

In addition, redundant satellites relying on satellites' elevation and azimuth angles. According to Wei *et al.* [21], if two satellites had extremely similar azimuth angles, one of them is removed based on its contribution to distribution to the overall distribution of satellites via elevation angles.

According to Wei *et al.* [51], rejecting the redundant satellites based on satellite elevation and azimuth angles is fast, as it avoids calculations and relying on elevation and azimuth angles to select the satellites. However, it provides less accurate results comparing to the LOS method. In contrast, the computational load in the LOS method is larger and sometimes results in an extremely high (poor) GDOP value [41]. To improve satellite selection, three enhanced methods are proposed in the following studies [51–53]. Two of them are based on LOS [52,53], while the third combines them [51]. In the three studies, the optimal satellite subsets were selected from a total of 9 GPS satellites. They were selected by Two techniques: i) LOS and ii) proposed technique. Compared to actual optimal

satellites, their proposed technique chose satellite subsets with GDOP value closer to actual optimal satellites than LOS. The positioning quality of the selected satellites from the three studies has not been evaluated.

3.2 Satellite Signals Power

The quality of satellite signals is critical for precise GNSS. [54] The carrier-to-noise density (C/N0) and signal-to-noise ratio (SNR) are two parameters that describe the strength of satellite signals. The C/N0 is the ratio of carrier power to noise power per unit bandwidth [55], and it is measured in decibels per hertz (dB-Hz) [38]. Whereas the SNR is the ratio of signal to noise power at a given bandwidth [55] and it is usually expressed in decibels (dB) [56]. However, in several studies they have been used in interchangeably, as in the following studies [56–58], as SNR was expressed by dB-Hz. C/N0 and SNR values are recorded by receiver [55], and they can be changed from one receiver to another [54,59,60]. The C/N0 value from an ideal receiver range between 37 and 45 dB-Hz [61].

Low C/N0 and SNR values indicates low satellite signal quality [62,63]. One of the factors that influence the satellite signal strength is multipath [64]. As a result, C/N0 and SNR values have been used to reduce multipath errors by different methods, and they can be classified into two categories: SNR value at single epoch and the fluctuation SNR value over period of time.

3.2.1 SNR Value

SNR value at single epoch / time is an approach for satellite selection. It determines a SNR threshold and rejects any satellite with an SNR value below it. The SNR threshold can be fix or variable based on elevation angle. For example, the SNR threshold was fix at 36 dB-Hz in [56]. It was variable based on the elevation angles in these studies [56,65,66]. Different positioning modes were used in three studies: SPP, D-GNSS, and RTK, respectively. The SNR or C/N0 threshold based on elevation requires 24 hours of statistical satellite data in open sky environment [65,66]. Based on this statistical data, the typical/reference signal strength (i.e., SNR or C/N0) for each satellite system and frequency is determined [65]. In three studies [56,65,66], the threshold for SNR or C/N0 was set below the reference signal power by 7-8 dB-Hz. This is because multipath reduce satellite signal power by 6 dB [43].

According to Tokura and Kubo [65], satellite selection using elevation-dependent threshold increased satellite availability by about (0.6%). Whereas it increased positioning accuracy by more than 50% compared to original D-GNSS [66]. According to Uaratanawong et al. [56], who applied the two techniques (fixed and elevation-dependent threshold) for SPP, the elevation-dependent SNR threshold provided a higher number of available satellites and better positioning availability, with an average of 6.12 available satellites and 91.60%

positioning availability, compared to 5.54 available satellites and 66.83% positioning availability for the fixed threshold. However, the fixed SNR threshold outperformed the elevation-dependent method in terms of positioning accuracy, improving horizontal accuracy by 46.80% and vertical accuracy by 12.88% compared to the original SPP method. In contrast, the elevation-dependent SNR threshold only improved horizontal accuracy by 5.83% and decreased vertical accuracy by 5.37% compared to the original SPP method.

3.2.2 SNR Fluctuation Value

SNR fluctuation is another approach that was used for satellite selection using signal strength. It technique checking the changing of SNR values over period of time. According to Fang et al. [43], SNR fluctuates get large as the signal quality decreases. Thus, they estimated the SNR fluctuation (i.e., stander deviation) of each satellites observed using Equation (3.3) If satellite's SNR fluctuation was over the threshold (Equation(3.4)), the satellite signal was rejected. Compared to the traditional relative positioning, SNR fluctuation selection method reduces the error in Easting, Northing and height by 87%, 80%, 80%, respectively.

$$std(SNR)_T = \sqrt{\frac{1}{N}\sum_{i=1}^{N}(SNR_i - \mu)^2} \tag{3.3}$$

$$std(SNR)_T < Threshold \tag{3.4}$$

where, $std(SNR)_T$ is SNR fluctuation for a satellite during T period, N is the total number observed (epochs), SNR_i is SNR value of i_{th} epoch, μ is the mean of SNR values over T period, and $Threshold$ is SNR fluctuation threshold, which was set to 4 dB because multipath affected satellite SNR values to have a std around 4 dB in preliminary tests [43] .

Low-elevation satellites generally have low signal quality as they are more vulnerable to multipath errors [43]. However, due to tall buildings in urban areas, even high-elevation satellites are affected by multipath [43]. In these scenarios, the benefit of the chosen satellites based on their signal quality (C/N0 and SNR) becomes obvious. Strong satellite signals can be chosen regardless of the satellite location (i.e., elevation). However, positioning accuracy is also affected by other factors, such as satellite geometry [67,68]. As a result, choosing satellites based on their signal quality alone is insufficient.

3.3 Geometric Dilution of Precision (GDOP)

The accuracy of GNSS solution relies on the quality of satellites measurements and satellite geometry, as shown in Equation (3.5) [24,32]. Dilution of Precision (DOP) is a parameter that

describes the quality of satellites geometry. It can be formed to express the impact of satellite geometry on horizontal positioning (HDOP), vertical positioning (VDOP), 3D positioning (PDOP), clock offset (TDOP), and all the above together (positioning and time) as Geometric Dilution of Precision (GDOP) [32]. The quality of satellite geometry improves as the satellites spread out in the sky. When satellites are concentrated in a single location, their quality decreases. As a results, this reduces positioning accuracy [69,70], as the uncertainty region grows (Figure 3.1). The DOP value is shown in Table 3.1, and it increases as the quality of satellite geometry decreases.

$$\sigma = UERE \times DOP \tag{3.5}$$

Where σ is the accuracy of GNSS solution, $UERE$ is the user equivalent range error, and DOP dilution of precision.

Table 3.1 DOP value ratings [71]

DOP value	Ratings
1	Ideal
2 - 4	Excellent
4 - 6	Good
6 - 8	Moderate
8 - 20	Fair
20 - 50	Poor

Due to the importance of GDOP in positioning accuracy, various studies used GDOP in satellite selection. The optimal satellite subset based on GDOP can be determined simply and accurately by checking the GDOP value for all possible satellite subsets using Equation (3.6). The satellite subset with the lowest GDOP value is then considered optimal. This exhaustive search technique is known as the traditional method (TM).

$$GDOP = \sqrt{tr(H^T H)^{-1}} \tag{3.6}$$

$$H = \begin{bmatrix} cosE_1 sinA_1 & cosE_1 cosA_1 & sinE_1 & 1 \\ cosE_2 sinA_2 & cosE_2 cosA_2 & sinE_2 & 1 \\ \vdots & \vdots & \vdots & \vdots \\ cosE_n sinA_n & cosE_n cosA_n & sinE_n & 1 \end{bmatrix} \tag{3.7}$$

where, tr: is the trace, H is the geometry matrix, H^T is a transpose of geometry matrix (H), and $(H^T H)^{-1}$ is the inverse of measurement matrix $(H^T H)$. The E_n and A_n are the elevation and azimuth angles of the n_{th} satellite. Each satellite system has its own time system, and

considering this difference in positioning will increases positioning accuracy [24]. As a result, this consideration will also improve the quality of satellite selection [14]. The *H* is calculated using Equation (3.8) taking into account the difference in satellite system timing.

$$H = \begin{bmatrix} cosE_{\mathrm{GPS1}}sinA_{\mathrm{GPS1}} & cosE_{\mathrm{GPS1}}cosA_{\mathrm{GPS1}} & sinE_{\mathrm{GPS1}} & 1 & 0 & 0 \\ \vdots & \vdots & \vdots & \vdots & \vdots & \vdots \\ cosE_{\mathrm{GPSn}}sinA_{\mathrm{GPSn}} & cosE_{\mathrm{GPSn}}cosA_{\mathrm{GPSn}} & sinE_{\mathrm{GPSn}} & 1 & 0 & 0 \\ cosE_{\mathrm{GLO1}}sinA_{\mathrm{GLO1}} & cosE_{\mathrm{GLO1}}cosA_{\mathrm{GLO1}} & sinE_{\mathrm{GLO1}} & 0 & 1 & 0 \\ \vdots & \vdots & \vdots & \vdots & \vdots & \vdots \\ cosE_{\mathrm{GLOn}}sinA_{\mathrm{GLOn}} & cosE_{\mathrm{GLOn}}cosA_{\mathrm{GLOn}} & sinE_{\mathrm{GLOn}} & 0 & 1 & 0 \\ cosE_{\mathrm{GAL1}}sinA_{\mathrm{GAL1}} & cosE_{\mathrm{GAL1}}cosA_{\mathrm{GAL1}} & sinE_{\mathrm{GAL1}} & 0 & 0 & 1 \\ \vdots & \vdots & \vdots & \vdots & \vdots & \vdots \\ cosE_{\mathrm{GALn}}sinA_{\mathrm{GALn}} & cosE_{\mathrm{GALn}}cosA_{\mathrm{GALn}} & sinE_{\mathrm{GALn}} & 0 & 0 & 1 \end{bmatrix} \quad (3.8)$$

The TM is a straightforward approach that selects the optimal satellite 100% accuracy as the efficiency (i.e., GDOP value) of all possible satellite subsets are checked. However, the inversion matrix that use to calculate GDOP (Equation (3.6)) is a computational load [72]. As a result, the TM can be time-consuming when it calculates the GDOP value of all possible satellite subsets [73], especially if their number was large. To avoid this computational load, various techniques including the closed-form solution, maximum volume, artificial neural network (ANN), and optimisation algorithms have been used to select optimal satellite subsets based on GDOP.

3.3.1 Closed-Form Formula

The close form is a mathematical expression refers to a mathematical operation that can be completed in a limited number of operations [74]. To avoid the huge computational burden of calculating the GDOP with the inversion matrix, different closed-form formulas were applied in these studies [75–78]. For example, Doong (2009) [76] proposed a closed-form formula to calculate the GDOP value for one satellite system, as shown in Equation (3.9).

$$GDOP = \sqrt{\frac{0.5h_1^3 - 1.5h_1h_2 + h_3}{3h_4}} \quad (3.9)$$

Where, h_1, h_2 and h_3 are the trace of *M*, M^2, and M^3, while h_4 is the determinant of *M*. The measurement matrix *(M)* is computed by the geometry matrix *(H), where M* = (H^TH).

The closed-form formula can significantly reduce the computational complexity of inversion matrix in TM, leading to compute GDOP value with less computation load using closed-form formula [79,80]. However, the number of calculations cannot be reduced with the closed-form formula, so it becomes time-consuming when the number of satellites increases [81]. Furthermore, the selected satellites by closed-form formula in the above four studies have not been used in positioning with any kind.

3.3.2 Maximum Volume

At least four satellites are required for positioning. The best geometry of four satellites is a tetrahedron, by one satellite directly above the receiver and three near the horizon, 120 degrees apart in azimuth (Figure 3.3) [82,83]. The GDOP value decreases (improves) as the tetrahedron's volume increases [82–84]. As a result, positioning accuracy increases by maximizing the tetrahedron volume [85]. Several studies [82,85,86] have selected the optimal four satellites based on maximizing the tetrahedral size. To select the optimal subset of more than four satellites, other studies [8,87,88] have maximized the polyhedron size. In addition, other studies [89,90] maximized the polygon area (i.e., orthogonal projection) to determine the optimal satellites subset.

From the above eight studies of satellite selection based on maximum volume, simulation GNSS data were used for satellite selection in three studies [8,87,89]. In addition, the satellites selected in the above eight studies were not evaluated in positioning except for one study [88]. In this study [88], the selected satellites based on maximum volume were implemented for SPP. Their 3D positioning accuracy was worse by about 44% than original SPP using all satellites (GPS and BDS).

Satellite selection based on maximum volume can be implemented by two methods: 1) volume computation and 2) satellites separation [85]. In the first approach, the tetrahedron/polyhedron volume of all possible satellite subsets is computed, and the largest satellite subset is chosen as the optimal. In the second method, satellite angles are used to determine the optimal satellite subset, which is the group of satellites that are the farthest apart. For example, Noe et al. chose the three satellites with the greatest separating in the Easting, Northing, and Zenith directions, then selected the fourth satellite that form the tetrahedron with the biggest volume [85].

According to Zuo-ya et al. [85], satellite selection based on maximum volume using both techniques is faster than TM, especially the satellite separation method. However, they are less accurate than TM [75,81,91], as the method focuses on maximizing the volume and not on the GDOP value [81,92]. Furthermore, the computation load is not effectively reduced in the volume computation method, as it increases with the number of satellites used [81,92].

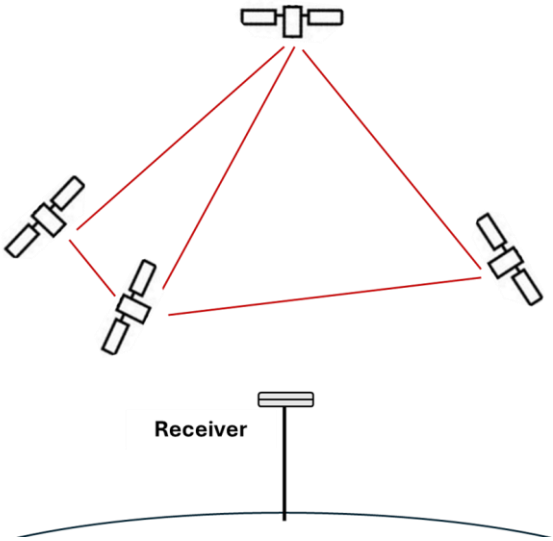

Figure 3.3 The tetrahedron of four satellites

3.3.3 Artificial Neural Network (ANN)

ANN is a machine learning algorithm that belongs to the field of artificial intelligence (AI). It was developed to simulate the biological neural networks of the human brain. ANN learn from input data just like humans [93], and the information gained from learning is stored as weights that influence the output [94]. ANN has broadly been used for different problems [95]. One of these issues is satellite selection based on the GDOP (e.g., [84,96–99]). However, the selected satellites in these studies have not been evaluated in positioning.

ANN is one of the most powerful AI algorithms [100]. The GDOP computational load can be reduced using ANN as it does not require the inversion matrix for GDOP determination [96,101,102]. However, ANN requires costly training, which becomes useless when the data deviates significantly from the training data [76,103]

3.3.4 Optimization Algorithms

Optimisation algorithms are mathematical procedures that aim to find the best solution to a given problem. They have been widely used in a variety of fields, including AI and machine learning. Furthermore, optimisation algorithms were used for satellite selection based on GDOP (e.g., [7,99,101,104–107]). Different optimalization algorithm was used in these studies for satellite selection. Despite the variation of optimization algorithms in these studies, their selected satellites have not been used for positioning.

Like ANN, optimization algorithms do not require the inversion matrix for GDOP computation [108]. This reduces the GDOP computation load. Compared to ANN,

optimisation algorithms do not require training, which make them faster than ANN [99]. In addition, optimization algorithms choose satellite subset with high quality [7,105]. They can successfully select the optimal satellite subset with high rate over 90% [99,106]. However, the successful selection rate of optimization algorithms is not fixed or grunted. This is because these algorithms were mainly designed to provide solutions in short time [109–111]. To do so, they tend to choose a reasonable solution, especially in complex problem that required long time to solve (ref). Furthermore, optimization algorithms relay on randomness in their selection this may lead to have different solution at each trail [110].

3.4 Weighted Geometric Dilution of Precision (WGDOP)

The positioning accuracy depends on satellites geometry (GDOP) and pseudo-range error (i.e., UERE), as shown in Equation (3.5). Thus, satellites were widely selected based on GDOP, as presented in Section 3.3. However, the quality of satellite pseudo-ranges varies depending on satellite system, atmospheric biases and multipath [112,113]. Thus, satellites' UERE should be considered when selecting satellites to improve outcomes [112]. To consider both GDOP and UERE at the same time, several studies chose satellites based on Weighted GDOP (WGDOP). WGDOP computes satellite geometry (GDOP) by assigning more weight to satellites with lower UERE. The WGDOP can be calculated using inversion matrix (Equation (3.10)). To reduce it computational load, closed-form solution [112,114], maximum volume [113], and artificial neural network (ANN) [73,92], were used to select the optimal satellite subset based on WGDOP.

The UERE is affected by the satellite signal power [115,116], which can be expressed by the SNR and C/N0. Since calculating the UERE value can be more complex compared to the value of signal power (SNR and C/N0) [50,92], which are directly calculated by the receiver. Therefore, three studies [50,92,117] chose satellites with WGDOP based on satellite signal power (SNR and C/N0) rather than UERE. Two of them [92,117] utilized optimization algorithms.

$$WGDOP = \sqrt{tr(H^T W H)^{-1}} \tag{3.10}$$

$$W = \begin{bmatrix} w_1 & 0 & \dots & 0 \\ 0 & w_2 & & 0 \\ \dots & & \ddots & \dots \\ 0 & 0 & \dots & w_n \end{bmatrix} \tag{3.11}$$

where, *H* is the geometry matrix determined based on the elevation and azimuth angles, as shown in Equations (3.7) and (3.8). *W* is the weighting matrix, where w_n is the weight of the

n_{th} satellite. In WGDOP based on UERE, the w_n is 1/UERE^2 [112,114]. In contrast, it is SNR in WGDOP based on SNR [92].

The selected satellites in the previous seven studies based on WGDOP using different satellite selection techniques: i) closed-form formal, ii) maximum volume, iii) ANN, and v) optimization algorithms, were not tested for positioning.

3.5 GDOP- RAIM (Receiver Autonomous Integrity Monitoring)

To verify the integrity of stand-alone positioning (i.e., SPP), Receiver Autonomous Integrity Monitoring (RAIM) was developed. It checks the consistency of satellite measurements by overdetermining positioning solution [24]. Then it detects and excludes abnormal satellite measurements to improve positioning accuracy. To determine receiver's coordinates (3D) and clock offset, four satellites are needed. Hence, five satellites are required for RAIM availability (i.e. fault detection). This is because the fifth satellite allows repeated position calculations using different measurements and finding abnormal satellite measurement. Six and more satellites are needed for RAIM exclusion.

After initial positioning, each satellite's pseudo-range residual, which is the differences between observed and estimated pseudo-range measurements, is determined. Then the sum squared residuals is computed. If the exceeds the error threshold, as determined by the Chi-square, the positioning solution consider invalid [118,119]. After that RAIM removes the satellite with high residual to improve positioning accuracy. The RAIM procedure can be expressed by the following steps [24,120]:

Step 1: Positioning determination using the following equations:

$$y = Hx + \varepsilon \tag{3.12}$$

$$\hat{x}_{LS} = (HH)^{-1}H^T y \tag{3.13}$$

$$\hat{y}_{LS} = H\hat{x}_{LS} \tag{3.14}$$

$$v = y - \hat{y}_{LS} \tag{3.15}$$

Where, y is observation vector, which is the different between the observed and the estimated measurements. Whereas H is the geometry matrix, x is the estimated vector for receiver three coordinates and clock offset, ε is the error vector, $\hat{x}_{LS}$ is the least square solution, and v is the residual vector.

Step 2: Solution validation based on sum squared residuals using Chi-square test

$$\frac{v^T v}{m-n-1} < x_\alpha^2(m-n-1) \tag{3.16}$$

Where, $v^T v$ is sum squared residuals, $(m-n-1)$ is the Chi-square degree of freedom. m is the total number of satellites tracked, n is the number of estimated parameters, x_α^2 is the chi-square distribution, and α is significance level, which is 0.001(0.1%) [118,119].

Step 3: Detection and exclusion fault satellite measurements via determining the contribution of each satellite in positioning error. This contribution of each satellite is given by a slope as shown in the following equations:

$$Slope_H(i) = \frac{\sqrt{A_{1i}^2 + A_{2i}^2}}{\sqrt{S_{ii}}} \tag{3.17}$$

$$Slope_V(i) = \frac{A_{3i}}{\sqrt{S_{ii}}} \tag{3.18}$$

$$A = H(H^T H)^{-1} H^T \tag{3.19}$$

$$S = \mathrm{I}_m - H(H^T H)^{-1} H^T \tag{3.20}$$

Where, $Slope_H(i)$ and $Slope_V(i)$ indicate the errors of i_{th} satellite horizontal and vertical, respectively. I_m is $m \times m$ identity matrix, m is total number of satellites observed. The satellite with the highest slope is excluded, as it contributes the most in positioning error.

RAIM only needs the satellite measurements observed by the receiver for positioning integrity (i.e., satellite exclusion) [14,121]. In addition, it considers positioning correction, as ionosphere and troposphere [122,123]. However, it is not suitable for satellite selection as RAIM excludes satellites based on criteria of positioning integrity. To take advantage of RAIM in satellite selection, several studies [14,121,124] used RAIM after satellite selection based on GDOP.

Meng et al. [121,124] chose satellites based on their geometrical distribution (GDOP) and RAIM using simulation GNSS data. They selected satellites three times in a row. Firstly, they chose satellites based on GDOP. Secondly, they check the quality of selected satellites using RAIM. Lastly, they applied satellite selection based on GDOP to replace the rejected selected satellites by RAIM. In other words, the satellite selection method was GDOP-RAIM-GDOP. The satellite selection based on their geometrical distribution (GDOP) was done

using satellite angles (elevation and azimuth). According to Meng et al. [99], the SPP positioning accuracy of the selected satellites GDOP-RAIM-GDOP was enhanced by 50% in comparison to the original SPP. According to Meng et al. [124], the SPP positioning accuracy of the selected satellites based on GDOP-RAIM was enhanced by more than 90% in comparison to the accuracy where only GDOP was applied. The SPP positioning accuracy of the satellite selected using GDOP-RAIM-GDOP was enhanced by more than 8% better than that of GDOP-RAIM.

In addition, Wang et al. [14] selected satellites based on GDOP and RAIM. Initially, they chose satellites based their geometrical distribution (GDOP) using satellite elevation angles (elevation and azimuth). Then they improved their set of selected satellites by adding more satellites to the selected set based on satellite contribution slope in RAIM algorithm. According to the authors, the horizontal accuracy of their proposed method was about 3 m higher (better) than that based on geometrical distribution.

3.6 Comparison of Satellite Selection Methods

This chapter presents various satellite selection methods. It shows how satellite selection method has two components: criterion and technique. Using the best of both provides the best method for selecting satellites. Below is a comparison of the criteria and techniques to find the best of both.

Satellites have been selected based on five criteria: i) satellite angles, ii) satellite signal power, iii) satellite geometry (GDOP), iv) satellite geometry and signal power (WGDOP), and v) GDOP and RAIM (GDOP-RAIM). Satellite geometry (GDOP) and signal power are the main factors affecting positioning solution. Satellite elevation angles were used to select satellites based on their signal power by abandoned satellite signal at low elevation angles (0-15 degrees), as they are more vulnerable to errors from multipath, ionospheric, and tropospheric. In addition, satellite elevation and azimuth angles were utilized to choose satellites based on their geometry distribution. Satellite selection methods based on satellite angle can be the fastest as it avoids computation [49,51]. However, their selected satellites cannot be the best. Poor satellite signals can be at elevation angles higher than 15 degrees. Using high elevation mask reduces satellite availability [49]. On the other hand, the quality of the selected satellites based on GDOP value were better using computation methods from satellites angles [14,51,52,105].

The quality of selected satellites increases as more positioning factors are considered. Thus, choosing satellites based on their geometry and signal power (WGDOP) could be better than selecting satellites based on GDOP or signal power alone. In addition, choosing satellites based on GDOP-RAIM could be even better than WGDOP. This is because RAIM considers more positioning factors than WGDOP. RAIM excludes satellites based on range

residuals, which are the different between the observed and the estimated pseudo-range measurements. To estimate pseudo-range measurements, it requires initial positioning considering satellite geometry, signal power and positioning correction. However, RAIM cannot be used for satellite selection, as it is a positioning integrity technique. Hence, RAIM was applied after GDOP-based satellite selection to improve the quality of the selected satellites in previous studies. Since satellite selection based on WGDOP is better than GDOP, WGDOP-RAIM could be the most suitable criterion for satellite selection.

RAIM is implemented via positioning. Whereas WGDOP can be carried out by various techniques, including TM, closed-form formal, maximum volume, ANN, and optimization algorithms. TM selects the optimal satellites with 100% selection accuracy, but it is time-consuming. The closed-form formal can reduce the TM computational complexity [125,126]. However, it could not reduce the number of calculations, so it becomes time-consuming when the number of satellites increase [72]. The maximum volume method is based on maximizing the volume of the tetrahedron or orthogonal projection created between the satellites [92,127]. The WGDOP value decreases (improves) as tetrahedron volume and maximum orthogonal projection increase. However, the positioning quality obtained with the selected satellites via this method is not guaranteed [72,128], as the method focuses on maximizing the volume of tetrahedron/orthogonal projection and not on the WGDOP value [92,128], and it is also a time-consuming technique [128]. On the other hand, ANN and optimization algorithms, which are broadly applied in artificial intelligence (AI) problems, can both provide good results in satellite selection [92,99,106]. However, the optimization algorithms, contrarily to ANN and generally to any AI or machine-learning algorithms, do not require any training and consequently any large dataset for the required training [129–131], which makes the optimization algorithms faster than ANN. In addition, ANN trained model could be difficult to apply due to the varying geometry of the tracked satellites due to the different revolution periods of the GNSS systems [129,130]. Thus, optimization algorithms are potentially more suitable for selection of satellites than ANN and similar AI techniques.

3.7 Summary

Satellite selection method has two components: criterion and technique. This chapter presents various types of criteria and techniques used for satellite selection. In addition, a comparison was made between the types of criteria and the types of techniques in the chapter too. This is to determine the best of both and used to form the most suitable satellite selection method. Precise positioning accuracy one of the main goals of satellite selection. Thus, positioning factors, as GDOP, have used as criteria for satellite selection. Since positioning is affected by all its factors, using as much as possible of them as criteria for satellite selection could be the best. Therefore, WGDOP-RAIM, including satellite signal

power, geometry, and positioning corrections, was considered the suitable criterion for satellite selection. On the other hand, optimization algorithm(s) was considered the appropriate technique for selecting satellites because it is efficient in terms of satellite selection accuracy and speed.

Chapter 4 Optimization Algorithms

4.1 Optimization Algorithms for Satellite Selection

There is a large number of optimization algorithms. According to Ostojić et al. [109], the optimization algorithms can be classified into three groups: i) Exact, ii) Heuristic, and iii) Meta-Heuristic. The exact algorithms provide the optimal solution but require a lot of time and resources. In contrast, the heuristic algorithms do not guarantee the optimal solution and outcomes' quality but usually they provide acceptable solutions in a short time. The main limitations of heuristic algorithms that are more suitable for specific problem [109,132], and they can be easily trapped in local optima [110,132]. The meta-heuristic algorithms are higher level of heuristic algorithms [132,133], designed to overcome heuristic drawbacks [110]. They are more flexible and reliable, handling various types of optimization problems and provide good results [110,111,134].

Many optimization algorithms are covered fall under the category of meta-heuristic, where 50 types of them were listed by Kaveh et al. in 2020 [135]. In satellite selection problem, five robust and well-known optimization algorithms have been used: i) Artificial Bee Colony (ABC) [99,106], ii) A (ACO) [92,106], iii) Genetic Algorithm (GA) [7,92,99,104,105,117], iv) Particle Swarm Optimization (PSO) [7,99,136], and v) Simulated Annealing (SA) [99,136]. In this chapter, these algorithms' principle, advantages, limitation, and application were shown. In addition, their efficiency was compared.

4.1.1 Artificial Bee Colony (ABC)

ABC is an algorithm developed by Karaboga (2005) to simulate the foraging behaviour of bees [137]. The algorithm is a population-based algorithm as it generates multiple numbers of artificial bees. ABC split these bees into three groups: employed bees, onlooker bees, and scout bees. Each type of bee is assigned to different research tasks. Through sharing the information of the discovered possible solutions (quality and location in the search space) among the bees, ABC can converge toward the optimal solution (Figure 4.1). ABC is flexible as it can be used for various types of problems, with the requirement of very few control parameters [138,139] which lead to reliable and robust results. However, ABC is relatively weak in local searching [140]. ABC algorithm has been used various applications, such as i) power system [141], ii) image processing [142], iii) clustering [143,144] , iv) biology [145], v) job scheduling [146], vi) engineering design [147], vii) AI training [148], and viii) GNSS satellite selection [99,106]. ABC can be implemented using the flowing steps [149]:

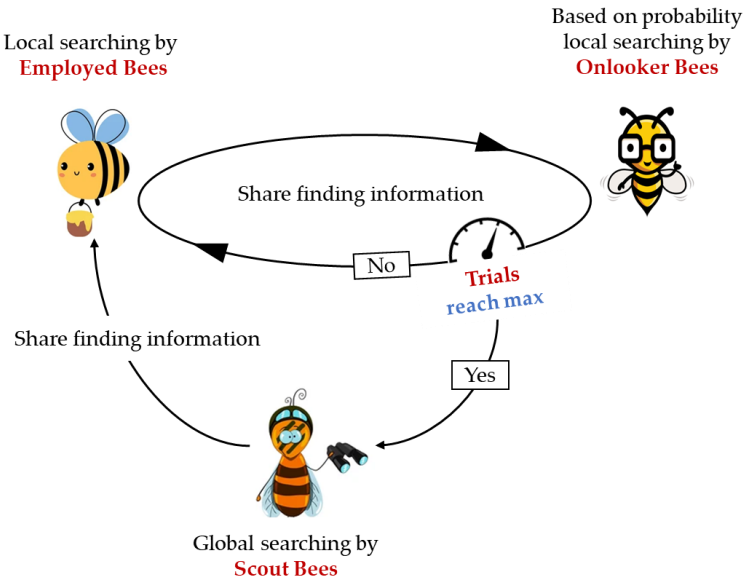

Figure 4.1 Representation of the ABC searching process and the roles of employed, onlooker, and scout and bees, adapted from [150].

1. **Parameter Initialization:** ABC It requires three parameters to be set: *iterMax*, *pSize*, and *limit*. *iterMax* is the maximum number of iterations allowed to find the optimal solution. *pSize* represents the number of bees searching for the best solution. Whereas *limit* is a threshold for abandoning a specified area in the issue search space. Typically, the *limit* value is calculated by multiplying the problem dimensions by the population size (*D* ×*pSize*) [151]. As a result, only two parameters (*iterMax* and *pSize*) are required setting in ABC [138].

2. **Food Source:** equivalent to *pSize*, a number of locations in the search space are selected at random. Any location in the search space is a possible solution, which is called food source in ABC algorithm. Food sources can be chosen randomly using Equation (4.1). After selecting the possible solutions, Equation (4.2) is used to calculate their fitness (quality).

$$x_{i,d} = l_d + r(u_d - l_d) \tag{4.1}$$

$$f(x_i) = \begin{cases} \dfrac{1}{1 + F(x_i)} & if \;\; f(x_i) \geq 0 \\ 1 + |F(x_i)| & else \end{cases} \tag{4.2}$$

where, x is the solution (food) location, i = [1,2,...,SN] is the solution number is the possible solution number, d=[1,2,...,D] is the d_{th} dimension within the search space, l_d and u_d are the lower and upper bounds of the problem search space, r is a random number ranging from 0-1, and $f(x_i)$ is the fitness of i_{th} solution, while $F(x_i)$ is the objective function of i_{th} solution.

3. **Employed Bees:** New possible solutions (i.e., food sources) are investigated by employee bees. Every employee bee presents a possible solution. They then change their current solutions (locations) using Equation (4.3). The new solutions are selected from the current solution neighborhood. The quality of these new solutions is evaluated using Equation (4.2). If a bee's new solution provides better quality, it is accepted and replaces the previous one. In addition, the abandon counter is reset to zero. Otherwise, the previous solution remains, and the abandoned counter increases by one.

$$v_{i,d} = x_{i,d} + \emptyset(x_{i,d} - x_{k,d}) \quad (4.3)$$

where, $v_{i,d}$ is a vicinity solution, $x_{i,d}$ is the current solution, $\emptyset$ is random number between [-1,1], $x_{k,d}$ is a random solution from the generated solution set ≠ the current solution ($x_{i,d}$).

4. **Onlooker Bees:** onlooker bees replace employed bees in this stage. Likewise, onlooker bees investigate neighbour solutions by changing their location in the search space using Equation (4.3). However, not all onlooker bees are allowed to change their location. An onlooker bee investigates/ changes its location if its searching probability (P) is greater than r, which is a random number between 0-1. P is calculated using Equation (4.4). After the onlooker bee finds a new solution, if the new solution quality is better than the previous one, it is accepted and replaces the previous one. In addition, the abandon counter is reset to zero. Otherwise, the previous solution remains, and the abandoned counter increases by one.

$$P_i = \frac{f_i}{\sum_{j=1}^{SN} f_j} \quad (4.4)$$

where, p_i is the probability of the current solution (i.e., onlooker bee), f_i is the fitness of the current solution, and $\sum_{j=1}^{SN} f_j$ is the sum of all solutions' fitness.

5. **Scout Bees:** When the solution abandonment counter reaches the specified threshold (*limit*), Scout Bees phase is activated. Bees in both the employee and onlooker stages investigate neighbour (local) solutions. However, if no better local

solution is discovered after a certain number of attempts, the solution's location is considered poor and abandoned. In such cases, a Scout Bee is assigned to change its (i.e., solution) location globally using Equation (4.1). As a result, the scout phase allows ABC to avoid local optimal trapped [152].

6. **Termination:** The number of iterations increases by one. If the number of iterations reaches the maximum (*IterMax*), the ABC search stops and solution with the highest fitness is considered the best solution for the given problem. Otherwise, ABC steps 2-6 are repeated until the stopping criterion is met.

4.1.2 Ant Colony Optimization (ACO)

ACO is an algorithm developed by Marco Dorigo et al. in 1996 [153]. The algorithm simulates the behaviour of ants in finding the shortest path between the food and the nest. In nature, ants search for food and secrete a substance known as pheromone to determine the food path. However, the pheromone evaporates over time. As a result, the pheromone rate increases as the food path decreases. This led ants to use the shortest food paths with high pheromone levels, as shown in Figure 4.2. The same concept is used in ACO, where a number of artificial ants is generated to find the best path (solution) for the given problem. In ACO, the optimal solution can be found after a number of iterations. At each iteration, each ant creates a new solution (path), and it is evaluated by the pheromone rate, which rises as the quality of the solution improves. The pheromone rates on the paths influence the ants' choice in finding the best path (solution) with the highest pheromone rate, as shown in Figure 4.3. ACO is a robust and flexible algorithm [154,155], suitable for the path planning problem [155,156], but it has a slow convergence [154]. ACO algorithm has been used various applications, such as i) power system [157], ii) clustering [158], iii) Medicine [159], iv) Transportation [160,161], v) water system design [162], and vi) GNSS satellite selection [92,106]. ACO can be implemented using the flowing steps [149]:

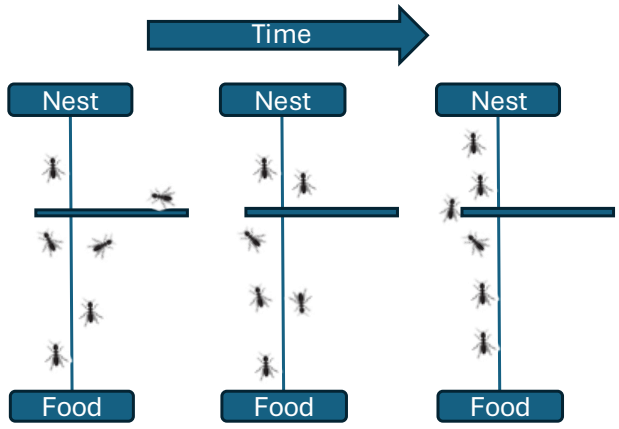

Figure 4.2 Ants food searching in nature, taking the shorted path for the food from the nest over time.

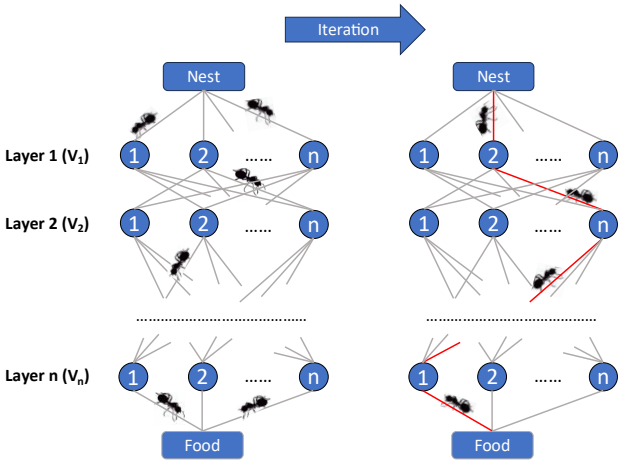

Figure 4.3 Artificial ants searching for the best possible solution, which is the path between nest and food. It is found (red line) over number of iterations, adapted from [150].

1. **Parameter Initialization:** The algorithm parameters are determined in this stage. Seven parameters needed to be set: (1) maximum number of iterations ($Iter_{max}$), (2) ant population size (*pSize*), (3) pheromone evaporation rate (ρ), (4) influence of pheromone rate creating a solution (α), (6) influence of desirability creating a solution (β), and (7) the quantity of pheromone laid by ant (Q).

2. **Creating new path (solution):** Each ant in the population creates one possible solution. The ant sequentially chooses solution variables to create one possible solution. In other words, it selects the path nodes one by one to form their path, as

shown in Figure 4.3. The node selection relies on probability, which is determined using the following equation.

$$p_{ij} = \frac{\tau_{ij}^{\alpha}\, \eta_{ij}^{\beta}}{\sum_{i,l=1}^{n} \tau_{il}^{\alpha}\, \eta_{il}^{\beta}} \tag{4.5}$$

where, p_{ij} is the probability of selecting j note, τ_{ij} is the pheromone rate on the path between notes i and j, η_{ij} is the desirability of selecting j note. While α and β are the influence parameters, which control the impact of the pheromone and the desirability value on the probability. The desirability is the distance between notes i and j. The rate of desirability increases as the distance between the two notes decreases in the distance minimization problem. Using Equation (4.5), ants choose notes to create their path (solution). However, they randomly select the notes to create the initial path as all paths initially have the same pheromone rates. The quality of each ants' possible solution is then evaluated.

3. **Update pheromone rate:** The pheromone rate of all possible paths between notes is updated. It is updated through two stages: (1) evaporation, which removes a portion of the pheromone rate on all possible paths, and (2) reinforcement, where an amount of pheromone is add on the paths based on their quality. Equation (4.6) can be used to update the pheromone rate, including evaporation and reinforcement.

$$\tau_{ij}\,(t+1) = \rho \cdot \tau_{ij}\,(t) + \sum_{k=1}^{K} \Delta\tau_{ij}^{k} \tag{4.6}$$

$$\Delta\tau_{ij}^{k} = \frac{Q}{f(T_k)} \tag{4.7}$$

where, $\tau_{ij}\,(t+1)$ is the amount of updated pheromone for the path between i and j, t is the current iteration value, ρ is the evaporation rate, $\tau_{ij}\,(t)$ the current amount of pheromone between i and j, and $\Delta\tau_{ij}^{k}$ is the amount of pheromone increase on the path i to j based on the tour (solution) fitness. While Q is the quantity of pheromone laid by ant, and $f(T_k)$ is the fitness of the k ant's tour.

4. **Termination:** The number of iterations increases by one. If the number of iterations reaches the maximum ($Iter_{max}$), the ACO search stops and tour (solution) with the highest pheromone rate is considered the best tour (solution) for the given problem. Otherwise, ACO steps 2-4 are repeated until the stopping criterion is met.

4.1.3 Genetic Algorithm (GA)

GA is an optimisation algorithm developed in the 1960s and 1970s by John Holland and his collaborators at the University of Michigan [149,163]. GA was developed to simulate Darwin's concept of evolution and natural selection. In GA, a problem's best solution is found by creating a number of random possible solutions. These possible solutions are evaluated and improved using various procedures to find the best possible solution ever. GA is a flexible and robust algorithm [149], but it is complex [149,164], sensitive to the value of parameters [149] and dependent on the initial population [164,165]. GA algorithm has been used various applications, such as i) AI training [166], ii) power system[167], iii) clustering [168], iv) Transportation [169], v) water system design [170,171], vi) Industry [172], vii) job scheduling [173], and viii) GNSS satellite selection [7,92,99,104,105,117]. The basic GA contains six main steps: population generation, fitness determination, selection, crossover, mutation, and population replacing [174]. Part of the first step, these steps are repeated for a number of iterations to find the best solution for a given problem, as shown in Figure 4.4.

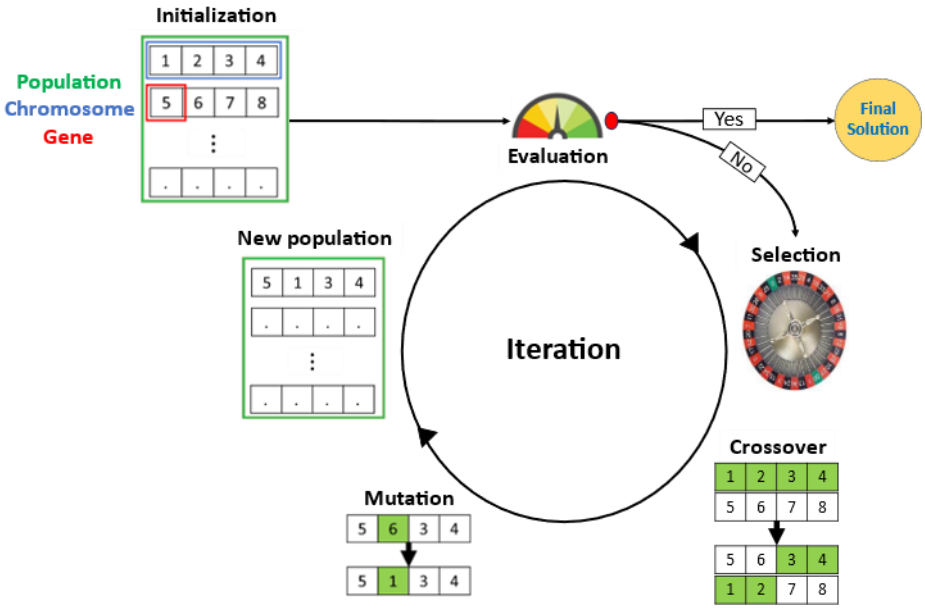

Figure 4.4 Representation of the GA processing steps [150].

1. **Population Generation:** To find the best solution for a given problem, GA initially generates a number of possible solutions that known as population of possible solutions. The population size/ the number of possible solutions is predefined. According to Yang (2014) [149], too small population size can cause GA to fall in the local optimum, while too large population size will lead to unnecessary computation load. A population size of 40 to 200 is sufficient for most problems. The possible

solutions in GA are represented as chromosomes, where each chromosome contains a number of genes (Figure 4.4). These genes indicate the problem variables. All chromosomes (possible solutions) have the same number of genes, which is equal to the number of problem variables were considered. The genes' value can be presented using the binary number system that is commonly used [149,174]. In addition, it can be presented as a real number, which is simpler as no conversion is required [174]. After determining the number of genes in the chromosomes and the number of chromosomes in the population, the GA randomly generates the initial set of possible solutions (chromosomes) using Equation (4.1).

2. **Fitness Determination:** Once a set of chromosomes (potential solutions) is generated, the quality (fitness) of each chromosome is evaluated to determine its efficiency in solving the given problem. The chromosome with highest fitness is required for problem solving. The fitness of chromosomes for maximization and minimization problems can be calculated using Equations (4.8) and (4.9), respectively.

$$F = f(x) \tag{4.8}$$

$$F = \frac{1}{f(x)} \tag{4.9}$$

where, *F is the fitness, and f* is the problem objective function of *x* possible solution.

3. **Selection:** In GA, the best solution to a given problem is discovered by improving the quality (fitness) of the current possible solutions (population) using crossover and mutation procedures. The selection step is the process of selecting the right current chromosomes to generate new set of chromosomes (i.e., new population). Iteratively, the selection procedure is carried out, with a number of iterations equivalent to half the total number of chromosomes. In each iteration, two chromosomes (parents) are chosen to produce new chromosomes (offspring). Chromosomes are chosen based on their fitness, but randomly. The roulette wheel is a selection technique widely used in GA [175]. Chromosomes with high fitness are more likely to be chosen using this technique.

4. **Crossover**: is a process aimed at creating two new possible solutions (chromosomes) from a pair of selected chromosomes. This can be done by switching chromosomes' genes in single or multiple points [176]. Single-point crossover

switches chromosome genes before/ after one point, whereas multi-point crossover flips chromosome genes at multiple locations, as shown in Figure 4.5. The multi-point crossover is more effective and commonly used [149]. The initial chromosomes are called parents, and the new solutions (chromosomes) are called offspring. Despite the crossover technique used (single/ multiple), the parents' genes switch (crossover) only if the crossover probability (*Pc*) is true (Pc> *r*). Usually, *Pc* value ranges between 0.7-1, and *r* is random number between 0 and 1 [149].

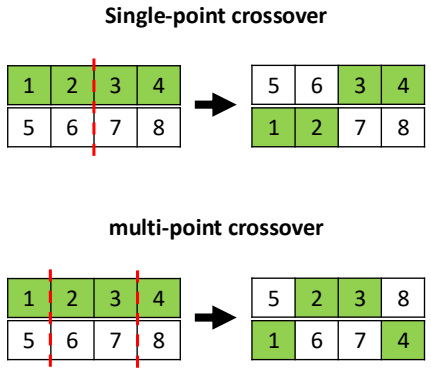

Figure 4.5 Genetic algorithm single- and multi-point crossover.

5. **Mutation:** After the crossover stage, the new set of chromosomes changes further by mutation. Mutation is another operation that seeks to create new possible solution (chromosome) by randomly changing the solution's variables (genes). It is only done if the mutation probability (*Pm*) is true (*Pm* > *r*). *Pm value* typically ranges from 0.001 - 0.05 [149]. In contrast to crossover, the mutation process occurs for each chromosome separately.

6. **Population Replacing:** After the mutation phase, the new set of chromosomes (population) replaces the initial one. In addition, the number of iterations increases by 1. Until the maximum number of iterations is met, the GA procedure is repeated from 2 to 6.

4.1.4 Particle Swarm Optimization (PSO)

PSO is an algorithm that simulates bird/fish foraging behaviour, and it was developed by Kennedy and Eberhart (1995) [177]. It is a population-based algorithm in which a number of particles are generated to find the optimal solution in the search space. By sharing information about the discovered possible solutions (quality and location in the search space), particles can converge towards optimal solutions. PSO is a flexible [149] and simple algorithm and it can be easily implemented compared to other optimization algorithms [149,178]. However, in a high-dimensional search space, PSO slowly converges toward the optimal solution, and the quality of its results decreases [179,180]. PSO algorithm has been

used various applications, such as 1) AI training [181], 2) power system [182], 3) clustering [183], 4) Transportation [184], 5) image processing [185], 6) Industry [186], 7) Farming [187], and 8) GNSS satellite selection [7,99,136]. According to [188], the PSO algorithm follows steps:

1. **Initialization:** a population of particles is generated and randomly distributed in the problem search space using Equation (4.1). Each location in the search space indicates a possible solution. As a result, particles represent the possible solutions of their positions.

2. **Updating:** The quality (fitness) of these particles (possible solution) is then calculated. Based on particles' fitness, the particle personal best (p_{best}) and global best (g_{best}) is repeatedly determined in each iteration. p_{best} is the best solution ever found by the same particle, while the best solution ever found by all particles is the g_{best}.

3. **Travelling:** particles velocity and location are determined/ updated in this stage. To find the best solution for the given problem, the particles move in the search space, investigating new locations (i.e., potential solutions). Particles' travelling depends on their velocity, p_{best} and $g_{best,}$ as shown in Figure *4.6*. Updating particles velocity and location can be done using Equations (4.10) and (4.11).

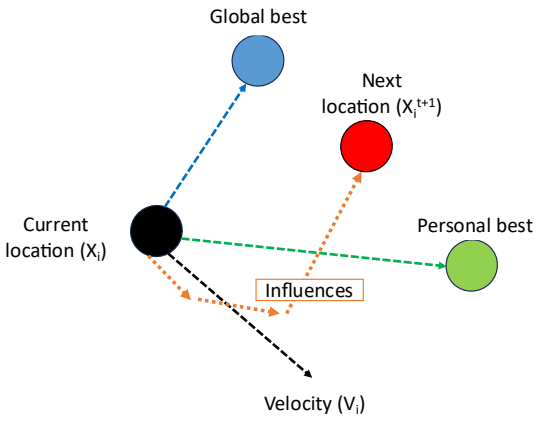

Figure 4.6 Representation of updating particle location based and on g_{best}, p_{best} and velocity [150].

$$X = X_0 + V \tag{4.10}$$

$$V = \omega V_0 + C_1 r_1 (pbest - X_0) + C_2 r_2 (gbest - X_0) \quad (4.11)$$

$$\omega = \omega_{max} - \frac{\omega_{max} - \omega_{min}}{Iter_{max}} * Iter \quad (4.12)$$

where, X is the new position, X_0 is the current (initial) position, V is the new velocity, V_0 is the current (initial) velocity, C_1 and C_2 are the acceleration factors, r_1 and r_2 are random number between 0-1, ω is the inertia weight, ω_{max} and ω_{min} are initial and final weights respectively, $Iter_{max}$ is the maximum number of iterations, and $Iter$: is current number of iterations. Typically, the value of the ω_{max} and ω_{min} are 0.9 and 0.4, respectively [189]. Whereas the value of C_1 and C_2 are 2 [190].

4. **Termination:** The number of iterations increases by one. If the number of iterations reaches $Iter_{max}$, the PSO search stops and g_{best} is considered the best solution for the given problem. Otherwise PSO steps 2-4 are repeated until the stopping criterion is met.

4.1.5 Simulated Annealing (SA)

SA is an optimization algorithm developed by Kirkpatrick et al. (1983) [191]. It is a single-based algorithm, where it generates one possible solution and iteratively optimizes to create the best solution for the given problem. To avoid the trap of local optimal solution, both better and worse solutions are acceptable. SA was designed to simulate annealing processes, where the metal is highly heated and slowly cooled to change its properties. Similarly, SA algorithm starts with a high temperature value, which allows it to accept worse solutions; as the temperature value decreases, the probability of accepting poor solutions declines. SA is a flexible algorithm [192] with the capacity to avoid local optima trap by accepting the worse solution [149]. However, slow convergence is required in SA to obtain the actual optimal solution [149,164,193]. In addition, it is a single solution-based algorithm, where only one solution is generated and optimized from local search [149]. SA algorithm has been used various applications, such as i) Industry [194], ii) clustering [195], iii) Transportation [196], iv) image processing [197], v) Security [198], vi) Water system [199], and vii) GNSS satellite selection [99,136]. According to [200,201], SA can be easily implemented using the following steps:

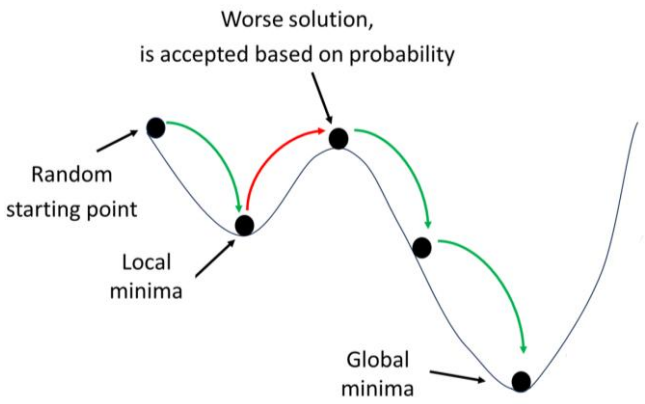

Figure 4.7 Schematic representation of SA algorithm procedure [150].

1. **Initialization:** The algorithm parameters and initial possible solution is determined in this stage. Three parameters needed to be set: (1) initial temperature (T_0), (2) the final temperature (T_f), (3) cooling factor (α), and (3) maximum number of iterations ($Iter_{max}$). According to [202], the T_0 and the α are very importance parameters in SA. Because the initial temperature determines whether non-good solutions are acceptable or not. If it is too low, weak solutions are rarely accepted. In contrast, if it is too high, all changes, good or bad, are accepted. Thus, a suitable initial temperature is needed. While the cooling factor responsible for lowering the temperature value during simulating. The value of the cooling factor usually ranges from 0.7-0.99. In addition, the initial possible solution is generated in this phase. It creates at random using Equation (4.1). Moreover, the solution quality is determined.

2. **New Solution:** A new possible solution is chosen at random from the currently chosen solution neighbourhood. Its fitness is calculated. If the new solution fitness was better than current (initial) one, the new solution accepted, i.e., replace the current one. Otherwise, the new solution is accepted if the probability ($P > r$) is true. P is calculated as follows:

$$P = \exp(-\Delta f / T_k) \tag{4.13}$$

where, P is the probability density function, r is a random number between 0-1, Δf is the fitness difference between the current and new solutions. T_k is the temperature at the current iteration.

3. **Termination:** The number of iterations increases by one, while the temperature value decreases using Equation (4.14). If a stopping criterion is met, such as reaching the

maximum number of iterations or the minimum number of temperatures, the algorithm stops its search for the best solution and considers the current solution the best. Otherwise, SA steps 2-3 are repeated until the stopping criterion is met.

$$T_{k+1} = T_k * \alpha \tag{4.14}$$

where T_{k+1} is the new temperature, T_k is the current temperature, and α is the cooling factor.

4.2 Comparison of Optimization Algorithms for GNSS satellite selection

The five optimization algorithms (ABC, ACO, GA, PSO, and SA) are uniquely designed, leading them work differently using different types of parameters. This makes each of them more suitable for different types of problems. In addition, their parameter values are affecting their result quality [203,204]. Hence, the value of algorithm parameters should be carefully adjusted to fit the problem. This can explain why the performance of the five optimization algorithms compared to each other changed from study to another (i.e., from one problem to another), as shown in Table 4.1.

Table 4.1 Comparison between optimization algorithms in different problems/studies

Algorithms	Problem	Best	Reference
ABC vs. GA	Benchmark functions	ABC	[205]
	Optimizing Heterogeneous wireless networks (HWNs)	GA	[206]
ABC vs. PSO	Benchmark functions	ABC	[207]
	Maximum power point tracking (MPPT) system	PSO	[208]
GA vs. PSO	Optimizing Heterogeneous wireless networks (HWNs)	GA	[206]
	Timetabling problem	PSO	[209]
PSO vs. SA	Satellite selection	PSO	[99]
	Multi-Objective Land Allocation (MOLA)	SA	[210]

Therefore, the performance of the five optimization algorithms should be considered from satellite selection problems. The five optimization algorithms (ABC, ACO, GA, PSO, and SA) were used to choose the optimal satellites in various studies. However, most of these studies have applied only one of these algorithms. Only three studies [92,99,106] were found that compared optimization algorithms.

Apart of ACO, Mosavi and Shiroie [106] chose the optimal subset of GPS satellites based on GDOP using the remaining four optimization algorithms. According to the selection results, the four algorithms were comparable in terms of selection speed and accuracy (i.e., matching the actual optimal satellites). According to their results, ABC was the most

superior as it was the most accurate and second fastest algorithm. The fastest algorithm was SA, but it was also the least accurate.

Xia et al. [106] chose the optimal subset of BeiDou satellites based on GDOP using ACO and modified ABC. To improve the performance of ABC, they combined ABC with another optimization algorithm (Tabu algorithm). This combination was called Tabu Search Artificial Bee Colony (TSABC). Comparing to the actual optimal satellites derived from TM (Exhaust Search), the TSABC outperformed ACO.

Du et al. [92] chose the optimal satellite subsets from multi-GNSS (GPS and BeiDou) using the minimum GDOP value (MGV), i.e., selecting satellites based on GDOP using TM. In addition, they chose the optimal satellites based on WGDOP using GA, ACO, and modified ACO, and Artificial neural network (ANN). To improve ACO, they combined it with polarized feedback (ACO-PF). **Error! Reference source not found.** shows the selection results of the a lgorithms. According to their results, ACO chose better satellites than GA, as their average WGDOP and RMS was better. However, GA was faster than ACO in satellite selection.

Accordingly, the suitable optimization algorithm for selecting satellites cannot be verified. This is because there are not adequate comparisons between them in satellite selection problem. Only three studies compared the performance of optimization algorithms in satellite selection. One of these studies compered four optimization algorithms (ABC, GA, PSO, and SA). The remaining studies compared two optimization algorithms. In addition, one of them was enhanced, leading to an unfair comparison.

4.3 Summary

This chapter presented the concept, pros, cons, applications, and implementation steps of five optimization algorithms (ABC, ACO, GA, PSO, and SA). All of them are considered robust and flexible as they were adapted to different types of problems. However, these algorithms were uniquely designed and work differently. Thus, they could be more suitable for one problem than another. In satellite selection problem, they have not been adequately compared. To find the most suitable optimization algorithm for satellite selection, the five algorithms should be tested in satellite satellites.

Chapter 5 Methodology to find the criterion and technique for PPP-selection

This chapter discuss the methodology that carried out to develop a satellite selection method for PPP, various steps were carried out. Mainly, they can be classified into three stages: 1) Define the suitable optimization algorithm, 2) Define the criteria and process for satellite selection, and 3) Experimental evaluation of Satellite Selection Method. This can be seen in Figure 5.1.

Each satellite selection method consists of two components: criterion and technique. The criterion is the factor based on which satellites are selected, while the technique is an approach for selecting satellites based on the criterion. Thus, technique performance is importance for criterion efficiency that indicate the efficiency of satellite selection method. Therefore, in the first stage of the project methodology, the performance of five optimization algorithms (techniques) was evaluated to find their best in satellite selection. In the second stage of the project methodology, the most suitable criterion for satellite selection was define. It can be a combination of criteria such as WGDOP including satellite signal strength and geometry. Hence, the appropriate criterion(s) and combination process were determined by testing different criteria and combination methods for satellite selection. Lastly, the results of the previous two phases were used to form the satellite selection method that were evaluated in several case studies in the third stage of the project methodology.

Analysing satellite data becomes more complex as it gets noisier due to GNSS error sources including receiver noise. To facilitate the development of satellite selection method, GNSS data were collected from geodetic GNSS receivers and antennas. This is because they provide results with lower noise levels than low-cost receivers and antennas [211]. GNSS data was collected from Leica GR10 and GS10 receivers and AR25.R4 and AS10 antennas. The antennas and receivers were designed to track and record precise satellite signals of multiple systems. However, the Leica receiver (GR10) and antenna (AR25.R4) are heavy and suitable for permanent jobs such as stations. Whereas the Leica receiver (GS10) and antenna (AS10) are lightweight, and easy to carry, making it suitable for field works. More information about these Leica receivers and antenna are shown in the tables below.

Table 5.1 Features of Leica GR10 and GS10 receivers

Receiver	Sat System	Frequency	Channel	Recording rate	Reference
Leica GR10	GPS	L1, L2, L5	120	Up to 1 Hz	[212]
	GLONASS	L1, L2			
	Galileo	E1, E2a, E2ab			
Leica GS10	GPS	L1, L2, L5	120	Up to 20 Hz	[213]
	GLONASS	L1, L2			
	Galileo	E1, E2a, E2ab			
	BeiDou	B1, B2			

Table 5.2 Features of Leica AR25.R4 and AS10 antennas

Antenna	Sat System	Frequency	Amplifier Gain	Noise figure	Design	Reference
Leica AR25.R4	GPS	L1, L2, L5	40 dB	< 1.2 dB	3D choke ring	[214]
	GLONASS	L1, L2, L3, L5				
	Galileo	E1, E5a, E5b, E5ab, E6				
	BeiDou	B1, B2, B3				
	QZSS	L1, L2, L5, L5				
	IRNSS	L5				
Leica AS10	GPS	L1, L2, L5	29 ±3 dB	Not specified	Compact	[213]
	GLONASS	Not specified				
	Galileo	Not specified				
	BeiDou	Not specified				

RTKLIB (demo5 b34d) was used for processing GNSS data. RTKLIB is an open-source software developed by Takasu and Yasuda (2006) for GNSS. It is a full package of GNSS software, including GNSS data conversion (RTKCONV), plotting (RTKPLOT), and processing (RTKPOST). RTKLIB can process GNSS data in multiple modes such as SPP, DGNSS, and PPP. Enormous number of studies have used RTKLIB proving its efficiency. In addition, RTKLIB is highly flexible and transparent as its code, processing configurations, and debug trace files are accessible. Thus, it is suitable for this project, as the performance of the selected satellites can be tracked and evaluated. Various versions of RTKLIB have been released since 2006. RTKLIB version demo5 b34d was used as it was the latest when this project started.

High Performance Computing (HPC) of the University of Nottingham was used for selecting satellites. HPC indicates combination of computing resources to achieve higher computing performance that is difficult or impossible to achieve using standard computers and

laptops. It is available to any research student and academic faculty member from any school or college. Users can use up to 600 CPU cores and 3000GB RAM simultaneously for up to 7 days. In addition, 1TB of storage is provided.

Figure 5.1 Flowchart of the project methodology

5.1 Define the suitable optimization algorithm

To find the most suitable and reliable optimization algorithm for satellite selection, the performance of five optimization algorithms (ABC, ACO, GA, PSO, and SA) was tested in satellite selection. Their algorithms were modified to fit to the satellite selection problem, while their common parameter values were adjusted and defined uniformly. They were

applied in several scenarios of satellite selection for various number of satellites and conditions. In all the cases, the cost-function of the five optimization algorithms was the CNR-WGDOP parameter, of which the minimum value would indicate the corresponding optimal GNSS satellite subset. The evaluation of the optimization algorithms was based on comparing the CNR-WGDOP value of their optimal satellite subset with that of the actual optimal satellite subset derived from the TM. The optimization algorithm with the best results in terms of satellite selection accuracy and speed was considered the appropriate algorithm for satellite selection, which then was applied for the development of the methodology of satellite selection (stage 2) and the various case studies applications (stage 3).

5.1.1 Adjust optimization algorithms

GNSS satellite selection is a discrete problem [127], while the five optimization algorithms are not explicitly designed for this type of problem. The five optimization algorithms follow an iterative search processing to find the optimal satellite subset. At the end of each iteration, new solution(s) are generated. ABC and PSO algorithms generate solution(s) with a fractional value as they were designed for the continuous problem. However, only an integer number is accepted in the satellite selection problem. This issue can be overcome by changing the algorithm design for a discrete problem [127,215,216], or simply rounding solution values [215,217]. To reduce complexity, the generated solutions from ABC and PSO were rounded to the nearest integer in each iteration.

In addition, the four optimization algorithms (apart from ACO) can provide results with duplicate values. In the case of the GNSS satellite problem, this would mean that the same satellite could be chosen twice in the solution of the optimized satellite constellation. To address this problem with less interference in the algorithm design, the algorithm solution was checked at the end of each iteration. If the solution contained a duplicated value, it was rejected, and a new solution was generated without consuming the number of searching iteration.

In this study, the optimal satellite subsets were chosen based on the criterion of minimising the CNR-WGDOP which indicates the best potential GNSS satellite combination for the given available GNSS satellites. That can be done without adjustment by all algorithms except for ACO. ACO originally was designed to simulate the foraging behaviour of ants, where ants search for the shortest path for the food source. Due to that ACO finds the optimal solution based on two criteria: (i) solution quality and (ii) the distance between solution members [153]. The weight of the two criteria (solution quality and distance between solution members) on finding the optimal solution can be determined through the values of alpha (α) and beta (β) parameters, respectively. In this problem, the quality of the

CNR-WGDOP and the distance between the satellites in a constellation represent the solution quality and the distance between solution members. To select the optimal satellites based on CNR-WGDOP only, the β value was set to zero [153].

5.1.2 Define the values of Optimization Algorithm parameters

The values of the algorithm parameters are critical as they directly affect the algorithm output and performance [203,204]. Choosing the appropriate value for algorithm parameters can be difficult due to their wide range [149,203], whereas homogeneity between these values should be considered [149]. In this study, parameter values were chosen based on their standards and previous studies (Table 5.3). However, this does not guarantee that the value of these parameters is the best for this problem.

To have an objective comparison of the performance of the five optimization algorithms, the algorithms' common parameters were standardized. In Table 5.3, the parameters of the five optimization algorithms are presented, and it is observed that the only common parameters were the searching iteration and population size. The values of both parameters were set to 100, which is considered a reasonable value and consistent with previous studies (Table 5.3). However, the SA algorithm was originally designed to have a single population size. To make up for this restriction of the population size in SA algorithm, the number of corresponding iterations was increased with respect to the other four optimization algorithms and defined to 1000 [218]. The number of iterations for the SA algorithm derived based on tests assessing the performance of the SA algorithm to reach the optimal solution while also retaining the SA iterations to a similar level of the performance of the other four optimization algorithms as defined by the number of iterations and population size.

Table 5.3 The parameter values of the five optimization algorithms [150].

Algorithm	Notation	Meaning	Value	References
ABC	D	The problem dimensions, indicating the satellite constellation size		
	maxIter	The maximum number of iterations	100	[106,107,127,219]
	pSize	The population size	100	[92,127,149,220]
	limit	The abandonment limit	D × pSize	[151]
ACO	maxIter	The maximum number of iterations	100	[92,149,153]
	pSize	The population size	100	
	ρ	The evaporation rate	0.5	
	α	The relative importance of the trail	1	
	β	The relative importance of the visibility	0	
	Q	The quantity of trails laid by ants	100	
GA	maxIter	The maximum number of iterations	100	[107,149]
	pSize	The population size	100	
	Pc	The probability of crossover	0.8	
	Pm	The probability of mutation	0.12	
PSO	maxIter	The maximum number of iterations	100	[136,149,219]
	pSize	The population size	100	
	Wmax	The initial weights	0.9	
	Wmin	The final weights	0.4	
	C1	The personal acceleration coefficient	2	
	C2	The social acceleration coefficient	2	
SA	maxIter	The maximum number of iterations	1000	[149,218]
	pSize	The population size	1	
	T0	The initial temperature	2000	
	Tf	The final temperature	0.01	
	α	The cooling factor	0.975	

5.1.3 GNSS Data

The 24-hour GNSS data was obtained from the BIGF (British Isles continuous GNSS Facility) station located on the roof of the Nottingham Geospatial Institute building (Figure 5.2), The GNSS station is equipped with a choke-ring antenna Leica AR25.R4 antenna with strong multipath rejection installed on the pillar of control point (NGB2) and a Leica GR10 receiver with the capacity of recording multi-GNSS signals (GPS, Galileo, GLONASS). On 20 September 2021, GNSS data were collected with a 30-sec sampling rate and zero-degree elevation mask. A total of 18-31 satellites were recorded including 7-13 GPS, 4-10 GLONASS, and 5-10 Galileo satellites (Figure 5.3).

Figure 5.2 (left) View at the roof of NGI building, with the location of control point NGB2 and (right) the GNSS antenna installed on the top of the pillar of NGB2 [150] .

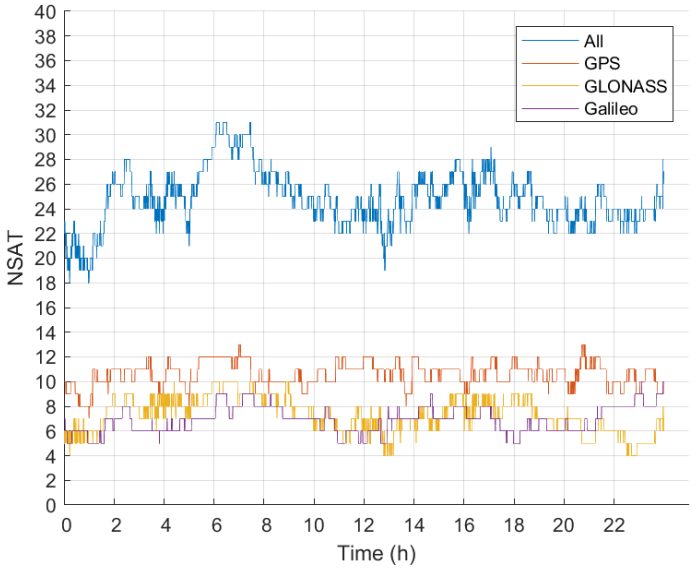

Figure 5.3 Number of available GNSS satellites at NGB2 GNSS station for the 24-hour period on 20 September 2021 [150].

5.1.4 Satellite Selection Implementation

To evaluate the five optimization algorithms, they should be applied for a long period of GNSS observation, where (i) the GNSS satellites systems (i.e. GPS, GLONASS, Galileo, etc.), (ii) the number of the corresponding GNSS satellites, and (iii) the position of the GNSS satellites (azimuth, elevation) varies with time. Therefore, a 24-hour period of GNSS observations were used. The optimization algorithms were applied to select the optimal GNSS satellites subset for specific time intervals where the change of the GNSS satellites position (azimuth and elevation) is adequate to affect the satellite constellation geometry.

For the given location of the GNSS station (i.e. Nottingham Geospatial Institute, Nottingham) and available GNSS satellites (i.e. GPS, Galileo, GLONASS), the required time for each GNSS satellite to move on its orbit by one degree was analysed. Figure 5.4 displays the required time of each available GNSS satellite to move by one degree, where the maximum required time reaches up to 3 minutes. In previous studies [107,117], 10 minutes satellite selection interval was used. However, in the current study, the satellite selection interval was set to 5 minutes to reduce the computation load of satellite selection while maintaining a large number of epochs for the satellite selection. Hence, the optimal satellite subsets were selected for 288 epochs, corresponding to 1 epoch per 5-minute interval, for the 24-hour GNSS dataset.

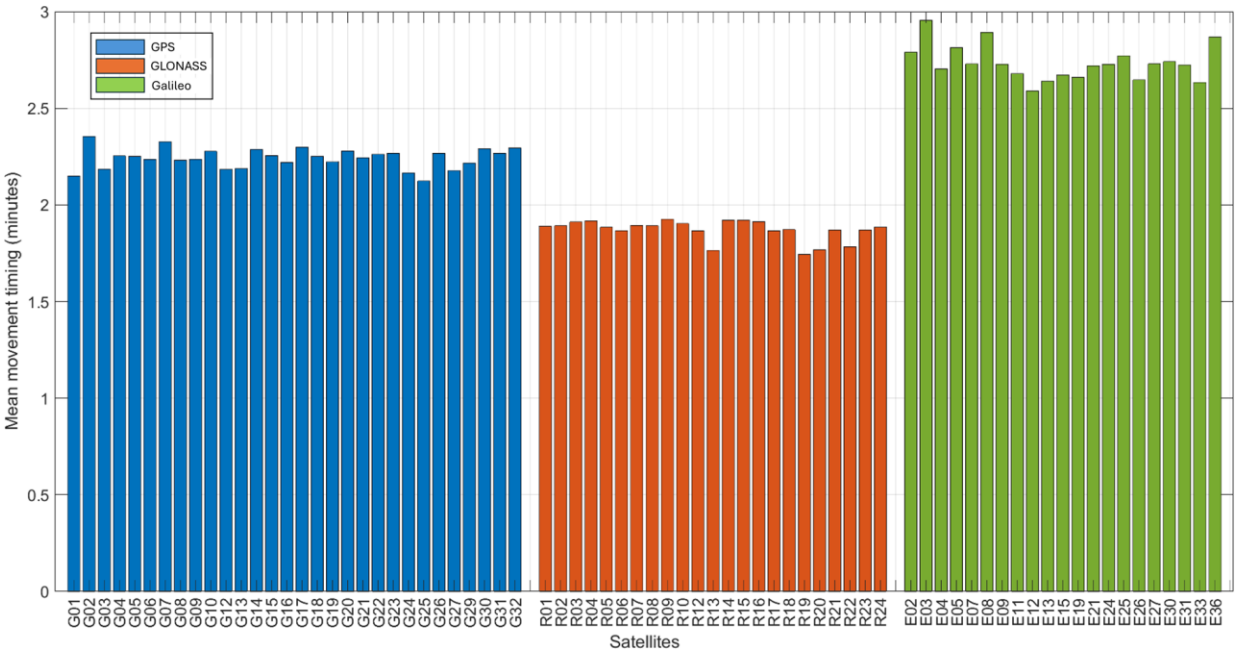

Figure 5.4 Time-period of satellites mean movement by one degree, considering satellite azimuth and elevation angles.

To choose the satellites based on the CNR-WGDOP, using the Equation (3.10), it is necessary to extract (i) satellite pseudorandom noise (PRN), (ii) satellite observation time, (iii) elevation angles, (iv) azimuth angles, and (v) the CNR values. The raw satellite data (range observations and navigation data) were introduced in RTKLIB (demo5 b34d) software to define the elevation and azimuth of each satellite, extract the required remaining information (satellite PRN, observation time and CNR) and save the information in a file, as shown in Figure 5.5. Using MATLAB (R2022b) software in HPC the optimal satellite subset was selection by the five optimization algorithms. The satellite selection was carried out every five minutes. They were selected sequentially using the standard serial for loop.

% TIME (GPST)	SAT	AZ(deg)	EL(deg)	CNR(dBHz)
2021/09/20 06:30:00.0	G01	242.1	4.2	34.95
2021/09/20 06:35:00.0	G01	243.2	6.1	37.10
2021/09/20 06:40:00.0	G01	244.3	8.0	39.25
2021/09/20 06:45:00.0	G01	245.4	10.0	38.35
2021/09/20 06:50:00.0	G01	246.5	11.9	39.45
2021/09/20 06:55:00.0	G01	247.7	13.9	40.50
2021/09/20 07:00:00.0	G01	248.9	15.8	42.45
2021/09/20 07:05:00.0	G01	250.1	17.8	41.10
2021/09/20 07:10:00.0	G01	251.3	19.8	41.75
2021/09/20 07:15:00.0	G01	252.5	21.8	44.65
2021/09/20 07:20:00.0	G01	253.8	23.9	41.15
2021/09/20 07:25:00.0	G01	255.1	25.9	44.95
2021/09/20 07:30:00.0	G01	256.4	28.0	41.05

Figure 5.5 Sample of the file of the GPS data information, which includes (i) date-time, (ii) satellite PRN, (iii) azimuth, (iv) elevation angle and (v) CNR (in dB-Hz) [150].

However, the GNSS satellite selection becomes more challenging as the number of possible satellite combinations increases, which occurs when there is a large number of available GNSS satellites in relation to the number of satellites in the subset. This can be described more clearly with Equation (5.1):

$$c_r^n = \frac{n!}{r!\,(n-r)!} \tag{5.1}$$

where c is the number of possible GNSS satellite combinations, expressed as factorial function of n, the number of available GNSS satellites, and r, the number of GNSS satellites in the subset (subset size).

Hence, by increasing the number of available satellites, the number of possible satellite combinations increase dramatically, making the evaluation of the five optimization algorithms more complex. In this study, satellite data were collected from multiple satellite systems (GPS, GLONASS, and Galileo). The number of available satellites exceed 20 (Figure 5.3), resulting in a large number of possible satellite combinations, making satellite selection more difficult. In Figure 5.6, the number of all possible combinations for GPS constellation and multi-GNSS constellation are depicted. The graphs illustrate the potential combinations for a number of given trackable satellites. It is evident that the possible satellite constellation combination increases significantly with the number of available satellites. With 8 GPS satellites available, the maximum number of 4-satellite combinations is 70, whereas in the case of 13 available GPS satellites, the maximum number of combinations is 1716 and occurs for GPS subsets of 6 and 7 satellites. For the case of the multi-GNSS constellation, where the available number of satellites increases, the number of possible combinations increases dramatically. Representative of this is the case of 31

available GNSS satellites, for which the maximum number of possible combinations is 300,540,195 and occurs for multi-GNSS satellite subsets of 15 and 16 satellites.

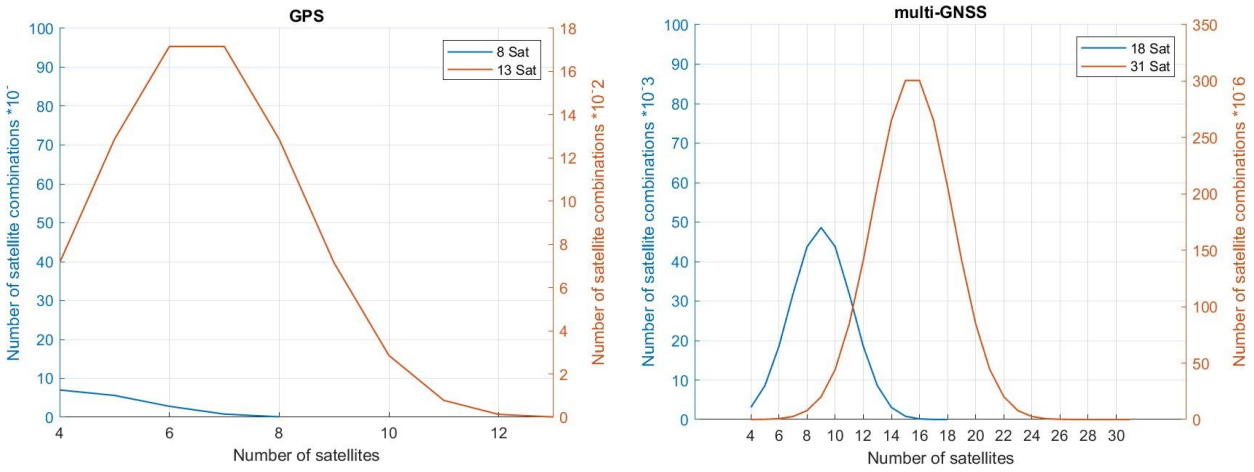

Figure 5.6 The possible combinations of satellite constellations for (left) GPS-only for the cases of 8 and 13 available GPS satellites, and (right) multi-GNSS satellites constellation, for the case of 18 and 31 available GNSS satellites [150].

Therefore, the optimization of the GNSS satellite subset was performed in two stages: (i) for GPS-only satellite constellation and (ii) for multi-GNSS satellite constellation (GPS, GLONASS and Galileo). Based on these two case studies, it is evaluated how the performance of the optimization algorithms is affected by the number of GNSS satellites. In the first stage, the performance of the five optimization algorithms was evaluated by optimizing GPS subsets in different sizes to change selection conditions. Based on the first stage of evaluation, the optimization algorithm with best performance, in terms of satellite selection accuracy and computation time requirement, was chosen. In the second stage, only the best-performed optimization algorithm was applied and evaluated to optimize different sizes of multi-GNSS satellite subsets under more challenging conditions as the number of available GNSS satellites is significantly high, resulting in a large number of possible satellite constellations. In addition, at the second stage, a parametric analysis of the best-performed optimization algorithm was conducted to evaluate the impact of the various settings, such as the number of iterations and the population size, on the performance of the optimization algorithm.

Accordingly, the performance of the five optimization algorithms in optimizing GPS satellite subsets of 4, 5, 6, and 7 satellites was examined. The most suitable optimization algorithm was chosen based on its overall performance. It was then tested for optimizing multi-GNSS satellite subsets of 4, 8, 12, and 15 satellites using various algorithm parameter values. In

all above tests, the algorithms quality in satellite selection was evaluated by comparing their selection with the actual optimal satellite subsets, which are identified by TM.

The TM checks the WGDOP value of all possible GNSS satellite subsets to define the optimal GNSS satellite subset with the lowest WGDOP value. Thus, it provides the actual optimal satellite subsets. However, finding the optimal satellite subset of 15 satellites when 31 satellites available requires checking 300,540,195 by TM. In MATLAB, a variable with one cell costs 8 bytes. Therefore, more than 40 GB of computer's RAM is required to generate only 300,540,195 of satellite subsets. As a result, High Performance Computing (HPC) Nottingham University was used to determine the optimal satellite subsets by TM and optimization algorithms.

5.1.5 Evaluation of the optimisation algorithms

The performance of optimization algorithms was evaluated based on two criteria: i) selection accuracy and ii) selection speed. Satellite selection of optimization algorithms was compared with the actual optimal satellite subsets, derived from TM. The WGDOP value of all possible satellite combinations (i.e., all possible solutions) was determined, and then the best satellite combination with least WGDOP value was define as the optimal combination. The optimization algorithm considers to be accurate when the WGDOP value of its selected optimal satellite subset exactly matches the WGDOP value of the TM optimal satellite subset, and consequently, the accuracy expresses how closely. On the other hand, the selection speed of optimization algorithm is processing time required for finishing the entire selection (288 selections). It was determined by MATLAB, which was used to perform satellite selection by TM and optimization algorithms.

5.2 Define the criteria and process of satellite selection subset

In section 3.6, WGDOP-RAIM was primarily chosen as the appropriate criteria for satellite selection. To improve the quality of satellite selection further, the performance of WGDOP-RAIM in satellite selection was evaluated along with satellite selection angle (Ele) and iv) Kalman Filter innovation threshold (KFITH). They were implemented for satellite selection in different combinations and order. In addition, the optimal satellites were selected in all possible subset sizes by WGDOP-RAIM in all combinations. The evaluation of WGDOP-RAIM selection combinations was based on (i) the positioning quality of the selected satellites, (ii) positioning availability, (iii) the number of actual selected satellites used in positioning solution, and (iv) the continuity of selected satellite subset. The selection combination with the best results in above evaluation criteria considered the appropriate one for satellite selection.

5.2.1 Define Possible Selection Factors with WGDOP-RAIM

There are many factors that affect positioning accuracy. Considering as many as possible of these factors can improve the quality of selecting satellites. WGDOP considers the satellite geometry and signal quality, which are the most important positioning factors. Whereas RAIM considers satellite geometry, signal quality, and positioning correction. As a result, WGDOP-RAIM could be the most appropriate criterion for satellite selection.

However, Satellite geometry (GDOP) improves with the use of low elevation satellites, so the GDOP/WGDOP-based satellite selection method tends to choose low elevation satellites. Satellite at low elevation angels (0°-15°) are more vulnerable to atmospheric and multipath errors. Thus, using cut-off elevation angle (CEA) may improve the selection quality of WGDOP-RAIM. Furthermore, using CEA will reduce the number of satellites observed. Consequently, the number of possible satellites combination will reduce, leading to decrease the difficulty of satellite selection.

On the other hand, RAIM was essentially design for Single Point Positioning (SPP) that has low positioning quality (meter level), where pseudo-range measurements are used to determine a positioning solution for each epoch separately (epoch-by-epoch) by least squares (LS). In contrast, PPP provides precise positioning (centimetre level), where both pseudo-range and carrier phase measurements are used to a sequential positioning using data processing approach such as Kalman Filter (KF). As a result, RAIM is not designed for PPP data process [221,222]. Several studies [123,223–225] have proposed a new RAIM algorithm that fit the KF's serial positioning residuals (KF innovation). Since satellite selection is for PPP, KF-RAIM should be used with WGDOP to improve selection quality.

However, RTKLIB (version demo5 b34d), used software, has the traditional RAIM and normal KF innovation thresholds [118,119]. In RTKLIB, the KF innovation threshold is set manually, and any residue exceeding it is rejected [118,119]. To perform a comprehensive evaluation of WGDOP-RAIM based on RTKLIB's traditional RAIM and standard KF innovation threshold, satellites were selected based on WGDOP-RAIM with or without the KF innovation threshold.

5.2.2 Define the suitable selection order for WGDOP-RAIM

In previous studies [14,121,124], satellites were chosen based on GDOP and RAIM. This selection was made sequentially. They chose satellites based on GDOP and then used RAIM to ensure the integrity of the selected satellites. In these two studies [121,124], satellites were selected again based on GDOP. Thus, their selection was GDOP-RAIM-GDOP. This selection order can be used with WGDOP to be as follows: WGDOP-RAIM-WGDOP. However, this selection order has a major limitation especially for PPP satellite selection.

Compared to SPP, PPP required various number of corrections such as satellite precise orbit and clock, as well as satellite and receiver phase antenna. WGDOP-based satellite selection ignores PPP correction because it only considers satellite geometry and signal power. On the other hand, RAIM considers positioning corrections when selecting satellites. As a result, selecting satellites based on WGDOP first may result in choosing inappropriate satellites for PPP. There is no guarantee that using RAIM later will improve this selection, especially if it the number of selected satellites was small, as satellites have already been filtered by WGDOP selection. Furthermore, satellites were selected based on WGDOP to meet a required level of geometry; removing some of these satellites using RAIM may impact their geometry.

In contrast, using RAIM first will check the integrity of satellite measurements, considering positioning corrections. This will improve WGDOP selection later because the integrity of the selected satellites by WGDOP for the positioning has been proved. Furthermore, few number of WGDOP selected satellites will be rejected by RAIM when it used again. Thus, RAIM-WGDOP-RAIM is better selection order. To verify the accuracy of the above hypotheses, the optimal satellites were selected by ten satellite selection cases, as shown in the Table 5.4.

Table 5.4 Ten satellite selection cases

Case	Selection technique
1	**WGDOP**
2	Ele + **WGDOP**
3	**WGDOP** + RAIM
4	**WGDOP** + RAIM +KFITH
5	RAIM + **WGDOP**
6	RAIM + KFITH + **WGDOP**
7	Ele + RAIM + **WGDOP**
8	Ele + RAIM + KFITH + **WGDOP**
9	Ele + RAIM + **WGDOP** + RAIM + KFITH
10	Ele + RAIM + KFITH + **WGDOP** + RAIM + KFITH

5.2.3 GNSS Data

To evaluate satellite selection of ten cases, satellites should be selected by them multiple times. In other words, satellites should be selected for a long period of GNSS data. Satellite signals are affected by various types of error sources, which reduce positioning accuracy, such as ionosphere, troposphere, and multipath. Compared to others, multipath effects cannot be mitigated by models. To reduce its effects, affected satellite signals should be minimized by avoiding multipath environments and using special antennas (e.g., choke ring

antenna). As a result, four days (20 September, 22 September, 27 September, and 01 October 2021) of satellite data were collected using choke ring antenna from open-sky environment.

GNSS data was obtained from the same BIGF station (NGB2) located on the roof of the NGI building (Figure 5.2). Figure 5.7 shows the number of GNSS satellites observed with a 30-sec sampling rate and zero-degree elevation mask.

To determine the true coordinates of NGB2, 15 days of relative positioning was implemented. GNSS data was obtained from NGB2 and the closest five BIGF stations (Keyworth, Lichfield, Lincoln, Church Lawford, Peterborough). They are 0.12 to 64.21 km away from NGB2, as shown in Table 5.5. Their 15 days of GNSS data was obtained from 20 September to 04 October 2021.

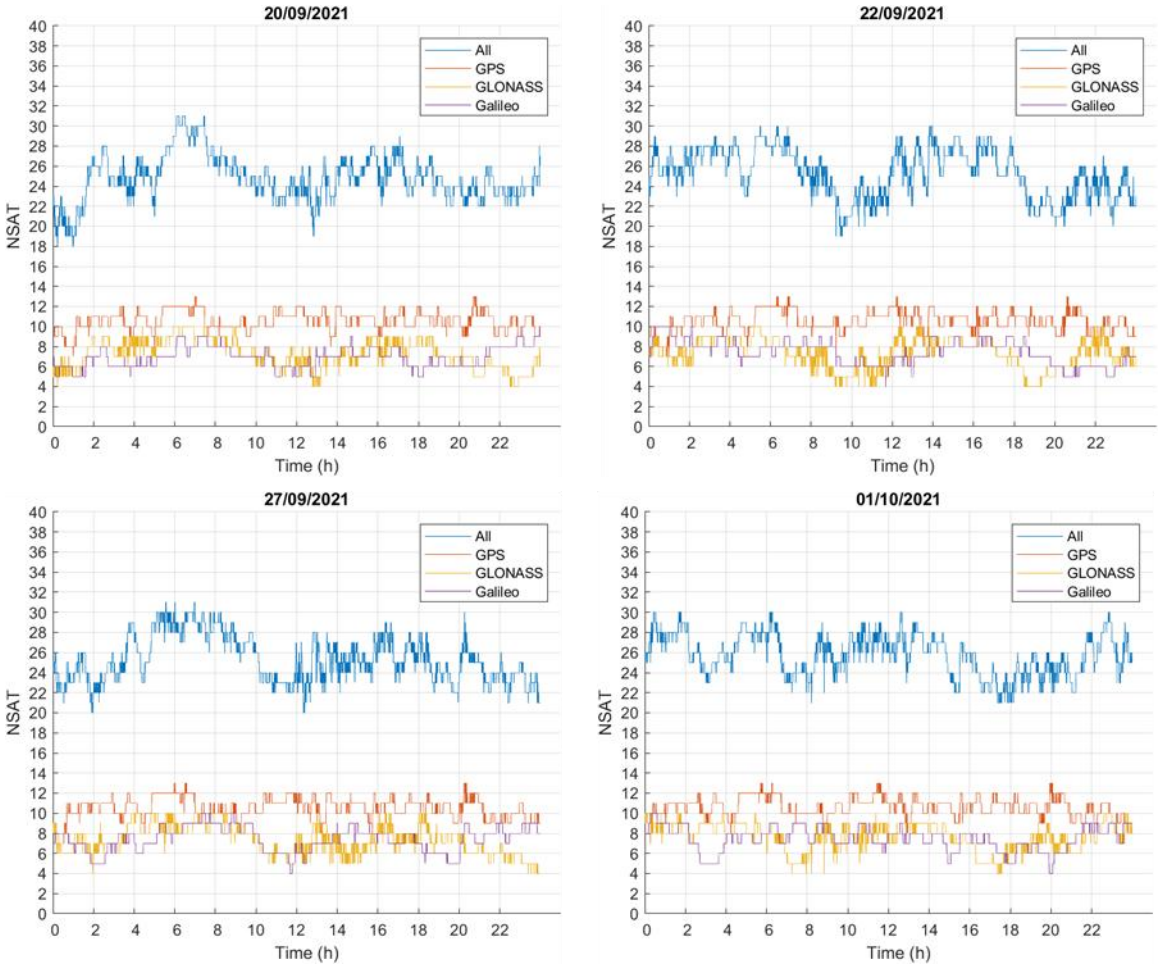

Figure 5.7 Number of GNSS satellites tracked at NGB2 GNSS station for a 24 h period on the four days: 20 September, 22 September, 27 September, and 1 October 2021.

Table 5.5 Information of the closest five BIGF stations to NGB2

#	Station name		Receiver	Antenna	Distance	
1	Keyworth	(KEYW)	SEPT POLARX5	LEIAR25	0.12	km
2	Lichfield	(LICF)	TRIMBLE ALLOY	LEIAR25	52.98	km
3	Lincoln	(LINO)	TRIMBLE ALLOY	LEIAR25	55.73	km
4	Church Lawford	(CLAW)	SEPT POLARX5	LEIAR25	60.40	km
5	Peterborough	(PETE)	SEPT POLARX5	LEIAR10	64.21	km

5.2.4 Satellite Selection Implementation

As mentioned earlier, in addition to WGDOP and RAIM, Ele and KFITH were considered in satellite selection. To evaluate the impact of RAIM, Ele, and KFITH on WGDOP selection, ten satellite selection cases were considered (Table 5.4). To improve satellite selection quality, the satellite selection of Ele, RAIM, and KFITH should be before WGDOP. In addition, the Ele selection should be before RAIM and KFITH. Whereas the satellite selection of RAIM and KFITH is done simultaneously using RTKLIB. Figure 5.8 shows the satellite selection order using the four selection factors.

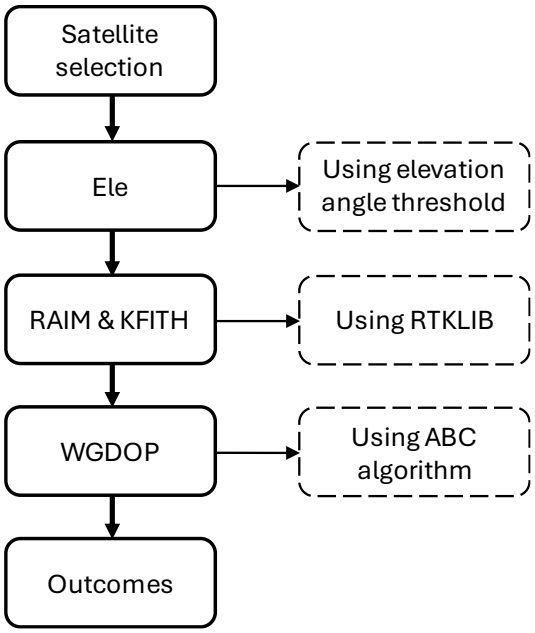

Figure 5.8 Satellite selection order using the Ele, RAIM, KFITH, and WGDOP.

5.2.4.1 Satellite Selection Based on Ele

Satellite selection based on elevation angles (Ele) is commonly used to remove satellite signals at low elevation angles that ranges from 0 -15 degrees, as they are more vulnerable to atmospheric and multipath errors. Ele satellite selection can be implemented with 5, 10, and 15 degrees. However, to investigate the impact of satellite selection by Ele with the least

number of trials/steps, the maximum threshold (15 degrees) was used only. This is suitable because it can show the maximum effect of satellite selection by Ele on WGDOP selection.

Ele satellite selection was carried out five times: once with WGDOP only (case 2), and the remine with RAIM/ RAIM-KFITH (cases 7–10), as shown in Table 5.4. In case 2, Ele selection was performed using MATLAB (R2022b) software before WGDOP selection using the ABC algorithm in MATLAB. When satellite characteristics file (Figure 5.5) was uploaded to MATLAB, any satellites with elevation angles less than 15 degrees were rejected. In other cases, Ele selection was done using RTKLIB's cut-off elevation angle (CEA), as RTKLIB will be used for RAIM/ RAIM and KFITH selection, which require satellite observation and navigation files.

5.2.4.2 Satellite Selection Based on RAIM and KFITH

RAIM and KFITH exclude satellites based on residual, which are the differences between the obtained/expected and computed measurements. Thus, the satellite selection of RAIM and KFITH require an initial positioning. RTKLIB (demo5 b34d) was utilized to performed RAIM and KFITH satellite selection. RTKLIB is equipped with the traditional RAIM, which deals with pseudo-range (code) measurements. Hence, RAIM's residuals is the differences between obtained and computed pseudo-range measurements. RTKLIB's RAIM uses chi-square test. If it is failed, RAIM remove the satellites to improve positioning accuracy. The chi-square test is shown in Equation (3.16).

Furthermore, RTKLIB has a threshold that exclude satellites based on Kalman filter innovate, which is the difference between the expected and computed measurements. These measurements are for both code and phase measurements. Kalman filter innovate threshold (KFITH) is a simple and straightforward threshold, where satellite measurements exclude if its residual (code/phase) exceeded the user pre-determined threshold. The code and phase thresholds are different but still connected in RTKLIB (demo5 b34d). The phase threshold is determined in meter by the used, and it multiplied by the code/phase error ratio to generate the code threshold [118]. Based on previous studies [13,226] and the default value [118,119], the phase threshold was set to 30 meters. The code/phase error ratio is a parameter defining how much accurate phase measurements than code. The code/phase error ratio was 300 using the default value [118].

As mentioned early, RAIM and KFITH satellite selection consider positioning correction as they chose satellite based on residuals, which are the different between the obtained/expected and computed measurements. Thus, an initial positioning is required for RAIM and KFITH selection. To consider the required PPP corrections and applied RAIM and KFITH selection, RTKLIB was implemented with following configurations:

Table 5.6 PPP configurations

Settings	Options
Position mode	PPP static
Satellite system	GPS, GLONASS, and Galileo
Frequency	L1/G1/E1, L2/G2/E5b, and L5/E5a
Filter type	Combined
Ocean tides loading	GOT4.7
Ionosphere correction	Ionosphere-free
Troposphere correction	Estimate ZTD (zenith total delay)
Satellite Ephemeris/Clock	Precise (final)
Satellite antenna PCV (phase centre variation)	igs14.atx
Receiver antenna PCV	igs14.atx
Phase windup correction (PhWindup)	ON
Reject eclipse	ON
Differential code bias (DCB) correction	ON
Integer Ambiguity Resolution	Continuous
RAIM	ON
KFITH of phase	30 meters
Code/phase error ratio	300

5.2.4.3 WGDOP Selection

WGDOP is a parameter that indicates satellite geometry while considering the quality of satellite measurements, either through pseudo-range error (UERE) or signal power (SNR/CNR). Compared to UERE, SNR and CNR are much easier to obtain as they are computed by the receiver. As a result, WGDOP based on CNR was used for satellite selection. WGDOP satellite selection can be classify into two main stages: (1) WGDOP determination and (2) WGDOP selection.

- **WGDOP Determination**

As discussed in Section 3.4, WGDOP can be computed either through the traditional method (TM) or closed-form formula. Although it can be calculated faster using the closed form formula, the traditional method was used for clarity and simplicity. In the TM, the geometry matrix (*H*) and the weighted matrix (*W*) are required to calculate the WGDOP using the inverse matrix, as shown in Equation (3.10). The *H* can be computed without and with the time difference between satellite systems using Equations (3.7) and (3.8), respectively. In multi-GNSS, it is crucial to consider the time difference between satellite systems to improve positioning accuracy [24]. Hence, considering this time difference is important when selecting multi-GNSS satellites to improve the quality of the selected satellites and

then positioning accuracy [14]. Therefore, the geometry matrix (*H*) was computed with the time difference consideration using Equation (3.8). On the other hand, the *W* matrix contains the CNR value of the satellites diagonally, as shown in Equation (3.11).

To calculate WGDOP based on CNR using the above three equations (3.10), (3.8), and (3.11), five satellite information is required: (1) satellite PRN, (2) observation time, (3) elevation angles, (4) azimuth angles, and (5) CNR values. These satellite data were obtained using RTKLIB (demo5 b34d). The raw satellite data (observations and navigation data) was imported in RTKLIB's PLOT to determine and extract the required the five satellite information, as shown in Figure 5.5. However, different satellite observation data were used in the ten satellite selection cases.

As shown in Table 5.4, there are ten cases of satellite selection. In the first four cases WGDOP satellite selection was done alone, after Ele, and before RAIM and before RAIM-KFITH, respectively. In these cases, the original satellites observation data obtained from receiver were used to generate the satellite characteristic file using RTKLIB. The satellite characteristic file was imported to MATLAB for WGDOP selection. However, the satellite characteristic file was filtered first to remove any satellites with an elevation angle less than 15 degrees before WGDOP selection in case 2.

In the last six cases, WGDOP satellite selection was performed after RAIM or RAIM-KFITH along with Ele in some of them. In these cases, a modified satellite observation file was used to generate the satellite characteristic file. RAIM or RAIM-KFITH selection was implemented before WGDOP. A positioning is implemented after RAIM selection. After RAIM selection (i.e., exclusion), the remaining satellites are then used for new positioning determination. As a result, the positioning status file was checked to find which satellites were rejected by RAIM and others (Ele and KFITH). These satellites were then excluded from the satellite observation file using MATLAB. This modified satellite observation file with the navigation massage were imported into RTKLIB's PLOT to obtain the satellite characteristic file for WGDOP selection.

- **WGDOP Selection**

Several techniques, as TM, ANN, and optimization algorithms, were used to find the optimal satellite subset based on WGDOP value. The optimization algorithms were considered the most suitable technique for the satellite selection based on their high result quality and computation speed, as discussed in Section 3.3. The performance of five optimization algorithms (ABC, ACO, GA, PSO, and SA) was evaluated in satellite selection in Chapter 6. The best-performing optimization algorithm was used for WGDOP-based satellite selection in the ten cases.

Satellite selection based on WGDOP/GDOP can be done by two ways: 1) fix subset size and 2) fix GDOP/WGDOP value. The fix subset size is an approach that finding the optimal satellites for a fix subset size (i.e., fix number of satellites in the subset). The fix GDOP/WGDOP value is an approach that finding the optimal satellite subset with the least size that reach the predetermined GDOP/WGDOP value. The optimal satellite subset based on WGDOP/GDOP was found for a fix number of satellites using optimization algorithms. To improve positioning accuracy with the lowest number of satellites, the optimization algorithms were carried out finding the optimal subset of fix number of satellites ranges between 4 – 18 (Table 5.7).

Table 5.7 Number of selected satellites using optimization algorithms in previous studies

NSAT selected	Reference
4	[101,105]
6	[107]
8	[106]
6, 8, 10, and 12	[7,117]
5 -18	[104]

The number of satellites is important for positioning accuracy because it increases as the number of satellites rises. To investigate the effect of the number of satellites on selection and positioning, the optimal satellites were selected with all possible subset sizes. When using one satellite system, at least four satellites are required for positioning. This minimum number of satellites (4) increases by one as the number of used satellites system increases. This is because the time difference between satellite system [22]. In this project, satellite data were collected from three satellites systems: GPS, GLONASS, and Galileo. Thus, the optimization algorithm was applied to find the optimal subset of 6 – maximum number of satellites observed.

Although GNSS data were collected for 24 hours with 30-sec interval (i.e., 2880 epochs), the optimal subset of large number of satellites was selected in few numbers of epochs less than 2880.This is because the number of satellites fluctuate over time, as the number of satellites increases the short it last. The satellites selection based on WGDOP was implemented per epoch. For each epoch, It was only applied if an epoch has a number of satellites greater or equal to the predetermined number of satellites for selection.

WGDOP-based satellite selection is selection based on the quality of satellite geometry (GDOP) and signal power (CNR). The optimal satellites were selected for multi-GNSS (GPS, GLONASS, and Galileo). Each one of these satellite system broadcasts their signal in multiple frequencies, as shown in Table 2.1. However, only satellite L1 frequencies were

considered in WGDOP selection. This is because the three satellite systems have different number and band of frequencies (Table 2.1).

5.2.5 Results Evaluation

The performance of the ten cases in satellite selection can be evaluated based on their selected satellite positioning quality, which includes positioning accuracy, precision, epochs, and the number of satellites used for positioning of the selected. The selection case with the best results in above evaluation criteria considered the appropriate one for satellite selection. However, four steps are required to implement positioning and estimate positioning accuracy, as shown in Figure 5.9

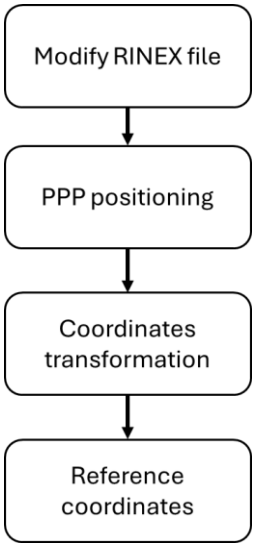

Figure 5.9 Flowchart of Implementing PPP positioning with the selected satellites and determine its accuracy

- **Modify RINEX**

Satellites travel around the Earth, so GNSS receiver track different satellites over time. As a result, different optimal satellites should be selected for different periods of time. RTKLIB, which was used for PPP positioning, can exclude different satellites for each epoch. Therefore, the original RINEX, obtained from receiver, was modified. It was imported to MATLAB to remove unselected satellites for each epoch Hence, the RINEX file was modified for every number of satellites selected in each case, as shown in Figure 5.10.

Case: 6 Selected: 6-Sat

```
> 2021 09 20 00 00 00.0000000  0 6
G06  23680380.100 1 124441273.11116        40.250
G12  20912213.020 1 109894485.92317        45.250
G22  25994644.820 1 136602749.05015        32.200
G24  24101322.960 1 126653325.47116        39.950
G25  19902207.820 1 104586823.52817        45.300
G32  22001572.140 1 115619071.03417        45.150
> 2021 09 20 00 00 30.0000000  0 6
G06  23685231.480 1 124466764.287 6        39.300
G12  20924118.400 1 109957047.530 7        45.850
G22  26003940.080 1 136651593.997 6        36.250
G24  24122363.600 1 126763895.127 6        39.200
G25  19902772.060 1 104589788.619 7        45.600
G32  22011205.080 1 115669691.137 7        44.500
> 2021 09 20 00 01 00.0000000  0 6
G06  23690195.560 1 124492849.926 6        38.350
G12  20936089.200 1 110019953.310 7        45.850
G22  26013310.260 1 136700832.169 5        34.850
G24  24143425.040 1 126874574.440 6        39.600
G25  19903423.880 1 104593214.017 7        45.100
G32  22020939.240 1 115720845.030 7        44.750
```

Case: 8 Selected: 6-Sat

```
> 2021 09 20 00 00 00.0000000  0 6
G06  23680380.100 1 124441273.11116        40.250
G12  20912213.020 1 109894485.92317        45.250
G24  24101322.960 1 126653325.47116        39.950
G25  19902207.820 1 104586823.52817        45.300
G31  22646321.440 1 119007226.58317        42.800
G32  22001572.140 1 115619071.03417        45.150
> 2021 09 20 00 00 30.0000000  0 6
G06  23685231.480 1 124466764.287 6        39.300
G12  20924118.400 1 109957047.530 7        45.850
G24  24122363.600 1 126763895.127 6        39.200
G25  19902772.060 1 104589788.619 7        45.600
G31  22629526.260 1 118918966.704 7        43.950
G32  22011205.080 1 115669691.137 7        44.500
> 2021 09 20 00 01 00.0000000  0 6
G06  23690195.560 1 124492849.926 6        38.350
G12  20936089.200 1 110019953.310 7        45.850
G24  24143425.040 1 126874574.440 6        39.600
G25  19903423.880 1 104593214.017 7        45.100
G31  22612781.520 1 118830972.281 7        43.950
G32  22020939.240 1 115720845.030 7        44.750
```

Case: 6 Selected: 7-Sat

```
> 2021 09 20 00 00 00.0000000  0 7
G03  25145643.320 1 132141245.92416        36.650
G06  23680380.100 1 124441273.11116        40.250
G12  20912213.020 1 109894485.92317        45.250
G22  25994644.820 1 136602749.05015        32.200
G24  24101322.960 1 126653325.47116        39.950
G25  19902207.820 1 104586823.52817        45.300
G32  22001572.140 1 115619071.03417        45.150
> 2021 09 20 00 00 30.0000000  0 7
G03  25148563.240 1 132156589.424 6        36.600
G06  23685231.480 1 124466764.287 6        39.300
G12  20924118.400 1 109957047.530 7        45.850
G22  26003940.080 1 136651593.997 6        36.250
G24  24122363.600 1 126763895.127 6        39.200
G25  19902772.060 1 104589788.619 7        45.600
G32  22011205.080 1 115669691.137 7        44.500
> 2021 09 20 00 01 00.0000000  0 7
G03  25151591.220 1 132172500.707 5        34.350
G06  23690195.560 1 124492849.926 6        38.350
G12  20936089.200 1 110019953.310 7        45.850
G22  26013310.260 1 136700832.169 5        34.850
G24  24143425.040 1 126874574.440 6        39.600
G25  19903423.880 1 104593214.017 7        45.100
G32  22020939.240 1 115720845.030 7        44.750
```

Case: 8 Selected: 7-Sat

```
> 2021 09 20 00 00 00.0000000  0 7
G06  23680380.100 1 124441273.11116        40.250
G12  20912213.020 1 109894485.92317        45.250
G24  24101322.960 1 126653325.47116        39.950
G25  19902207.820 1 104586823.52817        45.300
G29  22159658.020 1 116449808.58317        43.850
G31  22646321.440 1 119007226.58317        42.800
G32  22001572.140 1 115619071.03417        45.150
> 2021 09 20 00 00 30.0000000  0 7
G06  23685231.480 1 124466764.287 6        39.300
G24  24122363.600 1 126763895.127 6        39.200
G25  19902772.060 1 104589788.619 7        45.600
G31  22629526.260 1 118918966.704 7        43.950
E27  25892393.140 1 136065459.594 7        46.150
E30  22466574.340 1 118062662.913 8        49.100
E36  25611059.640 1 134587047.557 7        46.150
> 2021 09 20 00 01 00.0000000  0 7
G06  23690195.560 1 124492849.926 6        38.350
G12  20936089.200 1 110019953.310 7        45.850
G24  24143425.040 1 126874574.440 6        39.600
G25  19903423.880 1 104593214.017 7        45.100
G29  22124278.020 1 116263885.455 7        44.050
G31  22612781.520 1 118830972.281 7        43.950
G32  22020939.240 1 115720845.030 7        44.750
```

Figure 5.10 Sample modified RINEX files for 6 and 7 satellites selected from cases 6 and 8. They show L1 frequency in the first three epochs of the selected satellites (6 and 7). Left: satellites were selected from case 6, Right: satellites were selected from case 8.

- **PPP Configuration and Implementation**

After creating a RINEX file for every number of selected satellites in the ten cases, RTKLIB was used to determine the PPP positioning for the selected satellites. The previous PPP configurations, which was used for the initial PPP positioning (Table 5.6), was used again. However, RAIM and KFITH were disabled in PPP positioning of the selected satellites from all cases except for those in cases 9 and 10. This is to apply RAIM-KFITH selection after WGDOP selection. In RTKLIB, RAIM is turn on and off via ticking. Whereas KFITH can be disabled by increasing the threshold, and it was increased from 30 to 1000 metres.

- **Coordinates Transformation**

The positioning solution were determined in cartesian coordinate system (XYZ). In addition, the solution coordinates were obtained based on the satellite ephemeris' reference frame

because it was PPP solution. However, the positioning errors were evaluated in the east, north, and up directions of the British National Grid (BNG). This transformation was made to provide better representation of positioning errors.

According to El-Rabbany [30], satellite ephemeris contains satellite coordinates in the World Geodetic System 1984 (WGS84). If precise satellite ephemeris was used, the solution coordinates will be based on its reference frame. It was the International Terrestrial Reference Frame (ITRF) of 2014. To convert the solution coordinates from ITRF2014 to BNG based on OSTN15, was made three transformations: i) ITRF conversion, ii) datum conversion, ii) BNG conversion. These transformations are based on online services. The first two based on ETRF/ITRF Coordinate Transformation, while the last one is based on OSGB36 national grid coordinates.

- **Reference Coordinates**

To determine the positioning accuracy of the selected satellites, their positioning results were compared to truth. The truth was considered the results of relative positioning for 15 days (20 September to 04 October 2021). Five BIGF stations (Table 5.5) were used as reference stations. In addition, this relative positioning was implemented via Leica software with following configurations:

Table 5.8 Relative positioning configurations via Leica infinity

Setting	Options
Units of Lat/Long	DMS [0.00001]
Coordinate System	OSGB36(15)
Cut Off Angle	15-degree
Sample Rate	30-sec
Satellite System	GPS, GLONNAS, and Galileo
Ephemeris Type	Precise
Antenna Phase	igs14.atx
Solution Type	Phase Fixed
Tropospheric Model	Computed
Ionospheric Model	Automatic
Frequency	Automatic

5.3 Experimental evaluation of Satellite Selection Method

Different optimization algorithms and WGDOP-RAIM cases (combinations) were tested (Chapter 6 and 0) to determine the suitable satellite selection method. GNSS data, which was collected statically from open-sky environment, was used in these evaluations. To test the performance of the final proposed satellite selection method, it was implemented to

select satellites from GNSS data collected in three different scenarios. The first scenario of data collection is static open sky environment, which is the same data used before. This is to evaluate the new satellite selection method after the enhancement made based on the suggestion(s) derived from Chapter 6 and 0. The second scenario of data collection is kinematic open sky environment. The last scenario is static multipath environment.

To evaluate the performance of proposal satellite selection method for PPP. The satellite selection method was implemented in different scenarios. The optimal satellites were selected in all possible subset sizes. The evaluation of its selection was based on the positioning quality of their selected satellites, the number of positioning epochs, the number of selected satellites used in positioning, and the continuity of selected satellite subset.

5.3.1 GNSS Data

- **Static Open-Sky Environment**
  The same GNSS data on the 20th of September 2024 that was obtained from the same BIGF station (NGB2) located on the roof of the NGI building (Figure 5.2). Figure 5.3 shows the number of GNSS satellites observed with a 30-sec sampling rate and zero-degree elevation mask. The true coordinates of NGB2 were determined based on 15 days of relative positioning, using the closest five BIGF stations (Table 5.5).

- **Kinematic Open-Sky Environment**
  On 26 April 2023, GNSS data was collected kinematically. On the roof of the Nottingham Geospatial Institute building, a train was equipped with Leica AS10 antenna installed on a pillar (18 cm) and a Leica GS10 receiver with the capacity of recording multi-GNSS signals (GPS, Galileo, GLONASS, and BeiDou). For one-hour (13:16:45 – 14:16:45) GNSS data were collected while the train moving (Figure 5.11). To determine the true coordinates of train's path, GNSS data was collected from NGB2 station for the same period. This is to apply one-hour relative positioning using NGB2 station as a reference. Since NGB2 station collected only GPS, Galileo, and GLONASS satellite data, satellite data of these systems were collected with a 1-sec sampling rate and zero-degree elevation mask by the train and NGB2 receivers. Figure 5.12 shows the number of GPS, Galileo, and GLONASS satellites collected for one-hour by NGB2 and train receivers.

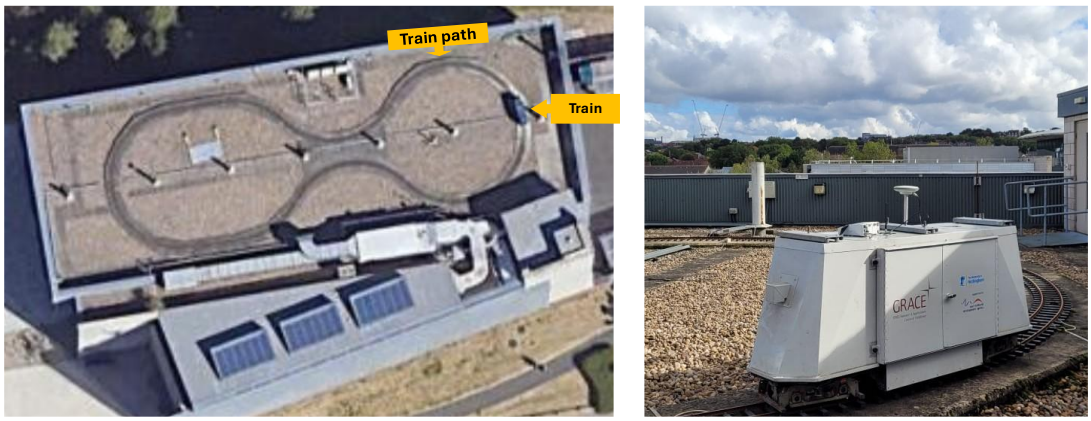

Figure 5.11 (left) The train and its path on the roof of NGI building, (right) the GNSS receiver and antenna on train collecting GNSS data.

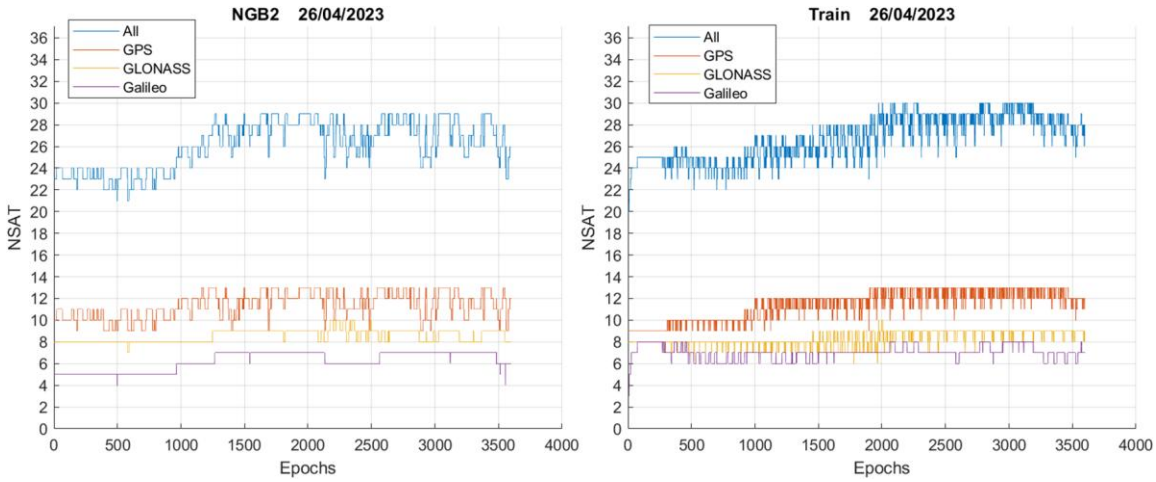

Figure 5.12 Number of GNSS satellites collected by NGB2 (left) and train (right) receivers for 1-hour period on April 26th, 2023.

- **Static Multipath Environment**

  To investigate the performance of the new satellite selection method under multipath environment, it was implemented for satellite selection in three locations with low and high multipath level. The first location has low multipath effect, and it is in the Jubilee campus next the tennis court. The second and the third locations are the control points NGB 11 and NGB 09 located fort and behind the NGI building. Both locations are surrounded by rise building creating high multipath environment. The GNSS data in these locations are shown below.

  On 08 October 2024, GNSS data was collected statically at Jubilee campus next the tennis court. Tripod, Leica AS10 antennas and Leica GS10 receiver were used to collect GNSS data, as shown in Figure 5.13. The GNSS data was collected for four hours

(09:40:00 – 13:40:00) with a 30-sec sampling rate and zero-degree elevation mask. Figure 5.14 shows the number of GPS, Galileo, and GLONASS satellites collected from.

Figure 5.13 (left) The receiver location at Jubilee campus next to the tennis court and (right) the GNSS receiver and antenna collecting GNSS data at the location.

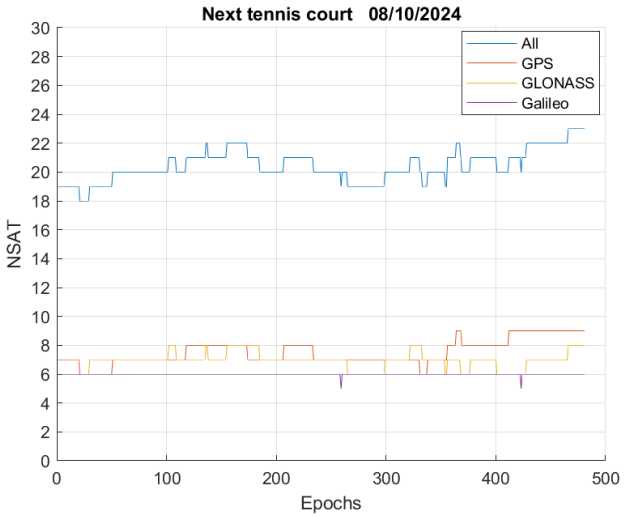

Figure 5.14 Number of GNSS satellites collected at Jubilee campus next to the tennis court for 4-hour period on October 08, 2024.

On 12 July 2023, GNSS data was collected statically from two control points (NGB9 and NGB11) around the Nottingham Geospatial Institute building (Figure 5.15). These control points are in multipath environment, as they surrounded by building. Tripods, Leica AS10 antennas and a Leica GS10 receivers were used (Figure 5.16) to collect GNSS data for four hours (11:01:21– 15:01:21) with a 30-sec sampling rate and zero-degree elevation mask. Figure 5.17 shows the number of GPS, Galileo, and GLONASS satellites collected from both locations (NGB9 and NGB11).

Figure 5.15 The location of NGB9 and NGB11, where GNSS data was collected.

Figure 5.16 The GNSS receiver, antenna, collecting GNSS data on NGB11 (left) and NGB9 (right), which are front and behind NGI building, respectively.

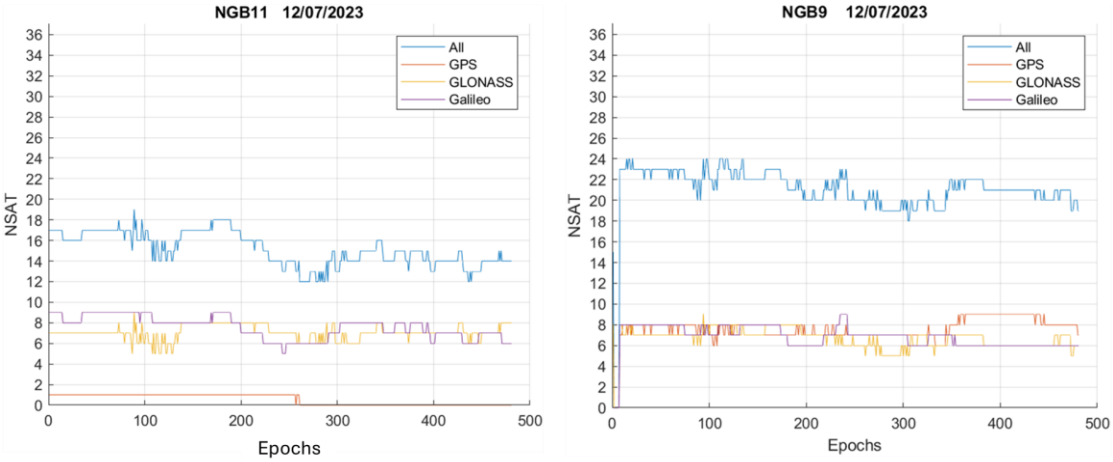

Figure 5.17 Number of GNSS satellites collected on NGB11 (left) and NGB9 (right) for 4-hour period on 12 July 2023.

5.3.2 Satellite Selection Implementation

Satellite selection method consists of two parts: i) selection techniques and ii) selection criterion. Satellite selection technique was evaluated in Chapter 6, as five optimization algorithms were tested. The best-performing optimization algorithm was used for WGDOP-based satellite selection. Whereas different satellite selection criteria were evaluated in Chapter 7, and the one with the best performance was used for satellite selection. To apply the best-performed selection technique and criterion, several steps were implemented, which are the same steps in section 5.2.4.

5.3.3 Results Evaluation

The performance of the satellite selectin method can be evaluated based on the positioning accuracy of its selected satellites. Four steps are required to apply the selected satellites for positioning and estimate positioning accuracy, as shown in Figure 5.9. These four steps were explained in section 5.2.5.

Chapter 6 Optimization Algorithms Performance

6.1 Results and Discussion

6.1.1 GPS Optimal Satellites

The five optimization algorithms were applied for the optimization of GPS-only satellite constellations of 4, 5, 6, and 7 GPS satellite constellations for the 24-hour GPS data. Optimal GPS satellites were selected every five minutes; hence the optimization algorithms selected optimal satellite constellation for 288 epochs (i.e. one epoch per 5 minutes) in the 24-hour period. Figure 6.1 shows (i) the quality of match of the GPS satellite subsets selected by the algorithms, which was determined by comparing the satellite selection results of the optimization algorithms with those of TM, and (ii) the selection time that was taken by the algorithms for the GPS satellite selection over 288 epochs.

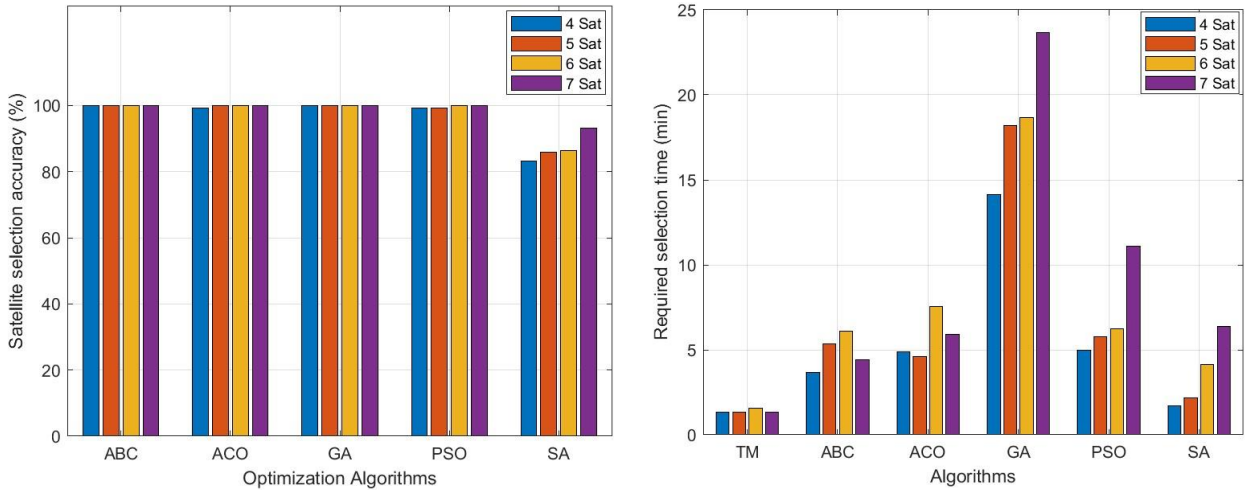

Figure 6.1 (left) The quality of match (accuracy) of the selection of the optimal GPS satellite subset by the optimization algorithms with respect to the actual optimal GPS satellite subset derived by the TM. (right) The required time of the TM and the optimization algorithms for the optimal GPS satellite subset selection[150].

According to Figure 6.1, all the optimization algorithms effectively selected the optimal GPS satellites, except for the SA algorithm. More specifically, for the cases of a GPS satellite constellation of 4, 5, 6, and 7 satellites, the four algorithms ABC, ACO, GA and PSO achieved a GPS satellite selection accuracy over 99%, with the algorithms ABC and GA achieving the best GPS satellite selection accuracy as they had 100% match with the GPS optimal satellite constellation as derived by the TM. In contrast, SA had the lowest accuracy in choosing the optimal GPS satellite constellation with a match ranging between 83% and 93%. However, the SA proved to be the fastest in satellite selection among the five optimization algorithms, but it was still slower than TM. The satellite selection speed is the time required to finish the selection session, which involves determining the optimal satellite subset sequentially from

288 epochs for a specific subset size. It was considered the processing time taken by MATLAB in HPC. The performance of optimization algorithms, and consequently the quality of their results, can be affected by the value of optimization algorithms' parameters. However, the main reason for lower SA quality in satellite selection is its design and specifically the technique of finding the optimal solution. ABC, ACO, GA, and PSO are population-based algorithms, which mean that they use groups of individuals to find the optimal solution [149]. In this project, the population size of these algorithms was determined as 100. In contrast, SA was originally designed to find the optimal solution by a single population size. Since increasing the population size can improve the quality of the algorithms' results [149] , the performance of SA was negatively affected by its low population.

On the other hand, it can be seen that the four algorithms (ABC, ACO, GA, and PSO) are equally accurate in selecting satellites. These algorithms achieved more than 99% accuracy in selecting the optimal GPS subsets of 4, 5, 6 and 7 satellites. ABC and GA constantly selected the optimal satellites with a quality of 100% in all cases. Whereas ACO and PSO had less accurate satellite selection (99.3%) in one and two cases, respectively. Since each case included 288 epochs the satellite selection accuracy of 99.3% means that the optimal GPS satellite subset was miss-selected in two epochs.

Figure 6.2 shows the fitness value (CNR-WGDOP) of the actual optimal satellite with the four subset sizes (4, 5, 6, and 7) over time (288 epochs), where they derived from TM. This is presented as a blue line that corresponds to life y-axis. The figure's right y-axis presents the difference between the fitness of actual optimal satellite subset and that of optimization algorithms (dABC, dACO, dGA, dPSO, and dSA). According to the Figure 6.2, no significant difference can be found between the ACO and PSO results and the TM results (actual results). This indicates that ACO and PSO fall at a local optimum that was too close to the best solution (i.e. satellite combination) ever found in the two epochs. ACO and PSO miss-selected the optimal subset of 4 satellites in two epochs. In Figure 6.3 and Figure 6.4, the actual optimal subset of 4 satellites, derived by TM, and the selected satellite combinations by ACO and PSO are displayed. The quality of these algorithms may vary from one trial to another, which could be due to the fact that these algorithms start randomly [149], which affects their results [164,165], or because the chosen values for the different parameters which can also affect the algorithms' results. However, the four algorithms (ABC, ACO, GA, and PSO) can generally be considered as equally accurate in satellite selection. This aligns with the results presented in [99], where ABC, GA, and PSO provided approximately the same high level of accuracy in GPS satellite selection, while SA provided slightly lower accuracy in the selection.

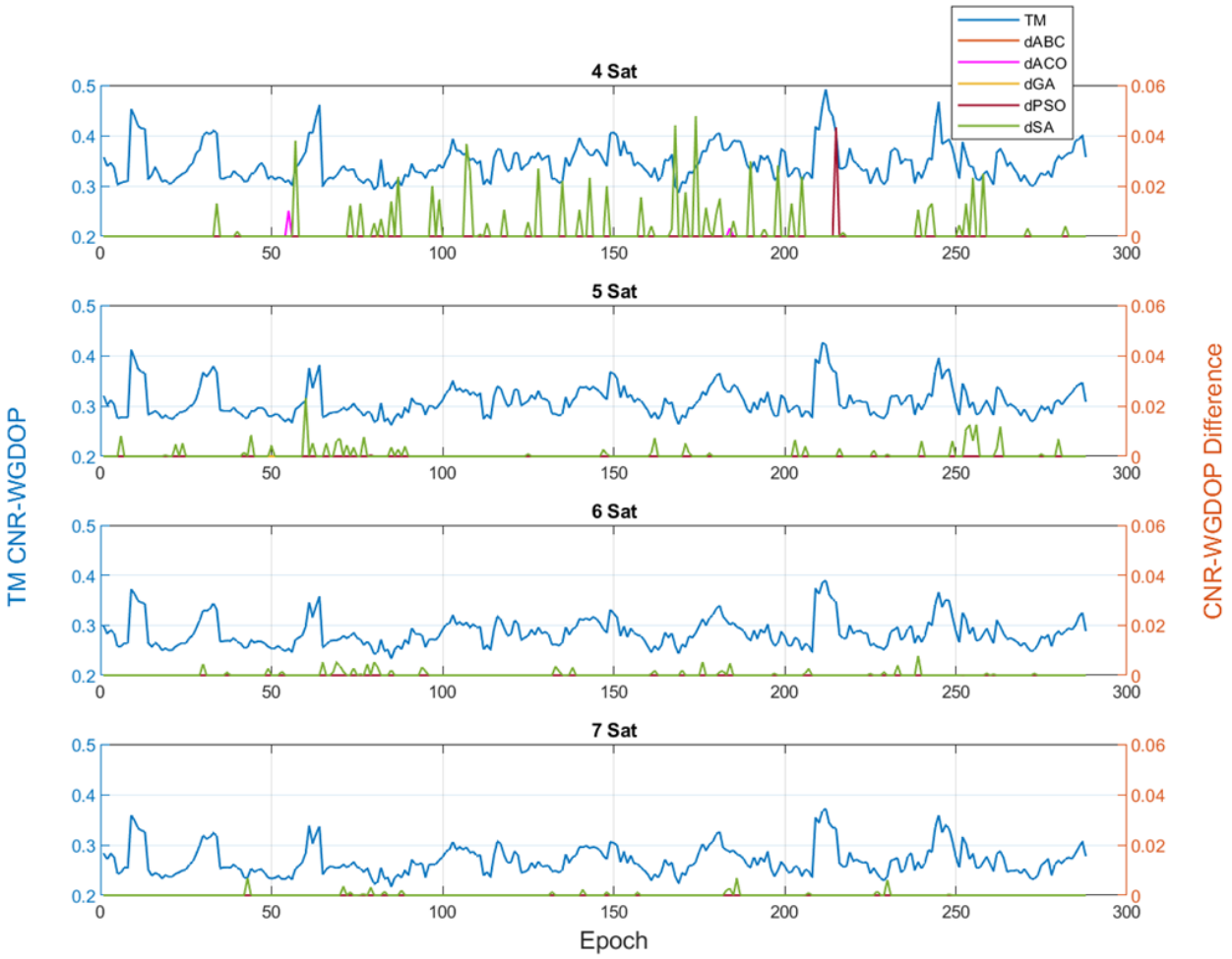

Figure 6.2 The comparison of the performance of the optimization algorithms with respect to TM, expressed as the difference between the CNR-WGDOP of the optimal satellite constellation of each optimization algorithm and the corresponding CNR-WDGOP of TM. The results of the four cases of GPS satellites constellations (4, 5, 6 and 7 satellites) are presented. On the left-axis, the CNR-WGDOP value of the optimal satellite constellation based on the TM is presented, and on the right-axis the difference between each of the optimization algorithm and the TM. Reprinted from [150].

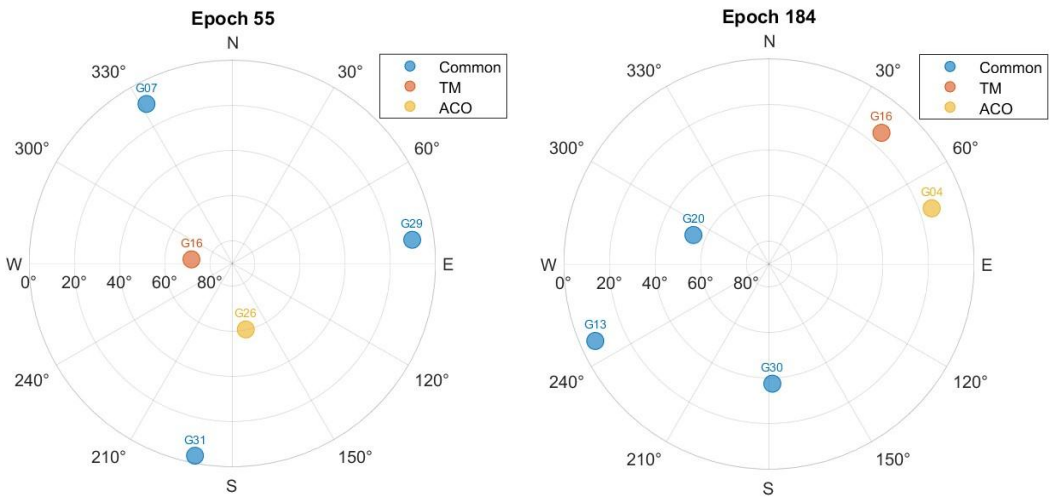

Figure 6.3 The sky plots of epoch 55 (left) and epoch 184 (right) presenting the selection of the optimal GPS satellite subset by the ACO and the TM, and showing the commonly selected satellites (blue) by the two methods, but also those who were differently selected by ACO (yellow) and TM (orange) [150].

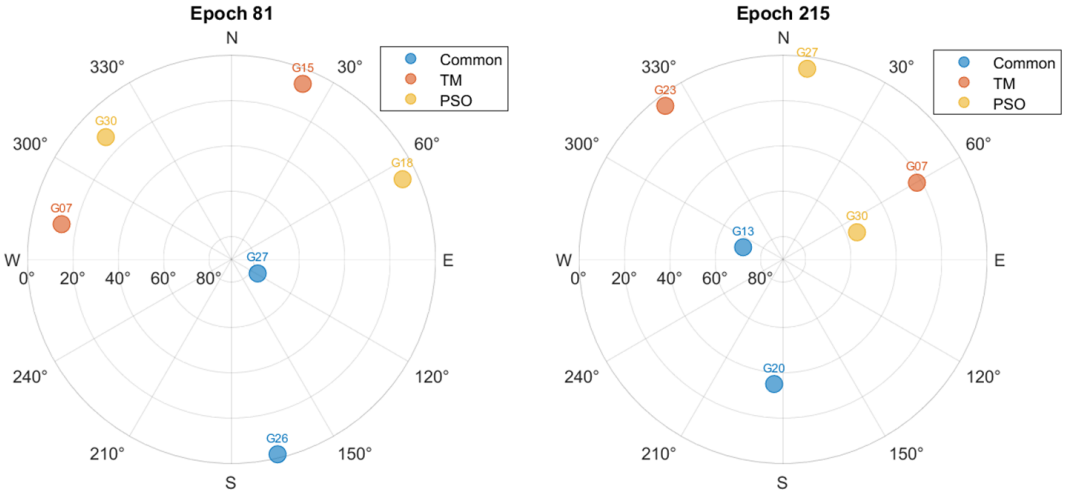

Figure 6.4 Same as Figure 13, presenting the sky plots for the epoch 81 (left) and epoch 215 (right), and differences between the selection of the optimal GPS satellite subset for PSO and TM [150].

In terms of satellite selection speed, the optimization algorithms were slow in selecting the optimal GPS satellites. Figure 6.1 represents the required time of the five optimization algorithms and TM to find the optimal GPS satellite selection for all 288 epochs: corresponding to the selection of GNSS satellite subset of 1-epoch per 5-minute interval, for the 24-hour GNSS data set. According to the figure, TM, which checks all possible satellite combinations, was faster than the optimization algorithms in finding the optimal satellite subset. TM selected the optimal satellites within about 2 minutes in all satellite selection cases. In contrast, the five optimization algorithms took more than 2 minutes in all cases,

with the required time varying depending on the number of the satellites in the constellation. In general, SA was the fastest algorithm among the five, whereas GA was the slowest. ABC, ACO, and PSO algorithms were similar in the required time (5 min) to complete the satellite optimization.

Unlike TM, optimization algorithms do not require a complete investigation of possible satellite combinations to determine the optimum. However, TM was faster in finding the best GPS satellites, as the optimization algorithms are computationally heavy for "small" problems by following indirect approaches that require additional processing time. For a small number of satellites that can be provided by a single system (e.g. GPS), this additional processing adds unnecessary burden to the problem. As a result, the TM was faster in finding the optimal GPS satellites, which aligns with the outcome in [92], as the TM is suitable for selecting satellites from one system.

Except for GA, the selection speed of the optimization algorithms is generally comparable. They took about 5 minutes to choose satellites in all selection cases. However, GA took much longer, ranging from 14 to 24 minutes. This contrasts with what was stated in [164], where GA is a fast algorithm. In addition, it contradicts the results presented by Du et al. [92], who showed that GA outperformed ACO in terms of satellite selection speed. GA took only 2 seconds, while ACO took 4.37 seconds to complete one selection. Furthermore, in [99], GA was as fast as ABC and PSO in selecting GPS satellites, completing approximately the same number of search iterations within 1, 1.5, and 2 seconds. The main reason for this unexpected delay in the speed of GA selection is the algorithm modification. GA finds the optimal solution by iteratively generating better new solutions. However, it may create solutions with a duplicate value, which is unacceptable in satellite selection. Thus, the solutions with a duplicate value were rejected, and new solutions were generated until no duplicates appeared. Obviously, this is time-consuming. Although the same modification was applied to ABC, PSO, and SA, these algorithms took much less time than GA. This is because GA creates new solutions by swapping the variables of two good solutions. As GA solutions converge, two nearly identical solutions are selected to create a new solution, which subsequently leads to more duplication.

Based on Equation (5.1), the number of possible satellite constellations changes due to the number of available satellites (8 and 13; Figure 5.6) and the constellation sizes (4, 5, 6, and 7; Figure 5.6). Compared to others, the subset of 6 GPS satellites has the highest number of possible combinations, which is a total of 1744. As a result, TM, which is checking all possible satellite combinations, took slightly longer time (13 sec) to find the optimal GPS subset of 6 satellites than others, as shown in Figure 6.1. In contrast to TM, the five optimization algorithms are unaffected by the number of possible satellite combinations, as

their number of searching iterations is predetermined. Although the five optimization algorithms were executed with the same number of iterations (100) at all satellite constellation sizes (4, 5, 6, and 7), the selection time for each algorithm varied from one satellite constellation size to another, as shown in Figure 6.1, due to the adjustment of duplication in the four algorithms (ABC, GA, PSO and SA). However, the difference in ACO processing time can be due to the number of possible GPS satellite subsets. In ACO, the pheromone rate on the paths influences the ants' path choice, which is stored in a pheromone matrix containing the pheromone rates of all possible paths. Since the size /burden of the pheromone matrix depends on the number of possible paths, which is equal to the number of possible satellite combinations, the ACO selection time changed with different satellite constellation sizes (4, 5, 6, 7), as they have different possible satellite constellations.

Among the five optimization algorithms, the most suitable one for satellite selection can be determined based on their satellite selection accuracy and speed. SA and GA are not suitable for satellite selection because of their low selection quality and speed, respectively. On the other hand, ABC, ACO, and PSO showed equivalent levels of selection quality and speed. However, the ABC algorithm was considered as the suitable algorithm for satellites selection, as only three parameters have to determined.

6.1.2 Multi-GNSS Optimal Satellites

Based on the evaluation of the optimization algorithms for the GPS-only satellite constellation, the ABC algorithm proved to be the most accurate and suitable for the optimization of GNSS satellite subsets. The next step was to apply and evaluate the ABC algorithm for the optimization of multi-GNSS satellite constellation. The same methodology as that for identifying the GPS-only satellite constellation was followed, by selecting the optimal GNSS satellite subset every five minutes. GPS, GLONASS and Galileo satellites were included for satellite selection, and four cases of satellite subset sizes (4, 8, 12 and 15 satellites) were examined. ABC was applied three times for each size of satellite subset, with different values for the parameters of (i) number of iteration and (ii) population size (Table 6.1), to evaluate their impact on algorithm performance and determine which parameters provide the best results.

The ABC algorithm requires the setting of three parameters: the maximum number of iterations (maxIter), population size (pSize), and abandoned limit (limit). In the case of the GPS-only satellite constellation, the maxIter, pSize, and limit values were set to 100, 100, and the product of problem dimensions and population size ($D \times pSize$), respectively. The value of abandoned limit ($D \times pSize$) is a dynamic value that automatically adapts to the problem size [151]; hence it does not need to be adjusted. On the other hand, higher values

of population size (pSize) and iteration (maxIter) can lead to better results, but they may cause slow convergence (longer processing times) [149,227]. Increasing the value of both pSize and maxIter could be unnecessary as the algorithm results can be improved with higher pSize and limited maxIter [227]. Based on previous studies pSize up to 200 is recommended [149]. As a result, pSize and maxIter were set to the values shown in Table 6.1.

Table 6.1 ABC parameter values [150].

Setting	maxIter	pSize	limit
1	100	100	D × pSize
2	100	200	D × pSize
3	200	200	D × pSize

Figure 6.5 shows the accuracy of the ABC algorithm in the GNSS satellite selection, which was determined by comparing ABC optimal GNSS satellite selection with the actual (TM selection), for each case of satellite subsets size (4, 8, 12 and 15) and for each case of parameters setting. In addition, Figure 6.5 illustrates the speed of the ABC algorithm and TM, expressed as the required selection time for the optimal satellite selection of all 288 epochs (GNSS satellites selection per 5 minutes for the 24-hour GNSS dataset). It is observed that satellite selection becomes more challenging due to the size of satellite subset, requiring higher parameter values and longer computation time. ABC showed better accuracy in selecting the optimum 4 GNSS satellites subset compared to the other sizes of satellite constellation (8, 12, 15) using the first two cases of parameter settings. This is due to the significant increase of the possible satellite combinations, which follows the increase of the number of satellites in the constellation (from 4 to 8, 12 and 15) (Figure 5.6). By increasing the value of the pSize and maxIter to 200, ABC accurately (100%) determined the optimal GNSS satellite subset for all sizes. However, the time required for selection increased by about 3.6 times, with respect to the first setting case using 100 for both pSize and maxIter. Therefore, satellite selection becomes more challenging due to constellation size. This requires higher values of population size and iteration, which leads to longer time of computation. This is consistent with what was reported in [149,227], as lower pSize and maxIter prevent achieving the best solution in complex problems, whereas increasing the value of these parameters increases the processing time.

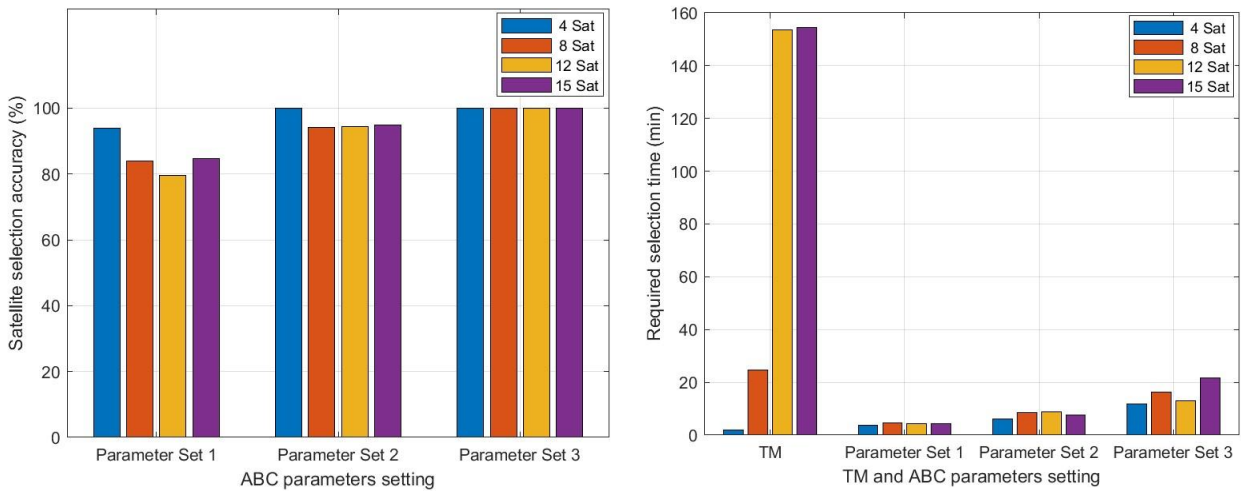

Figure 6.5 (left) The accuracy of the selection of the optimal GNSS satellite subset of ABC with respect to TM, for the various cases of satellite constellations and parameters settings and (right) the required time of the TM and ABC algorithm for the computation of the selection of optimal GNSS satellite subset. Reprinted from Alluhaybi et al. [150], licensed under CC BY 4.0.

The number of possible satellite combinations of 8 and 12 satellites-subsets is less than that for 15 satellites, and consequently the selection of the optimal satellite constellation should be easier than the 15 satellites. However, ABC was relatively more accurate in selecting the optimal 15 satellites than 8 and 12 satellites using the first parameter setting (Figure 6.5). The accuracy of choosing the optimal 8, 12 and 15 satellite constellation is 84%, 79.5% and 84.7%, respectively. Since similar parameter values were used for the three satellite constellation sizes, it is the initial randomly generated solution by the ABC algorithm which influences the produced solutions [165].

In terms of speed, the TM required an overall longer processing time to find the optimal satellites than the ABC algorithm, as the required time for the TM increases significantly with the satellite constellation size (increased from 4 to 15), since TM checks all possible satellite combinations which increase with the size of the satellite constellation. It should be noted that the TM required time for the case of 12 and 15 GNSS satellites constellation exceeds 150 minutes (i.e. >30 seconds per epoch).

On the other hand, the speed of ABC varies based on the parameters' settings. For the case of the first set of parameters (maxIter and pSize equal to 100), the ABC algorithm required approximately the same processing time (i.e. about 4.3 minutes; 0.9 seconds per epoch) for the four cases of satellites constellations (4, 8, 12 and 15), indicating that the number of satellite combinations does not affect speed of the ABC algorithm. For the other two settings an increased processing time was observed caused by the number of population size/iterations which was increased to 200. However, some slight difference of the required

processing time for the various satellite constellations (4, 8, 12 and 15) is reasoned by the adjustment of duplication of satellites in the solutions. The total number of GPS, GLONASS, and Galileo satellites reached 31, providing more than 300 million possible satellite combinations (Figure 5.6). However, ABC provides good results regardless of the setting used. According to Figure 6.5, ABC achieved a selection accuracy of 100% using setting 3, and its selection accuracy was no less than 80% with other settings. Figure 6.6 shows the fitness value (CNR-WGDOP) of the actual optimal satellite with the four subset sizes (4, 8, 12 and 15) over time (288 epochs), as they obtained from TM. This is presented as a blue line that corresponds to life y-axis. The right y-axis of the figure presents the difference between the fitness of actual optimal satellite subset and that of ABC with three settings (dSet1, dSet2, and dSet3). By reviewing the selection quality per epoch in Figure 6.6, it can be see that the fitness (CNR-WGDOP) of the miss-selected optimal GNSS satellite constellations differs by no more than 0.0063 in all cases (i.e. settings and constellation size) from those of the actual optimal GNSS satellite constellations determined by TM (Figure 6.6). The largest difference between the quality (i.e. CNR-WGDOP) of ABC satellite selection and the actual (TM) occurred in the selection of the four optimal satellites in setting 1. Figure 6.7 shows the sky plots of the satellites selected by ABC setting 1 and TM at epochs 20 and 88, which are the epochs with the largest difference of the CNR-WGDOP values between ABC setting 1 and TM; 0.0059 and 0.0063, respectively. In epoch 20, the selection of ABC setting 1 differed from TM in one satellite; the two different satellites of ABC and TM are of similar elevation angle and roughly symmetrical with respect azimuth. In epoch 88, ABC setting 1 selected three satellites different from those of TM. Similar to epoch 20, the six different satellites of ABC and TM are of similar elevation angle and roughly symmetrical with respect azimuth. Hence, even for the epochs where ABC satellite selection was not the actual optimal, its geometry was very close to the actual (as defined by TM), as shown in Figure 6.7. As a result, the ABC satellite subset had a very similar CNR-WGDOP value compared to the actual optimal satellite subset.

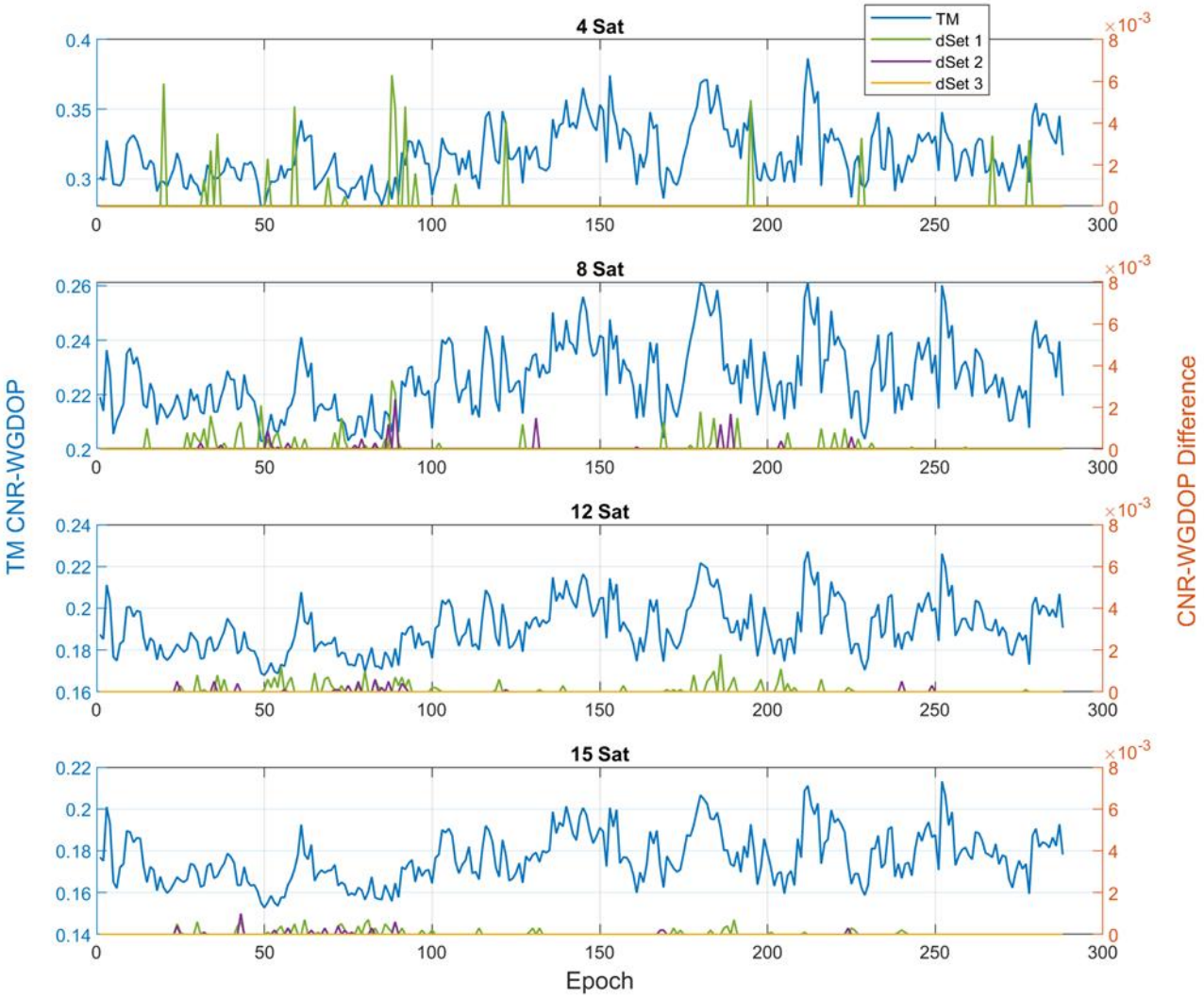

Figure 6.6 The comparison of the performance of the ABC algorithm for the three sets of parameter settings with respect to TM, expressed as the difference between the CNR-WGDOP of the optimal satellite constellation of each ABC parameter setting and the corresponding CNR-WDGOP of TM. On the left-axis the CNR-WGDOP value of the optimal satellite constellation based on the TM is presented, and on the right-axis the difference between each of the ABC parameter setting and the TM [150].

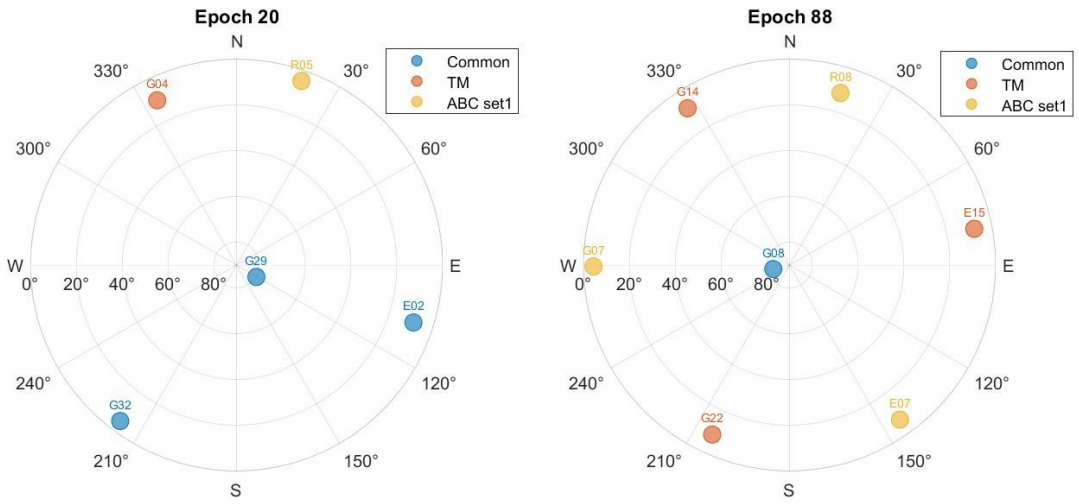

Figure 6.7 Sky plots of epochs 20 (left) 88 (right) presenting the difference in the selection of optimal GNSS satellite subset between ABC setting 1 and the actual-TM, by showing the common satellites (blue) and the differences of the ABC (yellow) and TM (orange) satellite selection[150].

As mentioned earlier, the satellite selection speed is the required time to complete the selection session of 288 selection for a single subset size. These 288 selections were done sequentially using the standard serial for loop in MATLAB. Despite the algorithm (TM or optimization algorithms), its selection speed can be improved by choosing the optimal satellite subsets parallelly using the parallel for loop (parfor) in MATLAB. However, this required more resources, including more CPU cores and RAM capacity. Furthermore, the selection speed/time can be improved by using compiled languages (e.g., C++), as they are faster than MATLAB (interpreted language) [228].

On the other hand, as revealed on the results above, TM has absolute accuracy (100%) in satellite selection, and the highest selection speed in single-GNSS selection. This raises a question. Can the satellite selection quality and speed of multi-GNSS be improved by selecting the optimal satellite subset from each satellite system individually by TM and then combining them to form the optimal satellite subset for multi-GNSS?

The speed of the multi-GNSS section will certainly increase greatly because the TM is so fast in single-GNSS selection. However, the quality of the selection is not guaranteed. TM selects satellites based on WGDOP, i.e., it chooses a number of satellites at the same time with the best signal power and distribution (WGDOP value). Since TM examines all possible solutions to determine the optimal one, the optimal subset of satellites derived from each system using TM is guaranteed. However, merging the optimal satellite subsets from different systems does not always provide the best subset of multi- GNSS satellites. This is because satellites from two or more GNSS systems can be close to each other leading to less optimal satellite distribution, as shown in Figure 6.8.

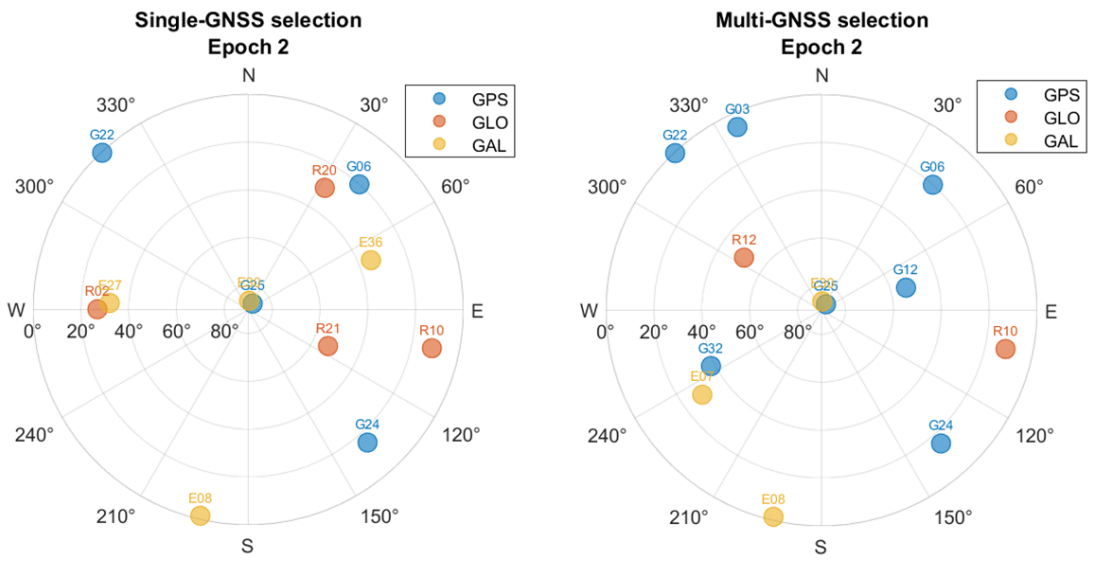

Figure 6.8 Sky plots of 12 multi-GNSS satellites selected by TM from the second epoch. Left, 4 satellites were selected from each system (GPS, GLONASS, and Galileo) individually. Right, 12 satellites were selected from multi-GNSS data directly.

6.2 Summary

This chapter focused on evaluating the performance of five optimization algorithms (ABC, ACO, GA, PSO, and SA) in satellite selection to determine the most suitable one, which was then further examined in more complex scenarios to determine its performance and suitable parameters' value. The evaluation was based on the selection accuracy and speed. The selection accuracy is how closely the CNR-WGDOP value of the optimal satellite subset selected by optimization algorithms matches that of the actual optimal subset, as determined by the TM. The selection speed is the required processing time to finish the selection session of 288 selections. The importance of this study is (i) the overall evaluation of the performance of the five optimization algorithms against each other and TM method, and (ii) the investigation of how the algorithms' principles and parameters setting affect their performance.

The five optimization algorithms were implemented to choose the optimal GPS satellites with different four subset sizes (4, 5, 6, and 7). According to the evaluation results, the ABC, ACO, and PSO algorithms had the highest accuracy in satellite selection, and they were efficient in terms of computation time. However, the ABC algorithm is more practical with the fewest parameters to adjust. The evaluation of the ABC algorithm in the more complex problem with multi-GNSS satellite constellation and even up to 31 available satellites revealed that the satellite selection accuracy of ABC algorithm improves significantly by increasing the values of the population size and iteration, which has though an effect on the required computation time (selection speed).

Also, it was shown that the TM is still the most efficient algorithm for selecting the optimal satellite combination from a single satellite-system system (i.e. GPS-only). However, this is not the case for multi-GNSS constellations with more simultaneously tracked satellites available, making the satellite selection problem too complex and time consuming for the TM.

Chapter 7 Define the criteria and process for satellite selection

7.1 Results and Discussion

The analysis of the performance of WGDOP in selecting the optimal subset of satellites was based on data selected on 20th September, 22nd September, 27th September, and 1st October 2021. The results based on the analysis of 20th September 2021 are presented in this chapter as representative of the entire analysis process, whereas the data of the other three days are presented in the appendix.

7.1.1 Availability

The optimal satellites were selected based on WGDOP in ten cases (Table 5.4). Except for the first case, the optimal satellites were chosen based on WGDOP with additional selection factors. Despite the additional selection factor (Ele, RAIM, or KFITH), satellites were mainly selected based on WGDOP. Satellite selection based on Ele, RAIM and KFITH were used to enhance WGDOP selection (i) before the application of WGDOP (cases 2, and 5 – 8), (ii) after the WGDOP (cases 3 and 4), and (iii) both, before and after the application of WGDOP (cases 9 and 10). The quality of selected satellites by WGDOP in the 10 cases can be evaluated by checking the number satellites initially selected for the solution with that were applied for the positioning solution. In positioning, weak satellite measurements are rejected by integrity functions (e.g., RAIM) to improve positioning accuracy. If all selected satellites were used in positioning, the quality of the selected satellites can be considered high and vis versa.

Figures 7.1, 7.2, and 7.3 show the availability results, including selection epochs availability (SEAva), positioning availability (PAva), and optimal positioning availability (OPAva). The optimal satellites were selected every 30 seconds for 24 hours, so they were chosen from 2880 epochs over 24 hours. As mentioned earlier in Section 5.2.4, The optimal satellites were chosen based on WGDOP for a fixed number of satellites from 6 to maximum number of observed satellites. They were selected separately for each epoch over the entire time. However, the number of observed satellites fluctuates over time. Therefore, satellite selection was implemented for specific number of satellites when the number of observed satellites in an epoch is greater than or equal to the number of selecting.

Out of 2880 epochs, the SEAva indicates the rate of epochs from which satellites were selected based on WGDOP. These epochs will be called WGDOP selection epochs. The PAva presents the rate of WGDOP selection epochs out of 2880 used in positioning. Whereas the OPAva indicates the rate of WGDOP selection epochs used in positioning out of 2880 without losing one WGDOP selected satellite. Moreover, the x-axis of Figure 7.1 represents the number of selected satellites out of 31, which is the total number of observed satellites over 24 hours.

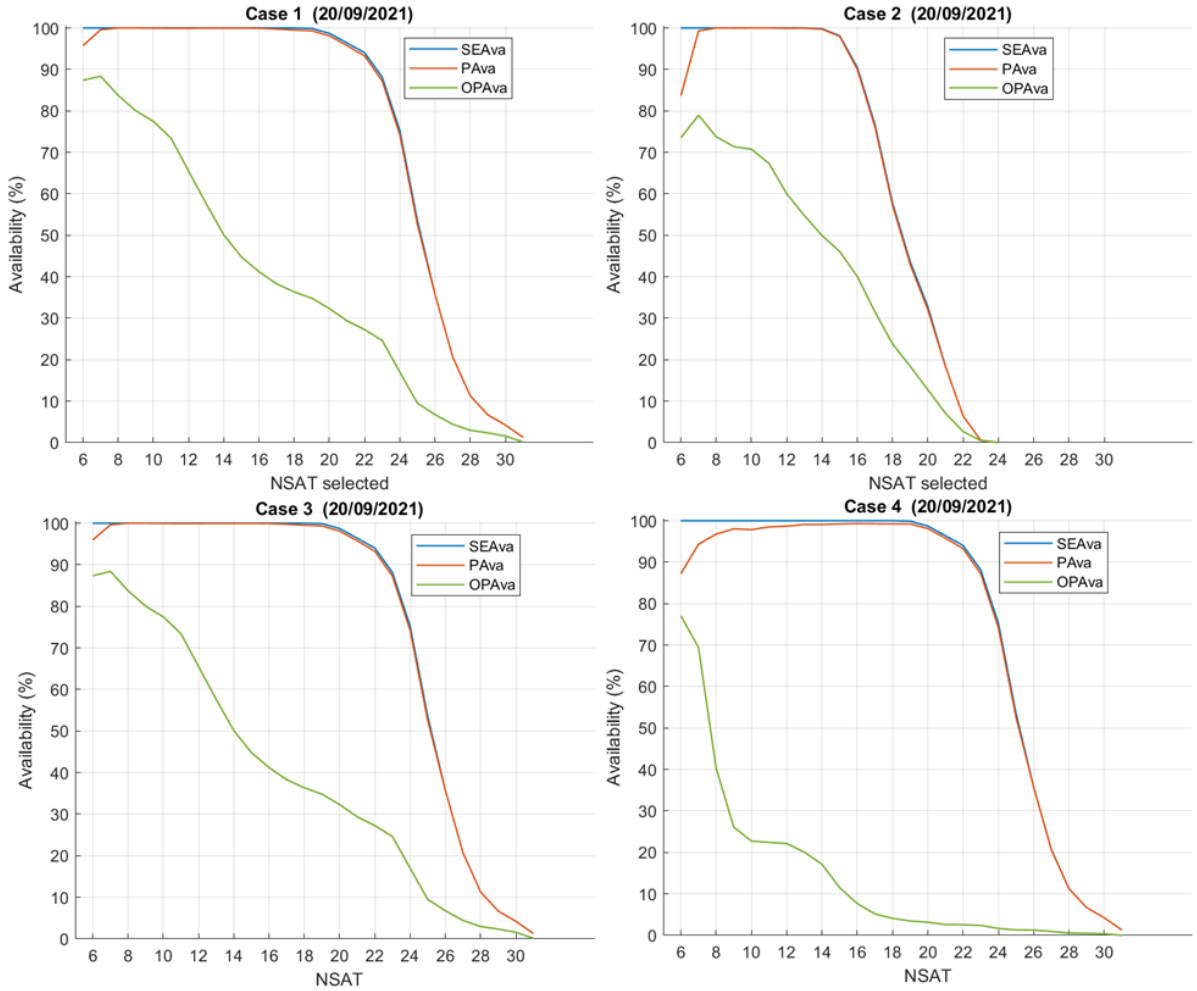

Figure 7.1 Comparison between satellite selection availability (SEAva), positioning availability (PAva), and optimal positioning availability (OPAva) from selection cases 1, 2, 3, and 4.

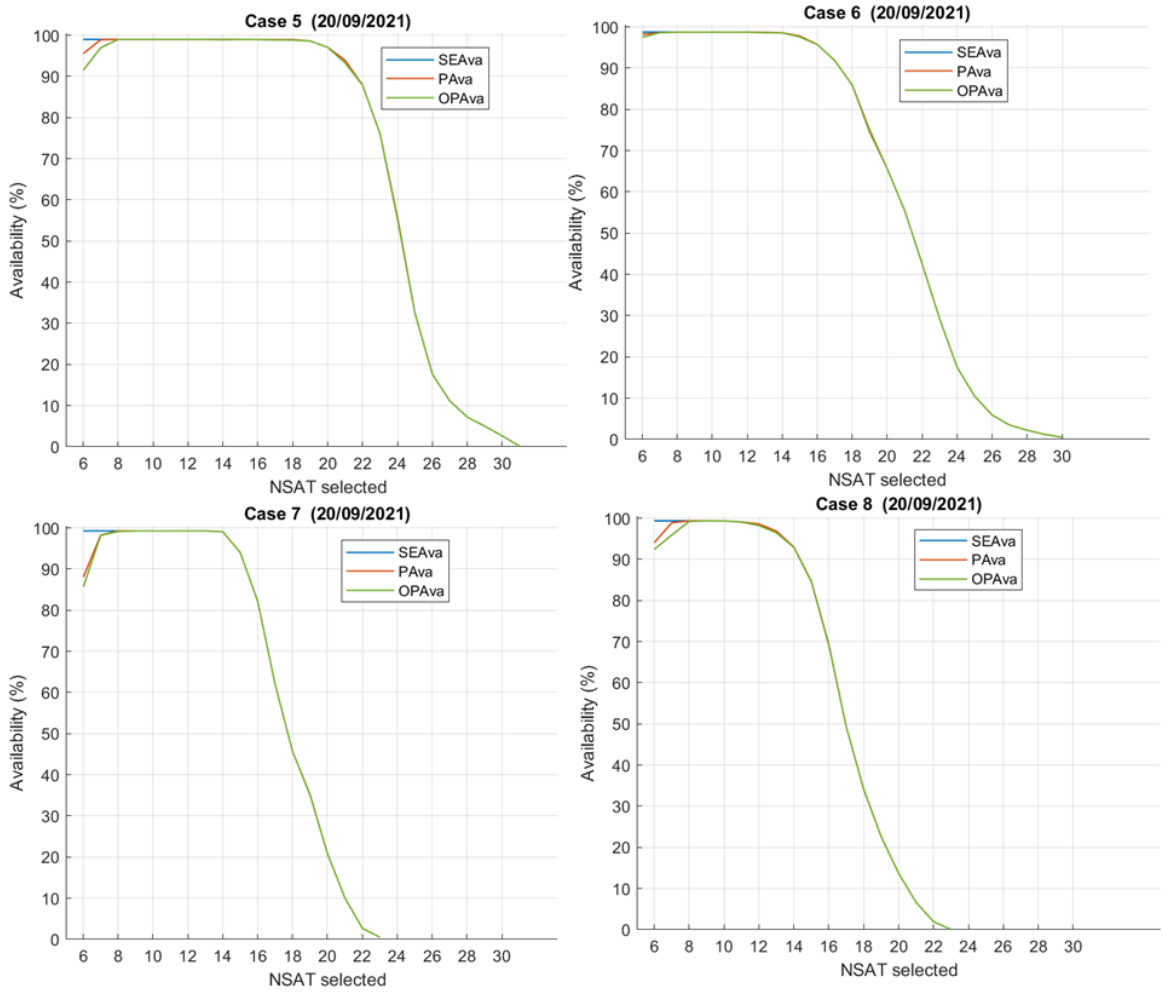

Figure 7.2 Comparison between satellite selection availability (SEAva), positioning availability (PAva), and optimal positioning availability (OPAva) from selection cases 5, 6, 7, and 8.

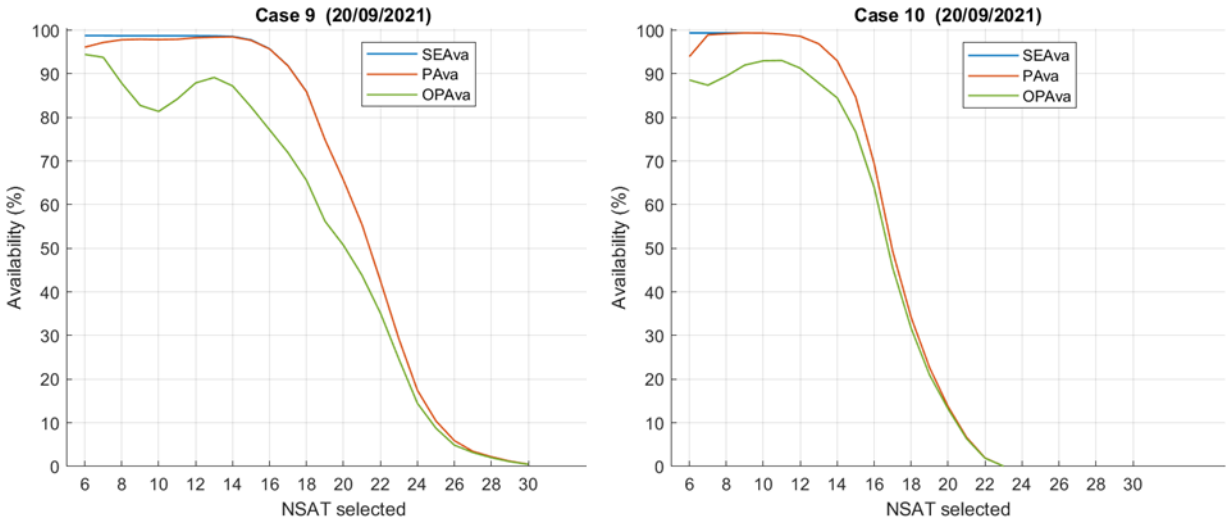

Figure 7.3 Comparison between satellite selection availability (SEAva), positioning availability (PAva), and optimal positioning availability (OPAva) from selection cases 9 and 10

According to Figures 7.1, 7.2, and 7.3, satellite availability was inconsistent in the ten selection cases. The maximum number of selected satellites is the largest in cases 1, 3, 4 and 5 with 31 satellites, while it is the lowest in cases 7, 8 and 10 with 23 satellites. The maximin number of selected satellites is 24 in case 2, while it is 30 in cases 6 and 9. Furthermore, SEAva was also inconsistent for the same number of satellites in the ten cases. For example, the SEAva for the six satellites was 100% (2880 epochs) in first four cases, while it was 98.99% (2851 epochs), 98.75% (2844 epochs), 99.27% (2859 epochs), 99.38% (2862 epochs), 98.75% (2844 epochs), and 99.38% (2862 epochs) for cases 5, 6, 7, 8, 9 and 10, respectively. The reason for this variation between cases is the satellite data used in WGDOP selection, as it were filtered differently in each case with the other selection factors (Ele, RAIM, and KFITH). Because the satellite data has not been filtered by them before WGDOP selection in cases 1, 3, and 4, SEAva in these cases was exactly the same.

On the other hand, the rate of SEAva decreased as the number of selected satellites increases in the same selection case. For example, the value of SEAva for 6 and 25 satellites in case 1 is 100% (2880 epochs) and 52.57% (1514 epochs), respectively. This is because the number of observed satellites fluctuates over time. Thus, a small number of satellites can be chosen most of the time, if not all. Whereas a large number of satellites can be selected only for short periods.

PAva refers to the rate of WGDOP selection epochs used in positioning. In all cases, it can be seen a small variation between the rate of epochs input for positioning (SEAva) and those used in positioning (PAva). In case 6, PAva is mostly aligned with SEAva in all selected satellites. In the remaining cases, the PAva is generally aligned with SEAva in all selected satellites except for those of 6 and 7 satellites. The alignment between PAva and SEAva means that all epochs input for positioning were used in positioning. In contrast, the

reduction of PAva compared to the corresponding SEAva means that a number of epochs have been excluded from the positioning determination.

There are two reasons for PAva reduction, i.e., losing epochs in the positioning solution. The first reason is solution validation. Both code and phase measurements are used in PPP. In RTKLIB, the quality of code solution is checked per epoch using chi-square test for the solution evaluation [118,119]. If the chi-square test for an epoch's solution fails, the epoch's solution is removed when RAIM is disable. However, weak satellite measurements are removed when RAIM is activated. This leads to the second reason for PAva reduction that is satellite exclusion. To maintain and improve an epoch solution, number of weak satellite measurements are removed by functions such as RAIM and KFITH. Nevertheless, the epoch solution is rejected when the number of the remaining satellites is less than four satellites.

The PAva reduction due to the second reason can be more affected with small number of selected satellites (e.g., 6 and 7), as their remain can easily be less than four satellites. Hence, the larger number of selected satellites are less affected by the second reason of PAva reduction. As a result, it can be assumed that the large number of selected satellites was affected only by the first reason for the PAva reduction. This can explain why 6 and 7 satellites have more PAva reduction than others.

Weak satellite measurements are rejected by RAIM and KFITH in RTKLIB. In case 4, both were only implemented before WGDOP selection. Therefore, PAva reduction was seen in more selected satellites (6 – 14) in case 4 compared to other cases.

In contrast to PAva, OPAva indicates the rate of epochs used in positioning without losing satellites, which were selected by WGDOP. Hence, the reduction of OPAva compared to the corresponding PAva indicates that a number of epochs were used for positioning after excluding a number of their WGDOP selected satellites. These satellites were removed due to their negative impact on positioning solution. According to Figure 7.1, there is a variation between OPAva and PAva in the ten selection cases with different rate. In the first four cases, the OPAva was significantly less than PAva in all selected satellites (6 – maximum number of selected satellites). In general, the variation between OPAva and the corresponding PAva was the largest in case 4, and the least in case 2. Whereas it was the same in case 1 and 3. The variation in OPAva rates between the four cases is accepted because different selection factors (Ele, RAIM, and KFITH) were used in them. Although RAIM was used in case 3 and not in case 1, their OPAva was identical. This is unacceptable, and it means that RAIM is not working. This is aligned with Angrisano et al. [226] outcomes, where no satellites were rejected by RAIM in PPP, using RTKLIB (v.2.4.2). It also supports what Zhang and Wang [222] stated, that RAIM is not mature enough for PPP.

Despite the differences between the first four cases in OPAva, the rate of OPAva decreases as the number of selected grows. In other words, the number of epochs with rejected satellites increases with the number of selected satellites. For example, in case 1, OPAva

rate was about 87%, 45%, and 3% for the 6, 16, and 28 selected satellites, respectively. Hence, the rate of their epochs with rejected satellites were about 9%, 55%, and 73% out of total number of epochs used in positioning 2736, 2880 and 316.8 (PAva: 95%, 100%, and 11%), respectively. This is because the satellites were selected based on a fixed number, which forces the selection algorithm (ABC) to provide a satellite constellation containing the exact number of satellites. As the number of selected satellites increases, more satellites with weak measurements are selected and will be rejected later, consequently, OPAva rate decreases.

On the other hand, the OPAva was almost aligned with PAva in all selected satellites in cases 5 to 8. In these cases, satellites were selected based on WGDOP along with Ele, RAIM, and KFITH. The WGDOP selection was applied as the last parameter of the method. This is the main reason for maintaining WGDOP selected satellites from rejection, i.e., increasing OPAva rates. Applying WGDOP selection first will lead to reject its selected satellites by the later selection technique (RAIM or KFITH). This can be seen in cases 3, 4, 9, and 10 when RAIM or RAIM-KFITH selection were performed after WGDOP selection. In addition, WGDOP selection uses satellites' raw information obtained from RINEX file, and it is not considering all positioning requirements. As a result, some of its selected satellites were rejected from positioning even without a later satellite selection. This can be seen in case 1 and 2, when satellites were selected bason on WGDOP-only and Ele-WGDOP, respectively. In these cases, satellites were excluded by two main factors: i) absent of satellites data and ii) post-fit residuals' threshold.

The selected satellites were excluded from positioning because of the absence of some of their data, which were due to precise satellite data and cycle slip. Precise satellite orbit and clock data are required for PPP, and they were collected from the Centre for Orbit Determination in Europe (CODE), which including satellite data from about 280 stations [229]. However, the precise satellite data from CODE did not contain a precise information for every satellite tracked by the GNSS receiver on NGB2. This led to reject these satellites from positioning, as shown in Figure 7.4. On the other hand, some of the selected satellites were rejected due to the absence of their clock data, which was caused by cycle slip, as shown in Figure 7.4.

```
prec ephem outage 2021/09/20 00:00:00 sat=42
no ephemeris 2021/09/19 23:59:59.922 sat=42
no broadcast ephemeris: 2021/09/20 00:00:00 sat=61 iode= -1
no broadcast clock 2021/09/19 23:59:59.916 sat=61
no broadcast ephemeris: 2021/09/20 00:00:00 sat=66 iode= -1
no broadcast clock 2021/09/19 23:59:59.913 sat=66
no broadcast ephemeris: 2021/09/20 00:00:00 sat=89 iode= -1
no broadcast clock 2021/09/19 23:59:59.925 sat=89
```

Figure 7.4 Sample of the debug trace file of 15-sat from case 1, showing four selected satellites were rejected. The first satellite (42) was excluded due to the absence of precise information, while the remaining were removed due to an ephemeris outage (i.e., cycle slip).

Furthermore, some of the selected satellites were rejected as they were outliers, as shown in Figure 7.5. In RTKLIB, PPP outliers determine by pre-fit and post-fit residuals' tests [230]. RAIM and KFITH are only eliminating the pre-fit outliers [119,231]. Since RAIM and KFITH were disabled in cases 1 and 2, the post-fit residuals' threshold was the main reason for these outliers' rejection (Figure 7.5). In cases 5 – 8, WGDOP selection were implemented the last, after RAIM or RAIM-KFITH. Nevertheless, few numbers of satellites were rejected from positioning, leading to OPAva reduction. This can be clearly seen in the selected 6 and 7 satellites. When RAIM and RAIM-KFITH selection were performed, both per-fit and post-fit residuals' thresholds were implemented, leading to exclude number of satellites with weak measurements. However, few satellites were rejected due to post-fit residuals again after WGDOP selection. This is because the status of satellite data used in positioning change after WGDOP selection, such as the number of satellite measurements. In cases 9 and 10, the selection of RAIM, KFITH, and post-fit residuals' threshold were implemented before and after WGDOP. Similarly, number of satellites were excluded by the after selection of RAIM, KFITH, and post-fit residuals' threshold due to the change of satellite status. The post-fit residuals' threshold is affected by the carrier phase errors, which was 0.003. The carrier phase errors is the base term of errors of carrier phase [118]. Increasing its value will increase the post-fit residuals' threshold and prevent satellites reduction. Figure 7.6 shows the number of used satellites in positioning when using 0.003 and 0.006 meters of carrier phase observations variation. It presents the number of satellites uses in positioning over 24 hours out of 6 selected satellites from case 7, which has the largest satellite reduction among the last four cases.

```
2021/09/20 23:57:00.00 sat=36 L1 res=   2.1313 sig=   0.0372 el=24.0
2021/09/20 23:57:00.00 sat=36 P1 res=   7.6536 sig=  10.7690 el=24.0
2021/09/20 23:57:00.00 sat=44 L1 res=  -0.7692 sig=   0.0224 el=66.3
2021/09/20 23:57:00.00 sat=44 P1 res=  -1.8723 sig=   6.0279 el=66.3
2021/09/20 23:57:00.00 sat=83 L1 res=  -0.1907 sig=   0.0172 el=57.2
2021/09/20 23:57:00.00 sat=83 P1 res=  -0.7868 sig=   4.1949 el=57.2
2021/09/20 23:57:00.00 sat=84 L1 res=   0.1674 sig=   0.0168 el=62.7
2021/09/20 23:57:00.00 sat=84 P1 res=   0.7193 sig=   4.0647 el=62.7
2021/09/20 23:57:00.00 sat=92 L1 res=   0.0428 sig=   0.0279 el=21.6
2021/09/20 23:57:00.00 sat=92 P1 res=   0.0903 sig=   7.8063 el=21.6
outlier (2) rejected 2021/09/20 23:57:00.00 sat=36 L1 res=   2.1313 el=24.0
```

Figure 7.5 Sample of the debug trace file of 15-sat from case 1, including satellites' code (P1) and phase (L1) residuals. Satellite 36 was rejected because its phases residual was considered an outlier.

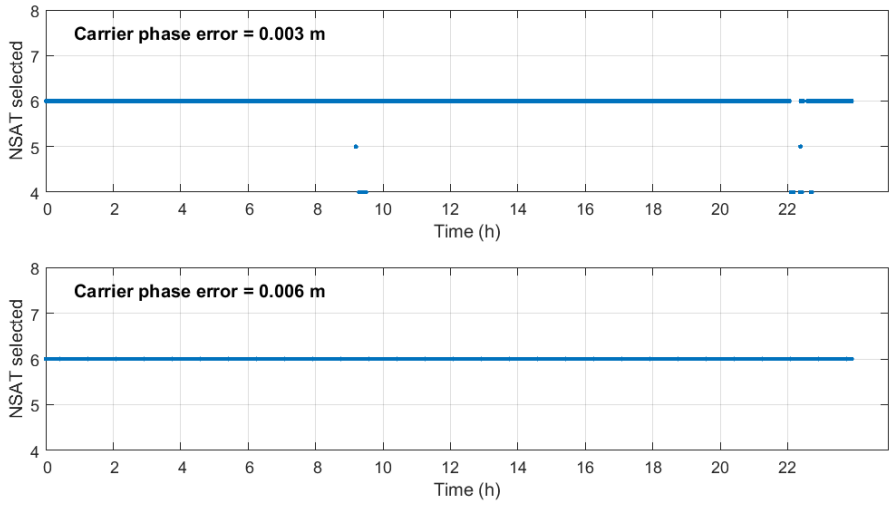

Figure 7.6 Comparison of the number of satellites used for 24-hour positioning out of six selected satellites from case 7. Top: the carrier phase error was set to 0.003 m, bottom: the carrier phase error was set to 0.006 m.

According to Table 5.4, satellites were selected by ten cases. Figures 7.7, 7.8, and 7.9 show the number of satellites used in positioning for all selected satellites in the ten cases. According to Figures 7.7, 7.8, and 7.9, the number of removed satellites was large in the first four cases compared to the others. As a result, the mean and median number of satellites used for positioning was often less than the number of selected satellites by one satellite. Whereas few numbers of satellites were excluded in cases 5 to 10. Thus, the exact number of selected satellites was mostly used in positioning. Apart from case 4, the maximum number of losing satellites can reach to 7 satellites. Figure 7.10 shows the number of satellites used in 24 hours positioning solution out of 10, 15, and 20 satellites selected from all cases. WGDOP selected satellites were mostly used in positioning in cases 5 – 8 because the WGDOP selection was the last selection.

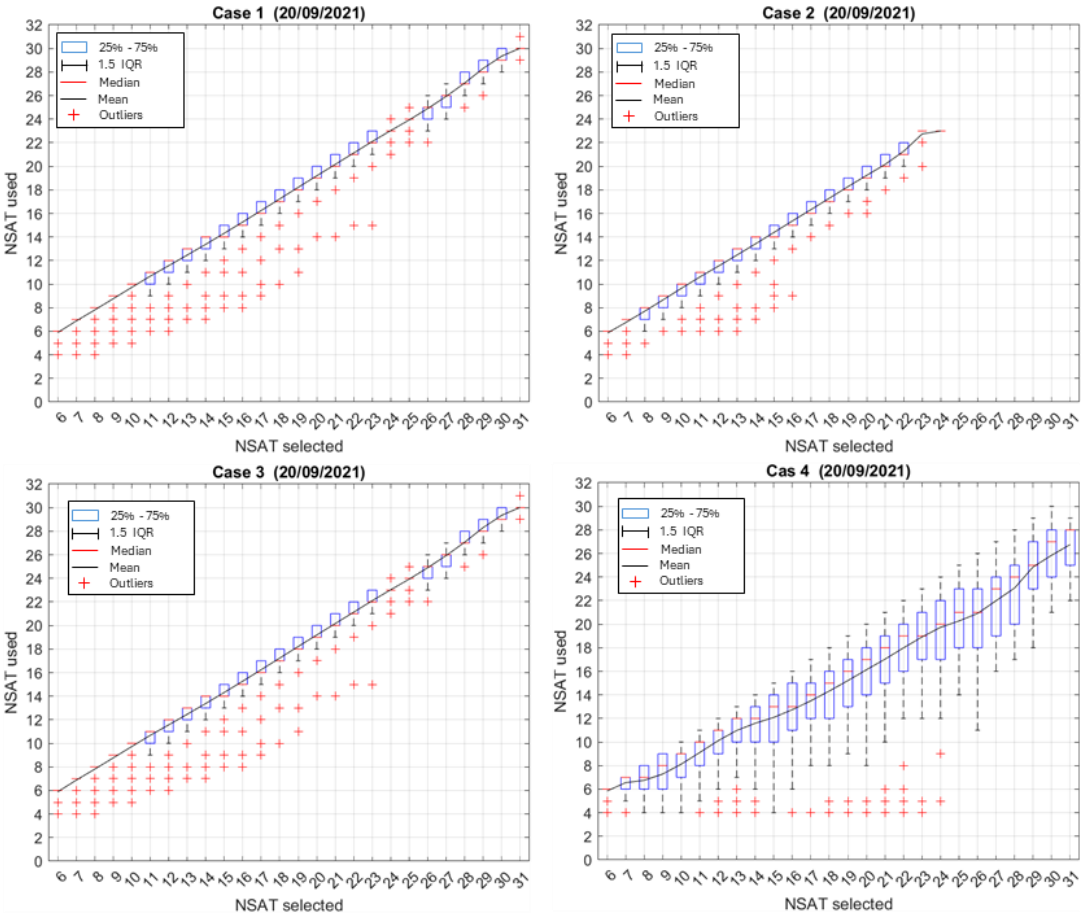

Figure 7.7 Number of satellites used in the 24-hour positioning solution from the selected satellites with all subset sizes. The satellites are chosen by the selection cases 1,2, 3, and 4.

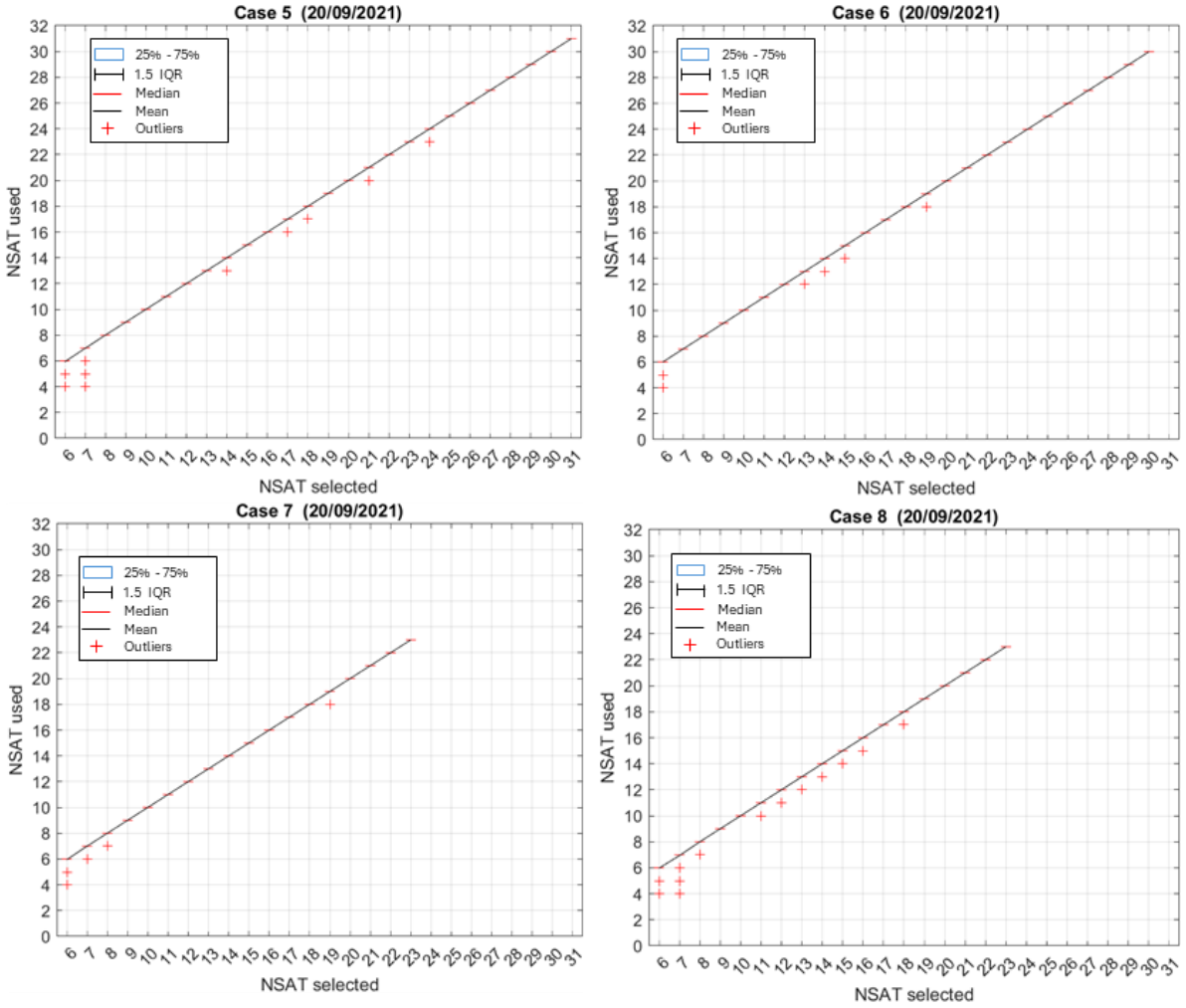

Figure 7.8 Number of satellites used in the 24-hour positioning solution from the selected satellites with all subset sizes. The satellites are chosen by the selection cases 5, 6, 7, and 8.

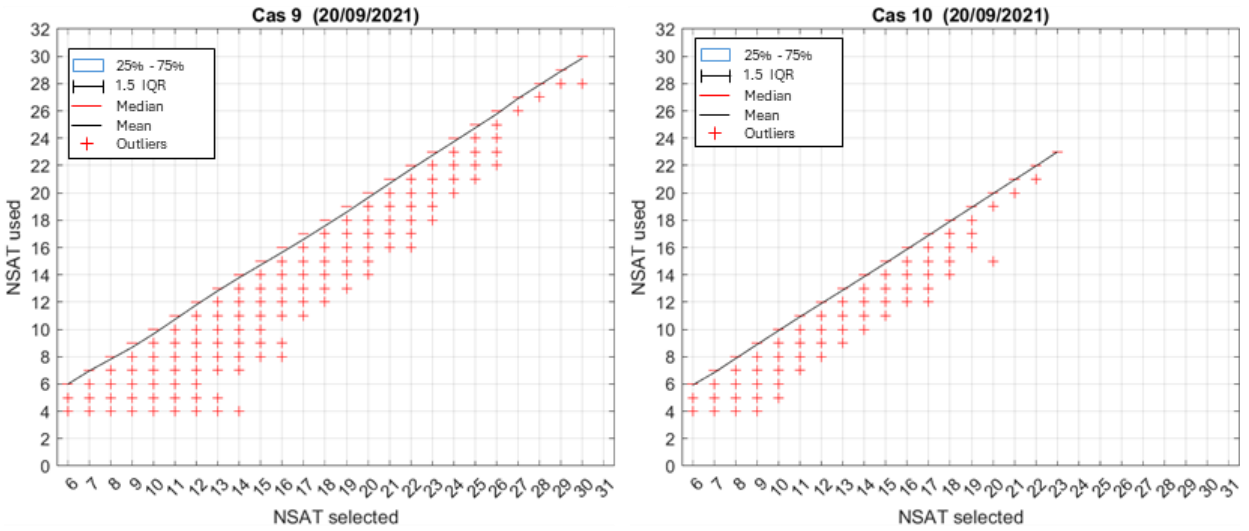

Figure 7.9 Number of satellites used in the 24-hour positioning solution from the selected satellites with all subset sizes. The satellites are chosen by the selection cases 9 and 10.

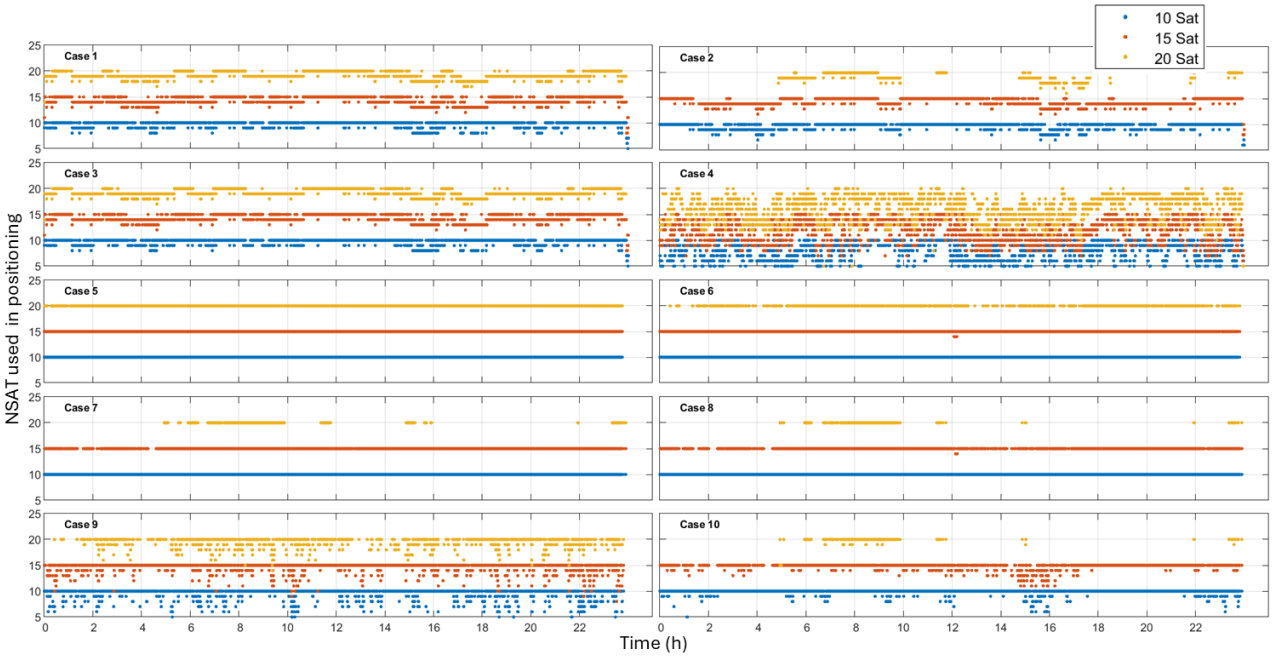

Figure 7.10 Time series of number of satellites used in 24 hours positioning solution from 10, 15, and 20 selected satellites from the ten cases.

7.1.2 Satellite Selection Status

Positioning accuracy is affected by various factors such as the quality of satellite geometry (GDOP) and measurement (code/phase). In addition, the system of used satellites can also affect positioning solution. Therefore, before evaluating the positioning quality of the selected satellites, their GDOP and WGDOP value were evaluated. In addition, the

continuity of the selected satellite combination, which affecting the carrier-phase's ambiguity resolution were also investigated. Finally, the system of selected satellites was displayed. As mentioned earlier, satellites were selected by different selection factors in ten cases although they were chosen mainly based on WGDOP. However, large number of WGDOP selected satellites were rejected in 6 cases (1-4 as well as 9 and 10). Thus, presenting the WGDOP selected satellites' status (GDOP, WGDOP, continuity, satellite system) is meaningless for these cases. As a result, the status of WGDOP selected satellites was shown only for the four cases 5 to 8, where the WGDOP selected satellites were mostly used in positioning solution.

7.1.2.1 GDOP/WGDOP

The optimal satellite subsets of 6 to max-observed satellites were selected for 2880 epochs, corresponding to 1 epoch per 30-sec interval, for the 24 hours. The quality of WGDOP improves as its value decreases, but no standards indicate how good the WGDOP value is. As a result, the GDOP value of the selected satellites were presented in Figure 7.11.

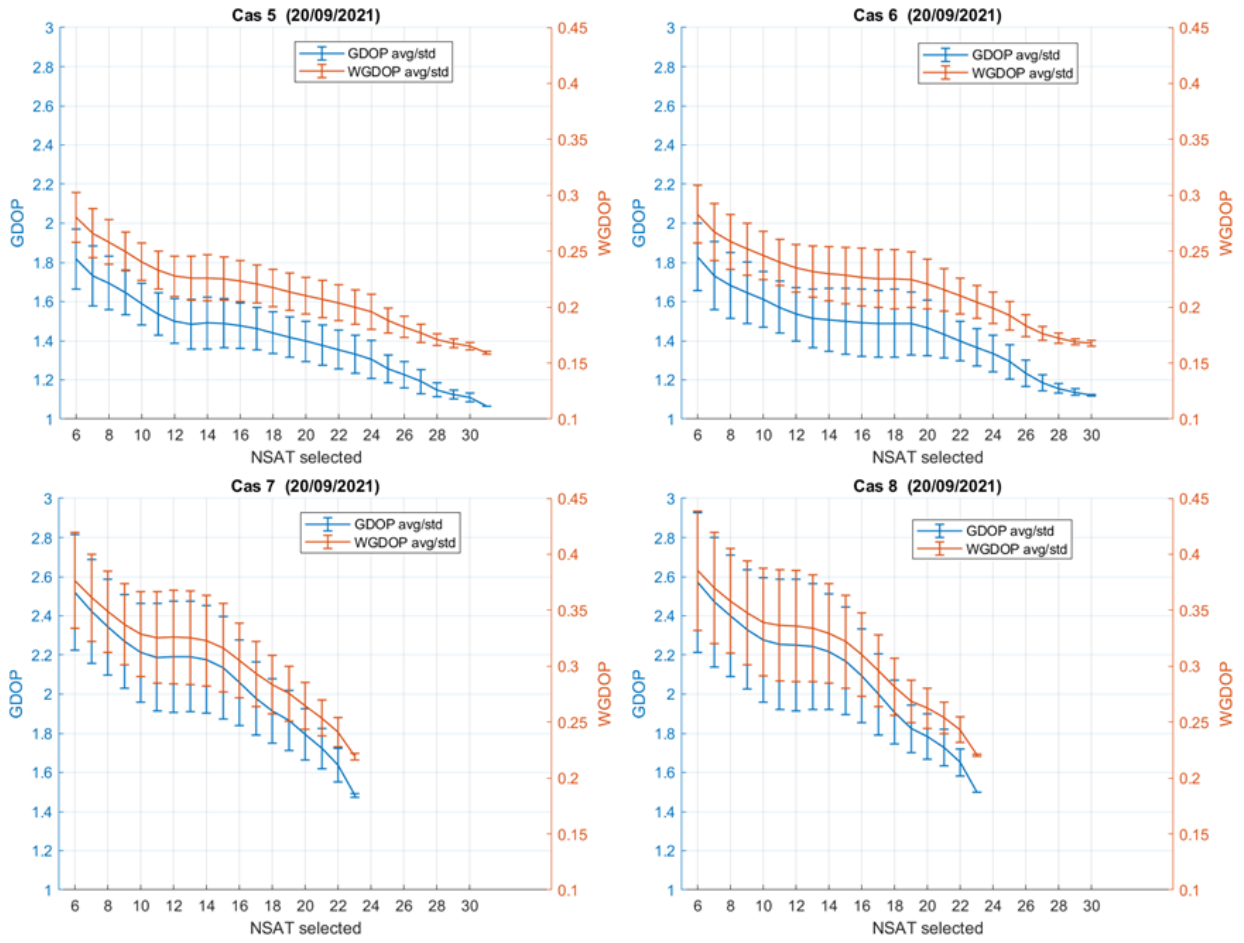

Figure 7.11 *Mean and stander deviation of the GDOP and WGDOP of the selected satellites with all possible subset sizes for 24 hours GNSS data (30 sec interval) collected over NGB2 on 20 September 2021. The value of selected satellite from cases 5, 6, 7 and 8 are only presented.*

Figure 7.11, presents the mean and the stander deviation (std) of WGDOP and GDOP for the selected subsets of six to maximum number of satellites observed. In the selection cases (5 – 8), the average and std of GDOP and WGDOP have a similar pattern as they improve (decrease) with the same rate as the number of satellites increases. Although satellite data were different in each case, the average and std of GDOP and WGDOP for the same number of satellites are almost the same in cases 5, and 6. In addition, it was the same in cases 7, and 8. To illustrate, in cases 5 and 6, the average value of GDOP and WGDOP for the optimal subsets of 6 to 30/31 satellites decrease from about 1.8 to 1.1 and from 0.27 to 0.16, respectively. In cases 7 and 8, the average value of GDOP and WGDOP for the optimal subsets of 6 to 23 decrease from about 2.5 to 1.5 and from 0.37 to 0.22, respectively. In terms of GDOP and WGDOP std, it was mostly the same for cases 5 and 6, as well as for cases 7 and 8. The difference between each pair in the std of GDOP for the same number of selected satellites is about 0.1, while is about 0.01 in the std of WGDOP.

Satellite geometry (GDOP) improves when using satellite at low elevation angles. Thus, GDOP and WGDOP values in cases 5, and 6 are lower (better) than those in cases 7, and 8 that used elevation angle mask (15^{o}). However, the variation between them is small and get smaller as the number of satellites increases. The differences between the average GDOP value for the same number of satellites (6, 17, and 23) is 0.7, 0.5 and 0.3, respectively.

7.1.2.2 Constellation Continuous

The optimal satellites were selected for 2880 epochs, and they were chosen separately for each epoch. They were selected without considering the continuity of selected satellites subset over time. Therefore, the optimal satellites can vary significantly from sequence epochs. Figure 7.12 displays the number of epochs having continuous optimal satellite subset (i.e., continuous epochs) for all selected satellites in cases 5 to 8. In addition, it shows the rate of these continuous epochs out of total number of epochs used in positioning solution. The selected optimal satellite subset was considered a continuous when the exact subset was selected in the pervious epoch.

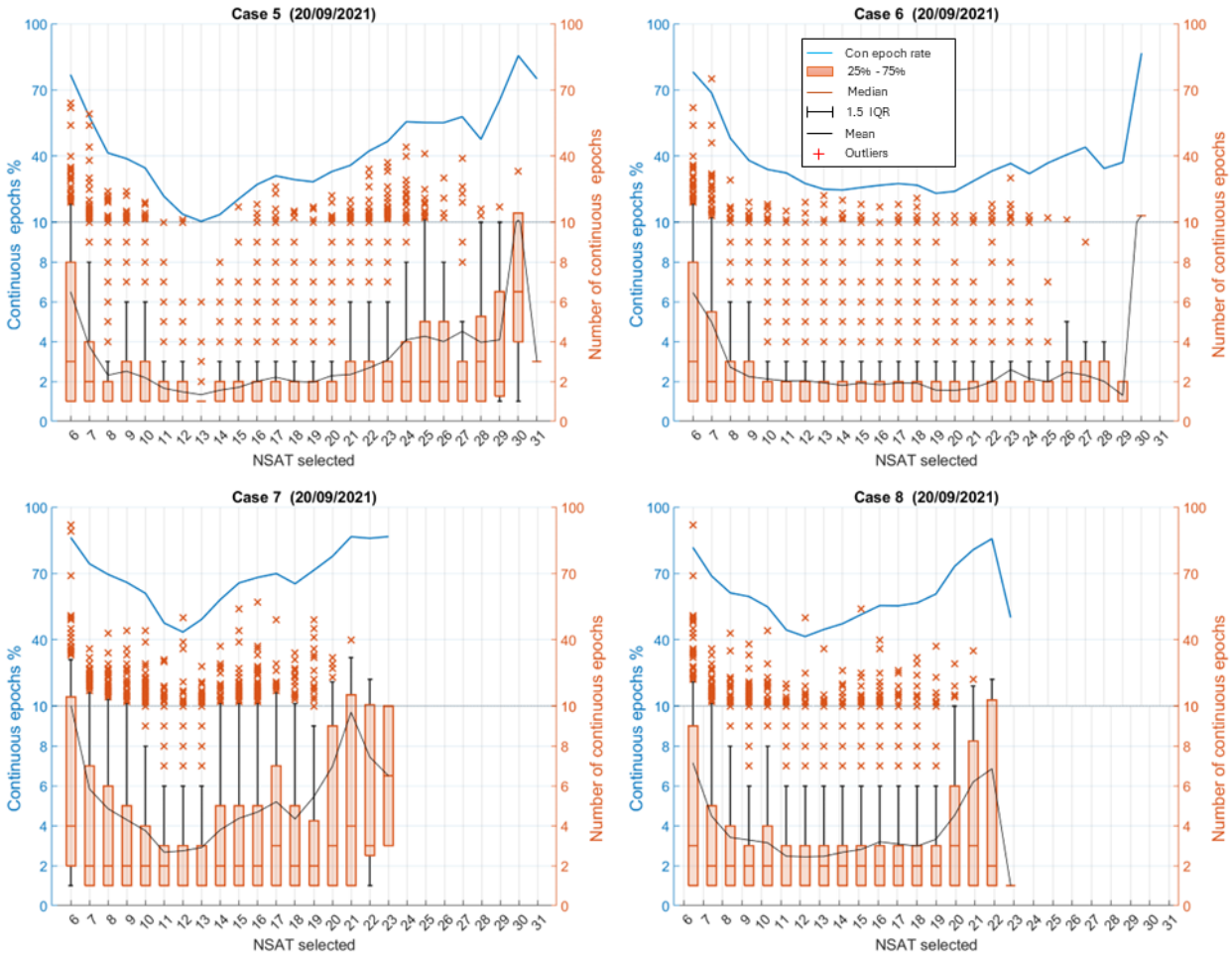

Figure 7.12 The number and the rate of continuous selection epochs from the selection cases 5, 6, 7, and 8 using 24 hours GNSS data collected on 20 September 2021.

Figure 7.12 shows similarity between the selection cases 5 and 6, as well as between the cases 7 and 8. The percentage of continuous epochs is less than 40% for the most satellite subset sizes in cases 5 and 6. In contrast, its value is more than 40% for all satellite subset sizes in cases 7 and 8. Furthermore, the number of continuous epochs in cases 7 and 8 are larger than those in the cases 5 and 6. For most satellite subset sizes, the average number of continuous epochs is about 2 in cases 5 and 6, and it is over than 2 in cases 7 and 8. Compared to cases 5 and 6, satellite elevation angle (15º) was used in cases 7 and 8. Thus, it can be considered it the reason for increasing the rate and number of continuous epochs in them.

Despite the difference between the four cases in rate or number of continuous epochs, they form a U-shape in the four cases. For example, the rate of continuous epoch was more than 70% for the six and maximum number of selected satellites, while it was less than 70% for the middle number of selected satellites in the four cases. Satellite data were collected from

three satellite systems (GPS, GLONASS, and Galileo). The time difference between these satellite systems was considered when selecting the optimal satellites by calculating the geometry matrix (*H*) using Equation (3.8) This supports the existence of more than one satellite of a system in the optimal satellite subset (Figure 7.13). As a result, this can be the reason for maintaining the same optimal satellite subset for larger number of sequential epochs, especially for the subset with a small number of satellites such as 6 and 7. On the other hand, the optimal satellite subset of larger and maximum number of selected satellites stayed langer because they were the only combination with that number of satellites.

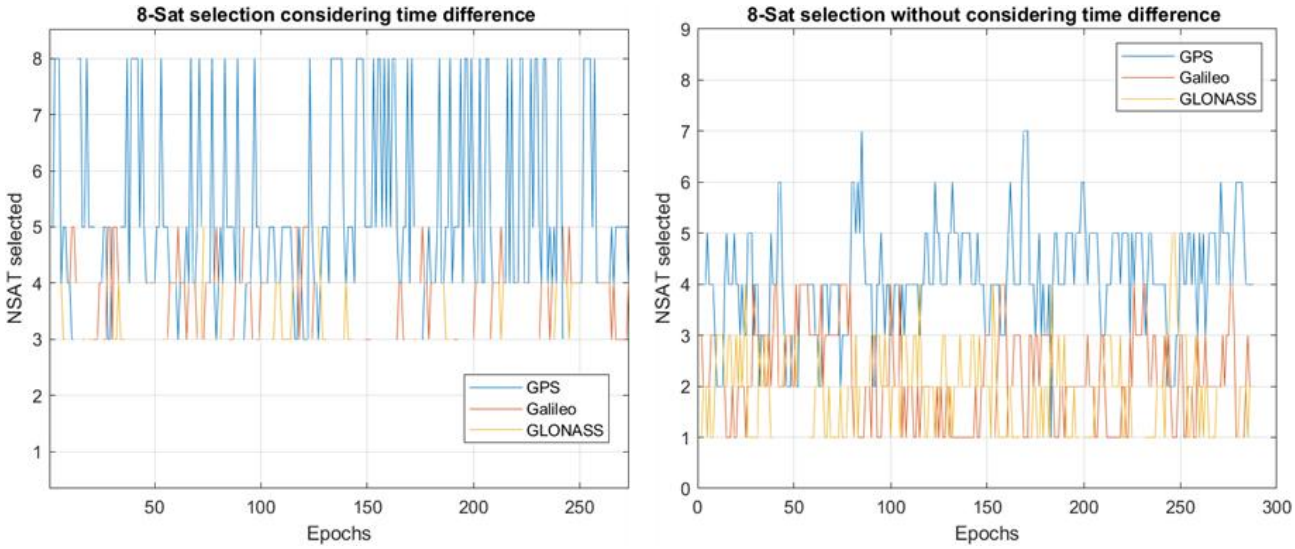

Figure 7.13 Comparison of selecting 8 satellites with (left) and without (right) considering the time difference between satellite systems.

The optimal satellites were selected separately for each epoch based on WGDOP without considering the continuity of the optimal satellite subset. Therefore, it is expected choosing different satellites combinations from one epoch to another due to the change of satellites' location and signal power over time. Figure 7.14 shows the difference in the WGDOP (fitness) value between the current and the pervious epochs' optimal satellite subset. Over the entire selection, the WGDOP value of the optimal satellites in the current and previous epochs was computed based on satellite information in the current epoch. The WGDOP value of the current epoch's optimal satellites subtracted from that of the previous epoch's optimal satellites. Satellites were selected based on WGDOP value, which is considered better when it decreases. Thus, the fitness of current epoch's optimal satellites is better than the old if the subtraction result is positive and vice versa.

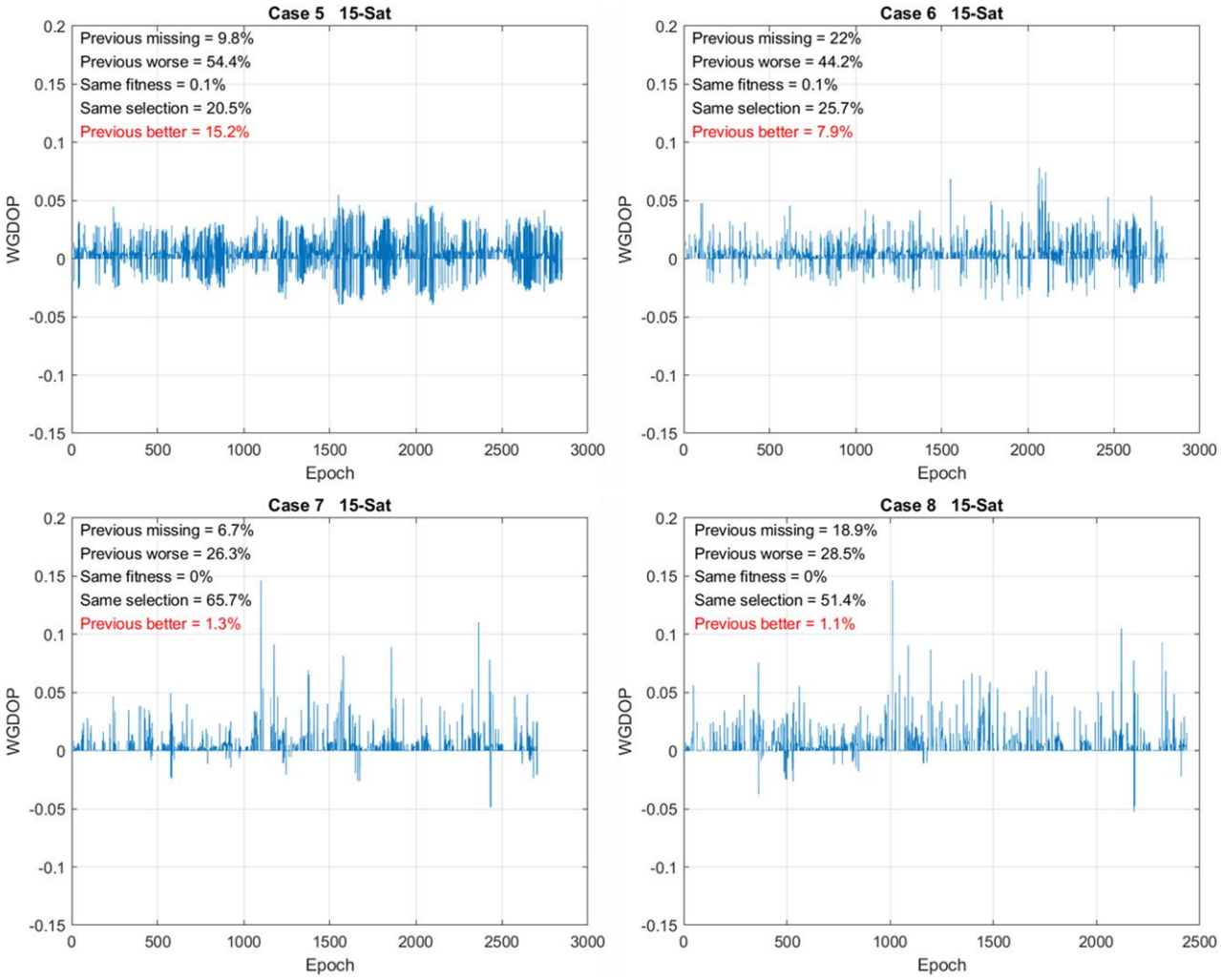

Figure 7.14 Comparison between the current and previous epochs' optimal subset of 15 selected satellites in their WGDOP value, using the current epoch's satellite information. The WGDOP value of the current epoch's optimal satellite subset was subtracted from that of the pervious epoch.

According to Figure 7.14, the current epoch's optimal satellite subset changed from the previous due to four reasons:

1) losing previous optimal satellite subset,
2) reduction the fitness of previous optimal satellite subset,
3) replacing previous optimal satellite subset with an equivalent one,
4) miss-selection.

The previous epoch's optimal satellite subset was missing in the later epoch, leading to choose another subset as the optimal. Since new satellite subset can be created by changing one satellite in a subset, losing previous epoch's optimal satellites can be due to the loss of one satellite. Thus, the new optimal satellite subset could differ from the previous by only one satellite. Over selection, the pervious epoch's optimal satellite subset was missing less than 10% in cases 5 and 7, while it was around 20 % in cases 6 and 8. KFITH

was applied in both cases 6 and 8. This could be the main reason why the missing rate of the previous subset of selected satellites increased to about 10%.

Satellites travel over time, leading to change their location and signal power through time. Thus, the fitness (WGDOP) value of the same satellite subset varies over time. The fitness (WGDOP) of previous epoch's optimal satellite subset was not the best in the later epoch, so another satellite subset with better fitness was chosen the optimal. This occurred most of the time during the selection in cases 5 and 6, as it happened more than 44%. In the other two cases 7 and 8, the optimal satellite subset changes from the previous due to decrease subset fitness with less rate 26.3 and 28.5%, respectively. This is due to the use of a 15° elevation mask in cases 7 and 8, where satellites with low elevation angles, which are more vulnerable to multipath and atmospheric errors, were not considered.

Since satellites were selected based on WGDOP without considering continuity, the previous epoch's optimal satellite subset was replaced by another subset has an equivalent fitness (WGDOP) value. This occurred only in cases 5 and 6 with few rates (0.1%).

Finaly, the current optimal satellites were miss-selected. Although the previous optimal satellite subset had better fitness (WGDOP) value, less quality satellite subset was chosen as the optimal. Over selection, this happened 15.2%, 7.9%, 1.3%, and 1.1% in cases 5 – 8, respectively. The main reason for this is efficiency of selection technique, i.e., optimization algorithm (ABC). The rate of miss-selection was significantly lower in the last two cases 7 and 8 because the selection difficulty was less. In both cases 15-degree elevation mask was used this lead to reduce the total number of satellites, consequently, decrease the selection difficulty.

As mentioned earlier, the previous epoch's optimal satellite subset could be loss and change by one satellite. Figure 7.15 shows the number of satellites in subset that differ from the previous epoch's optimal satellites subset. According to Figure 7.15, the number of changed satellites in the four cases is about the same. It is generally no more than 2 in all four cases. The maximum number of changed satellites is around 8 satellites for the most satellite subset sizes in the four cases.

Nonetheless, the number of changed satellites in cases 5 and 6 is slightly higher than that in cases 7 and 8 by few satellites. For example, the mean number of changed satellites of 13 selected satellites is 3, 2, 1, and 1 in cases 5, 6, 7, and 8, respectively. The maximum number of changed satellites of 13 selected satellites is 10, 10, 6, and 7 in in cases 5, 6, 7, and 8, respectively.

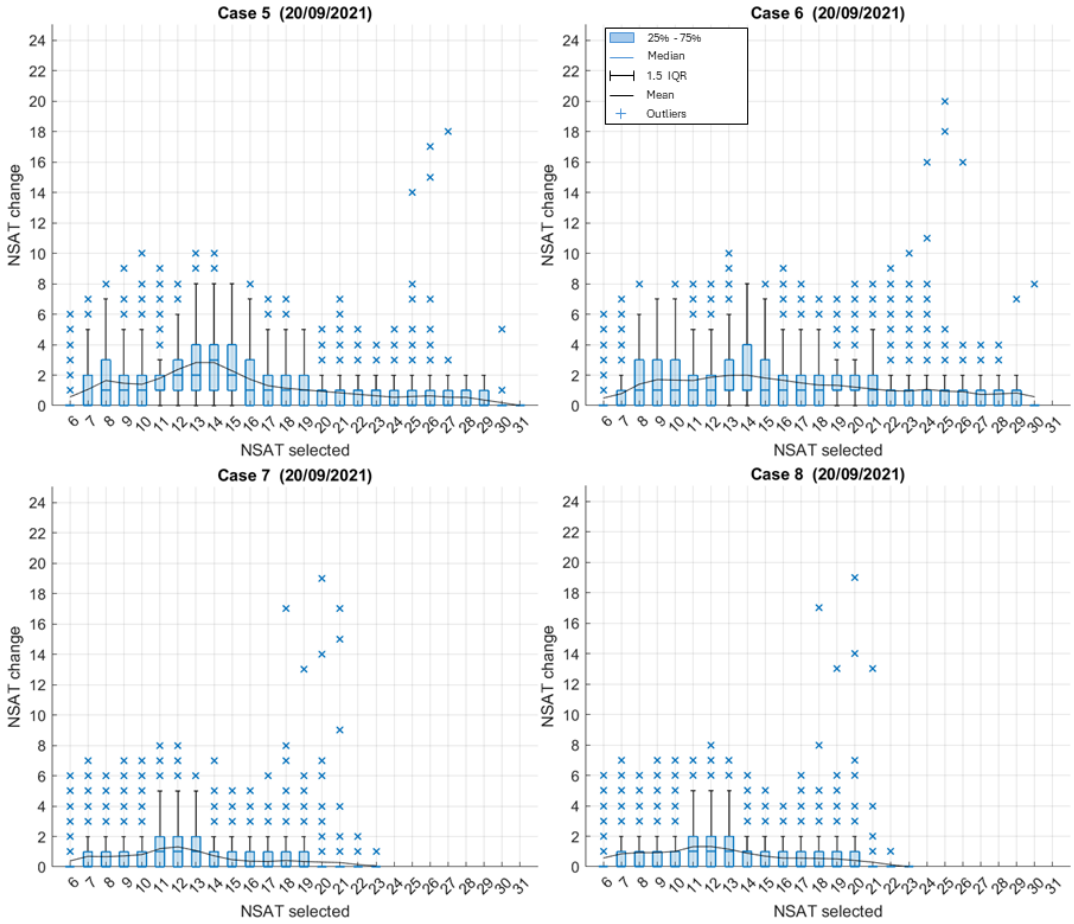

Figure 7.15 The number of satellites changed in the selected optimal subset over selection from the selection cases 5, 6, 7, and 8 using 24 hours GNSS data collected on 20 September 2021.

7.1.2.3 Satellite System Used

Three satellite systems (GPS, GLONASS, and Galileo) were tracked during the day (20/09/2021). Figure 7.16 illustrates the overall reliance on each system to form the optimal satellite subset in the four selection cases. The figure presents the average and standard deviation of the number of satellites from each system (GPS, GLONASS, and Galileo) that were included in the optimal subsets over 2880 epochs. In addition, it indicates the percentage of using the satellite system to form the optimal satellite subset over the total number of epochs (selection) for each satellite subset size. The contribution of the satellite system considered by one satellite.

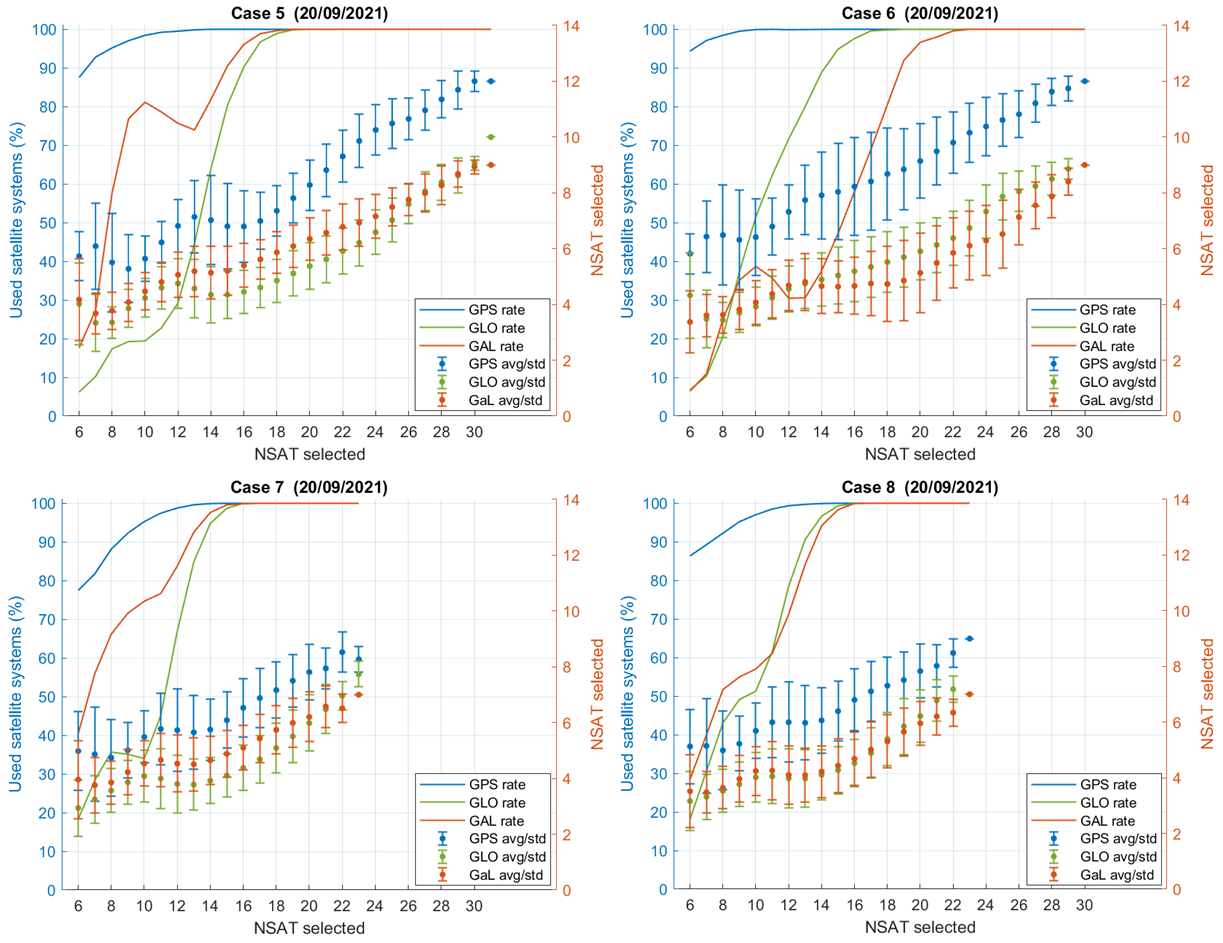

Figure 7.16 The mean and stander deviation of number of GPS, GLONASS, and Galileo satellites selected to form the optimal subsets with different sizes. The rate of using the system of satellite over the entire selection is also presented. Selected satellites from selection cases 5, 6, 7, and 8 are only presented. 24 hours GNSS data collected over NGB2 on 20 September 2021 are used.

Overall, GPS satellites were highly selected to form the optimal satellite subsets in the four selection cases. This can be seen from the percentage of using GPS satellites in the optimal satellite subset, and it was high for all satellite subset sizes with no less than 88% in all selection cases. In addition, the average number of GPS satellites used to form optimal satellite subsets was higher than other systems in all satellite subset sizes and in the four cases. This is because the number of GPS satellites observed was more than other two systems, as shown in Figure 5.7. On the other hand, the reliance on the GLONASS and Galileo satellite systems was approximately the same in terms of number of satellites. However, Galileo satellites were selected in more epochs than GLONASS. Galileo satellites were chosen more than GLONASS in two cases (5 and 7) out of the four and were chosen equally with GLONASS in case 8.

7.1.3 Positioning

In the ten selection cases (Table 5.4), the optimal satellites were selected in different number of satellites ranges from 6 to maximum number of satellites observed. To evaluate the quality of the ten selection cases in PPP selection, the PPP solution using the selected satellites from the ten cases was determined and presented. The positioning accuracy and precision of the selected satellites in the three directions (selE, selN, and selH) were illustrated. Their positioning availability (PAva) and the optimal positioning availability (OPAva), which can affect the positioning quality, are also shown. In order to assess the PPP solution of the selected satellites, it was compared with the original PPP solution, which included all satellites, a 15-degree elevation mask, RAIM, and KFITH (30-meter threshold).

The positioning solutions (accuracy and precision) of the selected satellites in the three directions (selE, selN, and selH) are presented as blue lines corresponding to left y-axis. Their PAva and OPAva are presented with red lines corresponding to right y-axis. To facilitate the comparison between the positioning solutions (accuracy and precision) of selected satellites with different subset sizes and the original PPP in the three directions (orgE, orgN, and orgH), the original PPP positioning solutions were presented with a green line starched over the selected satellites with different numbers (x-axis).

To have readable figure and clear presentation, the positioning solutions of the selected satellites from ten cases was divided into three figures. The first figure shows positioning solutions of the first 4 cases, where satellites were selected based on WGDOP before RAIM/RAIM-KFITH. The second figure covers the next 4 cases, selecting satellites based on WGDOP after RAIM/RAIM-KFITH. The third figure shows the last 2 cases, selecting satellites by RAIM/RAIM-KFITH before and after the WGDOP-selection.

- **Positioning solutions of cases 1, 2, 3, and 4**

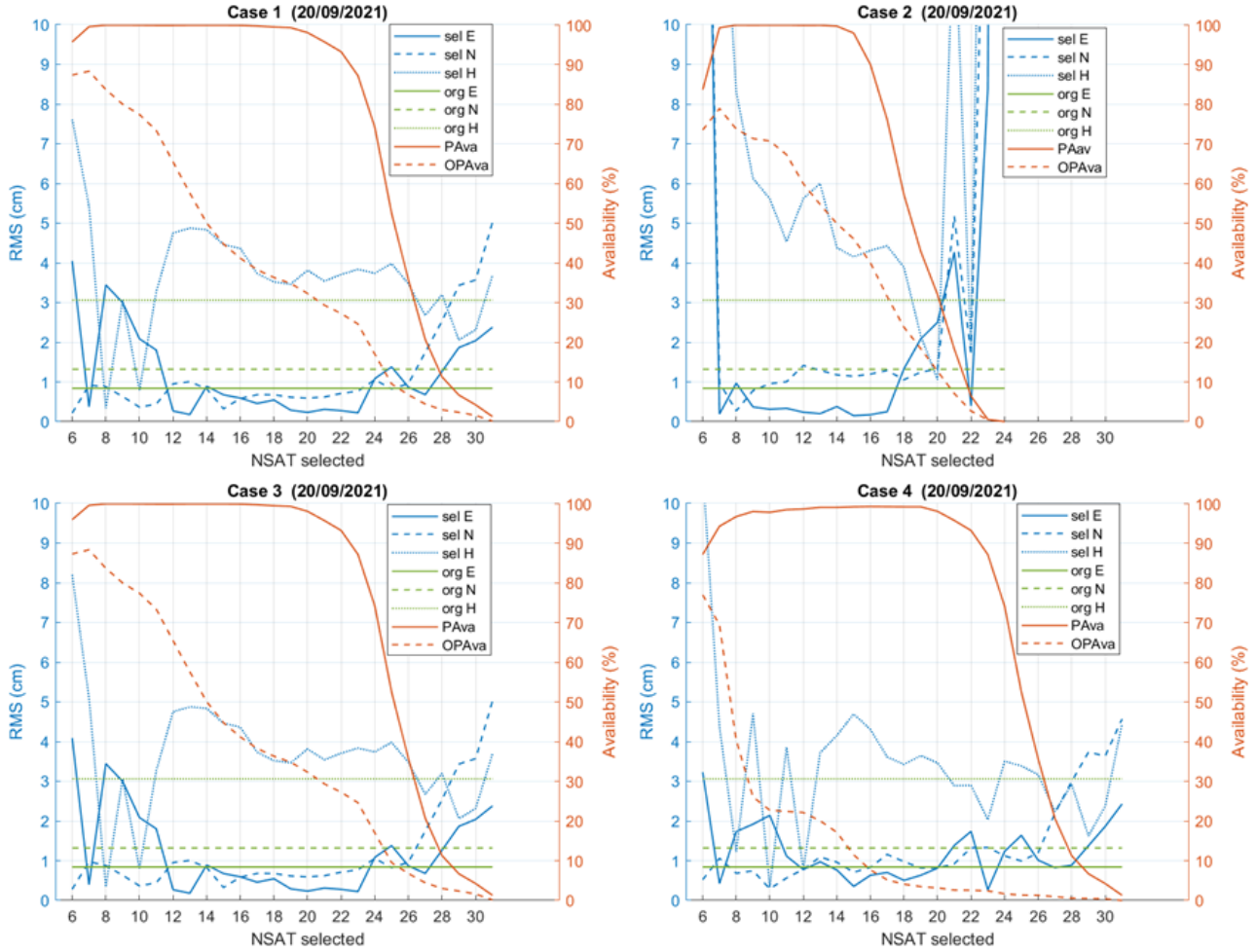

Figure 7.17 Comparison of the positioning accuracy of selected satellites from cases 1, 2, 3, and 4 with respect to the original PPP (all satellites). The life y-axis expresses the position accuracy of the selected satellites (blue) and original PPP (green). The right y-axis expresses the positioning availability of the selected satellites (red).

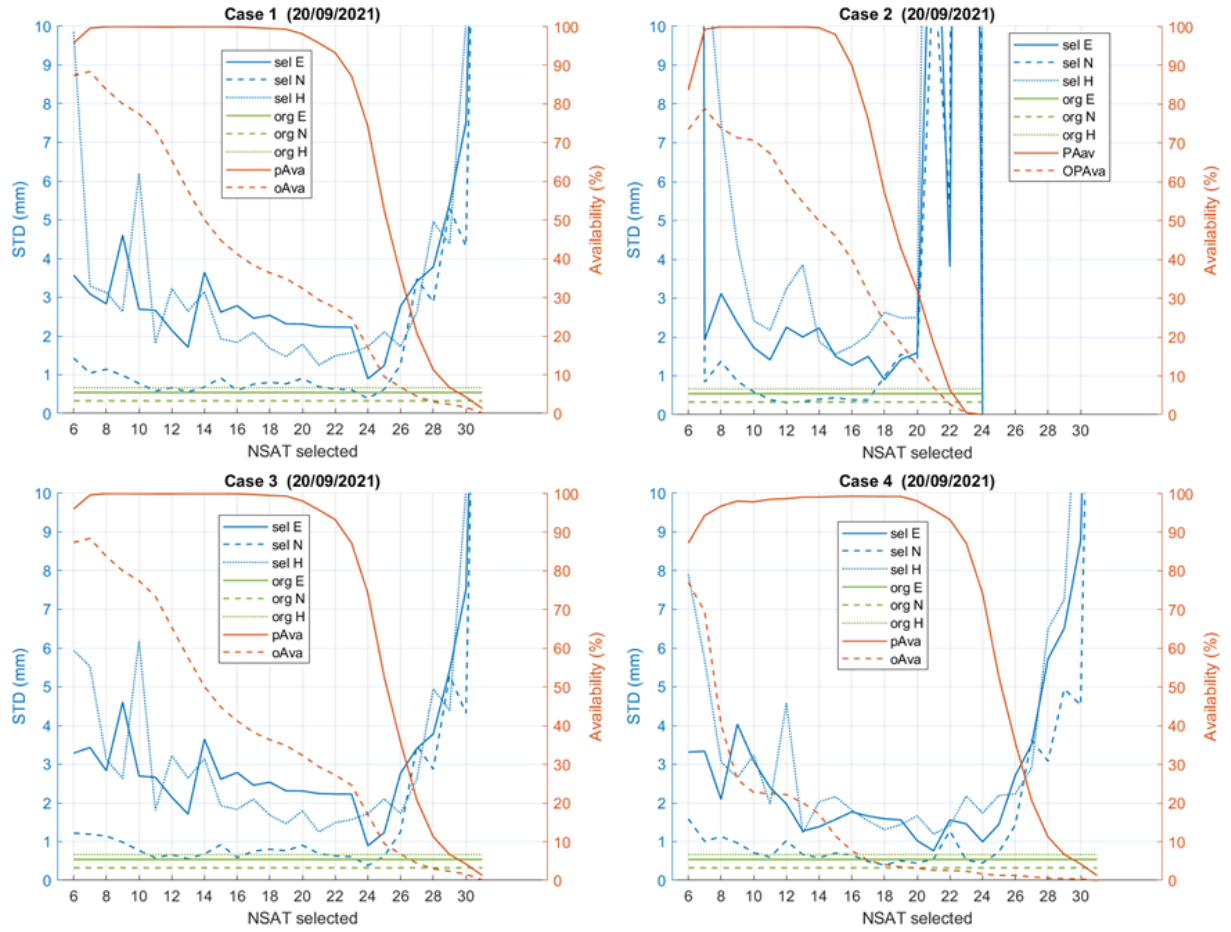

Figure 7.18 Comparison of the positioning precision of selected satellites from cases 1, 2, 3, and 4 with respect to the original PPP (all satellites). The life y-axis expresses the position precision of the selected satellites (blue) and original PPP (green). The right y-axis expresses the positioning availability of the selected satellites (red).

The positioning solutions of the selected satellites from cases 1, 2, 3, and 4 are presented Figure 7.17 and Figure 7.18, which indicate the positioning accuracy and precision, respectively. The common between these selection cases is satellites were selected by WGDOP before they be filtered by RAIM/RAIM-KFITH. Whereas these selection cases differ from each other by selecting satellites as follows: WGDOP-only, Ele-WGDOP, WGDOP-RAIM, and WGDOP-RAIM-KFITH, respectively.

Despite the selection variation in these selection cases, the cases' results have common pattern. The positioning solutions (accuracy and precision) of their selected satellites (blue lines) are unstable. In the same selection case, the positioning solutions change significantly as the number of selected satellites changes by one satellite, especially between the smallest and largest number of selected satellites. In general, it can be notice that the positioning accuracy and precision of the middle number of selected satellites is better than those of the smallest and the largest number of satellites. Furthermore, the

OPAva , indicating the rate of using the exact selected satellites in positioning solution, is noticeably low, indicating the low selection quality.

Because of the differences in selection for each case, the above common pattern has a different rate between cases 1, 2, and 4. However, they are same in cases 1 and 3 even though RAIM is considered in case 3, as shown in Figure 7.19. This is aligned with what Angrisano et al. [226] and Zhang and Wang [222] stated, that RAIM-snapshot (used in RTKLIB) is not suitable for PPP.

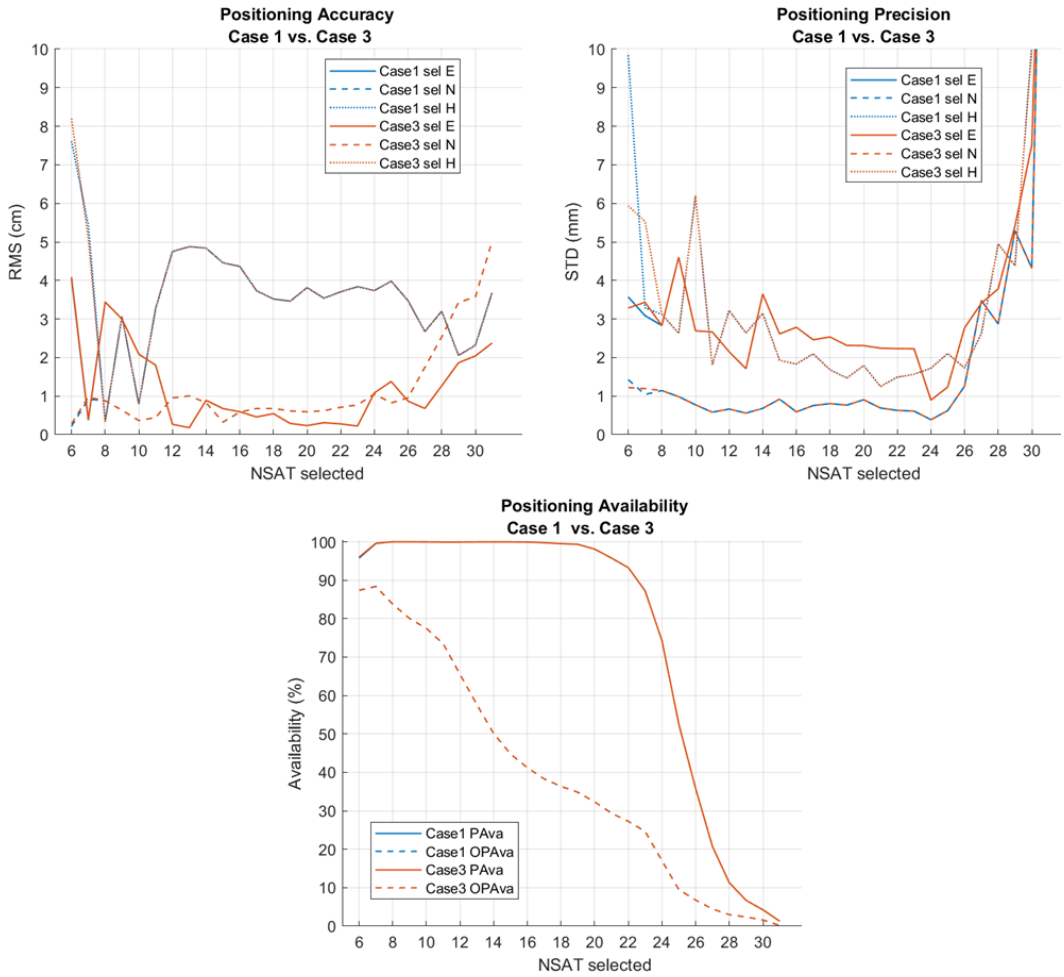

Figure 7.19 Comparison of the positioning accuracy, precision, and availability between cases 1 and 3.

Figure 7.17 and Figure 7.18 show the positioning solutions of the original PPP (green lines) along with that of the selected satellites (blue lines). The quality of positioning results of the selected satellites from the four cases can be evaluated by comparing them with that of the original PPP, using all satellites, a 15-degree elevation mask, RAIM, and KFITH with 30-meter threshold. Since the middle number of selected satellites in the above four cases provide the better and more stable results, their results were compared to original PPP.

Overall, the original PPP provided better vertical positioning accuracy, but worse horizontally positioning (easting and northing) accuracy compared to selected satellites. In precision, the original PPP had better results in three directions than the middle number of selected satellites. The middle number of selected satellites with most stable results.

Figure 7.20 and Figure 7.21 (below) illustrate the amount of differences in positioning solution between the original PPP and these middle number of selected satellites (12, 13, 14, 15 ,and 16) in the four cases. The positioning solutions (accuracy and precision) of original PPP subtracted from that of the selected satellites. If the product is positive, the positioning solution for the selected satellites is worse than the original PPP and vice versa. Based on the

Figure 7.20 and Figure 7.21, the exact difference in positioning solutions between the original PPP and the middle number of selected satellites (12-16) can be determined, which is no more than about 2 cm and 4 mm in accuracy and precision. Furthermore, the difference of the positioning solutions between the selected satellites from cases can be indicated. It is noticed that they are generally close to each other, with no more than around 4 cm in positioning accuracy, and 4 mm in precision.

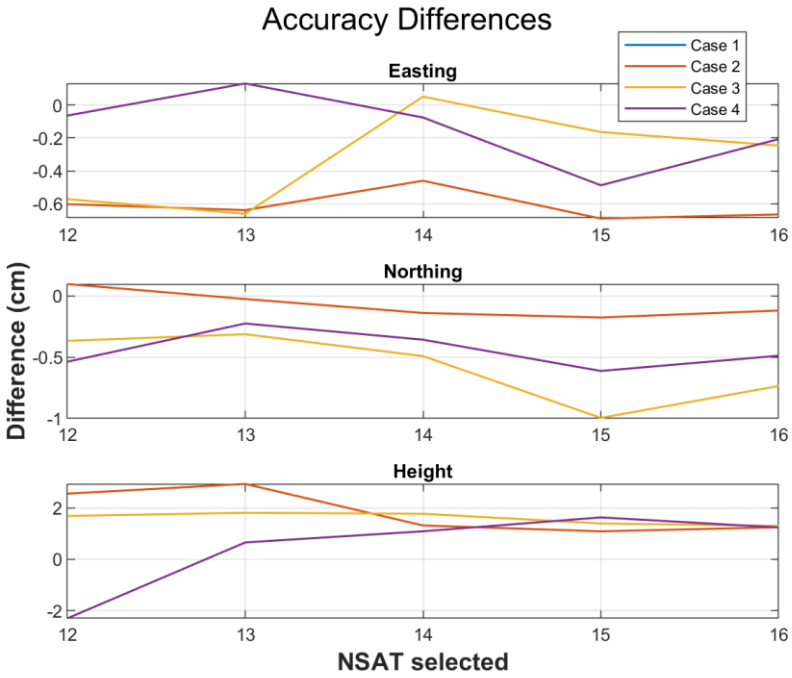

Figure 7.20 The differences of positioning accuracy between the original PPP and the selected satellites (12, 13, 14, 15 and 16) from cases 1, 2, 3, and 4.

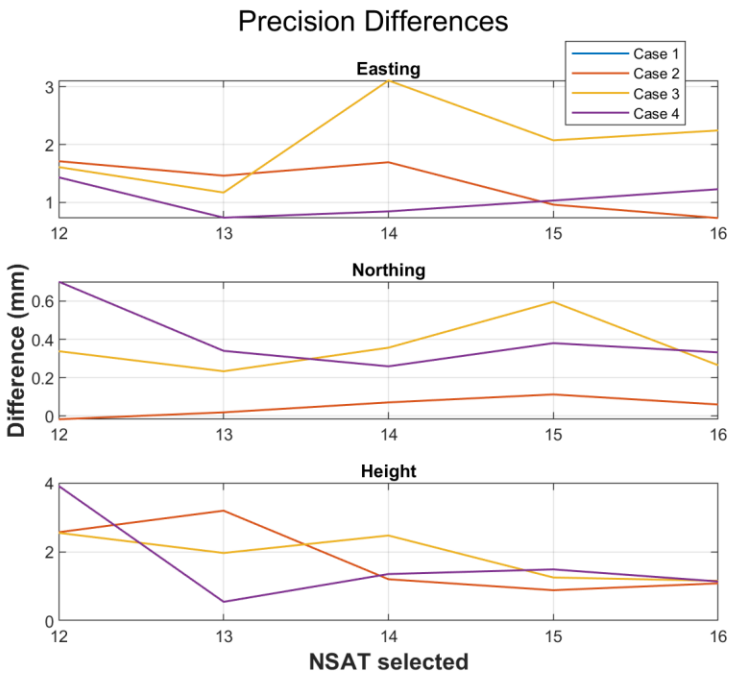

Figure 7.21 The differences of positioning precision between the original PPP and the selected satellites (12, 13, 14, 15 and 16) from cases 1, 2, 3, and 4.

- **Positioning solutions of cases 5, 6, 7, and 8**

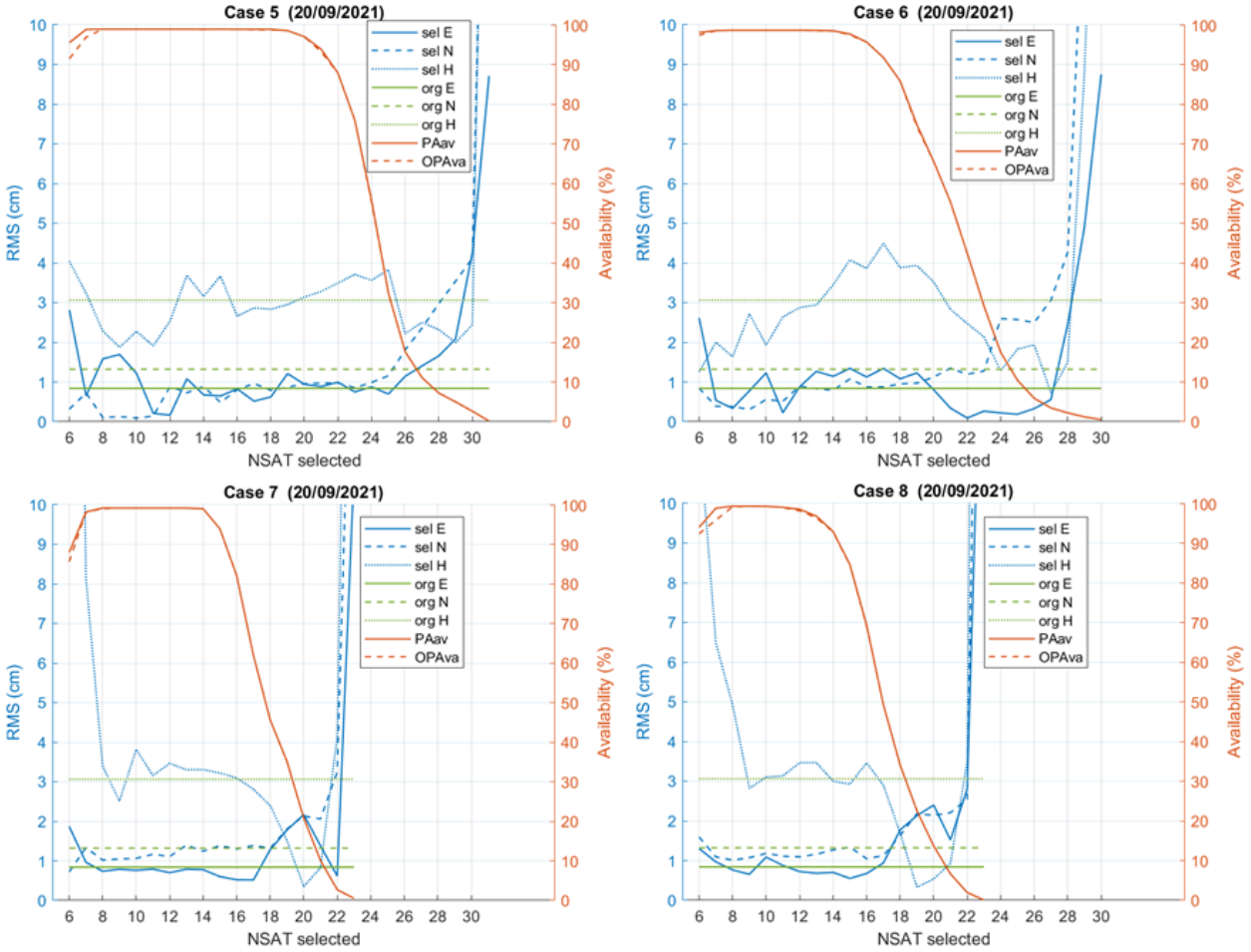

Figure 7.22 Comparison of the positioning accuracy of selected satellites from cases 5, 6, 7, and 8 with respect to the original PPP (all satellites). The life y-axis expresses the position accuracy of the selected satellites (blue) and original PPP (green). The right y-axis expresses the positioning availability of the selected satellites (red).

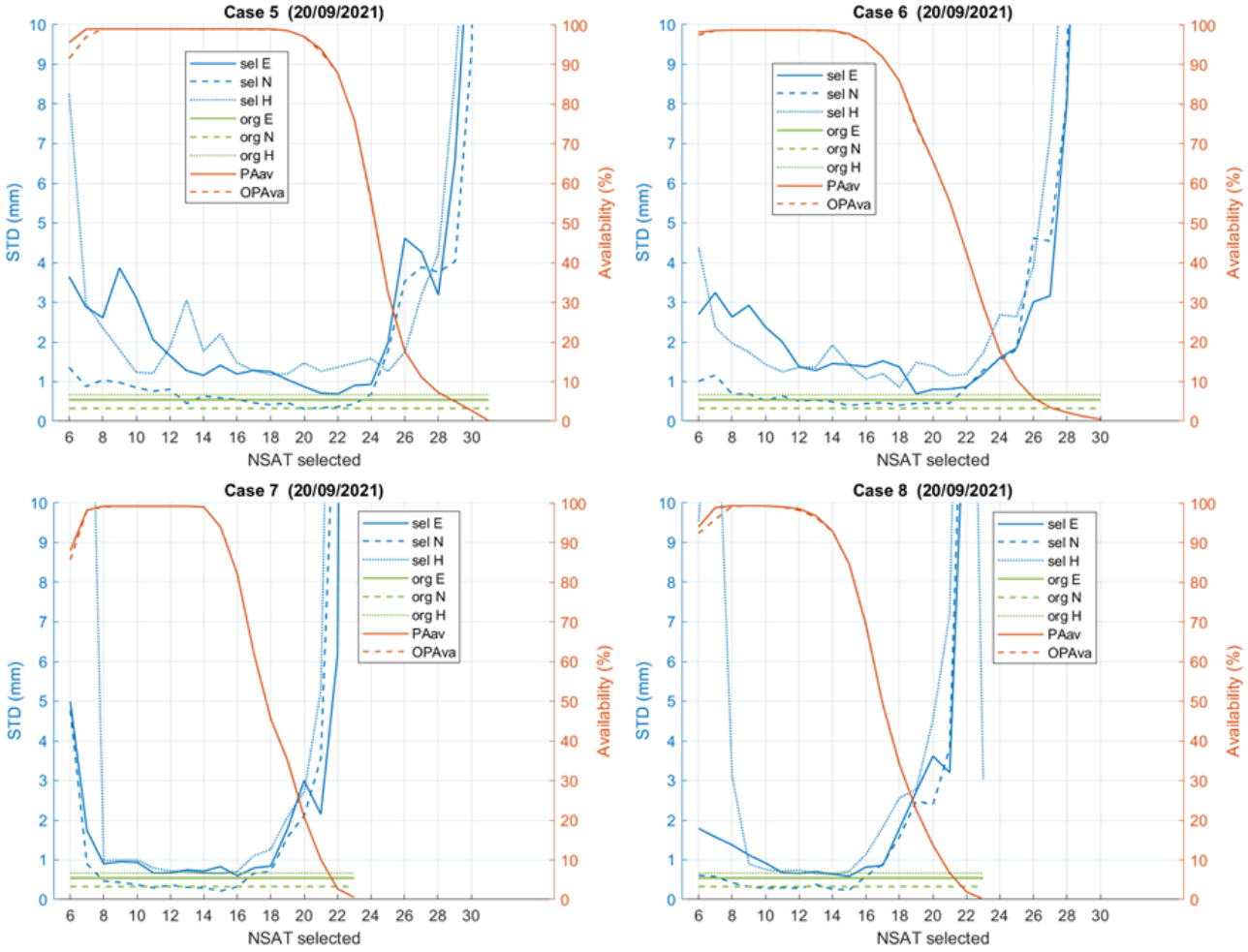

Figure 7.23 Comparison of the positioning precision of selected satellites from cases 5, 6, 7, and 8 with respect to the original PPP (all satellites). The life y-axis expresses the position precision of the selected satellites (blue) and original PPP (green). The right y-axis expresses the positioning availability of the selected satellites (red).

Figure 7.22 show the positioning accuracy of the selected satellites from cases 5, 6, 7, and 8. Figure 7.23 illustrates the precision of the positioning solutions of these selected satellites. The common between the four selection cases (5, 6, 7, and 8) is satellites were selected by WGDOP after RAIM/RAIM-KFITH selection as follows: RAIM-WGDOP, RAIM-KFITH-WGDOP, Ele-RAIM-WGDOP, and Ele-RAIM-KFITH-WGDOP, respectively.

According to Figure 7.22 and Figure 7.23, the OPAva is mostly aligned with the corresponding PAva over all satellite subset sizes at the four selection cases 5, 6, 7, and 8. This means that the satellites selected by these selection cases have been used in the positioning solution, indicating the selection quality. In terms of positioning accuracy and precision of the selected satellites (blue lines), they vary from one case to another. Overall, those of the small and the large number of selected satellites are fluctuated. Whereas the positioning

solutions of the middle number of satellites are more stable, especially those in cases 7 and 8.

Focusing on the middle number of satellites, their positioning accuracy in cases 5 and 6 are generally close to that of original PPP. However, their positioning precision are clearly worse than original PPP. On the other hand, the positioning accuracy and precision of the middle number of satellites from cases 7 and 8 are equivalent to the original PPP. To evaluate the differences, the original PPP solution was subtracted from the solutions of 12 to 16 selected satellites in cases 5 to 8.

Figure 7.24 shows the difference in positioning accuracy, while positioning precision presented in Figure 7.25. According to the figures, the variation between the original PPP and the middle number of satellites no more than about 1cm and 2 mm in positioning accuracy and precision respectively. The difference between cases results no more than about 1.5 cm in positioning accuracy, and 2 mm in precision.

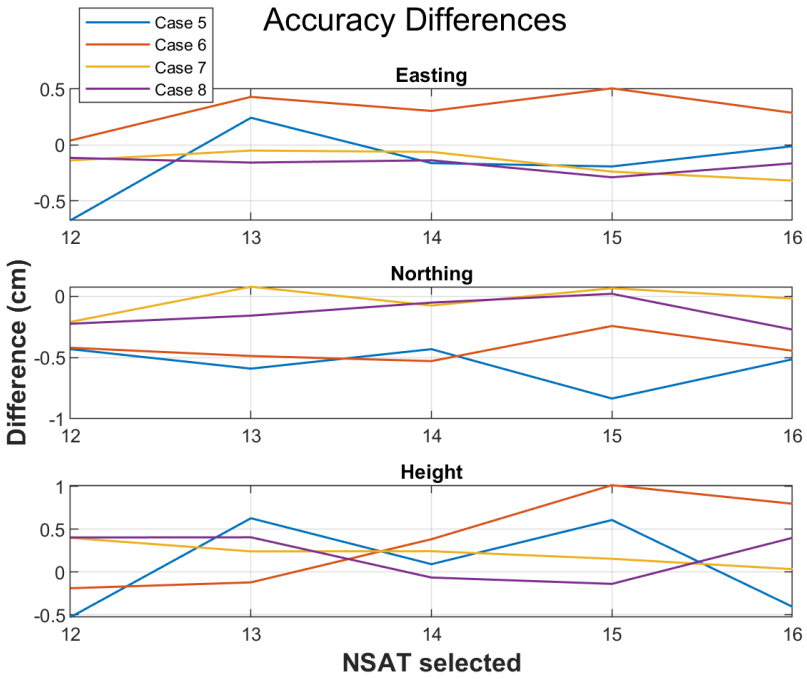

Figure 7.24 The differences of positioning accuracy between the original PPP and the selected satellites (12, 13, 14, 15 and 16) from cases 5, 6, 7, and 8.

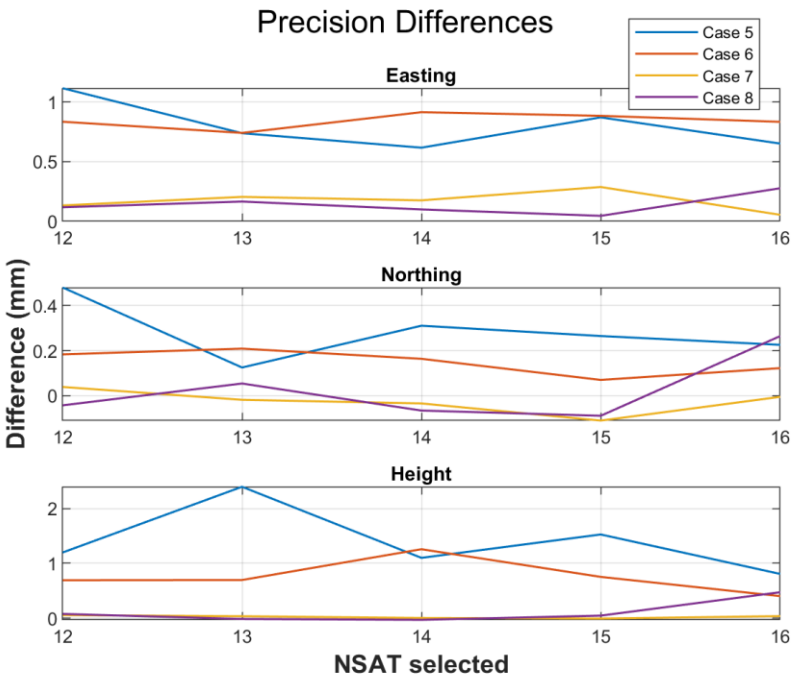

Figure 7.25 The differences of positioning precision between the original PPP and the selected satellites (12, 13, 14, 15 and 16) from cases 5, 6, 7, and 8.

- **Positioning solutions of cases 9 and 10**

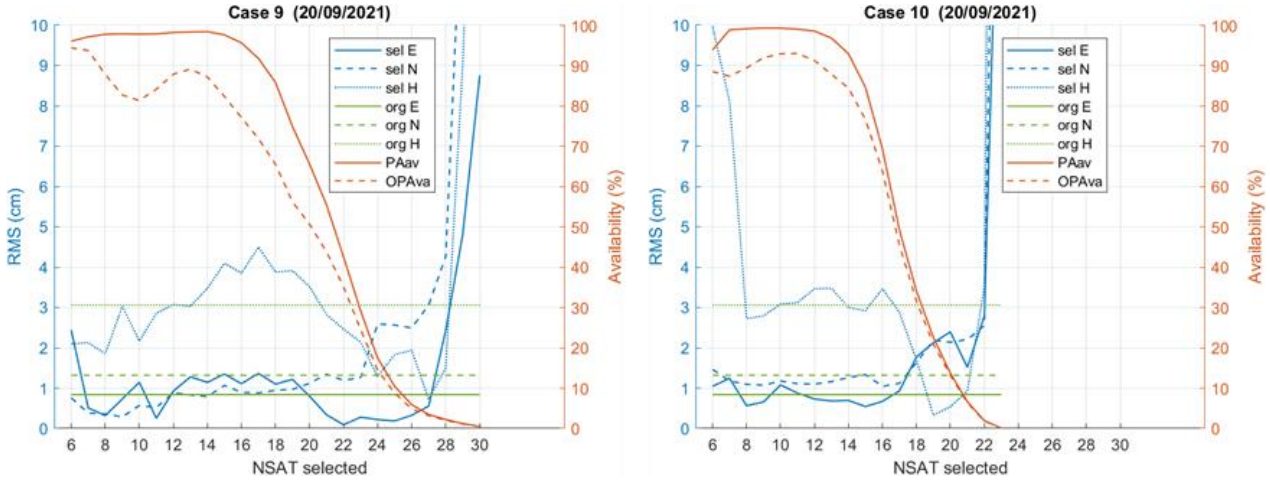

Figure 7.26 Comparison of the positioning accuracy of selected satellites from cases 9 and 10 with respect to the original PPP (all satellites). The life y-axis expresses the position accuracy of the selected satellites (blue) and original PPP (green). The right y-axis expresses the positioning availability of the selected satellites (red).

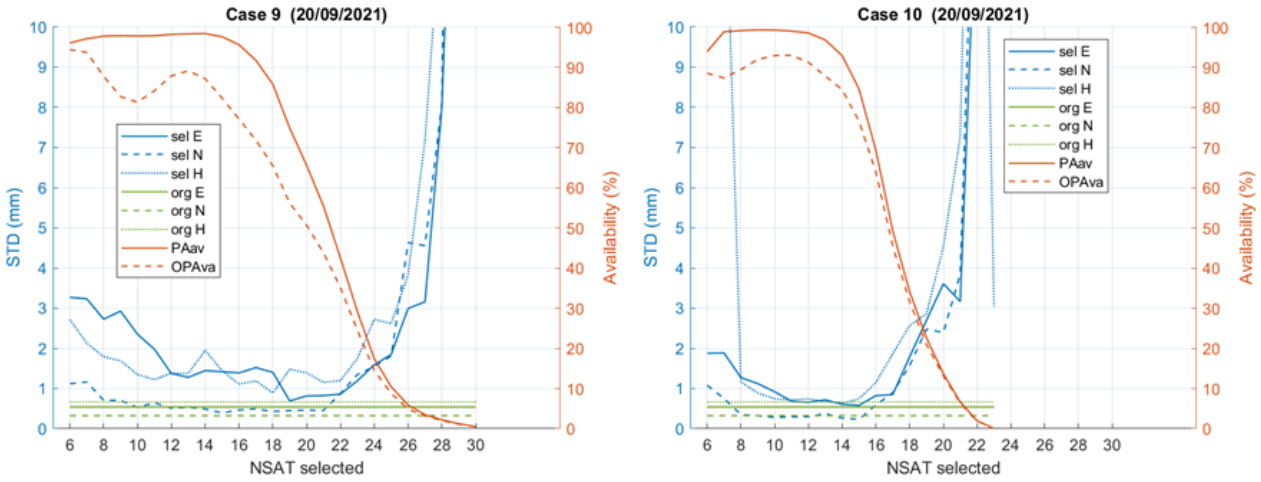

Figure 7.27 Comparison of the positioning precision of selected satellites from cases 9 and 10 with respect to the original PPP (all satellites). The life y-axis expresses the position precision of the selected satellites (blue) and original PPP (green). The right y-axis expresses the positioning availability of the selected satellites (red).

Figure 7.26 show the positioning accuracy of the selected satellites from cases 9 and 10. Figure 7.27 illustrates the precision of the positioning solutions of these selected satellites. The common between these two selection cases is satellites were selected by RAIM-KFITH before and after WGDOP selection as follows: RAIM-KFITH-WGDOP-RAIM-KFITH and Ele-RAIM-KFITH-WGDOP-RAIM-KFITH, respectively.

The satellites were selected by ten unique selection cases (Table 5.4), where each one considering different selection factors. The difference between cases 9 and 10 is a 15-degree satellite elevation mask (Ele), which was included in 10 cases only. According to Figure 7.26 and Figure 7.27, this leads to have different rate of OPAva and positioning solutions provided by each case. However, the positioning solutions of case 9 is almost the same to case 6 despite the differences in their selection factors. The same thing is noticeable between cases 8 and 10. The difference between cases 6 and 9, as well as between cases 8 and 10, lies in the RAIM-KFITH selection, which is considered further after WGDOP in cases 9 and 10. Figure 7.28 compares the difference between cases 6 and 9, while Figure 7.29 shows the comparison between cases 8 and 10.

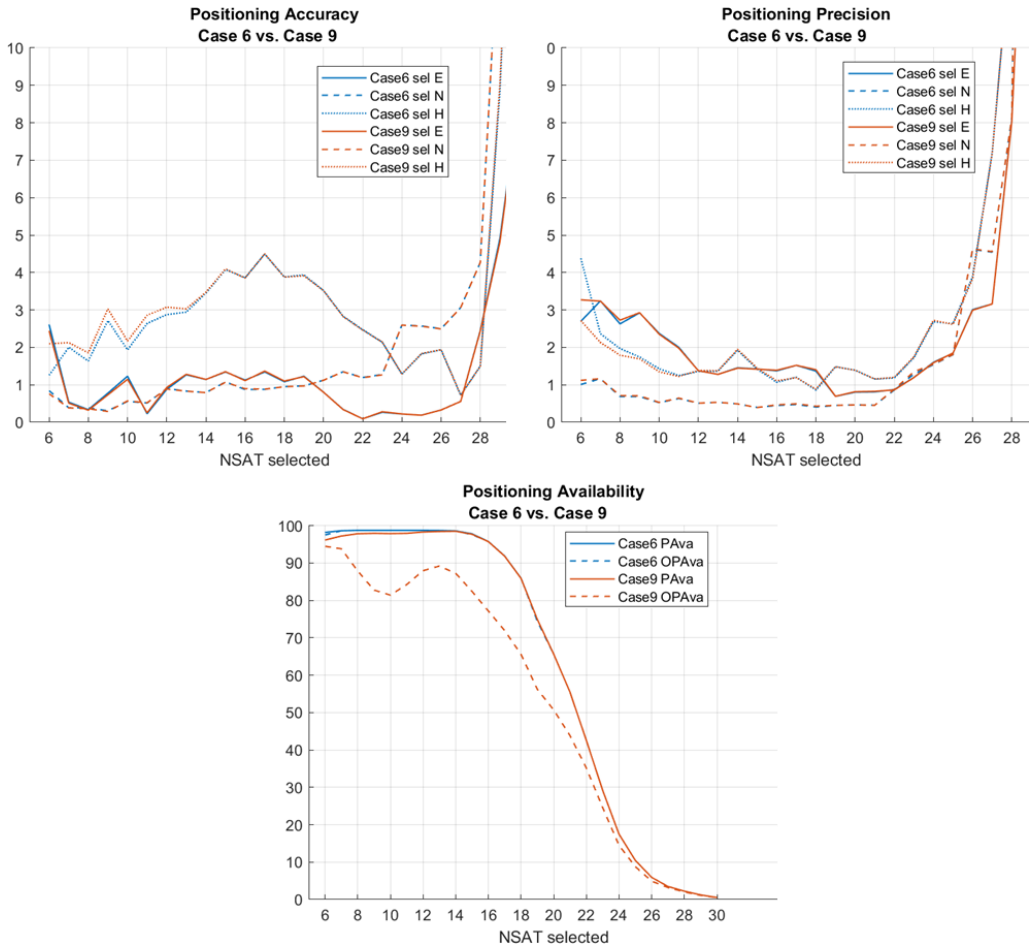

Figure 7.28 Comparison of the positioning accuracy, precision, and availability between cases 6 and 9.

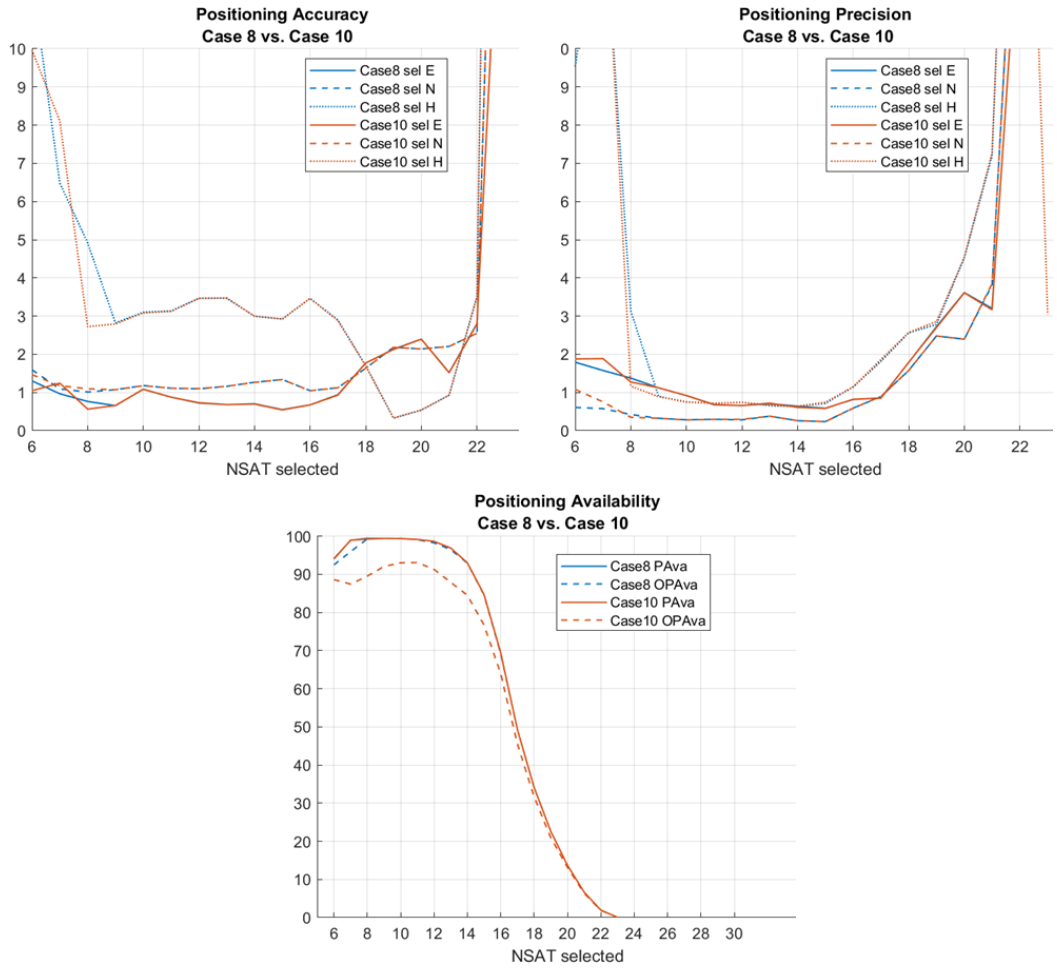

Figure 7.29 Comparison of the positioning accuracy, precision, and availability between cases 8 and 10.

According to Figure 7.28, the positioning solutions in cases 6 and 9 were almost identical. The same was true for cases 8 and 10, as shown in Figure 7.29. However, the OPAva rate in cases 9 and 10 was lower than that in cases 6 and 8. Lossing number of the selected satellites based on WGDOP in cases 9 and 10 was expected due to the RAIM-KFITH selection after WGDOP selection. However, the loss of these satellites did not improve the positioning solutions. This demonstrates the quality of selection in cases 6 and 8.

- **Comparison of satellite selection cases**

The optimal satellites were selected by ten unique selection cases, where different selection factor or order was considered in each case. Because of these differences, each selection case provides different results in positioning accuracy, precision, or availability, if not all of them together. In the first four cases, satellites were selected based on WGDOP before RAIM / RAIM-KFITH. Since WGDOP selection relied on the raw satellite data from the RINEX file, satellites with no correction (orbit and clock) and cycle slip were selected. These

satellites were then excluded during positioning process due to lack of information. As a result, the quality of the selected satellites from these cases is not good, and their positioning solution cannot be guaranteed as the positioning satellites cannot be controlled and predicted.

In cases 5, 6, 7, and 8, satellites were selected by RAIM or RAIM-KFITH first before WGDOP selection. RAIM and KFITH selection applied during positioning determination. Satellites with no correction and cycle slip were rejected through positioning due to lack of information. Poor satellite measurements were eliminated by RAIM and KFITH. This filtered satellite data and improved the quality of WGDOP selection leading to used most of its selected satellites in positioning solution.

RAIM only was applied before WGDOP selection in cases 5 and 7. Whereas both RAIM and KFITH (RAIM-KFITH) were used in cases 6 and 8. Since RAIM was found inefficient, as shown in Figure 7.19. The figure shows a comparison between case 1 and case 3. Satellites were selected based on WGDOP-only in case 1, while they were chosen based on WGDOP-RAIM in case 3. According to the Figure 7.19, both cases provided similar results in terms of positioning accuracy, precision, and availability. This means that RAIM was not effective, and no satellites were excluded by RAIM. The rejected satellites in case 1 were also eliminated in case 3 because their missing data (no correction / cycle slip). As a result, the selection cases 5 and 7, relying on RAIM-only, are not good enough. This this because RAIM is not working and does not provide anything for the selection.

In cases 6 and 8, satellites were selected based on RAIM-KFITH before WGDOP selection. In cases 9 and 10 satellites were chosen by RAIM-KFITH before and after WGDOP selection. 15-degrre satellite elevation mask (Ele) was included in cases 8 and 10. The only difference between cases 6 and 9, as well as between case 8 and 10, is applying RAIM-KFITH after WGDOP selection in cases 9 and 10. Despite the difference, the positioning solutions (accuracy and precision) provided by cases 6 and 9 are almost the identical. The same is true between cases 8 and 10. However, it can be notice that OPAva rate in cases 9 and 10 is lower than those in cases 6 and 8. In other words, number of WGDOP's selected satellites were rejected in cases 9 and 10. This is expected as RAIM-KFITH was implemented after WGDOP selection. Since excluding WGDOP selected satellites in cases 9 and 10 did not improve / change the positioning solutions provided by case 6 and 8, keeping these satellites may be more valuable to facilitate data analysis. As a result, it can be considered the selection quality of cases 6 and 8 better than that of cases 9 and 10.

From the ten cases, case 6 and 8 consider better than others. Satellites were chosen based on RAIM-KFITH-WGDOP in case 6, while they were selected based on Ele-RAIM-KFITH-WGDOP in case 8. Including satellite elevation mask (Ele) enhanced selection continuity more than 20%, as shown in Figure 7.12. Furthermore, it is improved satellite selection

accuracy by about 7%, as shown in Figure 7.14. Therefore, case 8 consider the most suitable selection case for PPP.

The ten selection cases were applied to choose satellites from four days of GNSS data. The selection results of the first day (20/09/2021) are the one shown above, while the rest are presented in the appendix. Overall, the performance of the ten selection cases were almost the same in four days / times. The positioning solutions (accuracy and precision) provided by cases 8 in the four times is shown below.

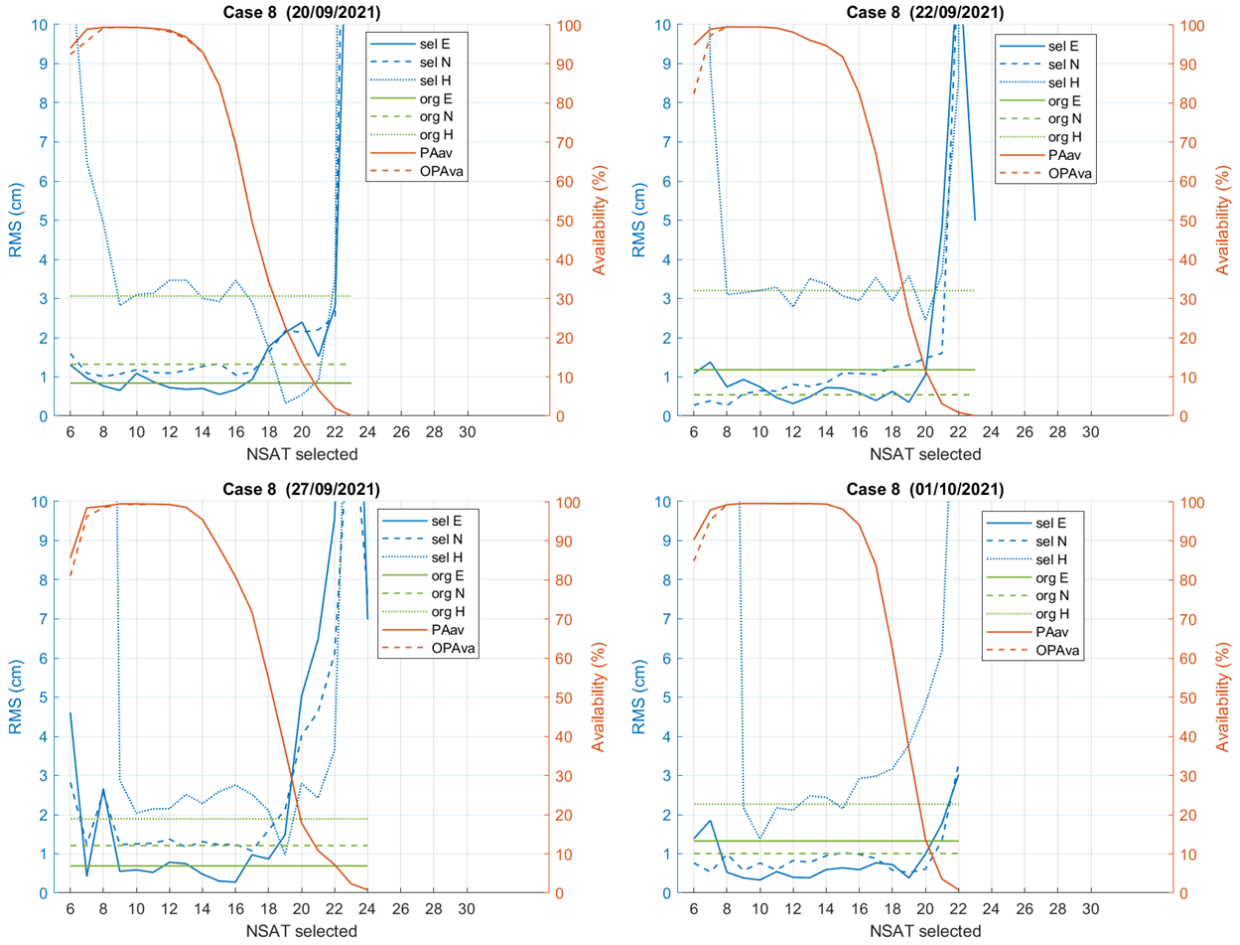

Figure 7.30 Positioning accuracy of case 8 from four days with respect to the original PPP (all satellites). The life y-axis expresses the position accuracy of the selected satellites (blue) and original PPP (green). The right y-axis expresses the positioning availability of the selected satellites (red).

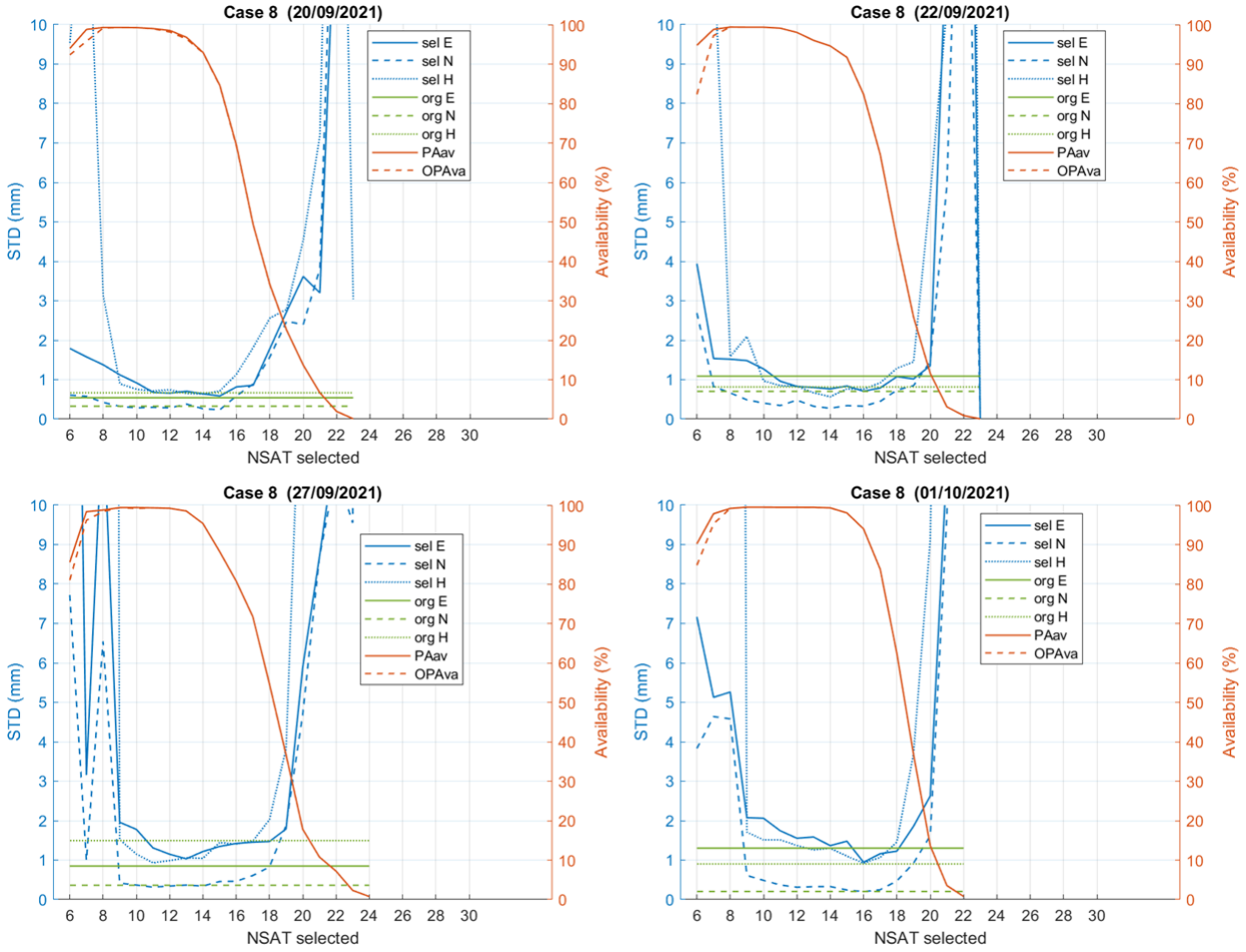

Figure 7.31 Positioning precision of case 8 from four days with respect to the original PPP (all satellites). The life y-axis expresses the position accuracy of the selected satellites (blue) and original PPP (green). The right y-axis expresses the positioning availability of the selected satellites (red).

7.2 Summary

This chapter focused on defending and investigating the performance of various criteria and selection orders for PPP-satellite selection and identifying the most suitable. As a result, satellites with all possible subsets were chosen based on ten selection combinations/cases of different criteria and selection orders. The importance of this study is (i) the overall evaluation of the performance of these selection combinations and (ii) the suitable subset size for PPP- satellite selection.

High PPP accuracy required corrections such as orbit and clock. In addition, excluding satellites signal at low elevation angle can also lead to improve PPP accuracy, as these satellites' signal are more vulnerable to atmospheric and multipath errors. As a result, the optimal satellites were selected based on WGDOP with and without satellite elevation angle and corrections in ten cases. The optimal satellites were selected in all possible subset

sizes as number of satellites affecting positioning quality. According to the results, PPP corrections are required for PPP satellite selection, otherwise a large number of poor satellite signals will be selected. Due to positioning validation functions, they will be rejected from positioning. Considering as more as possible of PPP corrections leads to better selection quality. Among the ten satellite selection cases, case 8 is the most suitable, as it considered the largest number of corrections using satellite elevation angle mask, RAIM, KFITH, and WGDOP. The least number of satellites suitable for selection is 12 to maintain continuous positioning with the same quality. The continuity of satellites over time is required for carrier phase ambiguity resolution, which improves PPP solution. Thus, the continuity of the selected optimal satellite subset over time should be considered for better quality PPP satellite selection.

Chapter 8 Experimental evaluation of Satellite Selection Method

Satellite selection method is combination of selection criterion and selection technique. To find the most suitable satellite selection method, various types of satellite criteria and techniques were evaluated. It was found that satellite selection based on multiple criteria is the best. This is because several factors affect positioning quality. Taking into account as many as possible of these factors will increase the quality of the selected satellites, and consequently, positioning accuracy. According to the results of 0, the most suitable criteria for satellite selection is satellite elevation angels, geometry (GDOP), signal power (CNR), and positioning residuals (RAIM and KFITH). They should be implemented with the following order: Ele then RAIM and KFITH, then WGDOP (Ele-RAIM+KFITH-WGDOP). Ele, RAIM, and KFITH can be implemented using positioning/navigation software (e.g., RTKLIB). Whereas WGDOP- based satellite selection can be implemented by various techniques. Optimization algorithms are more suitable technique than other for satellite selection based on WGDOP as discussed in Section 3.6. The ABC algorithm is the most suitable optimization algorithm as it is robust, fast, and has few parameters to set, as shown in Chapter 6.

In 0, the satellites were selected in ten cases one of them was based on Ele, RAIM, KFITH and WGDOP, using RTKLIB and ABC. The positioning accuracy of its selected satellites was the best and equivalent to the original PPP (all satellites). However, it did not support the continuity of the selected satellites. This is because it has mostly selected a different subset of satellites over successive epochs. The optimal satellites were change from one epoch to another due to four reasons: i) the previous selection was missing, ii) the pervious selection has worse fitness, iii) the previous and the new selection has the same fitness, and iv) miss-selection, as the previous selection has better fitness than the new selection although the new choice was chosen.

Since the continuity of satellites important for positioning, the continuity of the selected satellites was considered in this chapter. The satellites were selected based on Ele, RAIM, KFITH and WGDOP, using RTKLIB and ABC. The continuity of the selected satellites was considered in WGDOP-based satellite selection. For each epoch the pervious selection was compared with the new. If they are different and the previous selection has a WGDOP (fitness) value equal to or better than the new selection, the previous selection replaces the new choice.

To test the performance of the satellite selection method, it was implemented to select satellites from three different scenarios: i) static open-sky environment, ii) kinematic open-sky environment, and iii) static multipath environments. The results and their discussion are presented below.

8.1 Result And Discussion

8.1.1 Static Open-Sky Environment

The new satellite selection method is to choose satellite based on Ele, RAIM, KFITH and WGDOP, while considering the continuity of the selected satellites. This selection implement using RTKLIB and ABC algorithm as selection techniques. However, the same satellite selection method was applied in Chapter 7, but without continuity consideration. To evaluate the impact of continuity consideration, the positioning accuracy of selected satellites by the new method should be compared to that without continuity consideration. Therefore, satellites were selected using the proposed method from the same satellite data (static open-sky environment) used before.

Furthermore, the same positioning configurations (Table 5.6) were used. According to Table 5.6, combined KF, which has been used for PPP solution in several studies [226,232,233], was used. This is because its providers smoother positioning than forward and backword KF [118,119]. However, there is no convergence time when using the combined KF. To investigate the convergence time of the selected satellites by the new satellite selection method, the data of its selected satellites was processed also using forward KF. As a result, the data of the selected satellites by the new satellite selection method was processed twice: i) using the same positioning configurations (combined KF) to investigate the continuity consideration and ii) using forward KF to investigate the convergence time.

8.1.1.1 Satellite Selection with and without Continuity Consideration

To investigate the impact of considering the continuity of the selected satellites, the positioning solutions (accuracy and precision) of the selected satellites with and without continuity were compared. The satellites were selected for 24-hour every 30-sec (i.e., 2880 epochs). In addition, they were selected with all possible numbers of satellites (6–max number of observed satellites). Figure 8.1 shows the positioning solutions (accuracy and precision) for the selected satellites with and without continuity. In addition, it shows the positioning solutions (accuracy and precision) of original PPP, which is using all satellites, 15-degree elevation mask, RAIM, and 30-meter KFITH. Figure 8.2 shows the ENH errors timeseries of the 10, 15, and 20 selected satellites with and without continuity.

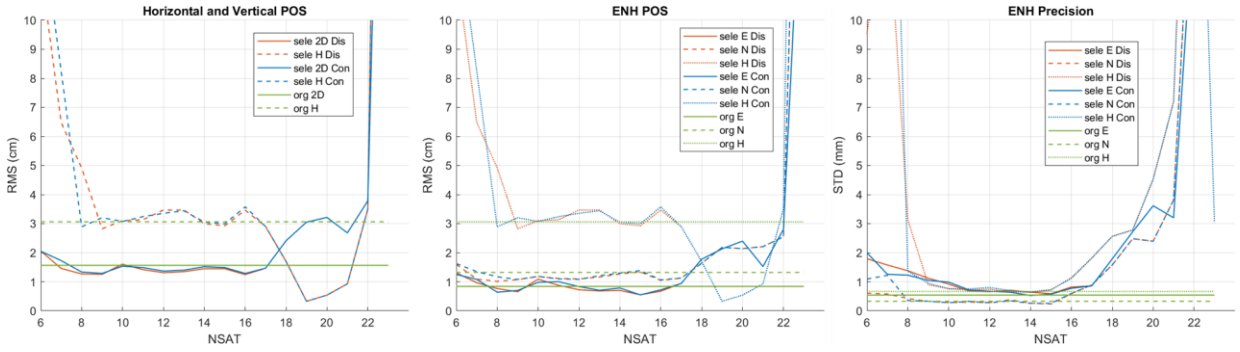

Figure 8.1 Positioning solutions (accuracy and precision) of the original PPP and the selected satellites with and without continuity.

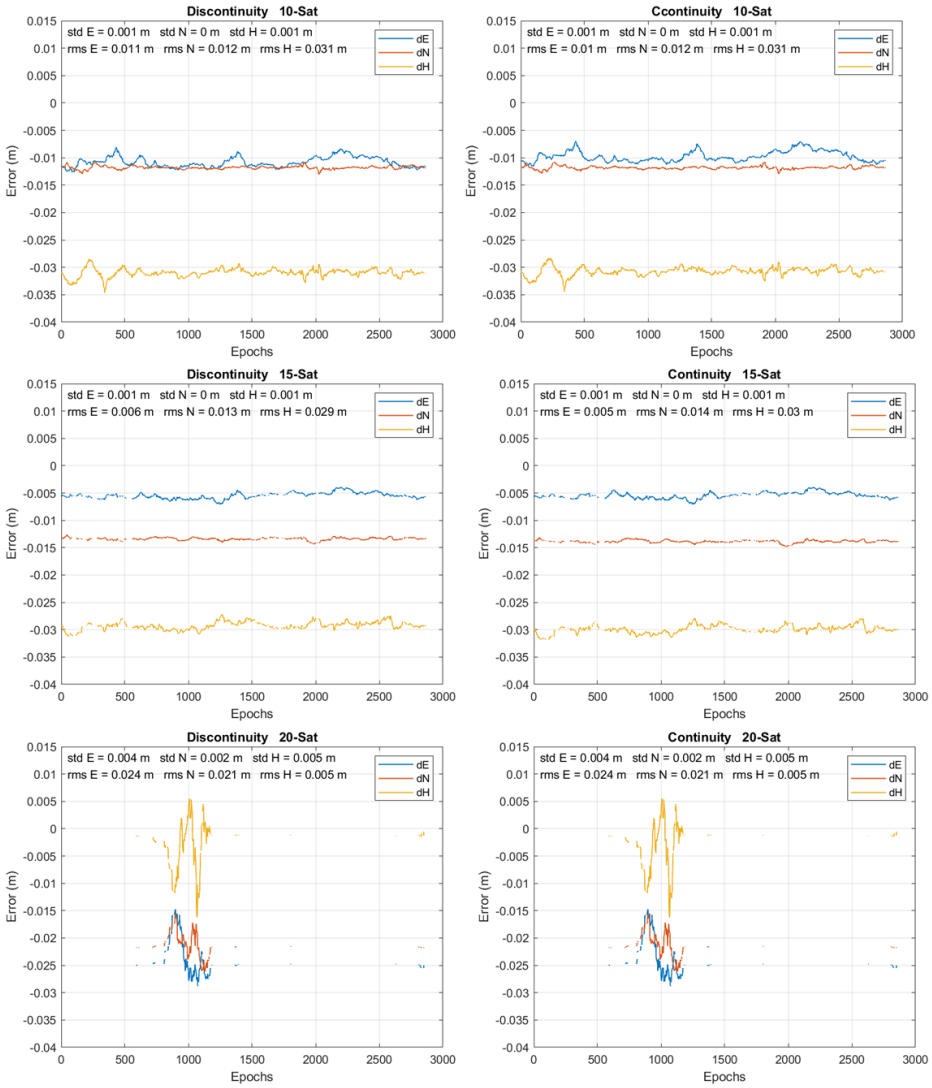

Figure 8.2 E/N/H error timeseries of the subset of 10, 15, and 20 selected satellites with and without continuous considerations. Left: the positioning error of the selected satellites without continuity, right: the positioning errors of the selected satellites with continuity.

Figure 8.2 presents E/N/H error timeseries of 10, 15, and 20 selected satellites with and without continuity. According to the figure, it can be seen how close the positioning solutions (accuracy and precision) of the satellites with and without continuity. The positioning accuracy of the selected 20 satellites with and without continuity was identical in the three directions (E/N/H). For 15 satellites, it varies by 1 mm in all three directions. For the 10 satellites, it was the same in northing and hight and differed by 1 mm in easting.

Checking the number of continuous epochs of the selected satellites with and without continuity (Figure 8.3), there is not a big different. For example, the average number of continuous epochs for middle number of selected satellites (10-19) is mostly 3 in both cases with and without continuity consideration. In addition, the average number of satellites change in the subset for the middle number of selected satellites is 2 for both cases. The continuity of the selected satellites was considered by comparing the pervious and current epoch's optimal selected satellites over each epoch. If the previous epoch's optimal satellites has equal or better fitness than the current, the previous epoch's optimal satellites replace the current. Despite the continuity consideration the selected satellites continuous did not increase a lot. This is could the reason why the positioning solutions (accuracy and precision) of the selected satellites with and without continuity are the same. In addition, RTKLIB (used software) apply PPP without carrier-phase ambiguity resolution [118]. This mean that continuity consideration has less effect on positioning, as the satellite continuity importance to carrier-phase ambiguity resolution [118,119]. This could be a second reason why the positioning solutions was almost the same for the selected satellites with and without continuity consideration.

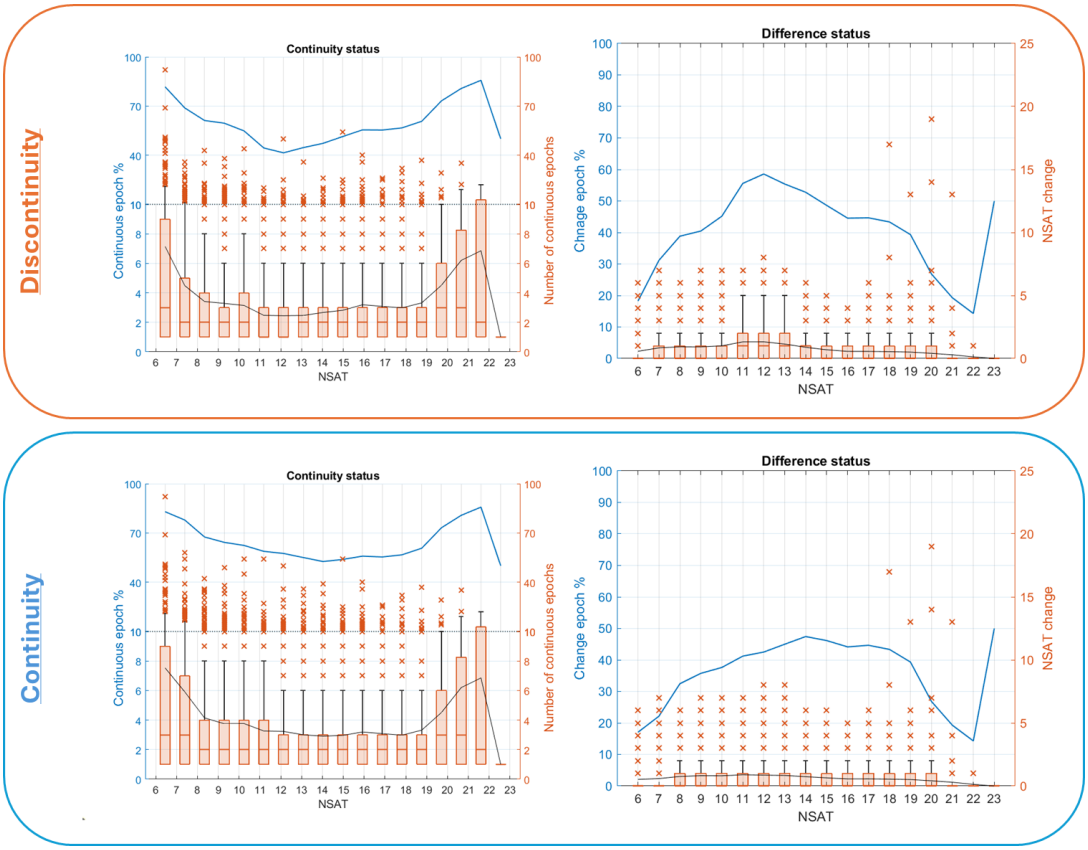

Figure 8.3 Comparison between satellite selection with and without continuity consideration in the number of continuous epochs and the number of satellites changed in the subset. Top: the number of continuous epochs and changed satellites without continuity consideration, Bottom: the number of continuous epochs and changed satellites with continuity consideration.

8.1.1.2 PPP Convergence Time

To investigates the positioning convergence time required for the selected satellites, forward KF setting was used in PPP positioning. Figure 8.4 shows the convergence time required for each number of selected satellites. Figure 8.5 shows the positioning solutions (accuracy and precision) after convergence for the original PPP and the selected satellites with different numbers and. Figure 8.6 presents the E/N/H error timeseries of the selected satellites and the original PPP. Lastly, Figure 8.7 shows a comparison between the positioning solutions (accuracy and precision), of the selected satellites using combined and forward KF.

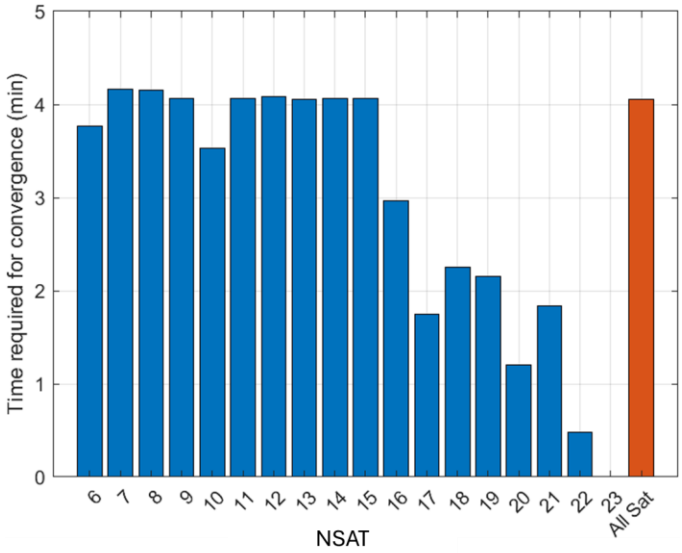

Figure 8.4 The time required for PPP convergence of the selected satellites with different number and original PPP (all satellites).

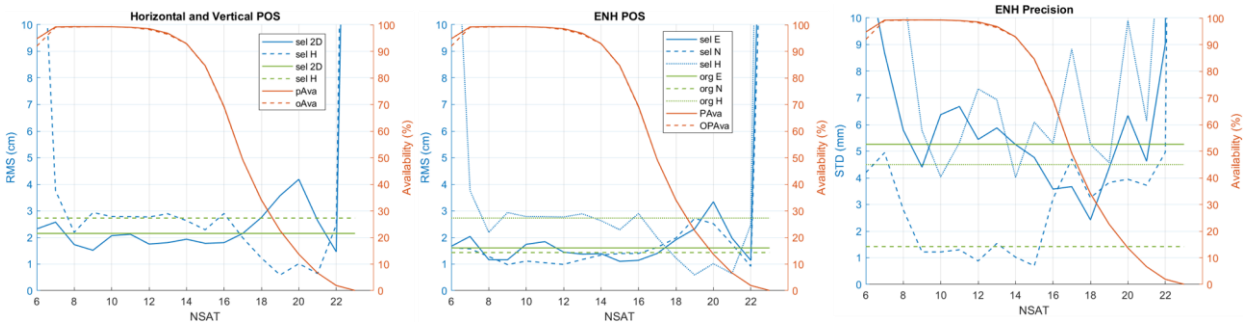

Figure 8.5 Positioning solutions (accuracy and precision) after convergence for the original PPP (all satellites) and the selected satellites with different numbers.

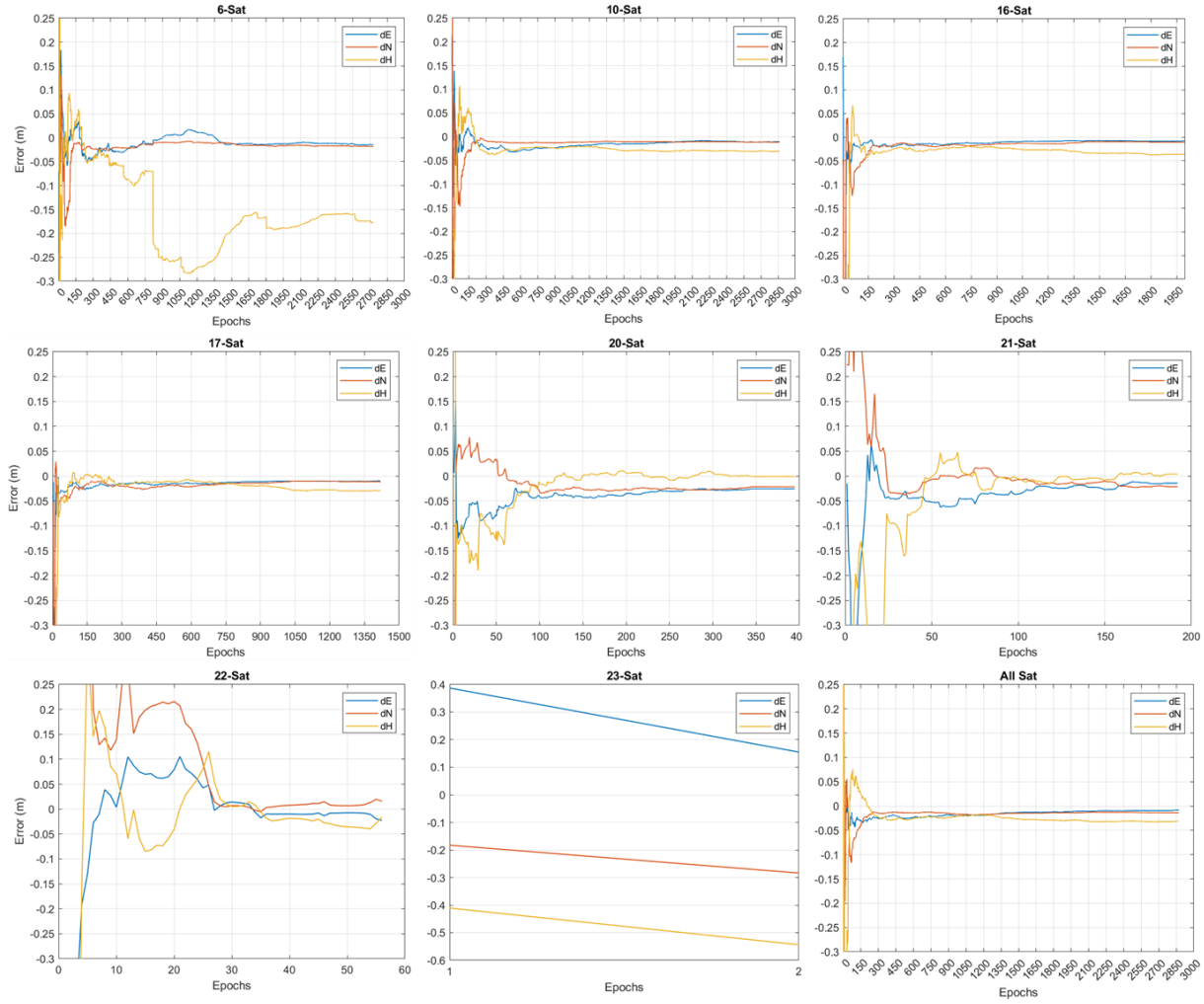

Figure 8.6 E/N/H error timeseries of the selected satellites and the original PPP (all satellites) with forward KF.

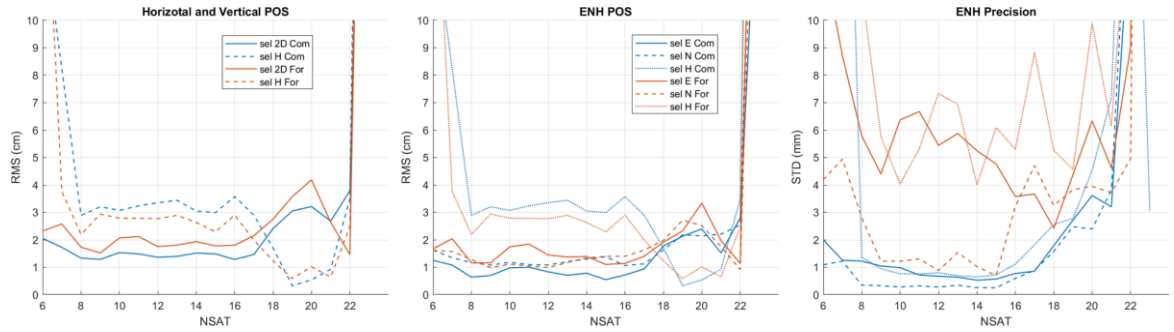

Figure 8.7 Comparison in positioning solutions (accuracy and precision) between the original PPP and selected satellites using forward and combined KF.

The convergence time is the time required to reach a stable absolute positioning error [234,235], which is a few centimetres [24,235]. According to Abou-Galala et al. [234], PPP convergence time is influenced by various factors, including the number of observed satellites and their geometry, the GNSS receiver's dynamic and environment, and the

observation quality and sampling rates. PPP convergence time is around 20 minutes when using single satellites systems [24,236]. It is several minutes, (~ 4 minutes) with multi-GNSS [25–27].

According to the Figure 8.4, the convergence time of the original PPP was about 4 minutes. The convergence time of the selected satellites varied based on the number of satellites selected. The convergence time of the subsets of 6 –15 selected satellites was like original PPP (about 4 minutes) except for the subsets of 6 and 10 satellites. Their convergence time was lesser, as it was about 3.5 minutes. The convergence times of the remaining selected satellites (16–23) was below 3 minutes. In general, their convergence time decreased as the number of selected satellites increased. For example, the convergence time of the subset of 16, 19, and 23 satellites was about 3, 2, and 0 minutes.

Various factors affecting the convergence time. The main reason for reducing the convergence time of the selected satellite with high number (16–23) is positioning availability. The positioning availability of the subset of 16–23 satellites decrease rapidly as the number of satellites increased (Figure 8.5), which is directly proportional to their convergence time. This explains why the convergence time was zero for the subset of 23 satellites, as it had only two epochs (Figure 8.6).

The convergence time of the original PPP and some of the selected satellites (7,8,9,11,12, 13,14, and 15) was about 4 minutes. The positioning accuracy of these selected satellites was better than original PPP apart of the 7 selected satellites. According to Figure 8.5, the vertical error of these selected satellites was almost like original PPP, which is 2.73 cm. However, their horizontal error was mostly 0.347 cm less than original PPP, which is 2.154 cm. On the other hand, the positioning accuracy of the selected satellites with convergence time less than 4 minutes (6,10, and 16-23). The positioning accuracy of 16, 17 and 22 selected satellites was better than the original PPP horizontally, vertically and both, respectively. The horizontal and vertical accuracy of 10 selected satellites was almost the same with original PPP, which were 2.154 and 2.73 cm. Whereas the horizontal accuracy of the selected satellites 18,19, 20, and 21 was worse than original PPP with no less than 0.5 cm. However, their vertical accuracy was better than original PPP with no less than1.5 cm. In terms of precision, the original PPP had better precision than the selected satellites in general.

According to Figure 8.7, the different between the positioning accuracy using forward and combined KF is mainly an offset. The horizontal accuracy of the selected satellites with combined KF was about 0.3 cm better than the forward KF accuracy. Whereas its vertical accuracy was worse than that of the forward KF by about 0.3 cm. In terms of precision, it is significantly better (lower) with combined KF. The positioning precision of most of the

selected satellites (8-17) was around 1 mm in the three directions (E/N/H). In contrast, the accuracy of the same selected satellites (8-17) was around 1 mm vertically and more than 4 mm in the easting and northing.

8.1.2 Kinematic Open-Sky Environment

The efficiency of the new satellite selection method was tested for kinematic PPP. Over one hour, the optimal satellites were selected for every second, i.e., they were selected 3600 times. They were selected in all possible subset sizes (6-max observed satellites). Figure 8.8 shows the overall positioning accuracy and precision of the selected satellites and original PPP, using all satellites, 15 degrees elevation mask, RAIM and 30 meters KFITH. In addition, it presents the positioning (PAva) and optimal positioning available of the selected satellites (OPAva). Figure 8.9 shows the E/N/H errors of timeseries of the original PPP and selected satellites. Figure 8.10 shows the track of the train based on the position of the original PPP and some of the selected satellites.

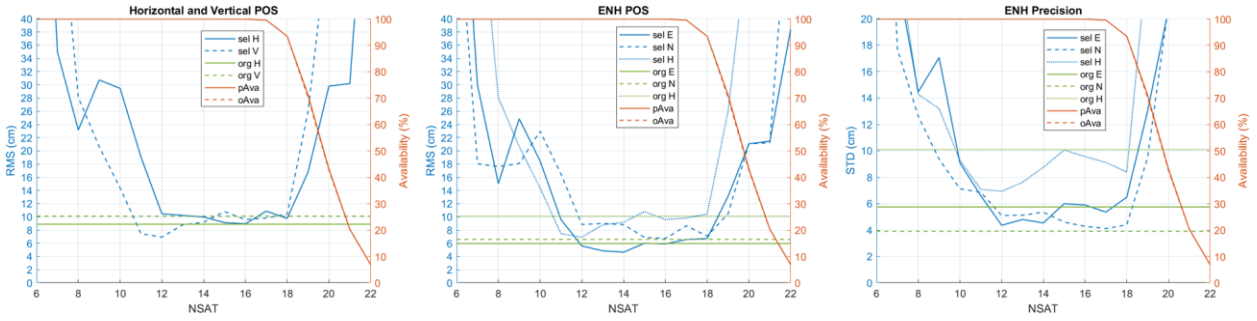

Figure 8.8 Overall kinematic positioning solutions accuracy and precision of the original PPP (all satellites) and the selected satellites with different numbers.

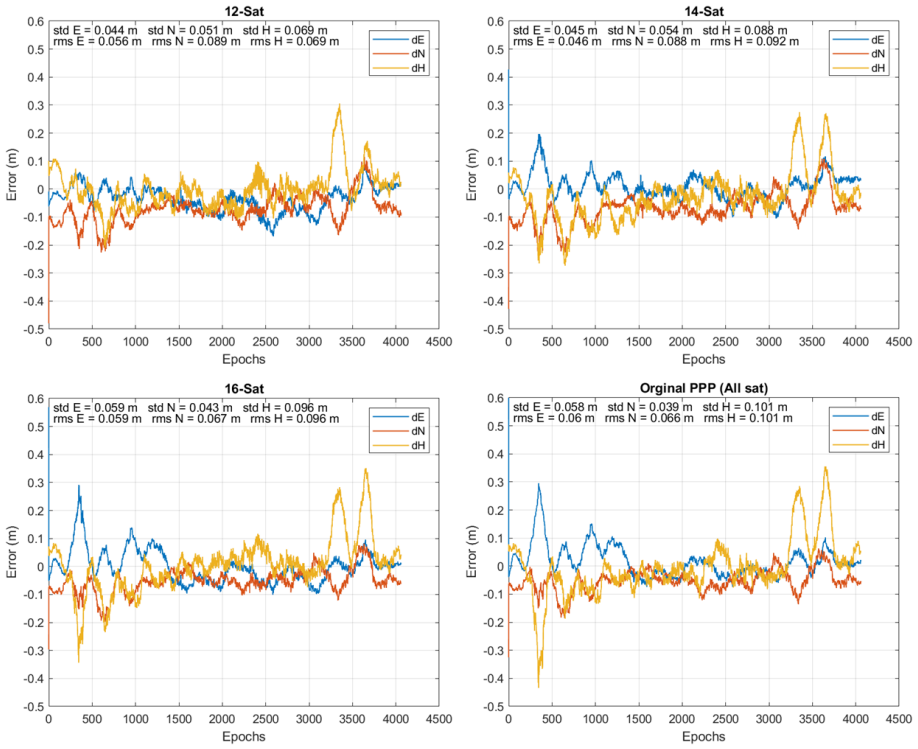

Figure 8.9 E/N/H error timeseries of original PPP (all satellites) and the subset of 12, 14, and 16 selected satellites for kinematic PPP.

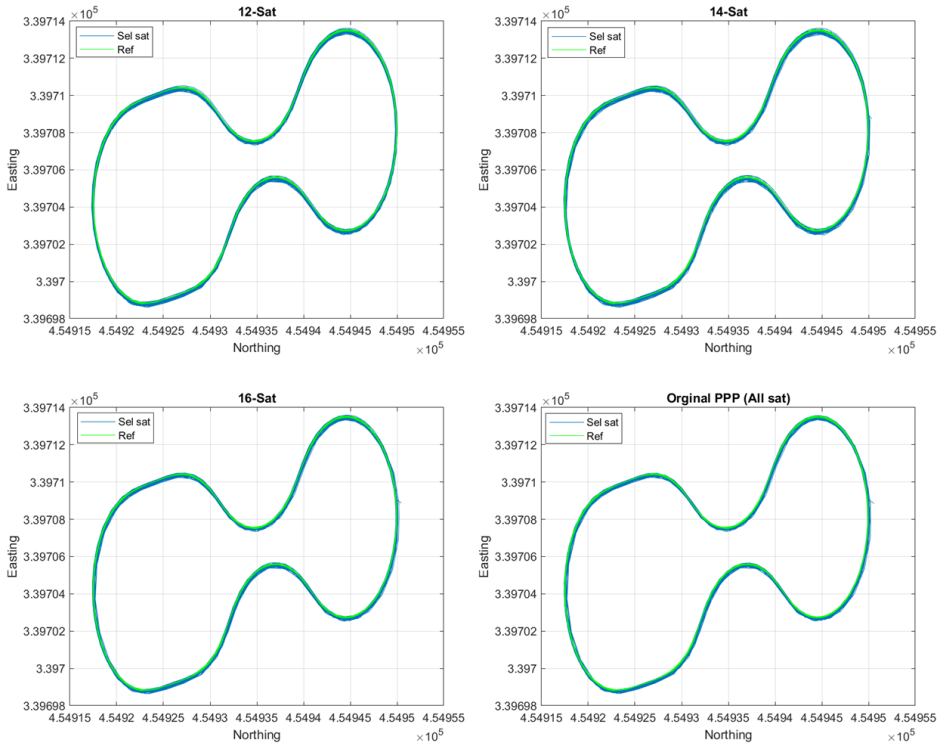

Figure 8.10 The train track based on the position of the selected satellites (12,14, and 16), original PPP (all satellites), and the relative positioning using all satellites (reference).

According to Figure 8.8, the overall positioning solutions (accuracy and precision) of the selected satellites creates U-shape. The positioning solutions of few and large number of selected satellites is high, while those of the middle number of satellites (12-18) is low (better). The positioning solutions of the middle number of selected satellites is equivalent to the original PPP, especially those of selected 15 and 16 satellites. The easting and northing errors of the original PPP and 15 and 16 selected satellites are about 6 cm. Whereas their high errors are about 10 cm. Their precision in the three directions (E/N/H) are about 4, 6, and 10 cm, respectively.

Figure 8.9 shows E/N/H timeseries of the original PPP and the selected 12, 14, and 16 satellites. The subset of 12 selected satellites provides easting and height positioning more precise than others. As the number of satellites increases (14, 16, to all satellites) the positioning accuracy in both directions becomes worse, which can be seeing in the following periods (50-1500 or 3500-3800). However, the difference between their overall positioning (RMS) is small, about 2 cm maximum. This explains why the train track based on them (Figure 8.10) looks almost identical.

8.1.3 Static Multipath Environment

To investigate the performance of the new satellite selection method under multipath environment, it was implemented for satellite selection in three locations with low and high multipath level. The first location has low multipath effect, and it is in the Jubilee campus next the tennis court. The second and the third locations are on the control points (NGB11 and NGB9) located fort and behind the NGI building. Both locations are surrounded by rise building creating high multipath environment. The positioning solution of the selected satellites in these locations are shown below.

- **Next Tennis Court**

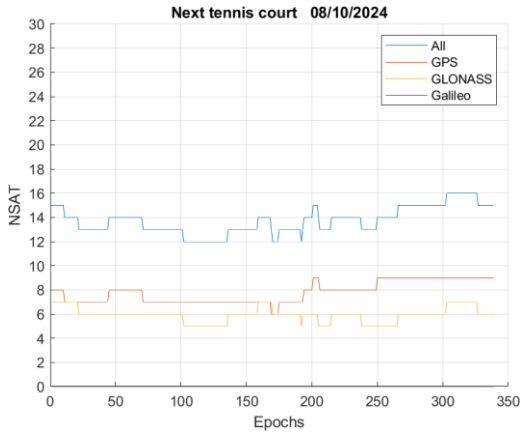

Figure 8.11 Number of satellites observed every 30 sec with 15 degrees elevation mask next the tennis court at Jubilee campus.

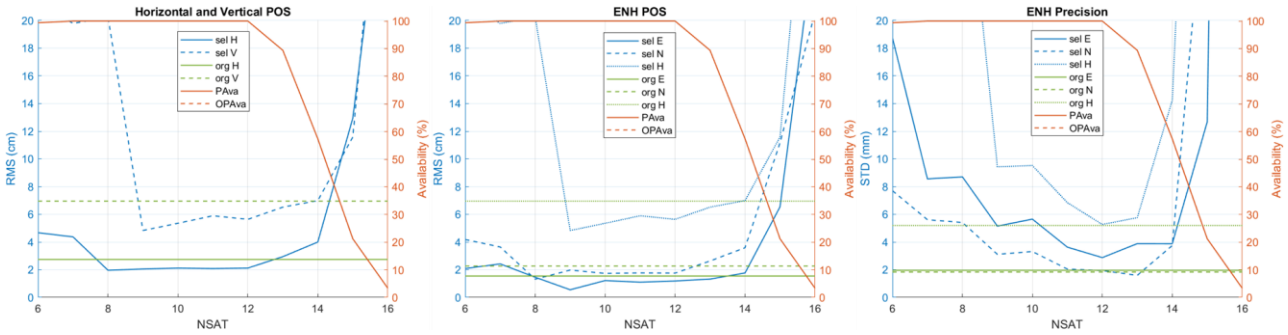

Figure 8.12 Positioning solutions (accuracy and precision) of the selected satellites and original PPP for the receiver location next the tennis court at Jubilee campus. In addition, the positioning available of the selected satellites.

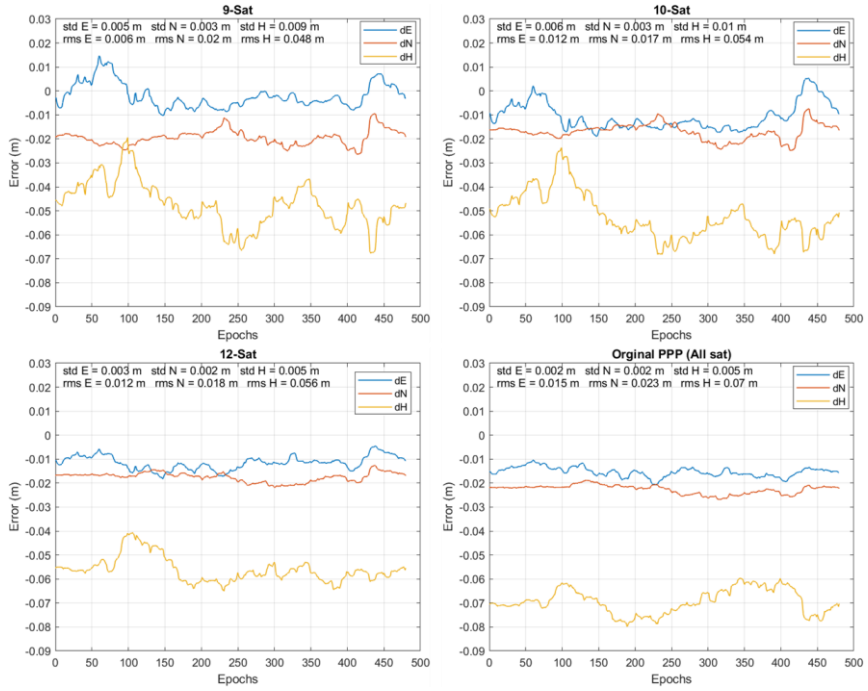

Figure 8.13 E/N/H errors timeseries of the original PPP and 14, 16, and 20 selected satellites from positioning receiver next to the tennis court at Jubilee campus.

According to Figure 8.11, 16 is the maximum number of satellites observed next to the tennis court when using a 15 degrees elevation mask. According to Figure 8.12, the horizontal and vertical positioning accuracy of original PPP, using all satellites, are 2.744 and 6.960 cm, respectively. The horizontal accuracy of 8 -12 selected satellites is stable at 2.048 cm, which is better than original PPP by 0.696 cm. The vertical accuracy of 9 -13 selected satellites is also better than original PPP, which gradually rises from 4.830 to 6.519 cm.

According to Figure 8.12, E/N/H precision of the original PPP are 1.958, 1.835, and 5.191 mm, respectively. The original PPP has better E/N/H precision than selected satellites except for the 13 selected satellites in the northing direction. The northing precision of the

subset of 13 satellites is better than that of original PPP by 0.242 mm. Compared to the selected satellites, the northing precision of the 12 selected satellites is the second best after 13 selected satellites. The E/N/H precision of the 12 selected satellites is the closest to the original PPP with 0.101, 0.916, and 0.076 mm difference.

Figure 8.13 shows a time series of E/N/H errors for the original PPP and a subset of 9, 10 and 12 selected satellites. E/N/H solutions of the original PPP are more precise than 9 and 10 selected satellites although they provide better overall positioning (RMS) in the three directions. E/N/H positioning accuracy of the 12 selected satellites is better than the original PPP although their E/N/H precisions are comparable.

Using a 15-degree elevation mask, the maximum number of available satellites was 16. Using the new satellite selection method, better position accuracy was achieved than all satellites (original PPP) with fewer number of satellites 9-12. This indicates the existence of weak satellite signals at high elevation angles (greater than 15º) even in low multipath environment (open area). This also proves the efficiency of the satellite selection method in this kind of environment. Compared to selected satellites, the 9-selected satellites provide the best positioning accuracy, but it does not have the best precision. According to Figure 8.12, the positioning precision of the selected satellites improve as the number of selected satellites increases up to 12 satellites. However, when the number of satellites exceeds 12, the positioning accuracy decreases gradually. Also, the positioning availability gradually decreases as the number of satellites exceeds 12. This means that the number of satellites and positioning availability are important for precision.

- **NGB 9**

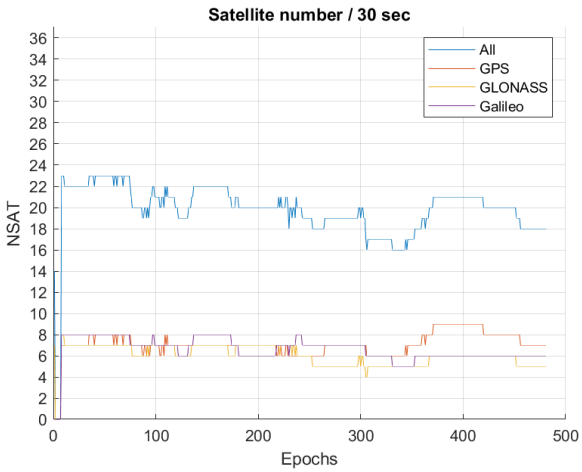

Figure 8.14 Number of satellites observed every 30 sec with 15 degrees elevation mask on NGB9.

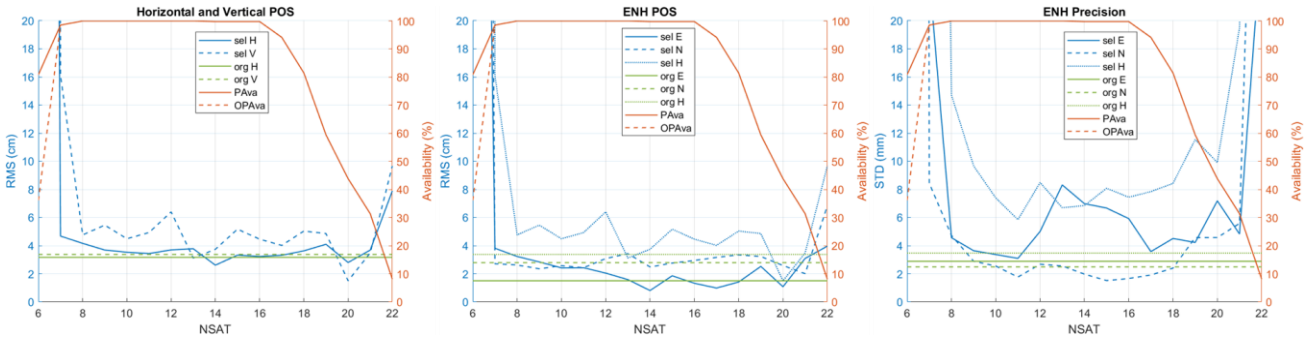

Figure 8.15 NGB9 positioning solutions (accuracy and precision) of the selected satellites and original PPP, as well as the positioning available of the selected satellites

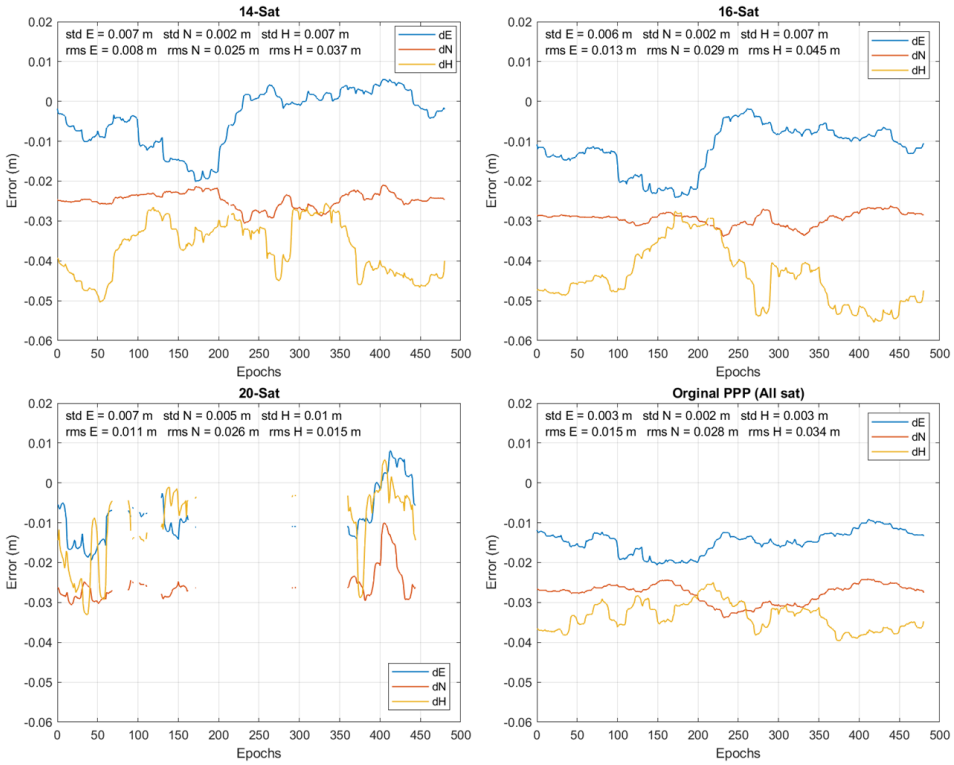

Figure 8.16 NGB9 E/N/H errors timeseries of the original PPP and 14, 16, and 20 selected satellites

The optimal satellites were found in all possible subset sizes. They were selected in subsets of 6 - the maximum number of satellites observed. According to Figure 8.14, 22 is the maximum number of available satellites using 15 degrees elevation mask. According to Figure 8.15, apart from 6, 7, 8, and 22 selected satellites, the horizontal positioning accuracy of the selected satellites is close to original PPP, which was 3.168 cm. The furthest horizontal accuracy from the original PPP is that of 13 selected satellites with a difference of 6.12 mm. The horizontal positioning accuracy of 14 and 20 selected satellites is better than original PPP with 5.57 and 3.66 mm difference. On the other hand, the vertical accuracy of original PPP was 3.378 cm. The vertical accuracy of most of the selected satellites was

worse than the original PPP by more than 1 cm. However, the vertical accuracy of 13 and 20 selected satellites was better than original PPP with 0.258 and 1.877cm difference.

According to Figure 8.15, E/N/H precision of the original PPP are 2.890, 2.486, and 3.470 mm, respectively. The original PPP significantly has better easting and height precision than selected satellites. However, most of the selected satellites (10–18) have equivalent or better precision than original PPP in northing direction. 15-selected satellites has the best northing precision (1.512 mm), which is better than the original PPP.

Figure 8.16 shows a time series of E/N/H errors for the original PPP and a subset of 14, 16, and 20 selected satellites. In general, E/N/H errors of the original PPP are more precise than selected satellites. However, its positioning accuracy was achieved by the subset of 14, and 16 selected satellites. In addition, the positioning accuracy of the original PPP in the three directions was overcome by the subset of 20 satellite selected that has positioning availability (44%) less than original PPP (100%).

According to Figure 8.14, the maximum number of available satellites using 15-degree elevation mask mainly ranges 16 – 22. A horizontal positioning accuracy equivalent to original PPP was achieved with 9 satellites using the new satellite selection method. In addition, better horizontal positioning than original PPP was obtained by 14 and 20 selected satellites by 0.557 and 0.361 cm, respectively. Better vertical positioning accuracy of the 13 and 20 selected satellites is better than original PPP by 0.258 and 1.877 cm, respectively. This can indicate the quality of satellites selection method.

- **NGB 11**

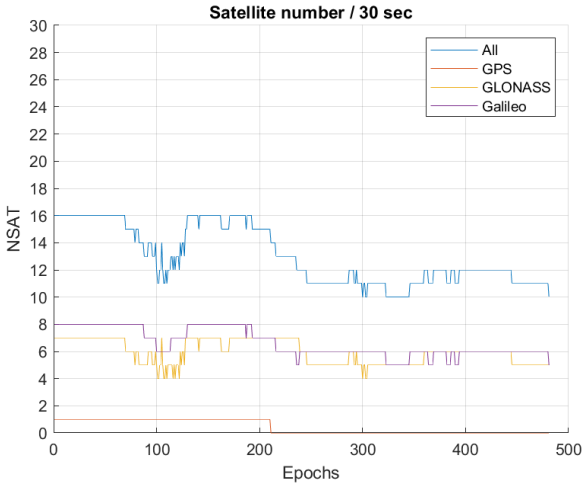

Figure 8.17 Number of satellites observed every 30 sec with 15 degrees elevation mask on NGB11

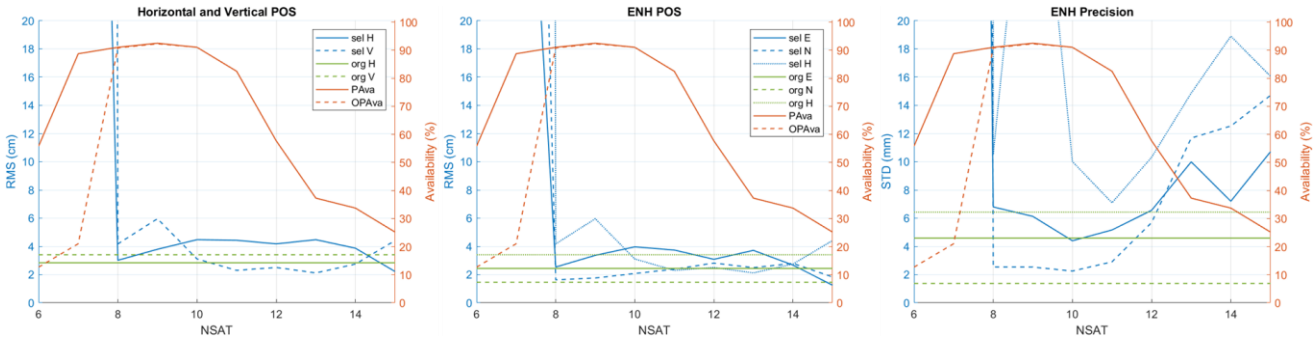

Figure 8.18 NGB11 positioning solutions (accuracy and precision) of the selected satellites and original PPP, as well as the positioning available of the selected satellites

Figure 8.19 NGB11 E/N/H errors timeseries of the original PPP and 8, 9, and 15 selected satellites

According to Figure 8.18, 15 is the maximum number of satellites observed on NGB11 when using a 15 degrees elevation mask. The horizontal and vertical accuracy when using all available satellites (original PPP) are 2.840 and 3.404 cm, respectively. Except for 6 and 7 selected satellites, the horizontal and vertical accuracy of the selected satellites are close to the original PPP. The horizontal positioning accuracy of the original PPP is mostly better than that of the selected satellites (10-14) by about 1.4 cm. Compared to the original PPP, the subset of 10-selected satellites is the furthest horizontally by 1.638 cm. The horizontal accuracy of the 8 selected satellites is the closest to the original PPP with 1.73 mm difference. Whereas the horizontal accuracy of the 15 selected satellites is better than

original PPP with 6.23 mm difference. In contrast, the vertical positioning accuracy of most of the selected satellites (10-14) better than original PPP by about 0.8 cm.

According to Figure 8.18, E/N/H precisions of the original PPP are 4.591, 1.371, and 6.426 mm, respectively. The original PPP significantly has better E/N/H precision than selected satellites except for the 10 selected satellites. Its easting precision is better than that of original PPP by 0.2 mm. The northing precision of the 8, 9, 10 and 11-selected satellites is approximately constant at about 2.5 mm and is noticeably better than that of the larger number of selected satellites.

Figure 8.19 shows a time series of E/N/H errors for the original PPP and a subset of 8, 9, and 15 selected satellites. In general, E/N/H errors of the original PPP are more precise than selected satellites. The easting and northing positioning of the subsets of 8 and 9 selected satellites are more precise than 15 selected satellites although they have a lower number of satellites.

8.2 Summary

This chapter focused on investigating the performance of the new satellite selection method under different scenarios (PPP modes). Satellites were chosen from kinematic GNSS data under low multi-path environment and from static GNSS data under low and high multipath environments. The importance of this study is the evaluation of the performance of satellite selection method in different PPP modes.

The efficiency of the new satellite selection method was excellent at low multipath environment regardless of the positioning modes: static, kinematic. This is because the kinematic positioning accuracy of original PPP (all satellites) was achieved by about half the number of satellites observed using the satellite selection method. Statically, a subset with half the number of satellites observed provided better positioning accuracy than the original PPP (all satellites). In addition, this level of positioning accuracy achieved by a subset with half the number of satellites observed was also obtained with optimal subsets with different number of selected satellites, which is less than the total.

In terms of high multipath environments, the performance of the new satellite selection method was less effective. From two different GNSS data, the satellites were selected in subsets with different number of satellites. In general, the positioning accuracy of original PPP was better than the selected satellites horizontally and vertically. However, the different between them was not big, it was less than 2 cm. In addition, one of the subsets with few numbers of satellites provided positioning accuracy was every close to original PPP. This proves the efficiency of the satellite selection method because selecting satellites based on a fixed number of satellites forces the algorithm to provide an optimal subset with an exact number of satellites. The satellite selection method is less effective in a high multipath

environment because it forced to choose poor satellite signals to complete the number of satellites predetermined.

Chapter 9 Conclusion and Recommendations

9.1 Conclusion

This thesis focuses on finding the most suitable satellite selection methods for PPP. For this purpose, various criteria and techniques for satellite selection were investigated. Satellites were selected from static and kinematic GNSS data at low and high multipath. Under these GNSS data scenarios, satellites were selected with all numbers of satellites (i.e. subset sizes) possible for positioning. The conclusion of these evaluations is given in the following:

9.1.1 Determining Satellite Selection Criteria

One of the main goals of satellite selection is obtaining precise positioning. Satellite geometry and signal power are the main factors affecting positioning solution. Therefore, satellites have been mainly selected based on them in one of five criteria: i) satellite angles, ii) satellite signal power, iii) satellite geometry (GDOP), iv) satellite geometry and signal power (WGDOP), and v) satellite geometry and positioning residuals (GDOP-RAIM). For example, satellite elevation angles were used to select satellites based on their signal power by abandoned satellite signal at low elevation angles, as they are more vulnerable to errors from multipath, ionospheric, and tropospheric. Satellite elevation and azimuth angles were adapted to choose satellites based on their geometry distribution.

Since positioning accuracy is affected by all its factors, considering them all for selecting satellites will improve satellite selection quality. Hence, choosing satellites based on their geometry and signal power (WGDOP) is better than selecting satellites based on GDOP or signal power alone. Choosing satellites based on GDOP-RAIM is even better than WGDOP especially for PPP-satellite selection. Corrections such as satellites ephemeris (orbit and clock) data, antenna phase centre variation (PCV), and ocean tide loading, are important factors for precise PPP. RAIM, which excludes satellites based on positioning residuals, takes these corrections into account. However, satellites cannot be selected by RAIM as it is a positioning integrity technique. Therefore, it was implemented after GDOP-based satellite selection to improve the quality of the selected satellites in previous studies. Since satellite selection based on WGDOP is better than GDOP, WGDOP-RAIM could be the most suitable criterion for satellite selection.

9.1.2 Determining Satellite Selection Techniques

RAIM is a technique for excluding satellites based on positioning residues. Satellite selection based on WGDOP can be carried out by various techniques, including TM, closed-form formal, maximum volume, ANN, and optimization algorithms. TM determines the optimal satellite subset after evaluating the fitness (WGDOP) of all possible satellite subsets (all possible solutions). Thus, it selects the optimal satellites with 100% selection

accuracy. However, it is time-consuming when the number of possible satellite subsets is huge. In this situation, the other techniques are faster than TM. The most effective in terms of selection accuracy and speed is optimization algorithms.

There are 50 types of optimization algorithms, and each was designed uniquely leading them to have different advantages and limitations. Five of the most popular and powerful optimization algorithms (ABC, ACO, GA, PSO, and SA) were tested in satellite selection based on WGDOP. They were implemented to choose the optimal GPS satellites for 288 epochs, corresponding to satellite selection every 5 minutes for 24-hour of GNSS dataset. In addition, the optimal GPS satellites were selected in four subset sizes (4, 5, 6, and 7). ABC, ACO, and PSO had the highest accuracy in determining the optimal GPS satellites and they were efficient in terms of computation time. However, the ABC algorithm is more practical, because it has the fewest parameters to adjust. maxIter and pSize are the only parameters that need adjustment in ABC algorithm.

The parameter values of optimization algorithm are critical for the results quality. Thus, the value of optimization algorithm parameters should be suitable for the given problem to obtain the best results. Satellite selection problem becomes more challenging as the number of possible satellite combinations (i.e., subsets) increases, corresponding to the increase of the total number of satellites tracked. Thus, the ABC algorithm was evaluated under complex satellite selection problem with different setting of parameters (maxIter and pSzie). It was implemented to select the optimal satellites from multi-GNSS data, where up to 31 satellites were tracked. The optimal multi-GNSS were selected satellites for 288 epochs, corresponding to satellite selection every 5 minutes for 24-hour of GNSS dataset. In addition, they were chosen in five subset sizes (4, 8, 10, 12, and 15). The evaluation of ABC algorithm revealed that the satellite selection accuracy of the ABC algorithm improves significantly (up to 100%) by increasing the values of population size and number of iterations, although this has an effect on the required computation time. This is consistent with what was reported in [149,227], as lower pSize and maxIter prevent achieving the best solution in complex problems, whereas increasing the value of these parameters increases the processing time.

Among the five optimization algorithms, the ABC algorithm is the most suitable in terms of selection accuracy and speed, as well as simplicity with only two parameters to set. This lines with what was stated in [99,138], as ABC is a robust algorithm between other optimization algorithms. Compared to TM, ABC is more efficient in multi-GNSS satellite selection because it is faster. However, it is significantly slower than TM in GPS satellite selection. As a result, TM is the most suitable algorithm (technique) for selecting the optimal

satellites from single satellite system (e.g., GPS). This aligns with what Du et al. [92] said that the TM is suitable for satellite selection from single satellite system.

9.1.3 Define the criteria and process for satellite selection

WGDOP-RAIM was considered as the most suitable criterion for PPP-satellite selection although it can be improved further. Satellite signals at low elevation angles could improve satellite geometry. However, they are vulnerable to errors due to multipath and ionosphere and troposphere biases. In addition, including them will increase the total number of satellites for selection, consequently, increasing the complexity of satellite selection problem. Thus, excluding these satellite signals could be useful. In addition, RAIM was originally designed for SPP, where it deals with pseudo-range residuals of least square. In contrast, PPP uses KF for positioning estimation based on pseudo-range and carrier phase measurements. Therefore, RAIM, carrier RAIM (CRAIM), and alternative technique, as KFITH, should be investigated for PPP-satellite selection. Furthermore, choosing satellites based on WGDOP-RAIM is applied sequentially. Hence, different selection order should be investigated as they can lead to different results quality.

As a result, the optimal satellites were selected based on WGDOP with and without Ele, RAIM, and KFITH in different combinations and orders. They were selected from multi-GNSS data for 2880 epochs, corresponding to satellite selection every 30 seconds for 24-hour of GNSS dataset. The selected optimal satellites were then utilized for positioning via PPP mode. It has been noticed that the optimal subset of satellites selected has changed frequently over sequential selections (epochs). Excluding satellite signals at low elevation angles (15^{o}) increased the continuity of the selected optimal satellites over selections (epochs) up to 40%. This led to increase the positioning precision. It was also revealed that traditional RAIM is not suitable for PPP, as it had no contribute to PPP-satellite selection. This is consistent with what Zhang and Wang [222] stated, that RAIM is not mature enough for PPP. It is also aligned with Angrisano et al. [226] outcomes, where no satellites were rejected by RAIM during PPP. Thus, CRAIM or KFITH is required for PPP-satellite selection. The most suitable selection combination and order is Ele-RAIM/KFITH-WGDOP, as it excludes low elevation satellites and considers PPP- corrections before satellite selection based on WGDOP.

9.1.4 Experimental evaluation of Satellite Selection Method

As mentioned, the most suitable satellite selection method is the combination of using Ele-RAIM/KFITH-WGDOP. However, it does not support the selection continuity. Thus, it was improved to consider the selection continuity. It was implemented to choose satellites with all possible subset sizes (6-max observed number of satellites). They were selected for PPP from different scenarios: static open-sky, static multipath and kinematic open-sky.

Compared to original PPP, the selected optimal satellites provided equivalent or even millimetres better positioning accuracy in one or more satellite subset sizes in all scenarios. The PPP convergence time of the original PPP (~ 4min) was equivalent to those of the optimal satellite subsets except for those with a large number of satellites. They had less time for convergence due to their low positioning availability.

The continuity of the selected optimal satellites increased as it was considered. However, it had no significant impact on positioning accuracy or precision. This is because its increasing rate was small, where it was less than 5% mostly. In addition, PPP was implemented without carrier phase ambiguity resolution (float-PPP); thus, continuity of selected satellites has low impact of positioning solution.

The optimal satellites were selected in subsets with a fix number of satellites (6-max observed number of satellites). In general, the optimal subsets of 12-15 satellites provided the best positioning accuracy and precision. This is because these number of satellites had high positioning availability as they are mostly available during the entire observation period. In addition, their optimal satellite subsets are less affected by changing satellites in the subset that ranging from 1-7 satellites. Hence, 12-15 satellites are the most suitable number of satellites for selection. This contrasts with most, if not all, studies that has investigated satellite selection with numbers ranging from 4 to 12 (e.g., [7,117]).

However, the subset of 12-15 satellites is only suitable at open-sky and low multipath areas. In high multipath environment, the maximum number of satellites available could be less than12, especially when using cut-off elevation mask. In addition, choosing satellites with a fixed number of satellites can result in selecting a weak satellite signal to complete the number of satellites predetermined. This can be more noticeable in complex environment (high multipath area). Thus, satellite selection with a fixed number is not the most suitable method for satellite selection, especially in high multipath environments.

9.2 Contribution Summary

This works aims to find the most suitable satellite selection method for PPP. It gives a comprehensive evaluation for satellite selection methods, determining their advantages and limitations in Chapter 3. In Chapter 6, comparison evaluation between five optimization algorithms (selection techniques) was conducted, showing their performance in satellite selection. In Chapter 7, ten cases with different selection criteria and selection orders were evaluated. Furthermore, the importance of considering the continuity of the chosen satellites during selection was demonstrated in Chapter 7. Based on the above, a new satellite selection method for PPP, considering all its corrections, was created. This work also defines the most suitable number of satellites (Chapter 7) and the environment for fixed satellite selection (Chapter 8).

9.3 Limitations and Future Work

GNSS results are affected by various factors such as positioning configurations, environment, mode, and equipment quality. To develop new method for selecting GNSS satellites, many of these factors were considered. For example, the satellites were selected with ten cases considering several positioning settings (Ele, RAIM, and KFITH). The performance of the new satellite selection method was assessed under open-sky environmental in statically and kinematically. Its performance was also evaluated statically at different levels of multipath rate. The GNSS data was collected by geodetic receivers and antennas.

However, still several factors were not covered in this study. In addition, the satellite selection method suffers from two main limitations. All these can be defined as the work limitations, which is as follows:

1. The proposed satellite selection method chooses satellites based on fixed number of satellites for the whole period. This is not the best way for satellite selection, especially, in multipath (e.g., urban) areas. In multipath areas, the number and geometry of the observed satellites change quickly. Therefore, choosing a fixed number of satellites at all times cannot accommodate the changing status of satellites over time.
2. The proposed satellite selection method was evaluated only for post-positioning and not for real time positioning.
3. The proposed satellite selection method took several seconds (> 4sec) to choose the optimal satellite subset from single epoch. Hence, the proposed satellite selection method is not quick enough for real-time positioning at 1Hz or more.
4. RAIM was used for selecting satellites. However, CRAIM has not been used, which may provide different results.
5. The positioning solution of the selected satellites was determined with float PPP. The positioning quality can be changed with fix PPP, fixing ambiguity resolution.
6. The performance of the new satellite selection has not been evaluated kinematically under multipath area.
7. GNSS data from low-cost receiver and antenna has not been considered.

The above limitations can be points for Future work for satellite selection.

References

1. GPS.GOV Space Segment Available online: https://www.gps.gov/systems/gps/space/ (accessed on 8 January 2024).
2. GLONASS Application Consumer Center About GLONASS Available online: https://glonass-iac.ru/en/about_glonass/ (accessed on 25 November 2024).
3. European GNSS Service Center Constellation Information Available online: https://www.gsc-europa.eu/system-service-status/constellation-information (accessed on 25 November 2024).
4. GPS.GOV Other Global Navigation Satellite Systems (GNSS) Available online: https://www.gps.gov/systems/gnss/ (accessed on 8 January 2024).
5. Quasi-Zenith Satellite System (QZSS) What Is the Quasi-Zenith Satellite System (QZSS)? Available online: https://qzss.go.jp/en/overview/services/sv02_why.html (accessed on 25 November 2024).
6. Indian Space Research Organisation, D. of S. Indian Regional Navigation Satellite System (IRNSS) : NavIC Available online: https://www.isro.gov.in/IRNSS_Programme.html (accessed on 25 November 2024).
7. Yu, Q.; Wang, Y.; Shen, Y. A Fast GNSS Satellite Selection Algorithm for Continuous Real-Time Positioning. *GPS Solutions* **2022**, *26*, doi:10.1007/s10291-022-01251-1.
8. Zhang, M.; Zhang, J.; Qin, Y. Satellite Selection for Multi-Constellation. In Proceedings of the IEEE/ION Position, Location and Navigation Symposium; 2008; pp. 1053–1059.
9. Xu, B.; Bingjun, S. Satellite Selection Algorithm for Combined GPS-Galileo Navigation Receiver. In Proceedings of the 2009 4th International Conference on Autonomous Robots and Agents; 2009; pp. 149–154.
10. Nie, Z.; Gao, Y.; Wang, Z.; Ji, S. A New Method for Satellite Selection with Controllable Weighted PDOP Threshold. *Survey review - Directorate of Overseas Surveys* **2017**, *49*, 285–293, doi:10.1080/00396265.2016.1171959.
11. Msaewe, H.A.; Hancock, C.M.; Psimoulis, P.A.; Roberts, G.W.; Bonenberg, L.; de Ligt, H. Investigating Multi-GNSS Performance in the UK and China Based on a Zero-Baseline Measurement Approach. *Measurement (Lond)* **2017**, *102*, 186–199, doi:10.1016/j.measurement.2017.02.004.
12. Lau, L.; Tateshita, H.; Sato, K. Impact of Multi-GNSS on Positioning Accuracy and Multipath Errors in High-Precision Single-Epoch Solutions-A Case Study in Ningbo China Real-Time Kinematic (RTK) Global Positioning System (GPS) Carrier Phase-Based Precise Positioning. *Journal of Navigation* **2015**, *68*, 999–1017, doi:10.1017/S0373463315000168.
13. Takahashi, S.; Kubo, N.; Yamaguchi, N.; Yokoshima, T. Real-Time Monitoring for Structure Deformations Using Hand-Held RTK-GNSS Receivers on the Wall. In Proceedings of the The Institute of Electrical and Electronics Engineers, Inc. (IEEE) Conference Proceedings; 2017; p. 1.

14. Wang, H.; Cheng, Y.; Cheng, C.; Li, S.; Li, Z. Research on Satellite Selection Strategy for Receiver Autonomous Integrity Monitoring Applications. *Remote Sens (Basel)* **2021**, *13*, doi:10.3390/rs13091725.

15. Nie, Z.; Gao, Y.; Wang, Z.; Ji, S. A New Method for Satellite Selection with Controllable Weighted PDOP Threshold. *Survey Review* **2017**, *49*, 285–293, doi:10.1080/00396265.2016.1171959.

16. Xue, C.; Psimoulis, P.; Horsfall, A.; Zhang, Q.; Meng, X. Assessment of the Accuracy of Low-Cost Multi-GNSS Receivers in Monitoring Dynamic Response of Structures. *Applied Geomatics* **2023**, *15*, 315–326, doi:10.1007/s12518-022-00482-8.

17. Poluzzi, L.; Tavasci, L.; Corsini, F.; Barbarella, M.; Gandolfi, S. Low-Cost GNSS Sensors for Monitoring Applications. *Applied Geomatics* **2020**, *12*, 35–44, doi:10.1007/s12518-019-00268-5.

18. Manzini, N.; Orcesi, A.; Thom, C.; Brossault, M.A.; Botton, S.; Ortiz, M.; Dumoulin, J. Performance Analysis of Low-Cost GNSS Stations for Structural Health Monitoring of Civil Engineering Structures. *Structure and Infrastructure Engineering* **2022**, *18*, 595–611, doi:10.1080/15732479.2020.1849320.

19. Xue, C.; Psimoulis, P.A. Monitoring the Dynamic Response of a Pedestrian Bridge by Using Low-Cost GNSS Receivers. *Eng Struct* **2023**, *284*, doi:10.1016/j.engstruct.2023.115993.

20. Wang, E.; Sun, C.; guo, J.; Qu, P.; Pang, T.; Zhang, J. GNSS Receiver Satellite Selection Algorithm Based on Particle Swarm Optimization. In Proceedings of the 15th IEEE Conference on Industrial Electronics and Applications (ICIEA); 2020; pp. 985–989.

21. Yang, L.; Gao, J.; Li, Z.; Li, F.; Chen, C.; Wang, Y. New Satellite Selection Approach for GPS/BDS/GLONASS Kinematic Precise Point Positioning. *Applied Sciences (Switzerland)* **2019**, *9*, doi:10.3390/app9245280.

22. Martini, I.; Susi, M.; Fernandez-Hernandez, I. PPP and Galileo High Accuracy Service with Satellite Selection Strategies for Kinematic Applications. In Proceedings of the 35th International Technical Meeting of the Satellite Division of the Institute of Navigation, ION GNSS+ 2022; 2022; pp. 635–650.

23. Rizos, C.; Janssen, V.; Roberts, C.; Grinter, T. Precise Point Positioning: Is the Era of Differential GNSS Positioning to an End? In Proceedings of the FIG Working Week 2012; Rome, Italy, May 2012.

24. Kaplan, E.D.; Hegarty, C.J. *Understanding GPS/GNSS: Principles and Applications, Third Edition*; Artech, 2017;

25. Aggrey, J.; Bisnath, S. Improving GNSS PPP Convergence: The Case of Atmospheric-Constrained, Multi-GNSS PPP-AR. *Sensors (Switzerland)* **2019**, *19*, doi:10.3390/s19030587.

26. Li, M.; Xu, T.; Guan, M.; Gao, F.; Jiang, N. LEO-Constellation-Augmented Multi-GNSS Real-Time PPP for Rapid Re-Convergence in Harsh Environments. *GPS Solutions* **2022**, *26*, doi:10.1007/s10291-021-01217-9.

27. Li, P.; Zhang, X. Integrating GPS and GLONASS to Accelerate Convergence and Initialization Times of Precise Point Positioning. *GPS Solutions* **2014**, *18*, 461–471, doi:10.1007/s10291-013-0345-5.

28. International GNSS Service (IGS) RINEX Version 3.04 Available online: http://acc.igs.org/misc/rinex304.pdf (accessed on 7 June 2024).

29. BeiDou Navigation Satellite System The Official BeiDou Site Available online: http://en.beidou.gov.cn/SYSTEMS/System/ (accessed on 10 January 2025).

30. El-Rabbany, A. *Introduction to GPS The Global Positioning System Second Edition*; Second Edition.; Artech House, 2009;

31. Robustelli, U.; Benassai, G.; Pugliano, G. Signal in Space Error and Ephemeris Validity Time Evaluation of Milena and Doresa Galileo Satellites. *Sensors (Basel)* **2019**, *19*, 1786, doi:10.3390/s19081786.

32. Sickle, J. Van *GPS and GNSS for Land Surveyors*; CRC Press, 2024;

33. de Lacy, M.C.; Reguzzoni, M.; Sansò, F. Real-Time Cycle Slip Detection in Triple-Frequency GNSS. *GPS Solutions* **2012**, *16*, 353–362, doi:10.1007/s10291-011-0237-5.

34. Zhou, H.; Wang, L.; Fu, W.; Li, T.; Li, W.; Chen, R. Real-Time GNSS Triple-Frequency Cycle Slip Detection Using Three Optimal Linear Combinations. *GPS Solutions* **2023**, *27*, doi:10.1007/s10291-023-01482-w.

35. Zhen Dai; Knedlik, S.; Loffeld, O.; Kaiser, T.; Kyamakya, K.; Jobmann, K. Real-Time Cycle-Slip Detection and Determination for Multiple Frequency GNSS. In Proceedings of the 2008 5th Workshop on Positioning, Navigation and Communication; IEEE: NEW YORK, 2008; pp. 37–43.

36. Li, T.; Melachroinos, S. An Enhanced Cycle Slip Repair Algorithm for Real-Time Multi-GNSS, Multi-Frequency Data Processing. *GPS Solutions* **2019**, *23*, doi:10.1007/s10291-018-0792-0.

37. Momoh, J.A.; Bhattarai, S.; Ziebart, M. Receiver Clock Jump and Cycle Slip Correction Algorithm for Single-Frequency GNSS Receivers. *GPS Solutions* **2019**, *23*, doi:10.1007/s10291-019-0832-4.

38. Park, C.; Kim, I.; Gyu Lee, J.; Jee, G.-I. A Satellite Selection Criterion Incorporating the Effect of Elevation Angle in GPS Positioning. *Control Eng Pract* **1996**, *4*, 1741–1746, doi:10.1016/S0967-0661(96)00192-X.

39. Rao, G.S.; Siripurapu, D.; Bagadi, L. Elevation and Position Uncertainty Based KF Model for Position Accuracy Improvement. *Procedia Comput Sci* **2018**, 914–920, doi:10.1016/j.procs.2018.10.362.

40. Wang, G.; Jiang, J. Fast Satellite Selection Algorithm Based on Satellite Elevation Angle and Satelte Contribution for Geometry Dilution of Precision in GPS / BEIDOU. **2018**, 4859–4863.

41. Wei, M.; Wang, J.; Li, J. A New Satellite Selection Algorithm for Real-Time Application. *In 2012 international conference on systems and informatics (ICSAI2012)* **2012**, 2567–2570.

42. Odolinski, R.; Teunissen, P.J.G. Single-Frequency, Dual-GNSS versus Dual-Frequency, Single-GNSS: A Low-Cost and High-Grade Receivers GPS-BDS RTK Analysis. *J Geod* **2016**, *90*, 1255–1278, doi:10.1007/s00190-016-0921-x.

43. Fang, Y.Y.; Hong, Y.; Zhou, O.G.; Liang, W.; WenXue, L. A GNSS Satellite Selection Method Based on SNR Fluctuation in Multipath Environments. *International Journal of Control and Automation* **2015**, *8*, 313–324, doi:10.14257/ijca.2015.8.11.30.

44. Kiliszek, D.; Kroszczyński, K. Performance of the Precise Point Positioning Method along with the Development of GPS, GLONASS and Galileo Systems. *Measurement (Lond)* **2020**, *164*, 108009, doi:10.1016/j.measurement.2020.108009.

45. He, H.; Li, J.; Yang, Y.; Xu, J.; Guo, H.; Wang, A. Performance Assessment of Single-and Dual-Frequency BeiDou/ GPS Single-Epoch Kinematic Positioning. *GPS Solutions* **2014**, *18*, 393–403, doi:10.1007/s10291-013-0339-3.

46. Odolinski, R.; Teunissen, P.J.G.; Odijk, D. Combined BDS, Galileo, QZSS and GPS Single-Frequency RTK. *GPS Solutions* **2015**, *19*, 151–163, doi:10.1007/s10291-014-0376-6.

47. Teunissen, P.J.G.; Odolinski, R.; Odijk, D. Instantaneous BeiDou+GPS RTK Positioning with High Cut-off Elevation Angles. *J Geod* **2014**, *88*, 335–350, doi:10.1007/s00190-013-0686-4.

48. Kaloop, M.R.; Yigit, C.O.; El-Mowafy, A.; Bezcioglu, M.; Dindar, A.A.; Hu, J.W. Evaluation of Multi-GNSS High-Rate Relative Positioning for Monitoring Dynamic Structural Movements in the Urban Environment. *Geomatics, Natural Hazards and Risk* **2020**, *11*, 2239–2262, doi:10.1080/19475705.2020.1836040.

49. Liu, X.; Zhang, S.; Zhang, Q.; Ding, N.; Yang, W. A Fast Satellite Selection Algorithm with Floating High Cut-off Elevation Angle Based on ADOP for Instantaneous Multi-GNSS Single-Frequency Relative Positioning. *Advances in Space Research* **2019**, *63*, 1234–1252, doi:10.1016/j.asr.2018.10.032.

50. Yong, Y.; Lingjuan, M. GDOP Results in All-in-View Positioning and in Four Optimum Satellites Positioning with GPS PRN Codes Ranging. In Proceedings of the PLANS 2004. Position Location and Navigation Symposium (IEEE Cat. No.04CH37556); 2004; pp. 723–727.

51. Wei, M.; Liu, Z.; Li, C.; Yang, R.; Li, B.; Xu, Q. A Combined Satellite Selection Algorithm. In Proceedings of the International Conference on Security, Pattern Analysis, and Cybernetics (SPAC); 2018; pp. 477–480.

52. Wei, M.; Wang, J.; Li, J. A New Satellite Selection Algorithm for Real-Time Application. In Proceedings of the International Conference on Systems and Informatics (ICSAI2012); IEEE, 2012; pp. 2567–2570.

53. Wei, M.; Wang, J.; Yang, X.B. An Improved Satellite Selection Algorithm. In Proceedings of the International Conference on Signal Processing Proceedings, ICSP; IEEE, 2012; Vol. 3, pp. 2258–2261.

54. Rapiński, J.; Tomaszewski, D.; Kowalski, M. Analysis of the Code and Carrier Phase Measurements Performed with LEA-6T GPS Receiver. In Proceedings of the 9th International Conference on Environmental Engineering, ICEE 2014; Vilnius Gediminas Technical University, Department of Construction Economics & Property, 2014; p. 1.

55. Richardson, T.; Hill, C.; Moore, T.; Toor, P. Analysis of Multi-Constellation GNSS Signal Quality. In Proceedings of the In Proceedings of the 2016 International Technical Meeting of The Institute of Navigation; 2016.

56. Uaratanawong, V.; Satirapod, C.; Tsujii, T. Optimization Technique for Pseudorange Multipath Mitigation Using Different Signal Selection Methods. *Artificial Satellites* **2020**, *55*, 77–86, doi:10.2478/arsa-2020-0006.

57. Aichinger-Rosenberger, M.; Aregger, M.; Kopp, J.; Soja, B. Detecting Signatures of Convective Storm Events in GNSS-SNR: Two Case Studies From Summer 2021 in Switzerland. *Geophys Res Lett* **2023**, *50*, doi:10.1029/2023GL104916.

58. Qing, Y.; Lin, J.; Liu, Y.; Dai, X.; Lou, Y.; Gu, S. Precise Orbit Determination of the China Seismo-Electromagnetic Satellite (CSES) Using Onboard GPS and BDS Observations. *Remote Sens (Basel)* **2020**, *12*, 1–17, doi:10.3390/rs12193234.

59. Phan, Q.H.; Tan, S.L.; McLoughlin, I. GPS Multipath Mitigation: A Nonlinear Regression Approach. *GPS Solutions* **2013**, *17*, 371–380, doi:10.1007/s10291-012-0285-5.

60. Steigenberger, P.; Thölert, S.; Montenbruck, O. Flex Power on GPS Block IIR-M and IIF. *GPS Solutions* **2019**, *23*, doi:10.1007/s10291-018-0797-8.

61. Arul Elango, G.; Sudha, G.F.; Francis, B. Weak Signal Acquisition Enhancement in Software GPS Receivers – Pre-Filtering Combined Post-Correlation Detection Approach. *Applied Computing and Informatics* **2017**, *13*, 66–78, doi:10.1016/j.aci.2014.10.002.

62. Zangenehnejad, F.; Gao, Y. GNSS Smartphones Positioning: Advances, Challenges, Opportunities, and Future Perspectives. *Satellite Navigation* **2021**, *2*, doi:10.1186/s43020-021-00054-y.

63. Huang, J.Y.; Tsai, C.H. Improve GPS Positioning Accuracy with Context Awareness. In Proceedings of the Proceedings - 2008 the 1st IEEE International Conference on Ubi-Media Computing and Workshops, U-Media2008; 2008; pp. 94–99.

64. Rost, C.; Wanninger, L. Carrier Phase Multipath Mitigation Based on GNSS Signal Quality Measurements. *Journal of Applied Geodesy* **2009**, *3*, doi:10.1515/JAG.2009.009.

65. Tokura, H.; Kubo, N. Efficient Satellite Selection Method for Instantaneous RTK-GNSS in Challenging Environments. *Trans Jpn Soc Aeronaut Space Sci* **2017**, *60*, 221–229, doi:10.2322/tjsass.60.221.

66. Tokura, H.; Yamada, H.; Kubo, N.; Pullen, S. Using Multiple GNSS Constellations with Strict Quality Constraints for More Accurate Positioning in Urban Environments. *Positioning* **2014**, *05*, 85–96, doi:10.4236/pos.2014.54011.

67. Kaplan, E.D.; Hegarty, C. *Understanding GPS/GNSS: Principles and Applications, Third Edition*; 2017;

68. Rajasekhar, C.; Srilatha Indira Dutt, V.B.S.; Sasibhushana Rao, G. Investigation of Best Satellite–Receiver Geometry to Improve Positioning Accuracy Using GPS and IRNSS Combined Constellation over Hyderabad Region. *Wirel Pers Commun* **2016**, *88*, 385–393, doi:10.1007/s11277-015-3126-3.

69. Shihab, R.H.; Tabassum, A.; Hossam-E-Haider, M. Comparison of DOP of GPS and Galileo in the South Asian Region. In Proceedings of the 1st International Conference on Electrical Engineering and Information and Communication Technology, ICEEICT; 2014; pp. 10–13.

70. Dutt, B.S.S.I.; Rao, G.S.B.; Rani, S.S.; Babu, S.R.; Goswami, R.; Kumari, C.U. Investigation of GDOP for Precise User Position Computation with All Satellites in View and Optimum Four Satellite Configurations. *Journal of Indian Geophysical Union* **2009**, *13*, 139–148.

71. Langley, R.B. Dilution of Precision. In *GPS World*; 1999; Vol. 10, pp. 52–59.

72. Jwo, D.-J. Efficient DOP Calculation for GPS with and without Altimeter Aiding. *Journal of Navigation* **2001**, *54*, 269–279, doi:10.1017/S0373463301001321.

73. Chen, C.S.; Lin, J.M.; Lee, C.T. Neural Network for WGDOP Approximation and Mobile Location. *Math Probl Eng* **2013**, *2013*, doi:10.1155/2013/369694.

74. Borwein, J.M.; Crandall, R.E. Closed Forms : What They Are and Why We Care. *Notices of the American Mathematical Society* **2013**, *60*, 50–65.

75. Jwo, D.J. Efficient DOP Calculation for GPS with and without Altimeter Aiding. *Journal of Navigation* **2001**, *54*, 269–279, doi:10.1017/S0373463301001321.

76. Doong, S.H. A Closed-Form Formula for GPS GDOP Computation. *GPS solutions* **2009**, *13*, 183–190, doi:10.1007/s10291-008-0111-2.

77. Meng, F.; Zhu, B.; Wang, S. A New Fast Satellite Selection Algorithm for BDS-GPS Receivers. *IEEE Workshop on Signal Processing Systems, SiPS: Design and Implementation* **2013**, *m*, 371–376, doi:10.1109/sips.2013.6674535.

78. Teng, Y.; Wang, J. A Closed-Form Formula to Calculate Geometric Dilution of Precision (GDOP) for Multi-GNSS Constellations. *GPS solutions* **2016**, *20*, 331–339, doi:10.1007/s10291-015-0440-x.

79. Chen, C. Weighted Geometric Dilution of Precision Calculations with Matrix Multiplication. *Sensors* **2015**, *15*, 803–817, doi:10.3390/s150100803.

80. Teng, Y.; Wang, J.; Huang, Q.; Liu, B. New Characteristics of Weighted GDOP in Multi-GNSS Positioning. *GPS Solutions* **2018**, *22*, 1–9, doi:10.1007/s10291-018-0740-z.

81. Abedi, A.A.; Mosavi, M.R.; Mohammadi, K. A New Recursive Satellite Selection Method for Multi-Constellation GNSS. *Survey Review* **2020**, *52*, 330–340, doi:10.1080/00396265.2019.1574113.

82. Dutt, B.S.S.I.; Rao, G.S.B.; Rani, S.S.; Babu, S.R.; Goswami, R.; Kumari, C.U. Investigation of GDOP for Precise User Position Computation with All Satellites in View and Optimum Four Satellite Configurations. *Journal of Indian Geophysical Union* **2009**, *13*, 139–148.

83. Sickle, J. Van *GPS for Land Surveyors, Fourth Edition*; Boca Raton, 2015; ISBN 9780429103353.

84. Jwo, D.-J.; Lai, C.-C. Neural Network-Based GPS GDOP Approximation and Classification. *GPS Solutions* **2007**, *11*, 51–60, doi:10.1007/s10291-006-0030-z.

85. Zuo-ya, Z.; Cheng, H.; Chu-gang, F.; Fei-peng, Z. Selection of GPS Satellites for the Optimum Geometry. *Chinese Astronomy and Astrophysics* **2004**, *28*, 80–87, doi:10.1016/S0275-1062(04)90009-4.

86. Hsu, D.Y. Relations between Dilutions of Precision and Volume of the Tetrahedron Formed by Four Satellites. In Proceedings of the Proceedings of 1994 IEEE Position, Location and Navigation Symposium - PLANS'94; 1994; pp. 669–676.

87. Zhang, M.; Zhang, J. A Fast Satellite Selection Algorithm: Beyond Four Satellites. *IEEE Journal on Selected Topics in Signal Processing* **2009**, *3*, 740–747, doi:10.1109/JSTSP.2009.2028381.

88. Kong, J.H.; Mao, X.; Li, S. BDS/GPS Satellite Selection Algorithm Based on Polyhedron Volumetric Method. In Proceedings of the 2014 IEEE/SICE International Symposium on System Integration, SII 2014; IEEE, 2014; pp. 340–345.

89. Blanco-delgado, N.; Nunes, F.D. Satellite Selection Method for Multi-Constellation GNSS Using Convex Geometry. *IEEE Trans Veh Technol* **2010**, *59*, 4289–4297.

90. Blanco-Delgado, N.; Nunes, F.D.; Seco-Granados, G. Relation between GDOP and the Geometry of the Satellite Constellation. In Proceedings of the 2011 International Conference on Localization and GNSS (ICL-GNSS); IEEE, 2011; pp. 175–180.

91. Zuo-ya, Z.; Cheng, H.; Chu-gang, F.; Fei-peng, Z. Selection of GPS Satellites for the Optimum Geometry. *Chinese Astronomy and Astrophysics* **2004**, *28*, 80–87, doi:10.1016/S0275-1062(04)90009-4.

92. Du, H.; Hong, Y.; Xia, N.; Zhang, G.; Yu, Y.; Zhang, J. A Navigation Satellites Selection Method Based on ACO with Polarized Feedback. In Proceedings of the IEEE Access; 2020; Vol. 8, pp. 168246–168261.

93. Flores, J.A. *Focus on Artificial Neural Networks*; 1st ed.; Nova Science Publishers, Incorporated, 2011;

94. Izgi, E.; Öztopal, A.; Yerli, B.; Kaymak, M.K.; Şahin, A.D. Short-Mid-Term Solar Power Prediction by Using Artificial Neural Networks. *Solar Energy* **2012**, *86*, 725–733, doi:10.1016/j.solener.2011.11.013.

95. Jwo, D.J.; Chin, K.P. Applying Back-Propagation Neural Networks to GDOP Approximation. *Journal of Navigation* **2002**, *55*, 97–108, doi:10.1017/S0373463301001606.

96. Azami, H.; Sanei, S. GPS GDOP Classification via Improved Neural Network Trainings and Principal Component Analysis. *International journal of electronics* **2014**, *101*, 1300–1313, doi:10.1080/00207217.2013.832390.

97. Zarei, N. Artificial Intelligence Approaches for GPS GDOP Classification. *Int J Comput Appl* **2014**, *96*, 16–21, doi:10.5120/16878-6877.

98. Simon, D.; El-Sherief, H. Navigation Satellite Selection Using Neural Networks. *Neurocomputing* **1995**, *7*, 247–258, doi:10.1016/0925-2312(94)00024-M.

99. Mosavi, M.R.; Shiroie, M. Efficient Evolutionary Algorithms for GPS Satellites Classification. *Arab J Sci Eng* **2012**, *37*, 2003–2015, doi:10.1007/s13369-012-0298-y.

100. Asadi, S.; Shahrabi, J.; Abbaszadeh, P.; Tabanmehr, S. A New Hybrid Artificial Neural Networks for Rainfall-Runoff Process Modeling. *Neurocomputing* **2013**, *121*, 470–480, doi:10.1016/j.neucom.2013.05.023.

101. Raja Sekhar, C.; Srilatha Indira Dutt, V.B.S.; Sasibhushana Rao, G. GDoP Estimation Using Simulated Annealing for GPS and IRNSS Combined Constellation. *Engineering Science and Technology, an International Journal* **2016**, *19*, 1881–1886, doi:10.1016/j.jestch.2016.09.017.

102. Simon, D.; El-Sherief, H. Navigation Satellite Selection Using Neural Networks. *Neurocomputing (Amsterdam)* **1995**, *7*, 247–258, doi:10.1016/0925-2312(94)00024-M.

103. Wu, C.H.; Su, W.H. A Comparative Study on Regression Models of GPS GDOP Using Soft-Computing Techniques. *IEEE International Conference on Fuzzy Systems* **2009**, 1513–1516, doi:10.1109/FUZZY.2009.5277243.

104. Huo, H.; Zheng, Z.; Zhang, X. An Optimal Satellite Selection Method Based on Genetic Algorithms. *International Journal of Simulation: Systems, Science and Technology* **2016**, *17*, 40.1-40.9, doi:10.5013/IJSSST.a.17.25.40.

105. Song, J.; Xue, G.; Kang, Y.; Wang, Y. A Novel Method for Optimum Global Positioning System Satellite Selection Based on a Modified Genetic Algorithm. *PLoS One* **2016**, *11*, e0150005–e0150005, doi:10.1371/journal.pone.0150005.

106. Xia, J.; Wang, Y.; Li, Y. A Navigation Satellite Selection Method Based on Tabu Search Artificial Bee Colony Algorithm. In Proceedings of the IEEE 3rd International Conference on Electronic Information and Communication Technology (ICEICT); 2020; pp. 421–425.

107. Meng, X.; Nie, P.; Sun, J.; Niu, Z.; Zhu, B. A Novel Satellite Selection Method Based On Genetic Algorithm. In Proceedings of the 11th UK-Europe-China Workshop on Millimeter Waves and Terahertz Technologies, UCMMT 2018 - Proceedings; 2018; Vol. 1, pp. 1–3.

108. Mosavi, M.R.; Shiroie, M. Efficient Evolutionary Algorithms for GPS Satellites Classification. *Arab J Sci Eng* **2012**, *37*, 2003–2015, doi:10.1007/s13369-012-0298-y.

109. Ostojić, D.; Ramljak, D.; Urošević, A.; Jolović, M.; Drašković, R.; Kakka, J.; Jakšić Krüger, T.; Davidović, T. Systematic Literature Review of Optimization Algorithms for P||Cmax Problem. *Symmetry (Basel)* **2025**, *17*, doi:10.3390/sym17020178.

110. Mohammadi, A.; Sheikholeslam, F. Intelligent Optimization: Literature Review and State-of-the-Art Algorithms (1965–2022). *Eng Appl Artif Intell* **2023**, *126*, doi:10.1016/j.engappai.2023.106959.

111. Stefanoni, M.; Sarcevic, P.; Sárosi, J.; Odry, A. Optimization Techniques in the Localization Problem: A Survey on Recent Advances. *Machines* **2024**, *12*, doi:10.3390/machines12080569.

112. Chen, C.-S. Weighted Geometric Dilution of Precision Calculations with Matrix Multiplication. *Sensors (Basel)* **2015**, *15*, 803–817, doi:10.3390/s150100803.

113. Blanco-delgado, N.; Nunes, F.D. Satellite Selection Based on WDOP Concept and Convex Geometry. In Proceedings of the 2010 5th ESA Workshop on Satellite Navigation Technologies and European Workshop on GNSS Signals and Signal Processing (NAVITEC) (2010): 1-8. Web.; IEEE, 2010.

114. Teng, Y.; Wang, J.; Huang, Q.; Liu, B. New Characteristics of Weighted GDOP in Multi-GNSS Positioning. *GPS Solutions* **2018**, *22*, 1–9, doi:10.1007/s10291-018-0740-z.

115. Sairo, H.; Akopian, D.; Takala, J. Weighted Dilution of Precision as Quality Measure in Satellite Positioning. *IEE Proceedings: Radar, Sonar and Navigation* **2003**, *150*, 430–436, doi:10.1049/ip-rsn:20031008.

116. Rost, C.; Wanninger, L. Carrier Phase Multipath Mitigation Based on GNSS Signal Quality Measurements. *Journal of Applied Geodesy* **2009**, *3*, doi:10.1515/JAG.2009.009.

117. Meng, X.; Wang, S.; Nie, P.; Niu, Z.; Zhu, B. An Efficient Genetic Algorithm of Multi-Constellation Satellite Selection. In Proceedings of the 2018 IEEE 4th International Conference on Computer and Communications, ICCC 2018; IEEE, 2018; pp. 2200–2204.

118. Takasu, T. RTKLIB - Demo5 Manual Available online: https://rtkexplorer.com/pdfs/manual_demo5.pdf (accessed on 7 June 2024).

119. Takasu, T. RTKLIB Ver. 2.4.2 Manual Available online: https://www.rtklib.com/prog/manual_2.4.2.pdf (accessed on 7 June 2024).

120. Angrisano, A.; Gaglione, S.; Crocetto, N.; Vultaggio, M. PANG-NAV: A Tool for Processing GNSS Measurements in SPP, Including RAIM Functionality. *GPS Solutions* **2020**, *24*, doi:10.1007/s10291-019-0935-y.

121. Meng, F.; Xing, C.; Sun, P.; Zhu, Z.; Li, N. Identification and Exclusion Multiple Outliers in GNC Microsystem. *American Journal of Science, Engineering and Technology* **2020**, *5*, 61, doi:10.11648/j.ajset.20200502.12.

122. Angrisano, A.; Gaglione, S. Smartphone GNSS Performance in an Urban Scenario with RAIM Application. *Sensors* **2022**, *22*, doi:10.3390/s22030786.

123. Feng, S.; Ochieng, W.; Samson, J.; Tossaint, M.; Hernandez-Pajares, M.; Juan, J.M.; Sanz, J.; Aragón-Àngel, À.; Ramos-Bosch, P.; Jofre, M. Integrity Monitoring for Carrier Phase Ambiguities. *Journal of Navigation* **2012**, *65*, 41–58, doi:10.1017/S037346331100052X.

124. Meng, F.; Xing, C.; Sun, P.; Zhu, Z.; Li, N. *IEEE Aerospace and Electronic Systems Magazine*. Institute of Electrical and Electronics Engineers Inc. 2015, pp. 14–27.

125. Meng, F.; Zhu, B.; Wang, S. A New Fast Satellite Selection Algorithm for BDS-GPS Receivers. In Proceedings of the SiPS 2013 Proceedings; IEEE, 2013; pp. 371–376.

126. Teng, Y.; Wang, J. A Closed-Form Formula to Calculate Geometric Dilution of Precision (GDOP) for Multi-GNSS Constellations. *GPS solutions* **2016**, *20*, 331–339, doi:10.1007/s10291-015-0440-x.

127. Hong, Y.; Xu, S. A Navigation Satellite Selection Method Based on Optimized DPSO Algorithm. In Proceedings of the Proceedings - 2020 IEEE 6th Intl Conference on Big Data Security on Cloud, BigDataSecurity 2020, 2020 IEEE Intl Conference on High Performance and Smart Computing, HPSC 2020 and 2020 IEEE Intl Conference on Intelligent Data and Security, IDS 2020; 2020; pp. 174–179.

128. Abedi, A.A.; Mosavi, M.R.; Mohammadi, K. A New Recursive Satellite Selection Method for Multi-Constellation GNSS. *Survey Review* **2020**, *52*, 330–340, doi:10.1080/00396265.2019.1574113.

129. Doong, S.H. A Closed-Form Formula for GPS GDOP Computation. *GPS solutions* **2009**, *13*, 183–190, doi:10.1007/s10291-008-0111-2.

130. Wu, C.H.; Su, W.H. A Comparative Study on Regression Models of GPS GDOP Using Soft-Computing Techniques. *IEEE International Conference on Fuzzy Systems* **2009**, 1513–1516, doi:10.1109/FUZZY.2009.5277243.

131. Habboub, M.; Psimoulis, P.A.; Bingley, R.; Rothacher, M. A Multiple Algorithm Approach to the Analysis of GNSS Coordinate Time Series for Detecting Geohazards and Anomalies. *J Geophys Res Solid Earth* **2020**, *125*, doi:10.1029/2019JB018104.

132. Liu, H.; Yan, G.; Duan, Z.; Chen, C. Intelligent Modeling Strategies for Forecasting Air Quality Time Series: A Review. *Appl Soft Comput* **2021**, *102*, doi:10.1016/j.asoc.2020.106957.

133. Ali, A.O.; Elmarghany, M.R.; Abdelsalam, M.M.; Sabry, M.N.; Hamed, A.M. Closed-Loop Home Energy Management System with Renewable Energy Sources in a Smart Grid: A Comprehensive Review. *J Energy Storage* **2022**, *50*, doi:10.1016/j.est.2022.104609.

134. Tomar, V.; Bansal, M.; Singh, P. Metaheuristic Algorithms for Optimization: A Brief Review. *Engineering Proceedings* **2023**, *59*, doi:10.3390/engproc2023059238.

135. Kaveh, A.; Javadi, S.M.; Moghanni, R.M. Emergency Management Systems after Disastrous Earthquakes Using Optimization Methods: A Comprehensive Review. *Advances in Engineering Software* 2020, *149*.

136. Wang, E.; Sun, C.; Wang, C.; Qu, P.; Huang, Y.; Pang, T. A Satellite Selection Algorithm Based on Adaptive Simulated Annealing Particle Swarm Optimization for the BeiDou Navigation Satellite System/Global Positioning System Receiver. *Int J Distrib Sens Netw* **2021**, *17*, 155014772110317, doi:10.1177/15501477211031748.

137. Karaboga, D. AN IDEA BASED ON HONEY BEE SWARM FOR NUMERICAL OPTIMIZATION. *Technical Report TR06, Erciyes University, Engineering Faculty, Computer Engineering Department* **2005**, *200*, 1–10, doi:10.2320/materia.44.24.

138. Abu-Mouti, F.S.; El-Hawary, M.E. Overview of Artificial Bee Colony (ABC) Algorithm and Its Applications. In Proceedings of the 2012 IEEE International Systems Conference SysCon 2012; IEEE, 2012; pp. 1–6.

139. Pian, J.; Wang, G.; Li, B. An Improved ABC Algorithm Based on Initial Population and Neighborhood Search. *IFAC-PapersOnLine* **2018**, *51*, 251–256, doi:10.1016/j.ifacol.2018.09.308.

140. Zhu, G.; Kwong, S. Gbest-Guided Artificial Bee Colony Algorithm for Numerical Function Optimization. *Appl Math Comput* **2010**, *217*, 3166–3173, doi:10.1016/j.amc.2010.08.049.

141. Secui, D.C. A New Modified Artificial Bee Colony Algorithm for the Economic Dispatch Problem. *Energy Convers Manag* **2015**, *89*, 43–62, doi:10.1016/j.enconman.2014.09.034.

142. Chidambaram, C.; Lopes, H.S. A New Approach for Template Matching in Digital Images Using an Artificial Bee Colony Algorithm. In Proceedings of the 2009 WORLD CONGRESS ON NATURE & BIOLOGICALLY INSPIRED COMPUTING (NABIC 2009); IEEE: NEW YORK, 2009; pp. 146–151.

143. Zhang, C.; Ouyang, D.; Ning, J. An Artificial Bee Colony Approach for Clustering. *Expert Syst Appl* **2010**, *37*, 4761–4767, doi:10.1016/j.eswa.2009.11.003.

144. Karaboga, D.; Ozturk, C. A Novel Clustering Approach: Artificial Bee Colony (ABC) Algorithm. *Applied Soft Computing Journal* **2011**, *11*, 652–657, doi:10.1016/j.asoc.2009.12.025.

145. Manuel Vargas Benítez, C.; Silvério Lopes, H. Parallel Artificial Bee Colony Algorithm Approaches for Protein Structure Prediction Using the 3DHP-SC Model. In Proceedings of the Intelligent Distributed Computing IV: Proceedings of the 4th International Symposium on Intelligent Distributed Computing - IDC 2010, Tangier, Morocco; 2010; pp. 255–264.

146. Santhi, V.; Nandhini, S. An Efficient Algorithm for Job Scheduling Problem-Enhanced Artificial Bee Colony Algorithm. *Asian Journal of Information Technology* **2016**, *15*, 2210–2216, doi:10.3923/ajit.2016.2210.2216.

147. Akay, B.; Karaboga, D. Artificial Bee Colony Algorithm for Large-Scale Problems and Engineering Design Optimization. *J Intell Manuf* **2012**, *23*, 1001–1014, doi:10.1007/s10845-010-0393-4.

148. Huang, S.J.; Liu, X.Z. Application of Artificial Bee Colony-Based Optimization for Fault Section Estimation in Power Systems. *International Journal of Electrical Power and Energy Systems* **2013**, *44*, 210–218, doi:10.1016/j.ijepes.2012.07.012.

149. Yang, X.-S. *Nature-Inspired Optimization Algorithms 1st Edition*; 2014;

150. Alluhaybi, A.; Psimoulis, P.; Remenyte-Prescott, R. An Evaluation of Optimization Algorithms for the Optimal Selection of GNSS Satellite Subsets. *Remote Sens (Basel)* **2024**, *16*, doi:10.3390/rs16101794.

151. Veček, N.; Liu, S.H.; Črepinšek, M.; Mernik, M. On the Importance of the Artificial Bee Colony Control Parameter 'Limit.' *Information Technology and Control* **2017**, *46*, 566–604, doi:10.5755/j01.itc.46.4.18215.

152. Nseef, S.K.; Abdullah, S.; Turky, A.; Kendall, G. Knowle Dge-Base d Systems An Adaptive Multi-Population Artificial Bee Colony Algorithm for Dynamic Optimisation Problems. **2016**, *104*, 14–23, doi:10.1016/j.knosys.2016.04.005.

153. Dorigo, M.; Maniezzo, V.; Colorni, A. Ant System: Optimization by a Colony of Cooperating Agents. *IEEE Transactions on Systems, Man, and Cybernetics, Part B: Cybernetics* **1996**, *26*, 29–41, doi:10.1109/3477.484436.

154. Ab Wahab, M.N.; Nefti-Meziani, S.; Atyabi, A. A Comprehensive Review of Swarm Optimization Algorithms. *PLoS One* **2015**, *10*, doi:10.1371/journal.pone.0122827.

155. Dai, X.; Long, S.; Zhang, Z.; Gong, D. Mobile Robot Path Planning Based on Ant Colony Algorithm with A∗ Heuristic Method. *Front Neurorobot* **2019**, *13*, 15–15, doi:10.3389/fnbot.2019.00015.

156. Wang, W.; Zhao, J.; Li, Z.; Huang, J. Smooth Path Planning of Mobile Robot Based on Improved Ant Colony Algorithm. *Journal of Robotics* **2021**, *2021*, 1–10, doi:10.1155/2021/4109821.

157. Pothiya, S.; Ngamroo, I.; Kongprawechnon, W. Ant Colony Optimisation for Economic Dispatch Problem with Non-Smooth Cost Functions. *International Journal of Electrical Power and Energy Systems* **2010**, *32*, 478–487, doi:10.1016/j.ijepes.2009.09.016.

158. Shelokar, P.S.; Jayaraman, V.K.; Kulkarni, B.D. An Ant Colony Approach for Clustering. *Anal Chim Acta* **2004**, *509*, 187–195, doi:10.1016/j.aca.2003.12.032.

159. Rahman Lingkon, M.L.; Ahmmed, M.S. Application of an Improved Ant Colony Optimization Algorithm of Hybrid Strategies Using Scheduling for Patient Management in Hospitals. *Heliyon* **2024**, *10*, doi:10.1016/j.heliyon.2024.e40134.

160. Wu, C.; Zhou, S.; Xiao, L. Dynamic Path Planning Based on Improved Ant Colony Algorithm in Traffic Congestion. In Proceedings of the IEEE Access; Institute of Electrical and Electronics Engineers Inc.: Piscataway, 2020; Vol. 8, pp. 180773–180783.

161. Armond, A.M.; Prasetyo, Y.D.; Ediningrum, W. Application of Ant Colony Optimization (ACO) Algorithm to Optimize Trans Banyumas Bus Routes. In Proceedings of the Proceedings - 2022 IEEE International Conference on Cybernetics and Computational Intelligence, CyberneticsCom 2022; Institute of Electrical and Electronics Engineers Inc.: Malang, Indonesia, 2022; pp. 132–137.

162. Zecchin, A.C.; Simpson, A.R.; Maier, H.R.; Leonard, M.; Roberts, A.J.; Berrisford, M.J. Application of Two Ant Colony Optimisation Algorithms to Water Distribution System Optimisation. *Math Comput Model* **2006**, *44*, 451–468, doi:10.1016/j.mcm.2006.01.005.

163. Simon, D. *Evolutionary Optimization Algorithms*; Newark : John Wiley & Sons, Incorporated, 2013;

164. Yang, L.; Yang, X.; Wu, Y.; Liu, X. Applied Research on Distributed Generation Optimal Allocation Based on Improved Estimation of Distribution Algorithm. *Energies (Basel)* **2018**, *11*, 2363, doi:10.3390/en11092363.

165. Li, Q.; Liu, S.Y.; Yang, X.S. Influence of Initialization on the Performance of Metaheuristic Optimizers. *Applied Soft Computing Journal* **2020**, *91*, doi:10.1016/j.asoc.2020.106193.

166. Domashova, J. V.; Emtseva, S.S.; Fail, V.S.; Gridin, A.S. Selecting an Optimal Architecture of Neural Network Using Genetic Algorithm. *Procedia Comput Sci* **2021**, *190*, 263–273, doi:10.1016/j.procs.2021.06.036.

167. Chiang, C.L. Genetic-Based Algorithm for Power Economic Load Dispatch. *IET Generation, Transmission and Distribution* **2007**, *1*, 261–269, doi:10.1049/iet-gtd:20060130.

168. Maulik, U.; Bandyopadhyay, S. Genetic Algorithm-Based Clustering Technique. *Pattern Recognit* **2000**, *33*, 1455–1465.

169. Pisinger, D.; Ropke, S. A General Heuristic for Vehicle Routing Problems. *Comput Oper Res* **2007**, *34*, 2403–2435, doi:10.1016/j.cor.2005.09.012.

170. Istvan Lippai, B.; Heaney, J.P.; Laguna, M. ROBUST WATER SYSTEM DESIGN WITH COMMERCIAL INTELLIGENT SEARCH OPTIMIZERS. *JOURNAL OF COMPUTING IN CIVIL ENGINEERING* **1999**.

171. Wu, Z.Y.; Boulos, P.F.; Orr, C.H.; Ro, J.J. Using Genetic Algorithms to Rehabilitate Distribution Systems. *Journal AWWA* **2001**, *93*, 74–85, doi:10.1002/j.1551-8833.2001.tb09335.x.

172. D'Addona, D.M.; Teti, R. Genetic Algorithm-Based Optimization of Cutting Parameters in Turning Processes. *Procedia CIRP* **2013**, *7*, 323–328, doi:10.1016/j.procir.2013.05.055.

173. Essafi, I.; Mati, Y.; Dauzère-Pérès, S. A Genetic Local Search Algorithm for Minimizing Total Weighted Tardiness in the Job-Shop Scheduling Problem. *Comput Oper Res* **2008**, *35*, 2599–2616, doi:10.1016/j.cor.2006.12.019.

174. Katoch, S.; Chauhan, S.S.; Kumar, V. A Review on Genetic Algorithm: Past, Present, and Future. *Multimed Tools Appl* **2021**, *80*, 8091–8126, doi:10.1007/s11042-020-10139-6.

175. Pham, V.H.S.; Nguyen Dang, N.T.; Nguyen, V.N. Enhancing Engineering Optimization Using Hybrid Sine Cosine Algorithm with Roulette Wheel Selection and Opposition-Based Learning. *Sci Rep* **2024**, *14*, doi:10.1038/s41598-024-51343-w.

176. Chong, E.K.P.; Żak, S.H. Genetic Algorithms. In *An introduction to optimization*; Wiley: Hoboken, New Jersey , 2013; pp. 285–301.

177. Kennedy, J.; Eberhart, R. Particle Swarm Optimization. In Proceedings of the Proceedings of ICNN'95 - International Conference on Neural Networks; IEEE, 1995; Vol. 4, pp. 1942–1948.

178. Lee, K.Y.; Park, J.-B. Application of Particle Swarm Optimization to Economic Dispatch Problem: Advantages and Disadvantages. *In 2006 IEEE PES Power Systems Conference and Exposition (pp. 188-192).* **2006**.

179. Gad, A.G. Particle Swarm Optimization Algorithm and Its Applications: A Systematic Review. *Archives of Computational Methods in Engineering* **2022**, *29*, 2531–2561, doi:10.1007/s11831-021-09694-4.

180. Li, M.; Du, W.; Nian, F. An Adaptive Particle Swarm Optimization Algorithm Based on Directed Weighted Complex Network. *Math Probl Eng* **2014**, *2014*, 1–7, doi:10.1155/2014/434972.

181. Mendes, R.; Cortez, P.; Rocha, M.; Neves, J. Particle Swarms for Feedforward Neural Network Training. In Proceedings of the PROCEEDING OF THE 2002 INTERNATIONAL JOINT CONFERENCE ON NEURAL NETWORKS; IEEE: NEW YORK, 2002; pp. 1895–1899.

182. Chaturvedi, K.T.; Pandit, M.; Srivastava, L. Particle Swarm Optimization with Time Varying Acceleration Coefficients for Non-Convex Economic Power Dispatch. *International Journal of Electrical Power and Energy Systems* **2009**, *31*, 249–257, doi:10.1016/j.ijepes.2009.01.010.

183. De Falco, I.; Della Cioppa, A.; Tarantino, E. Facing Classification Problems with Particle Swarm Optimization. *Applied Soft Computing Journal* **2007**, *7*, 652–658, doi:10.1016/j.asoc.2005.09.004.

184. Reda, M.; Onsy, A.; Ghanbari, A.; Haikal, A.Y. Path Planning Algorithms in the Autonomous Driving System: A Comprehensive Review. *Rob Auton Syst* **2024**, *174*, doi:10.1016/j.robot.2024.104630.

185. Omran, M.; Engelbrecht, A.P.; Salman, A. Particle Swarm Optimization Method for Image Clustering. *Intern J Pattern Recognit Artif Intell* **2005**, *19*, 297–321.

186. Jerald, J.; Asokan, P.; Prabaharan, G.; Saravanan, R. Scheduling Optimisation of Flexible Manufacturing Systems Using Particle Swarm Optimisation Algorithm. *International Journal of Advanced Manufacturing Technology* **2005**, *25*, 964–971, doi:10.1007/s00170-003-1933-2.

187. Zhang, H.; Li, D. Applications of Computer Vision Techniques to Cotton Foreign Matter Inspection: A Review. *Comput Electron Agric* **2014**, *109*, 59–70, doi:10.1016/j.compag.2014.09.004.

188. Rezaee Jordehi, A.; Jasni, J. Particle Swarm Optimisation for Discrete Optimisation Problems: A Review. *Artificial intelligence review* **2015**, *43*, 243–258, doi:10.1007/S10462-012-9373-8.

189. Kennedy, J.F.; Eberhart, R.C.; Shi, Yuhui. *Swarm Intelligence*; San Francisco : Morgan Kaufmann, 2001;

190. Yang, X.-S. Particle Swarm Optimization. In *Nature-Inspired Optimization Algorithms. First edition. Elsevier*; Elsevier, 2014; pp. 99–110.

191. Kirkpatrick, S.; Gelatt, C.D.; Vecchi, M.P. Optimization by Simulated Annealing. *Science (American Association for the Advancement of Science)* **1983**, *220*, 671–680.

192. Aydin, L.; Artem, H.S. Design and Optimization of Fiber Composites. In *Fiber Technology for Fiber-Reinforced Composites*; Elsevier, 2017; pp. 299–315 ISBN 9780081009932.

193. Austbø, B.; Wahl, P.E.; Gundersen, T. Constraint Handling in Stochastic Optimization Algorithms for Natural Gas Liquefaction Processes. *23 EUROPEAN SYMPOSIUM ON COMPUTER AIDED PROCESS ENGINEERING* **2013**, *32*, 445–450.

194. Erchiqui, F. Application of Genetic and Simulated Annealing Algorithms for Optimization of Infrared Heating Stage in Thermoforming Process. *Appl Therm Eng* **2018**, *128*, 1263–1272, doi:10.1016/j.applthermaleng.2017.09.102.

195. Bonab, M.B.; Mohd Hashim, S.Z.; Haur, T.Y.; Kheng, G.Y. A New Swarm-Based Simulated Annealing Hyper-Heuristic Algorithm for Clustering Problem. *Procedia Comput Sci* **2019**, *163*, 228–236, doi:10.1016/j.procs.2019.12.104.

196. Wei, L.; Zhang, Z.; Zhang, D.; Leung, S.C.H. A Simulated Annealing Algorithm for the Capacitated Vehicle Routing Problem with Two-Dimensional Loading Constraints. *Eur J Oper Res* **2018**, *265*, 843–859, doi:10.1016/j.ejor.2017.08.035.

197. Fang, L.; Zuo, H.; Pang, L.; Yang, Z.; Zhang, X.; Zhu, J. Image Reconstruction through Thin Scattering Media by Simulated Annealing Algorithm. *Opt Lasers Eng* **2018**, *106*, 105–110, doi:10.1016/j.optlaseng.2018.02.020.

198. Jiang, Y.; Zhao, S.; Li, H.; Qin, Y.; Yang, X. A Hybrid Spectral Clustering Simulated Annealing Algorithm for the Street Patrol Districting Problem. *Complex and Intelligent Systems* **2023**, *9*, 1791–1807, doi:10.1007/s40747-022-00880-w.

199. Cunha, M.; Marques, J. A New Multiobjective Simulated Annealing Algorithm—MOSA-GR: Application to the Optimal Design of Water Distribution Networks. *Water Resour Res* **2020**, *56*, doi:10.1029/2019WR025852.

200. Chong, E.K.P.; Żak, S.H. Simulated Annealing Algorithm. In *An Introduction to Optimization. Fourth edition. Wiley*; 2013; pp. 279–283.

201. Arora, J.S. Chapter 15 - Discrete Variable Optimum Design Concepts and Methods. In *Introduction to Optimum Design, 2nd edition. San Diego, Calif.: Elsevier Academic Press*; 2004; pp. 513–530.

202. Yang, X.-S. Simulated Annealing. In *Nature-Inspired Optimization Algorithms. First edition. Elsevier*; Elsevier, 2014; pp. 67–75.

203. Eiben, Á.E.; Hinterding, R.; Michalewicz, Z. Parameter Control in Evolutionary Algorithms. In Proceedings of the IEEE Transactions on Evolutionary Computation; 1999; Vol. 3, pp. 124–141.

204. Krink, T.; Ursem, R.K. Parameter Control Using the Agent Based Patchwork Model. In Proceedings of the Proceedings of the 2000 Congress on Evolutionary Computation, CEC 2000; IEEE Computer Society, 2000; Vol. 1, pp. 77–83.

205. Karaboga, D.; Akay, B. A Comparative Study of Artificial Bee Colony Algorithm. *Appl Math Comput* **2009**, *214*, 108–132, doi:10.1016/j.amc.2009.03.090.

206. Goudarzi, S.; Hassan, W.H.; Anisi, M.H.; Soleymani, S.A. Comparison between Hybridized Algorithm of GA–SA and ABC, GA, DE and PSO for Vertical-Handover in Heterogeneous Wireless Networks. *Sadhana - Academy Proceedings in Engineering Sciences* **2016**, *41*, 727–753, doi:10.1007/s12046-016-0509-4.

207. Karaboga, D.; Basturk, B. On the Performance of Artificial Bee Colony (ABC) Algorithm. *Applied Soft Computing Journal* **2008**, *8*, 687–697, doi:10.1016/j.asoc.2007.05.007.

208. Sathasivam, K.; Garip, I.; Saeed, S.H.; Yais, Y.; Alanssari, A.I.; Hussein, A.A.; Hammoode, J.A.; Lafta, A.M. A Novel MPPT Method Based on PSO and ABC Algorithms for Solar Cell. *Electric Power Components and Systems* **2024**, *52*, 653–664, doi:10.1080/15325008.2023.2228795.

209. Wihartiko, F.D.; Wijayanti, H.; Virgantari, F. Performance Comparison of Genetic Algorithms and Particle Swarm Optimization for Model Integer Programming Bus Timetabling Problem. *IOP Conf Ser Mater Sci Eng* **2018**, *332*, 12020, doi:10.1088/1757-899X/332/1/012020.

210. Song, M.; Chen, D.M. A Comparison of Three Heuristic Optimization Algorithms for Solving the Multi-Objective Land Allocation (MOLA) Problem. *Ann GIS* **2018**, *24*, 19–31, doi:10.1080/19475683.2018.1424736.

211. Xue, C.; Psimoulis, P.; Zhang, Q.; Meng, X. Analysis of the Performance of Closely Spaced Low-Cost Multi-GNSS Receivers. *Applied Geomatics* **2021**, *13*, 415–435, doi:10.1007/s12518-021-00361-8/Published.

212. Leica Geosystems Leica GR10/GR25 User Manual Available online: chrome-extension://efaidnbmnnnibpcajpcglclefindmkaj/https://www.ecomexico.net/proyectos/soporte/LEICA/ESTACION%20DE%20REFERENCIA/GR10/Leica%20GR10_GR25_UserManual_2.5.0_en.pdf (accessed on 18 December 2024).

213. Leica Geosystems Leica Viva GNSS GS10 Receiver Datasheet Available online: chrome-extension://efaidnbmnnnibpcajpcglclefindmkaj/https://www.sccssurvey.co.uk/downloads/leica_viva/Leica_Viva_GNSS_GS10_Datasheet.pdf (accessed on 18 December 2024).

214. Leica Geosystems Leica AR25-Constellation GNSS Antenna Design, Built to Last Available online: file:///C:/Users/alluh/Downloads/Leica-AR25-LR-FLY.pdf (accessed on 18 December 2024).

215. Strasser, S.; Goodman, R.; Sheppard, J.; Butcher, S. A New Discrete Particle Swarm Optimization Algorithm. In Proceedings of the GECCO 2016 - Proceedings of the 2016 Genetic and Evolutionary Computation Conference; 2016; pp. 53–60.

216. Zhao, D.; Cai, C.; Li, L. A Binary Discrete Particle Swarm Optimization Satellite Selection Algorithm with a Queen Informant for Multi-GNSS Continuous Positioning. *Advances in Space Research* **2021**, *68*, 3521–3530, doi:10.1016/J.ASR.2021.08.013.

217. Chen, Q.; Peng, Y.; Zhang, M.; Yin, Q. Application Analysis on PSO Algorithm in the Discrete Optimization Problems. *J Phys Conf Ser* **2021**, *2078*, doi:10.1088/1742-6596/2078/1/012018.

218. de Andrade, L.N.; Mauri, G.R.; Mendonça, A.S.F. General Multiobjective Model and Simulated Annealing Algorithm for Waste-Load Allocation. *J Water Resour Plan Manag* **2013**, *139*, 339–344, doi:10.1061/(asce)wr.1943-5452.0000257.

219. Faisal, S.F.; Beig, A.R.; Thomas, S. Time Domain Particle Swarm Optimization of PI Controllers for Bidirectional VSC HVDC Light System. *Energies (Basel)* **2020**, *13*, doi:10.3390/en13040866.

220. Piotrowski, A.P.; Napiorkowski, J.J.; Piotrowska, A.E. Population Size in Particle Swarm Optimization. *Swarm Evol Comput* **2020**, *58*, 100718, doi:10.1016/J.SWEVO.2020.100718.

221. Zhang, W.; Wang, J.; El-Mowafy, A.; Rizos, C. Integrity Monitoring Scheme for Undifferenced and Uncombined Multi-Frequency Multi-Constellation PPP-RTK. *GPS Solutions* **2023**, *27*, doi:10.1007/s10291-022-01391-4.

222. Zhang, W.; Wang, J. Integrity Monitoring Scheme for Single-Epoch GNSS PPP-RTK Positioning. *Satellite Navigation* **2023**, *4*, doi:10.1186/s43020-023-00099-1.

223. Feng, S.; Ochieng, W.; Moore, T.; Hill, C.; Hide, C. Carrier Phase-Based Integrity Monitoring for High-Accuracy Positioning. *GPS Solutions* **2009**, *13*, 13–22, doi:10.1007/s10291-008-0093-0.

224. Joerger, M.; Pervan, B. Integrity Risk of Kalman Filter-Based RAIM. In Proceedings of the PROCEEDINGS OF THE 24TH INTERNATIONAL TECHNICAL MEETING OF THE SATELLITE DIVISION OF THE INSTITUTE OF NAVIGATION (ION GNSS 2011); Portland, OR, 2011; pp. 3856–3867.

225. Joerger, M.; Pervan, B. Kalman Filter Residual-Based Integrity Monitoring Against Measurement Faults. In Proceedings of the AIAA Guidance, Navigation, and Control Conference 2012; Minneapolis, MN., 2012.

226. Angrisano, A.; Dardanelli, G.; Innac, A.; Pisciotta, A.; Pipitone, C.; Gaglione, S. Performance Assessment of PPP Surveys with Open Source Software Using the GNSS GPS-GLONASS-Galileo Constellations. *Applied Sciences (Switzerland)* **2020**, *10*, doi:10.3390/APP10165420.

227. Tsoy, Y.R. The Influence of Population Size and Search Time Limit on Genetic Algorithm. In Proceedings of the In 7th Korea-Russia International Symposium on Science and Technology, Proceedings KORUS 2003.(IEEE Cat. No. 03EX737); 2003; pp. 181–187.

228. MATLAB MATLAB Performance Available online: https://www.mathworks.com/products/matlab/performance.html (accessed on 13 May 2025).

229. University of Bern CODE - Analysis Centre Available online: https://www.aiub.unibe.ch/research/code___analysis_center/index_eng.html (accessed on 28 September 2024).

230. Takasu, T. PPP-Models, Algorithms and Implementations (2) Available online: chrome-extension://efaidnbmnnnibpcajpcglclefindmkaj/https://gpspp.sakura.ne.jp/ppp/JAXA_PPP_2019 1018.pdf (accessed on 8 September 2024).

231. Alonso, M.T.; Ferigato, C.; Ibanez Segura, D.; Perrotta, D.; Rovira-Garcia, A.; Sordini, E. Analysis of 'Pre-Fit' Datasets of GLAB by Robust Statistical Techniques. *Stats (Basel)* **2021**, *4*, 400–418, doi:10.3390/stats4020026.

232. Everett, T.; Taylor, T.; Lee, D.K.; Akos, D.M. Optimizing the Use of RTKLIB for Smartphone-Based GNSS Measurements. *Sensors* **2022**, *22*, doi:10.3390/s22103825.

233. Zhang, J.; Wang, X.; Li, Z.; Li, S.; Qiu, C.; Li, H.; Zhang, S.; Li, L. The Impact of Different Ocean Tide Loading Models on Gnss Estimated Zenith Tropospheric Delay Using Precise Point Positioning Technique. *Remote Sens (Basel)* **2020**, *12*, doi:10.3390/RS12183080.

234. Abou-Galala, M.; Rabah, M.; Kaloop, M.; Zidan, Z.M. Assessment of the Accuracy and Convergence Period of Precise Point Positioning. *Alexandria Engineering Journal* **2018**, *57*, 1721–1726, doi:10.1016/j.aej.2017.04.019.

235. Liu, T.; Yuan, Y.; Zhang, B.; Wang, N.; Tan, B.; Chen, Y. Multi-GNSS Precise Point Positioning (MGPPP) Using Raw Observations. *J Geod* **2017**, *91*, 253–268, doi:10.1007/s00190-016-0960-3.

236. Guo, J.; Geng, J.; Wang, C. Impact of the Third Frequency GNSS Pseudorange and Carrier Phase Observations on Rapid PPP Convergences. *GPS Solutions* **2021**, *25*, doi:10.1007/s10291-020-01079-7.

Appendix A

The coordinates of NGB2 based on relative positioning

Leica Geosystems AG
Heinrich Wild Strasse
CH-9435 Heerbrugg
St. Gallen, Switzerland

Phone: + 41 71 727 3131
Fax: + 41 71 727 4674

- when it has to be right

Leica Geosystems

Points Quality Report

Report created: 15/01/2024 11:52:37

Project Details

General		Customer Details	
Project Name:	NGB2 15Days	Customer Name:	-
Owner:	-	Contact Person:	-
Lead Surveyor:	Abdulaziz Alluhaybi	Number:	-
Date Created:	15/01/2024 10:11:17	Email:	-
Last Accessed:	15/01/2024 10:11:18	Skype:	-
Application Software:	Infinity 4.0.1	Website:	-

Master Coordinate System	
Coordinate System Name:	OSGB36(15)
Transformation Type:	-
Residual Distribution:	None
Ellipsoid:	GRS 1980
Projection Type:	Transverse Mercator
Geoid Model:	OSGM15GB
CSCS Model:	OSTN15(GB)

Path:	C:\Users\evxaa58\Desktop\NGB2 15Days\NGB2 15Days.iprj
Size:	4,091.8 MB
Comments:	-

Summary

#	Point ID	Point Role	Easting [m]	Northing [m]	Ortho. Height [m]	Ellips. Height [m]	Code	Tilt [gon]	3D CQ [m]	2D CQ [m]	1D CQ [m]	Date/Time
1	NGB2	Averaged	454,920.9715	339,703.9087	42.7162	91.2067		-	0.0092	0.0038	0.0084	05/10/2021 00:59:12

Averaged Points Summary

Max. Distance between Average and Measurement:

Position:	0.1000 m
Height:	0.1000 m
Weighted Average:	Yes

#	Point ID	Easting [m]	Northing [m]	Ortho. Height [m]	SD Easting [m]	SD Northing [m]	SD Height [m]	Code	Code Group	Code Attributes	Date/Time
1	NGB2	454,920.9715	339,703.9087	42.7162	0.0035	0.0017	0.0084	-	-	-	05/10/2021 00:59:12
	Use	**Source**	**Station**	**Date/Time**	**3D CQ [m]**	**ΔPos. [m]**	**ΔHeight [m]**	**ΔPos. & Height [m]**	**Easting [m]**	**Northing [m]**	**Ortho. Height [m]**
	Auto	3D	LINO	05/10/2021 00:59:12	0.0002	0.0082	-0.0009	0.0083	454,920.9737	339,703.9008	42.7171
	Auto	3D	LEEK	05/10/2021 00:59:12	0.0001	0.0099	0.0106	0.0145	454,920.9813	339,703.9103	42.7055
	Auto	3D	KEYW	05/10/2021 00:59:12	0.0001	0.0056	-0.0118	0.0130	454,920.9661	339,703.9077	42.7280
	Auto	3D	BUXT	05/10/2021 00:59:12	0.0002	0.0131	0.0207	0.0245	454,920.9834	339,703.9142	42.6954
	Auto	3D	LICF	05/10/2021 00:59:12	0.0002	0.0087	0.0374	0.0384	454,920.9782	339,703.9143	42.6787

Figure 0.1 Leica report of estimating the coordinates of NGB2 using relative positioning and relying on five GNSS reference stations.

Appendix B

Positioning solutions of NGB2 based on the selected satellites on 22/09/2021

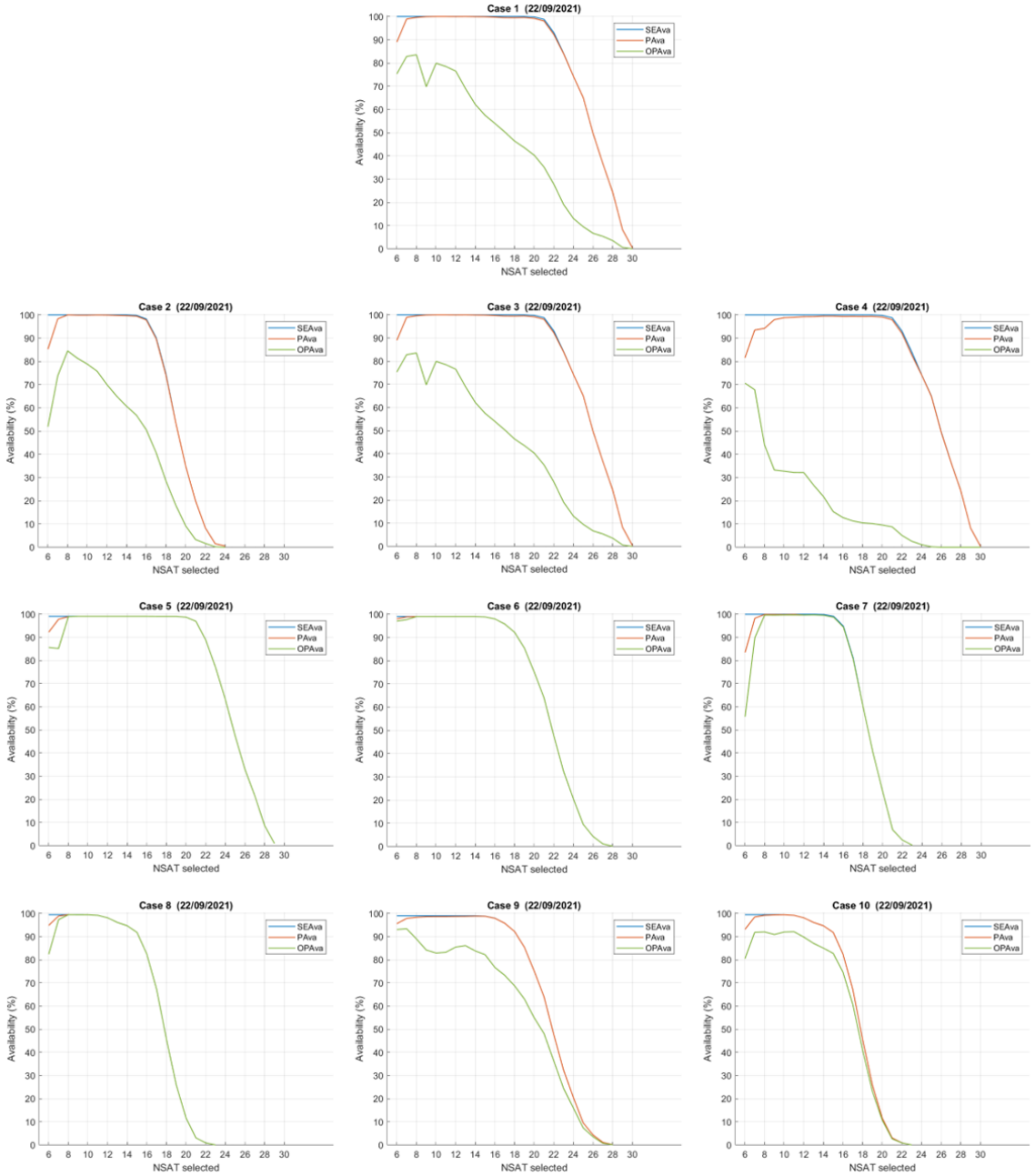

Figure B.0.1 Satellites availability (blue line) on 24 hours GNSS data collected over NGB2 on 22 September 2021. In addition, the availability of positioning (red line) and optimal positioning (green line) using the selected satellites with all subset sizes from the ten selection cases.

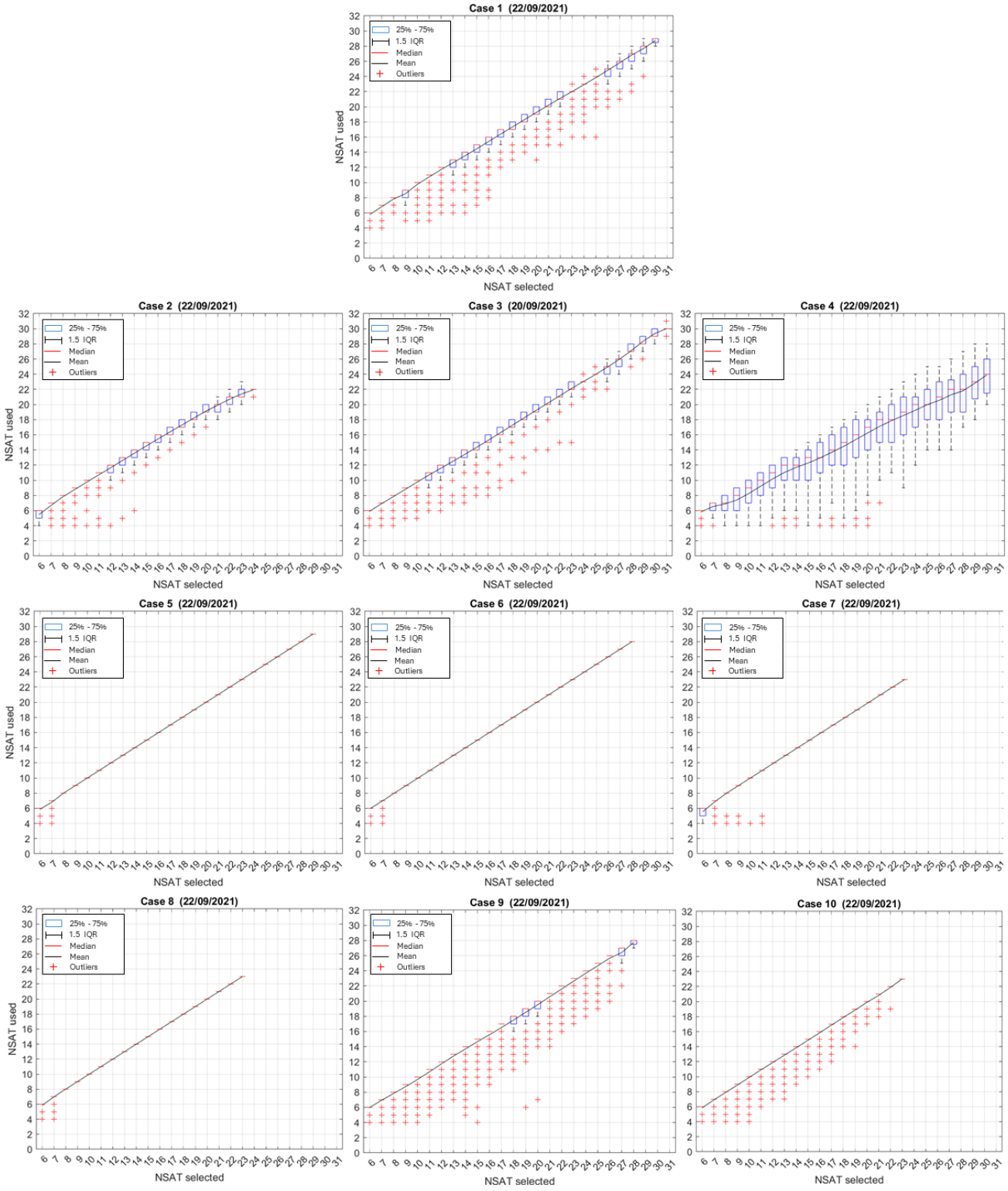

Figure B.0.2 Number of satellites used in the 24-hour positioning solution from the selected satellites with all subset sizes. The satellites are chosen by ten selection cases from GNSS data collected over NGB2 on 22 September 2021.

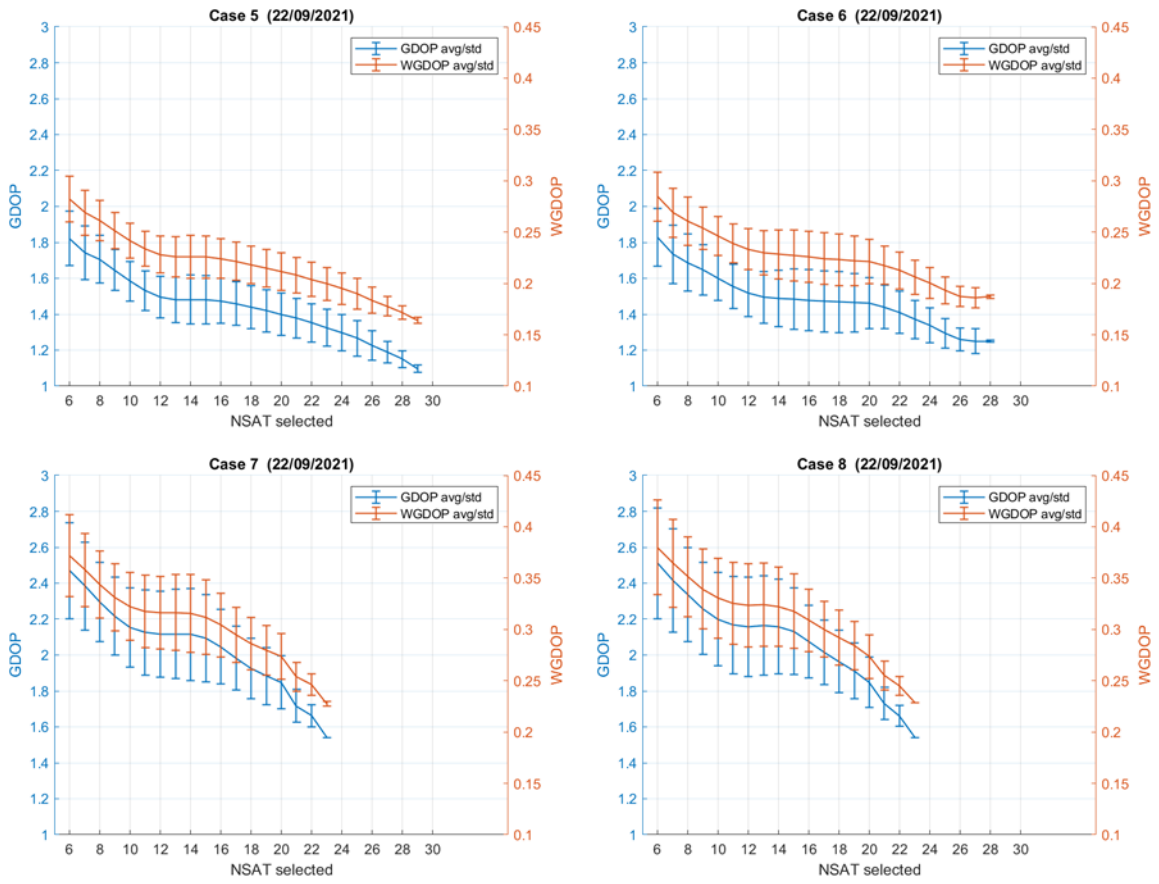

Figure B.0.3 Mean and stander deviation of the GDOP and WGDOP of the selected satellites with all possible subset sizes for 24 hours GNSS data (30 sec interval) collected over NGB2 on 22 September 2021. The value of selected satellite from cases 5, 6, 7 and 8 are only presented.

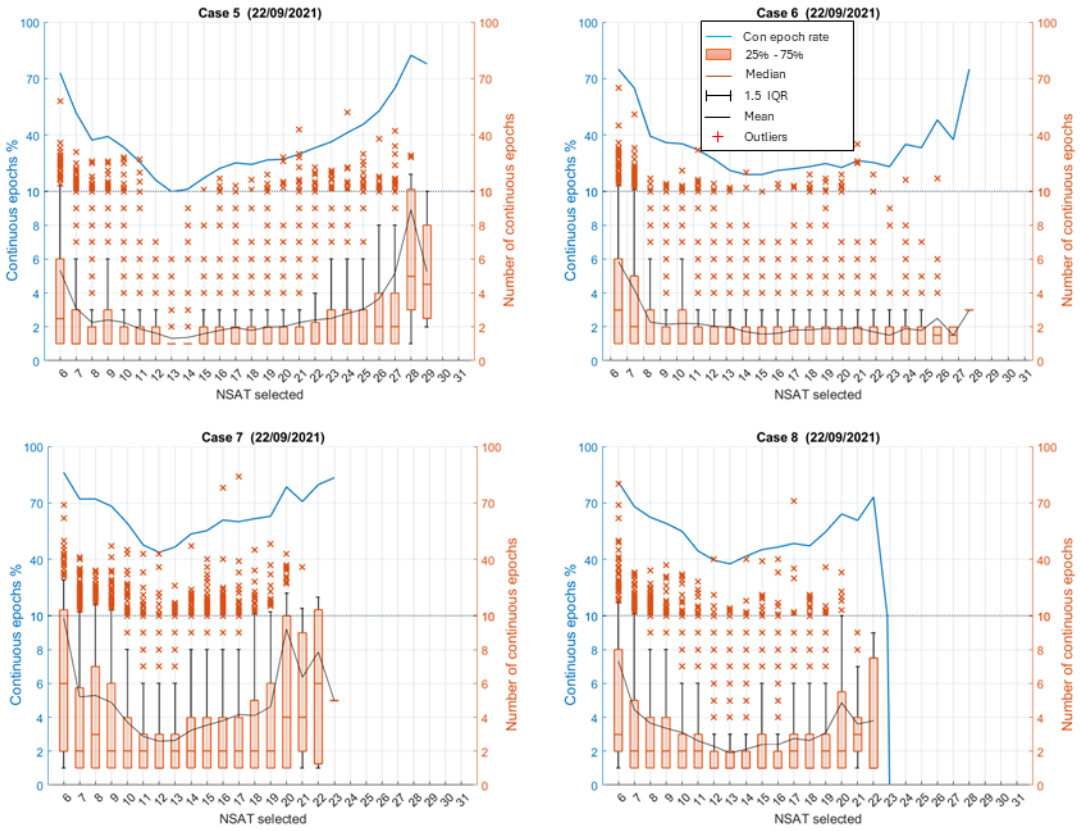

Figure B.0.4 The number and the rate of continuous selection epochs from the selection cases 5, 6, 7, and 8 using 24 hours GNSS data collected on 22 September 2021.

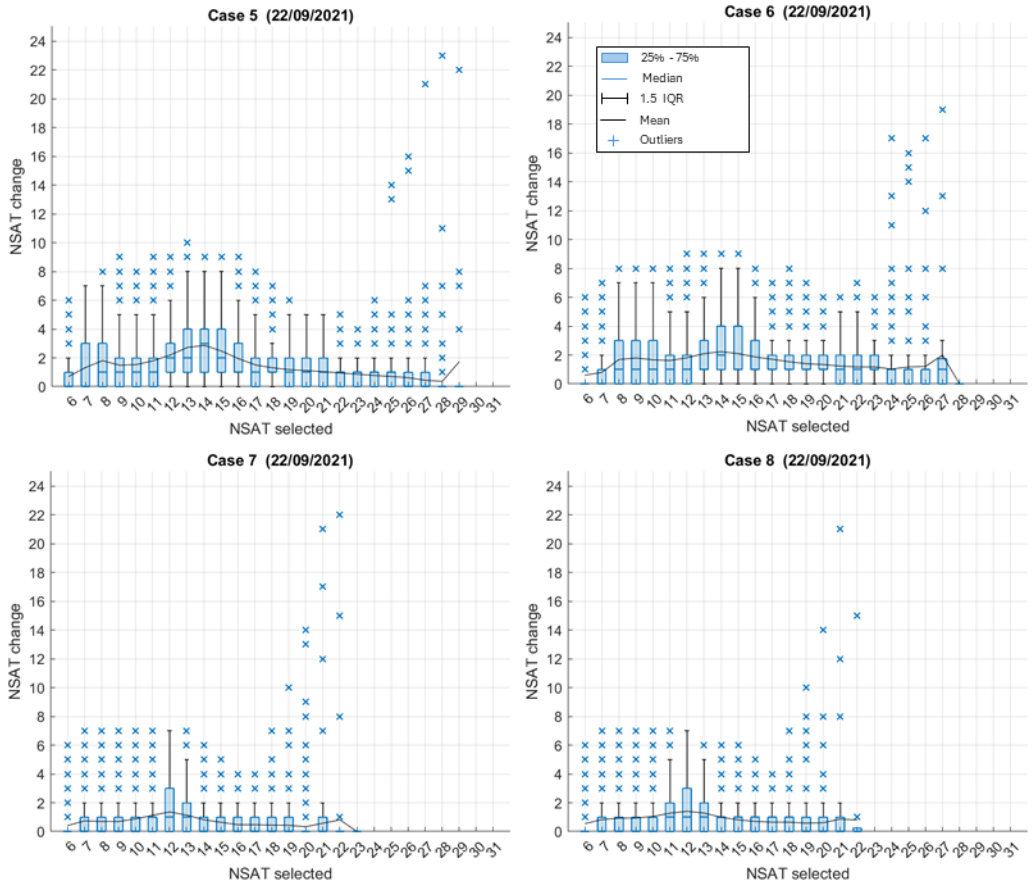

Figure B.0.5 The number of satellites changed in the selected optimal subset over selection from the selection cases 5, 6, 7, and 8 using 24 hours GNSS data collected on 22 September 2021.

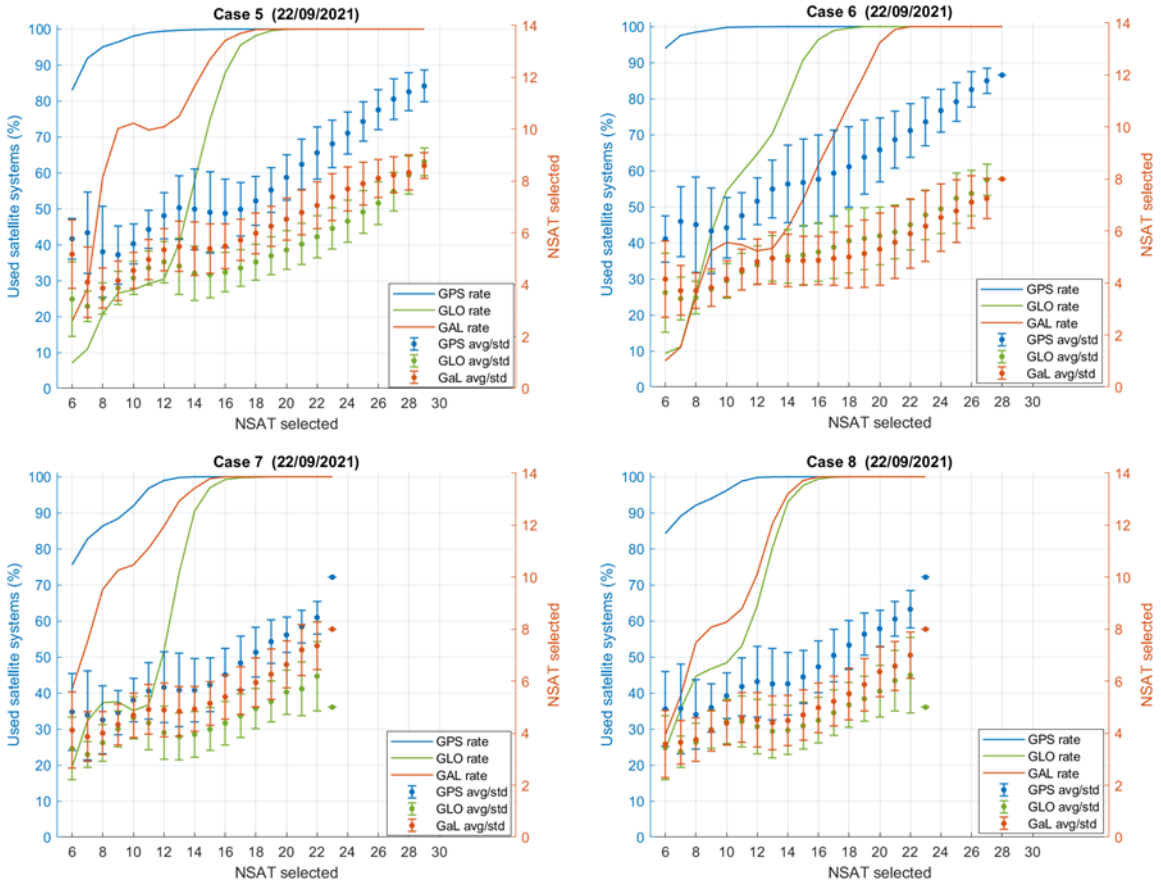

Figure B.0.6 The mean and stander deviation of number of GPS, GLONASS, and Galileo satellites selected to form the optimal subsets with different sizes. The rate of using the system of satellite over the entire selection is also presented. Selected satellites from selection cases 5, 6, 7, and 8 are only presented. 24 hours GNSS data collected over NGB2 on 22 September 2021 are used.

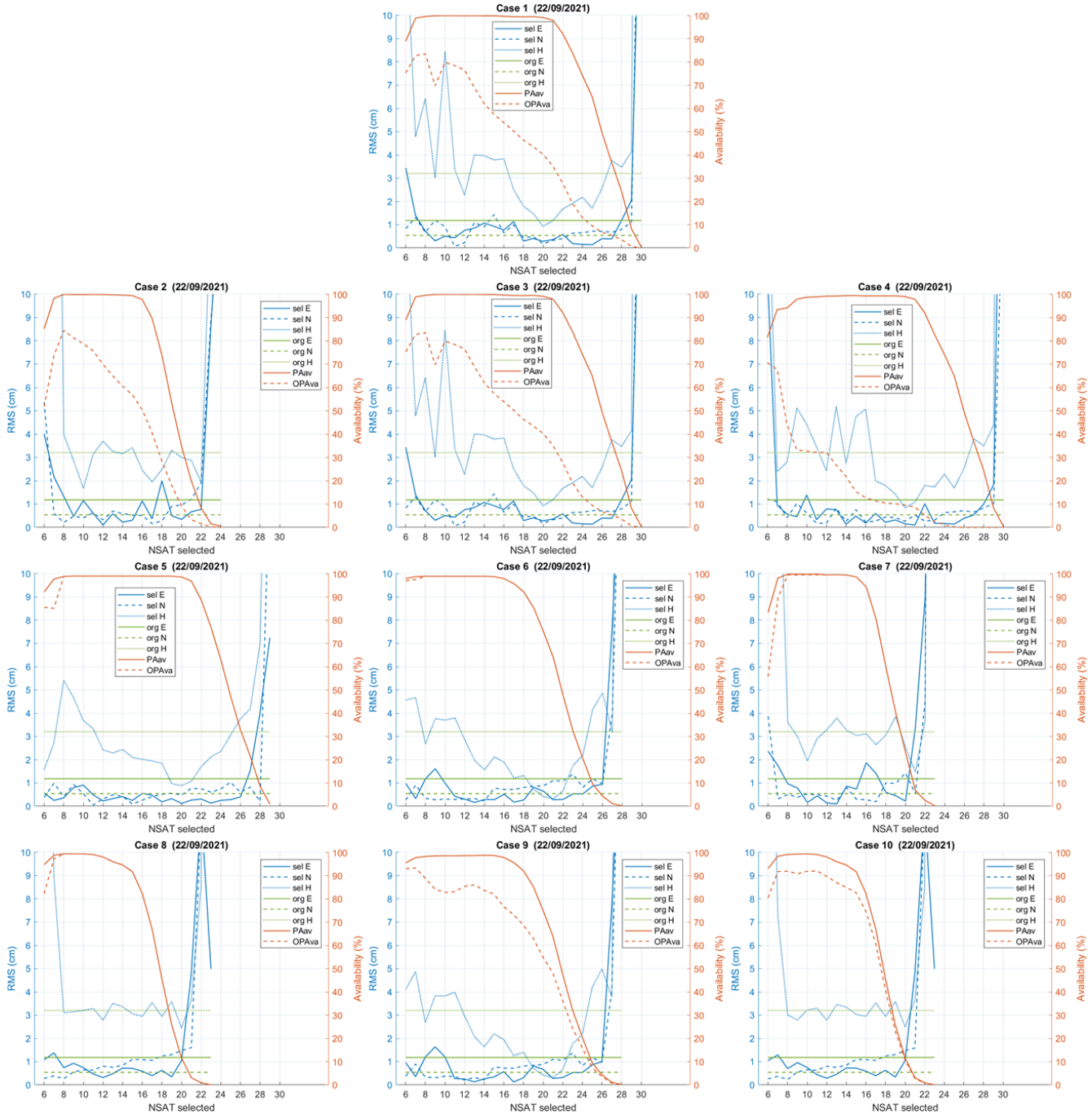

Figure B.0.7 Positioning accuracy in Easting, Northing, and Hight using the original PPP and the selected satellites from the ten selection cases. In addition, the availability of positioning and optimal positioning of the selected satellites is presented. The positioning is based on 24 hours GNSS data collected over NGB2 on 22 September 2021.

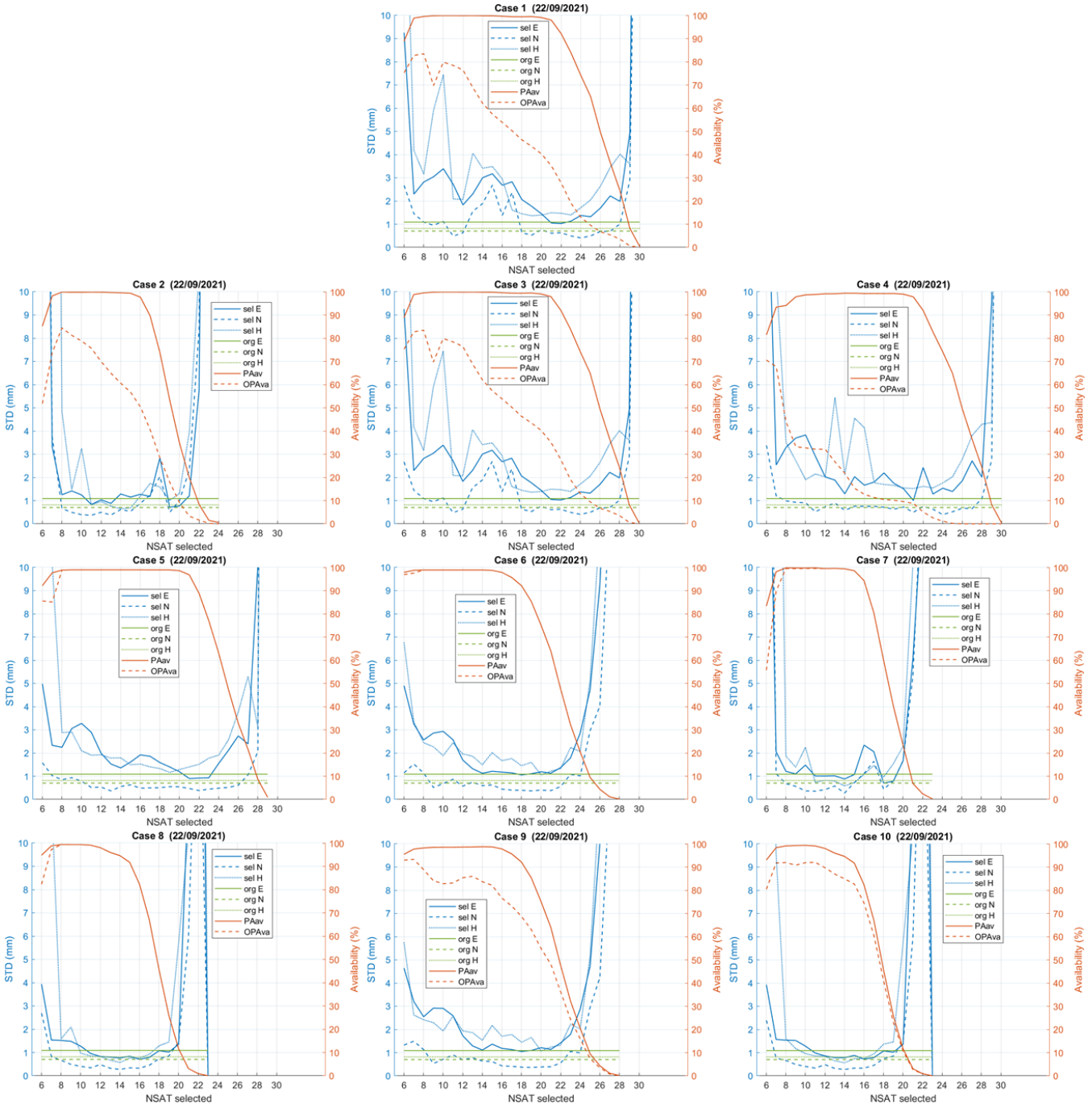

Figure B.0.8 Positioning precision in Easting, Northing, and Hight using the original PPP and the selected satellites from the ten selection cases. In addition, the availability of positioning and optimal positioning of the selected satellites is presented. The positioning is based on 24 hours GNSS data collected over NGB2 on 22 September 2021.

Positioning solutions of NGB2 based on the selected satellites on 27/09/2021

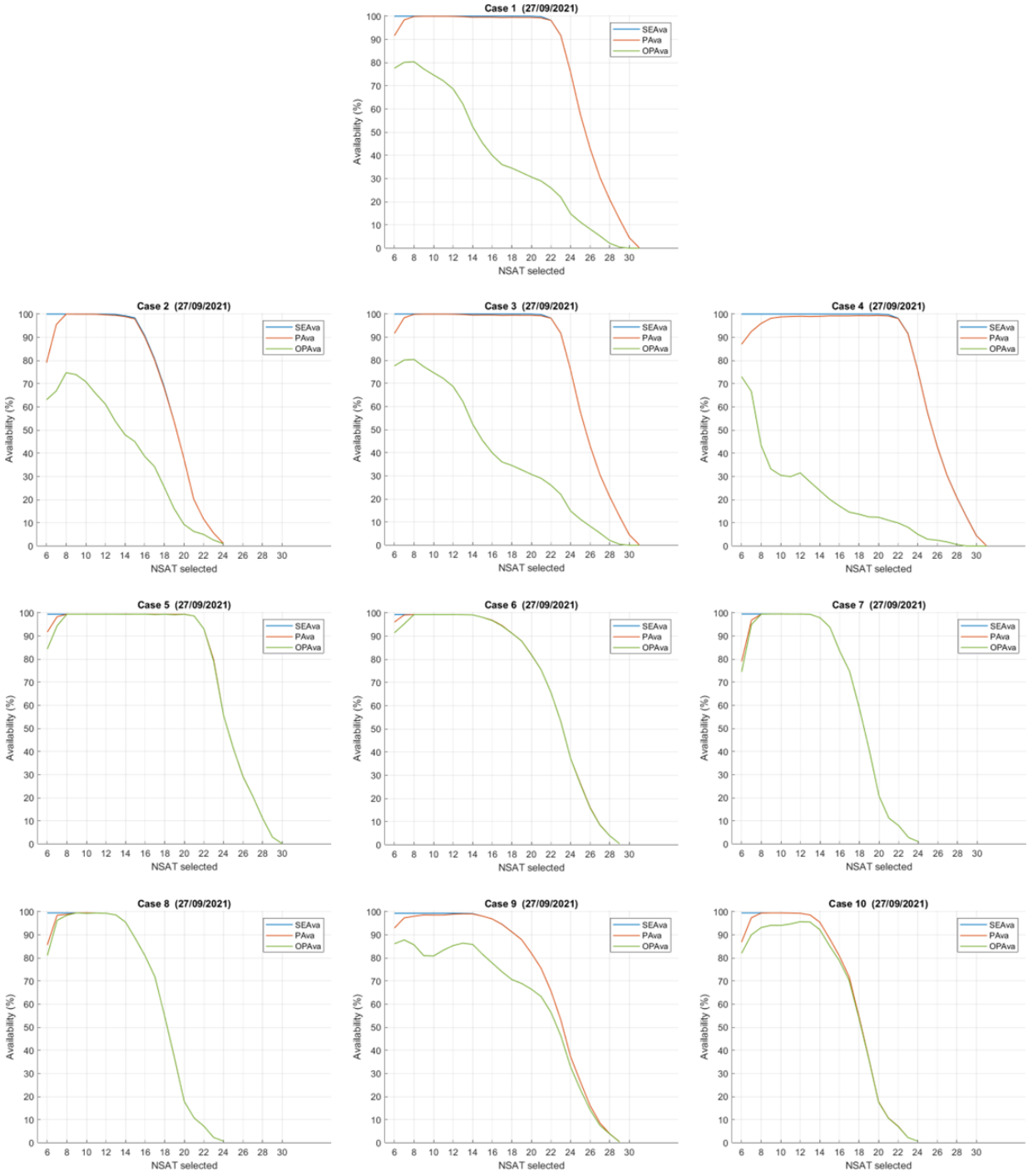

Figure B.0.9 Satellites availability (blue line) on 24 hours GNSS data collected over NGB2 on 27 September 2021. In addition, the availability of positioning (red line) and optimal positioning (green line) using the selected satellites with all subset sizes from the ten selection cases.

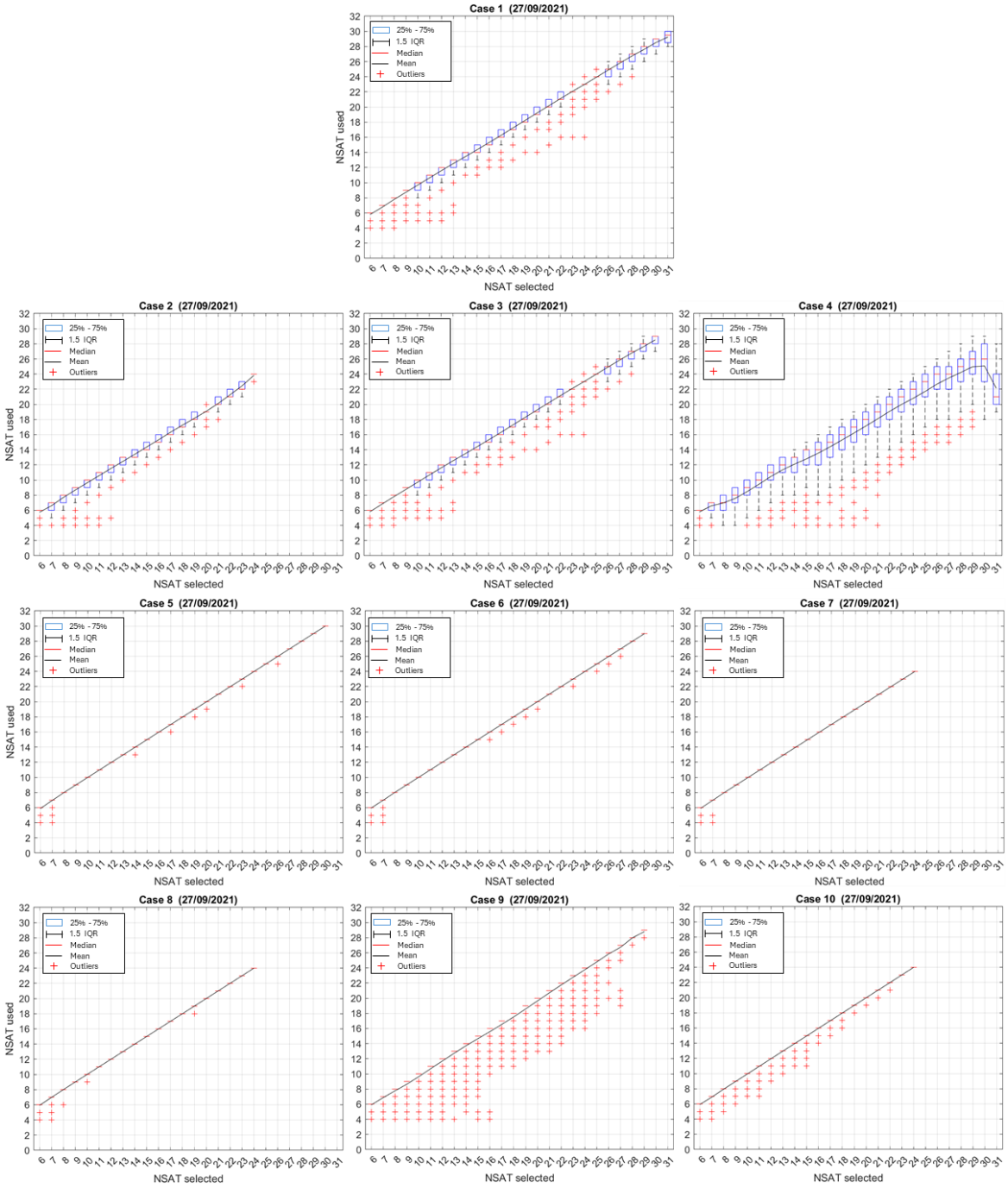

Figure B.0.10 Number of satellites used in the 24-hour positioning solution from the selected satellites with all subset sizes. The satellites are chosen by ten selection cases from GNSS data collected over NGB2 on 27 September 2021.

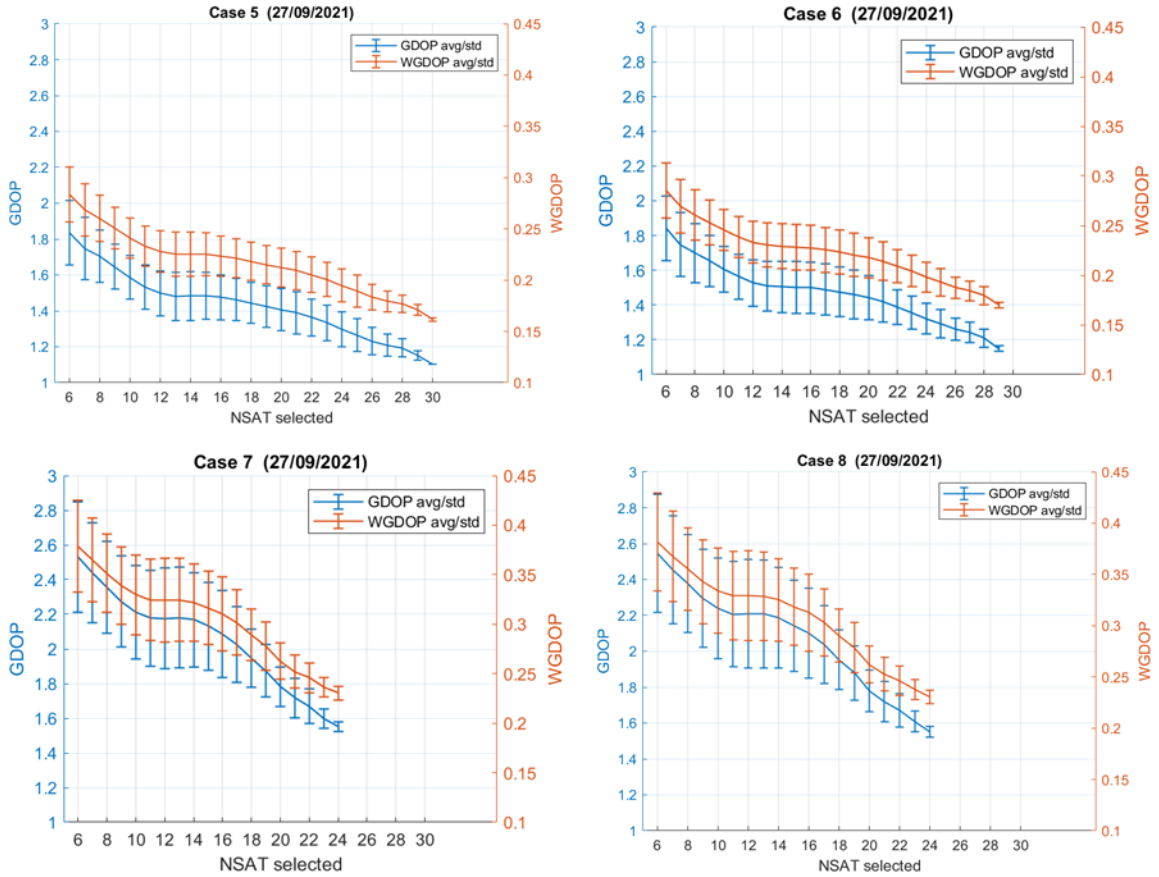

Figure B.0.11 Mean and stander deviation of the GDOP and WGDOP of the selected satellites with all possible subset sizes for 24 hours GNSS data (30 sec interval) collected over NGB2 on 27 September 2021. The value of selected satellite from cases 5, 6, 7 and 8 are only presented.

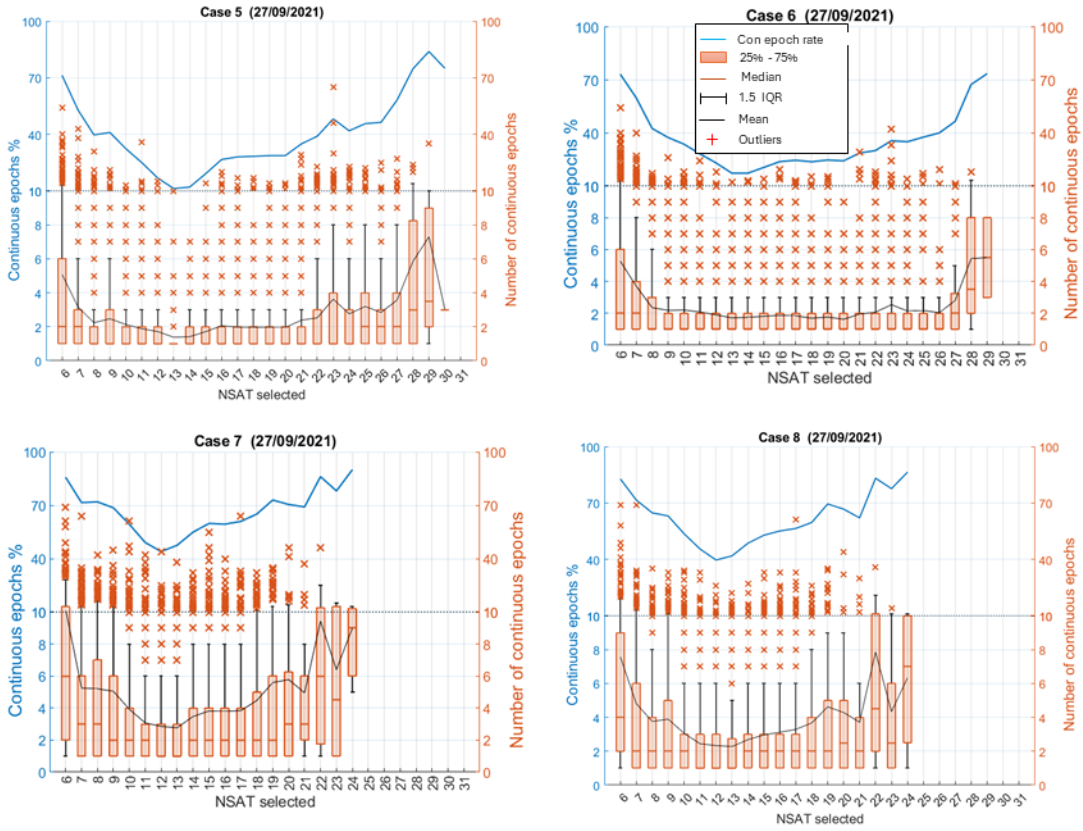

Figure B.0.12 The number and the rate of continuous selection epochs from the selection cases 5, 6, 7, and 8 using 24 hours GNSS data collected on 27 September 2021.

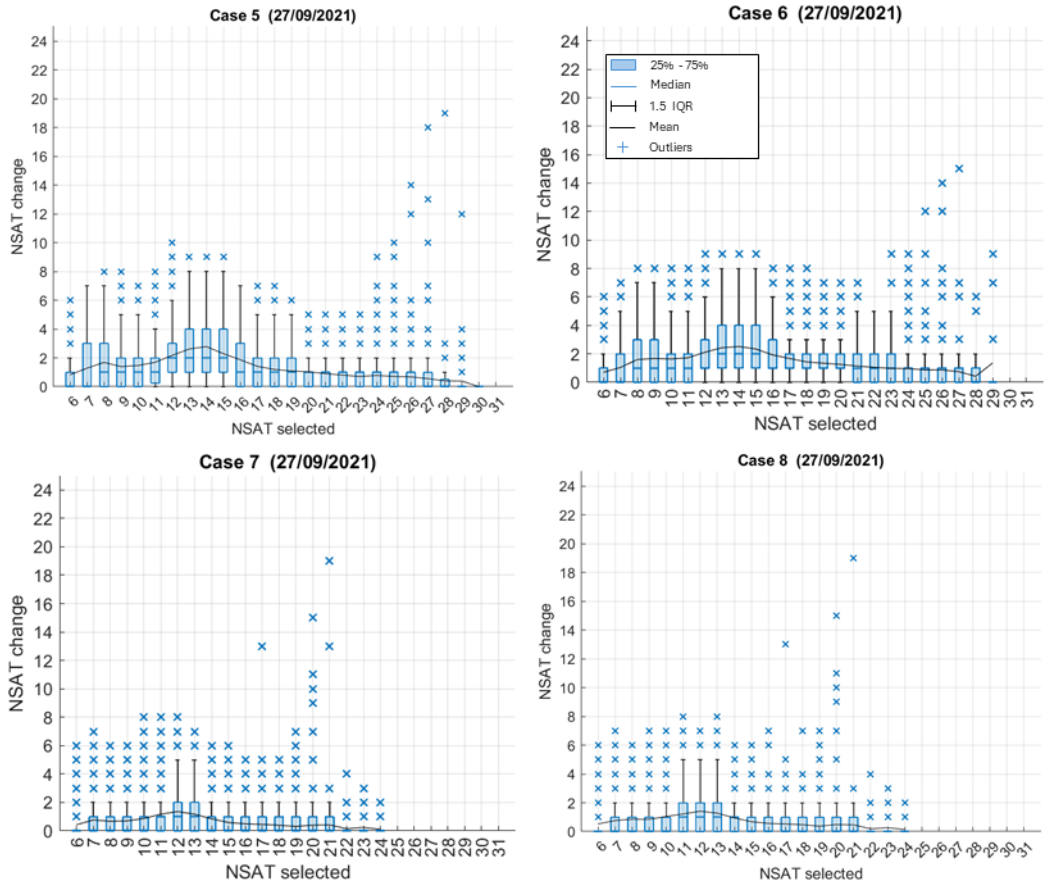

Figure B.0.13 The number of satellites changed in the selected optimal subset over selection from the selection cases 5, 6, 7, and 8 using 24 hours GNSS data collected on 27 September 2021.

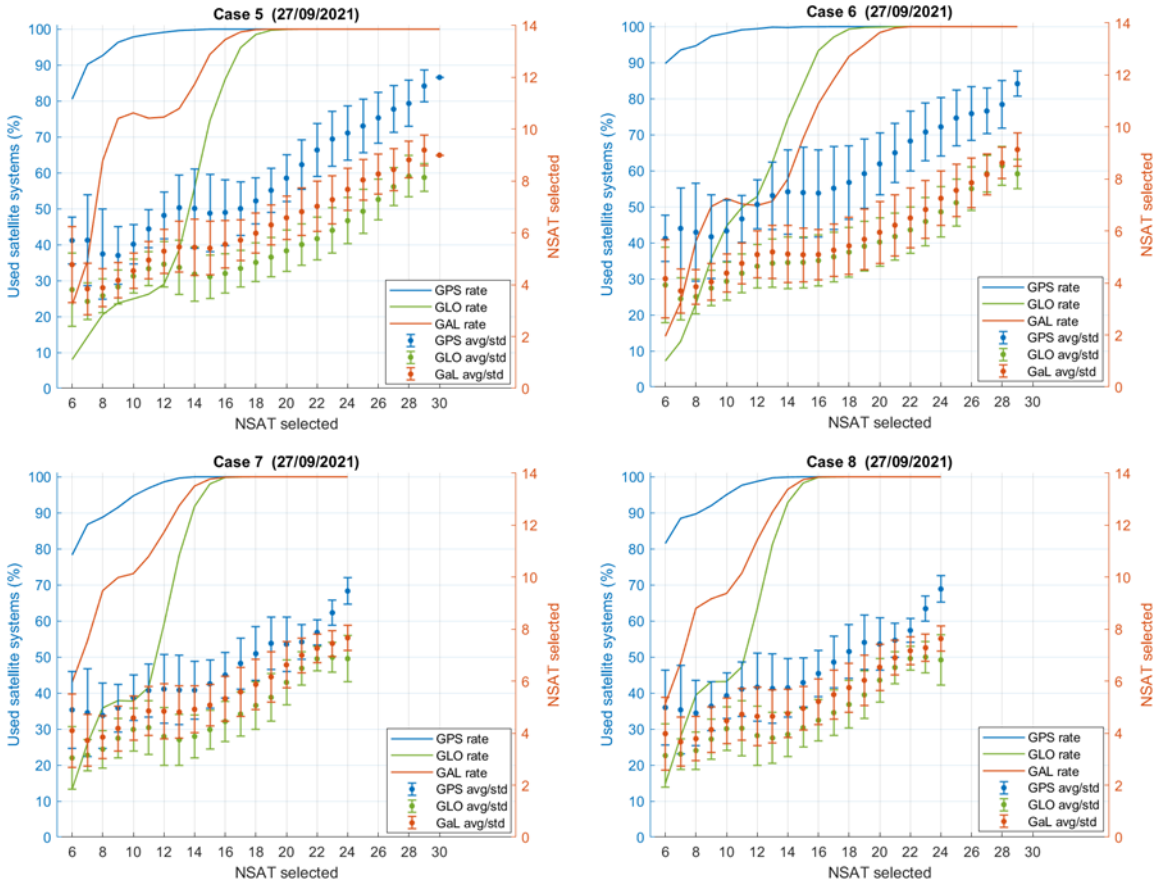

Figure B.0.14 The mean and stander deviation of number of GPS, GLONASS, and Galileo satellites selected to form the optimal subsets with different sizes. The rate of using the system of satellite over the entire selection is also presented. Selected satellites from selection cases 5, 6, 7, and 8 are only presented. 24 hours GNSS data collected over NGB2 on 27 September 2021 are used.

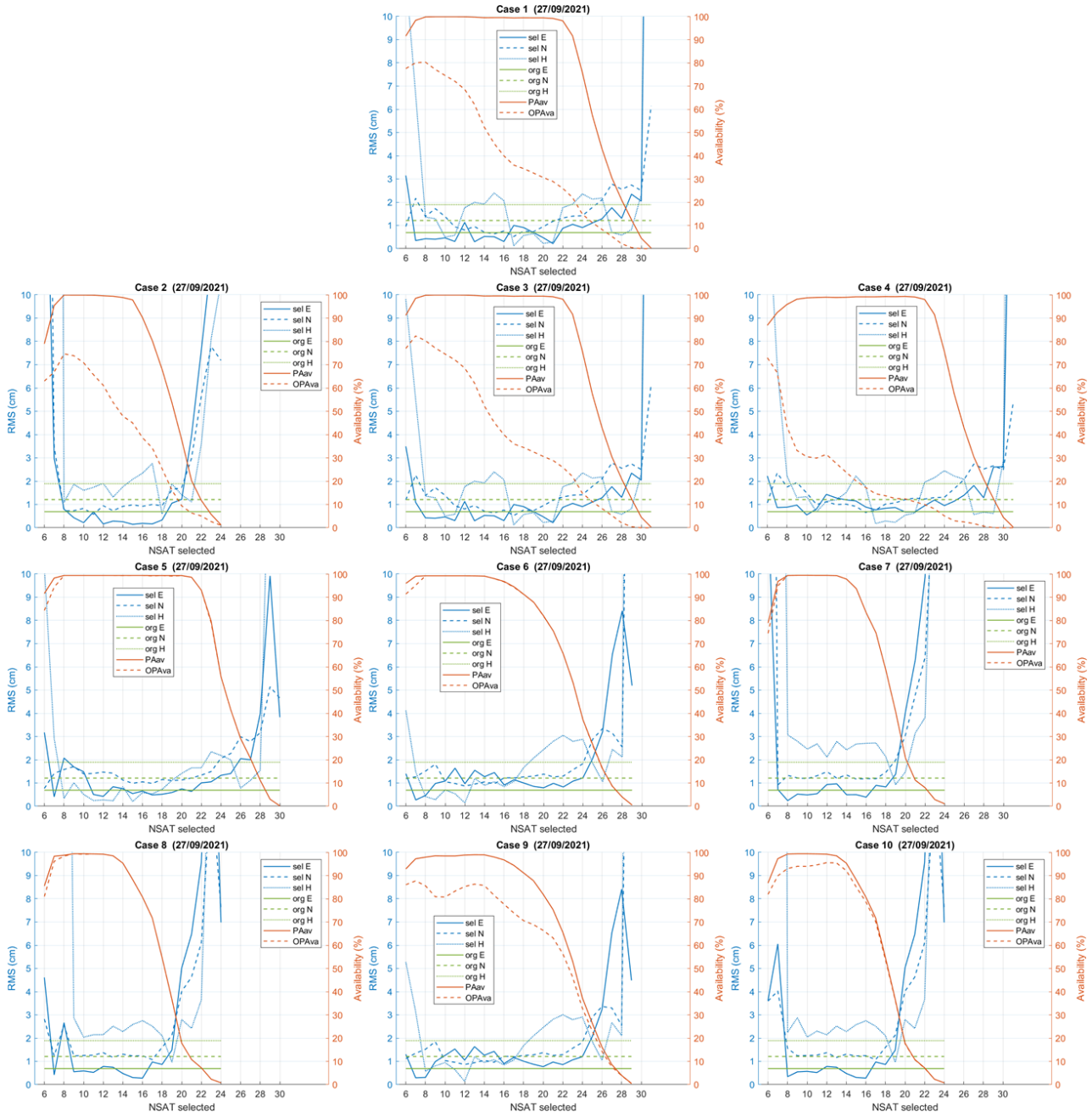

Figure B.0.15 Positioning accuracy in Easting, Northing, and Hight using the original PPP and the selected satellites from the ten selection cases. In addition, the availability of positioning and optimal positioning of the selected satellites is presented. The positioning is based on 24 hours GNSS data collected over NGB2 on 27 September 2021.

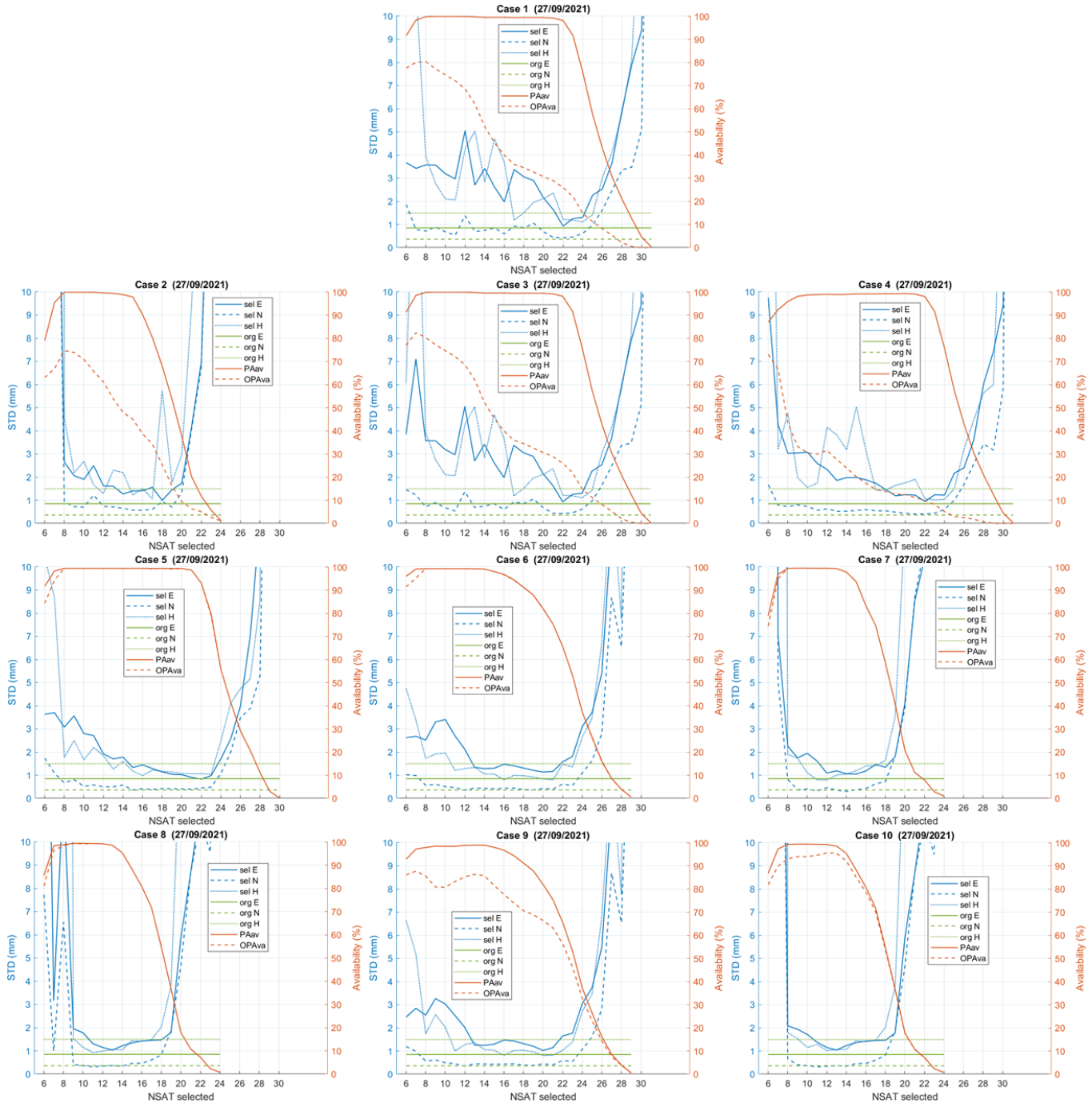

Figure B.0.16 Positioning precision in Easting, Northing, and Hight using the original PPP and the selected satellites from the ten selection cases. In addition, the availability of positioning and optimal positioning of the selected satellites is presented. The positioning is based on 24 hours GNSS data collected over NGB2 on 27 September 2021.

Positioning solutions of NGB2 based on the selected satellites on 01/10/2021

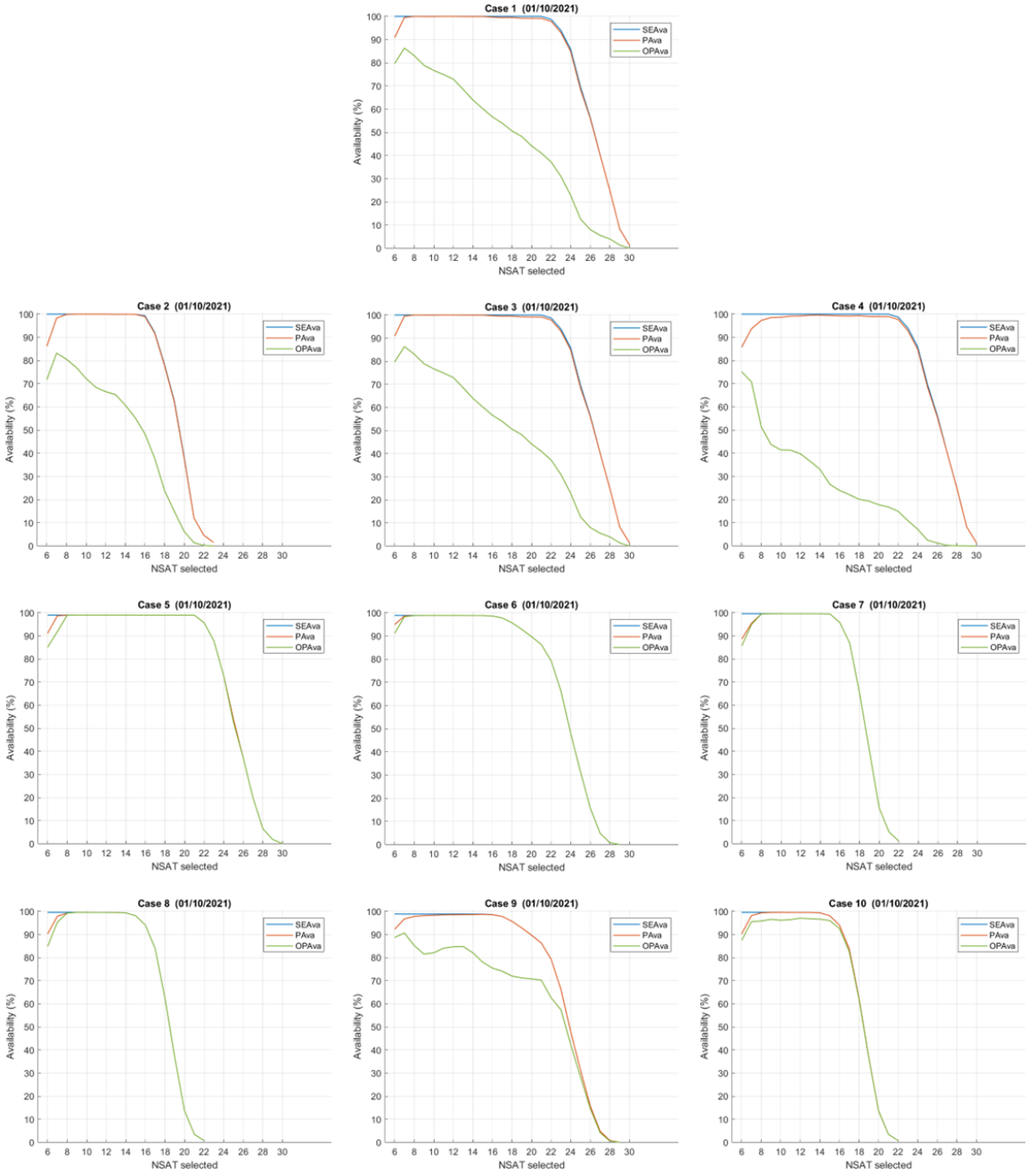

Figure B.0.17 Satellites availability (blue line) on 24 hours GNSS data collected over NGB2 on 1st October 2021. In addition, the availability of positioning (red line) and optimal positioning (green line) using the selected satellites with all subset sizes from the ten selection cases.

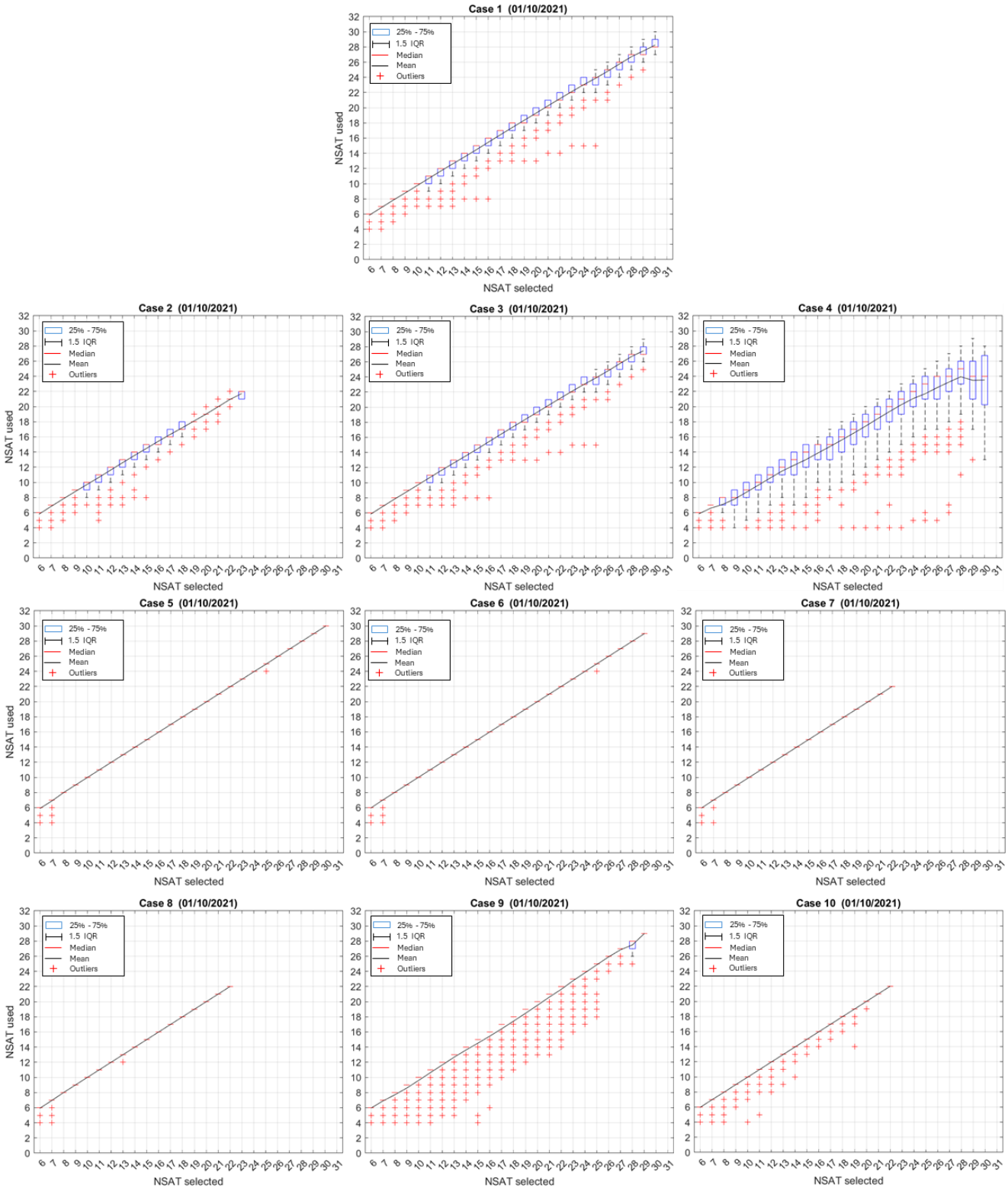

Figure B.0.18 Number of satellites used in the 24-hour positioning solution from the selected satellites with all subset sizes. The satellites are chosen by ten selection cases from GNSS data collected over NGB2 on 1st October 2021.

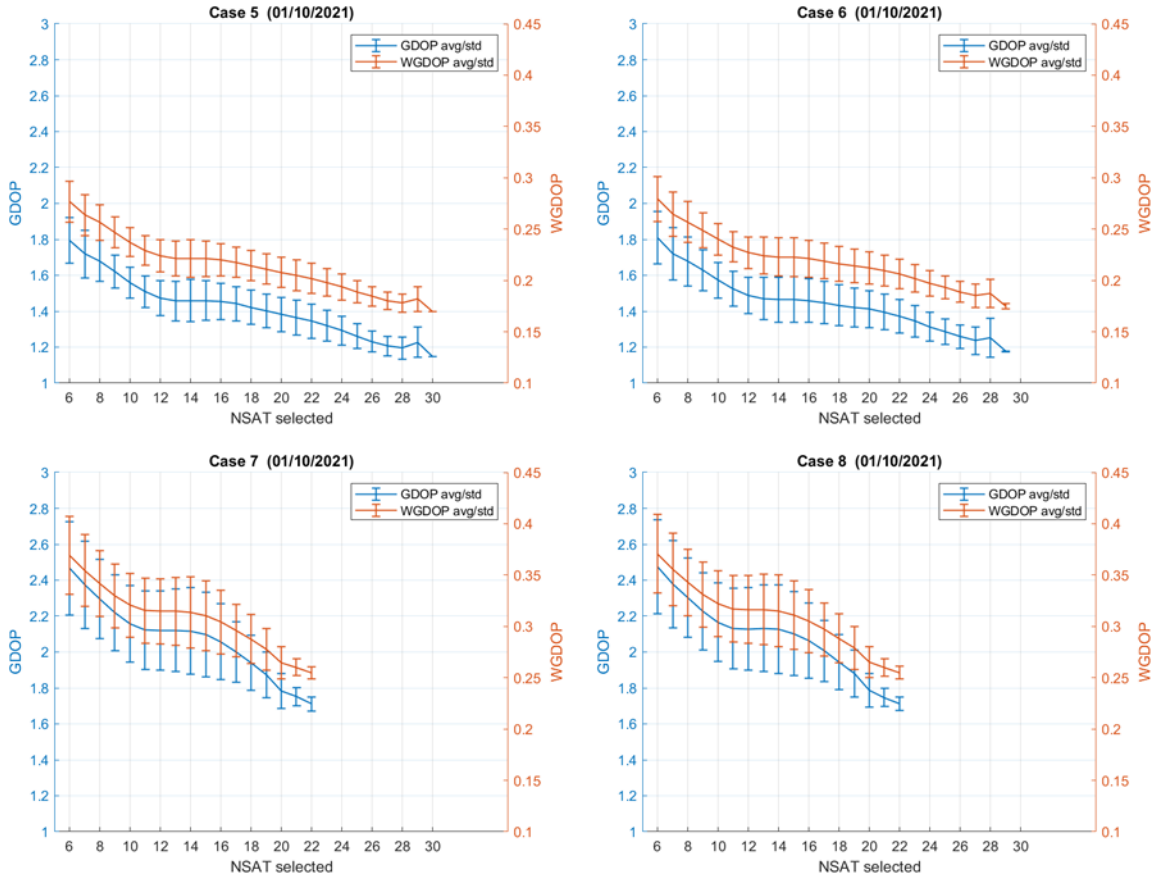

Figure B.0.19 Mean and stander deviation of the GDOP and WGDOP of the selected satellites with all possible subset sizes for 24 hours GNSS data (30 sec interval) collected over NGB2 on 1st October 2021. The value of selected satellites from cases 5, 6, 7 and 8 are only presented.

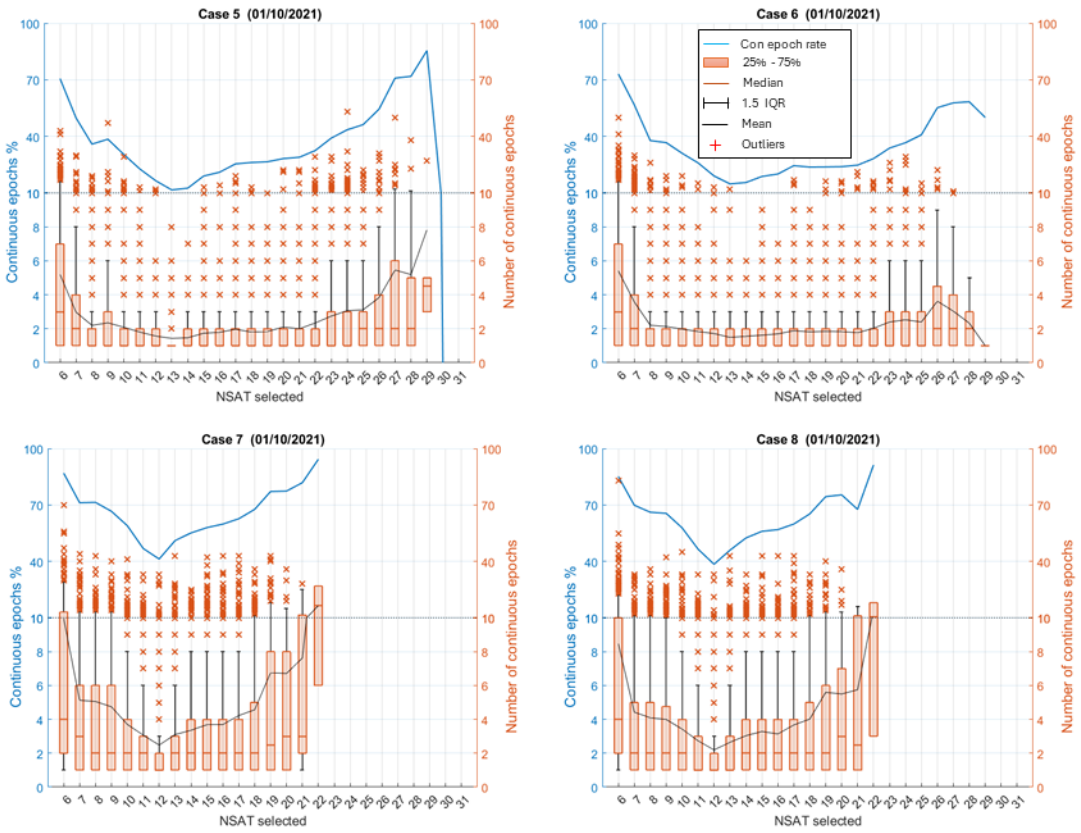

Figure B.0.20 The number and the rate of continuous selection epochs from the selection cases 5, 6, 7, and 8 using 24 hours GNSS data collected on 1st October 2021.

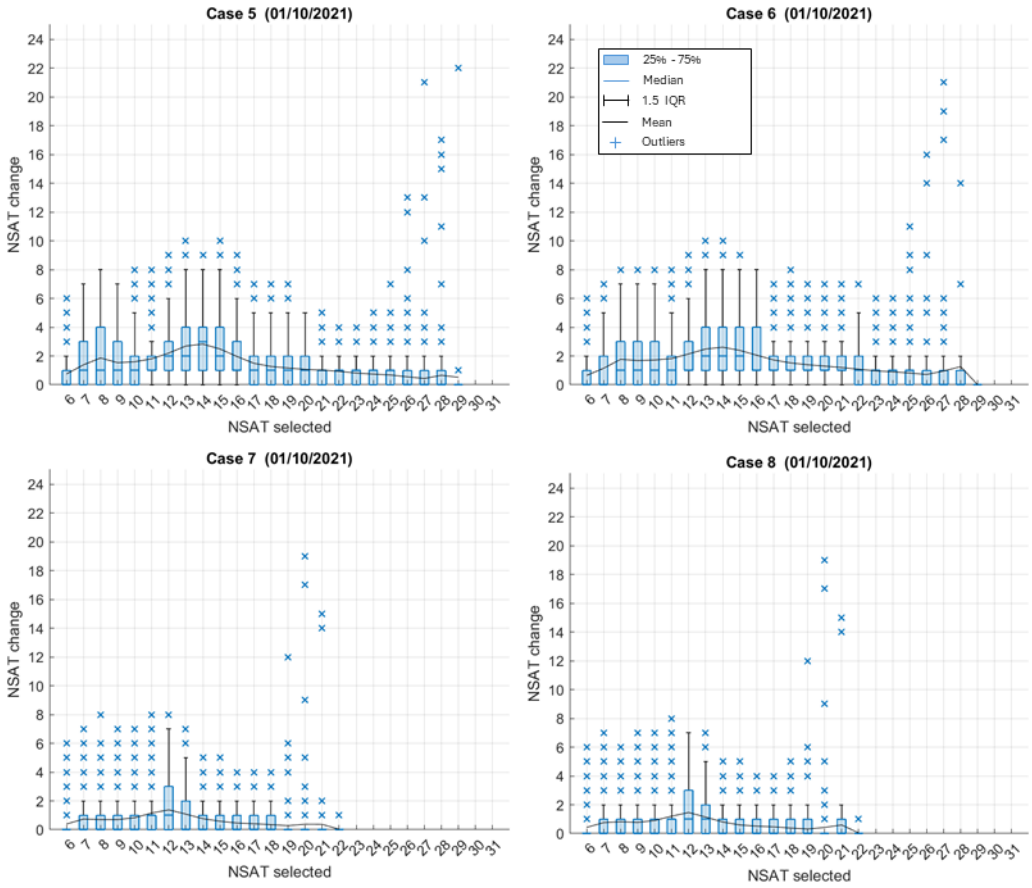

Figure B.0.21 The number of satellites changed in the selected optimal subset over selection from the selection cases 5, 6, 7, and 8 using 24 hours GNSS data collected on 1st October 2021.

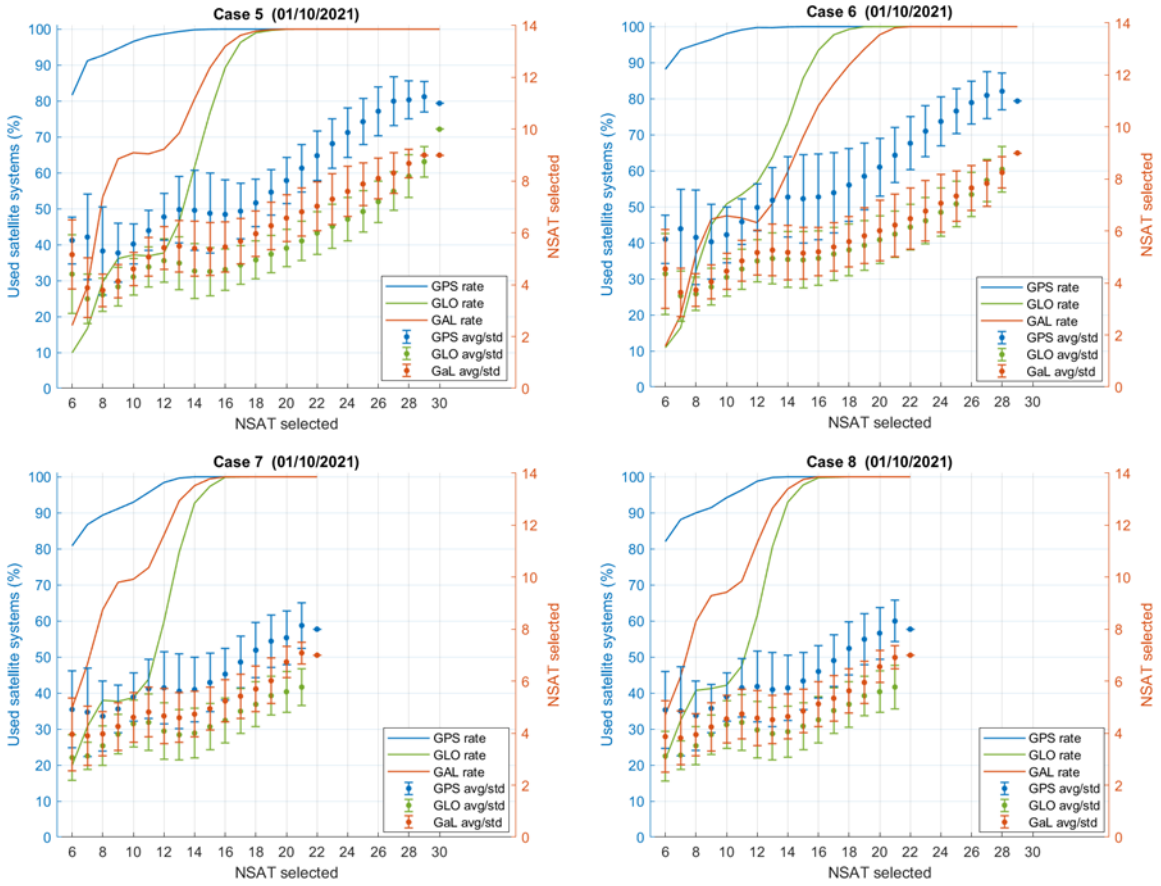

Figure B.0.22 The mean and stander deviation of number of GPS, GLONASS, and Galileo satellites selected to form the optimal subsets with different sizes. The rate of using the system of satellite over the entire selection is also presented. Selected satellites from selection cases 5, 6, 7, and 8 are only presented. 24 hours GNSS data collected over NGB2 on 1st October 2021 are used.

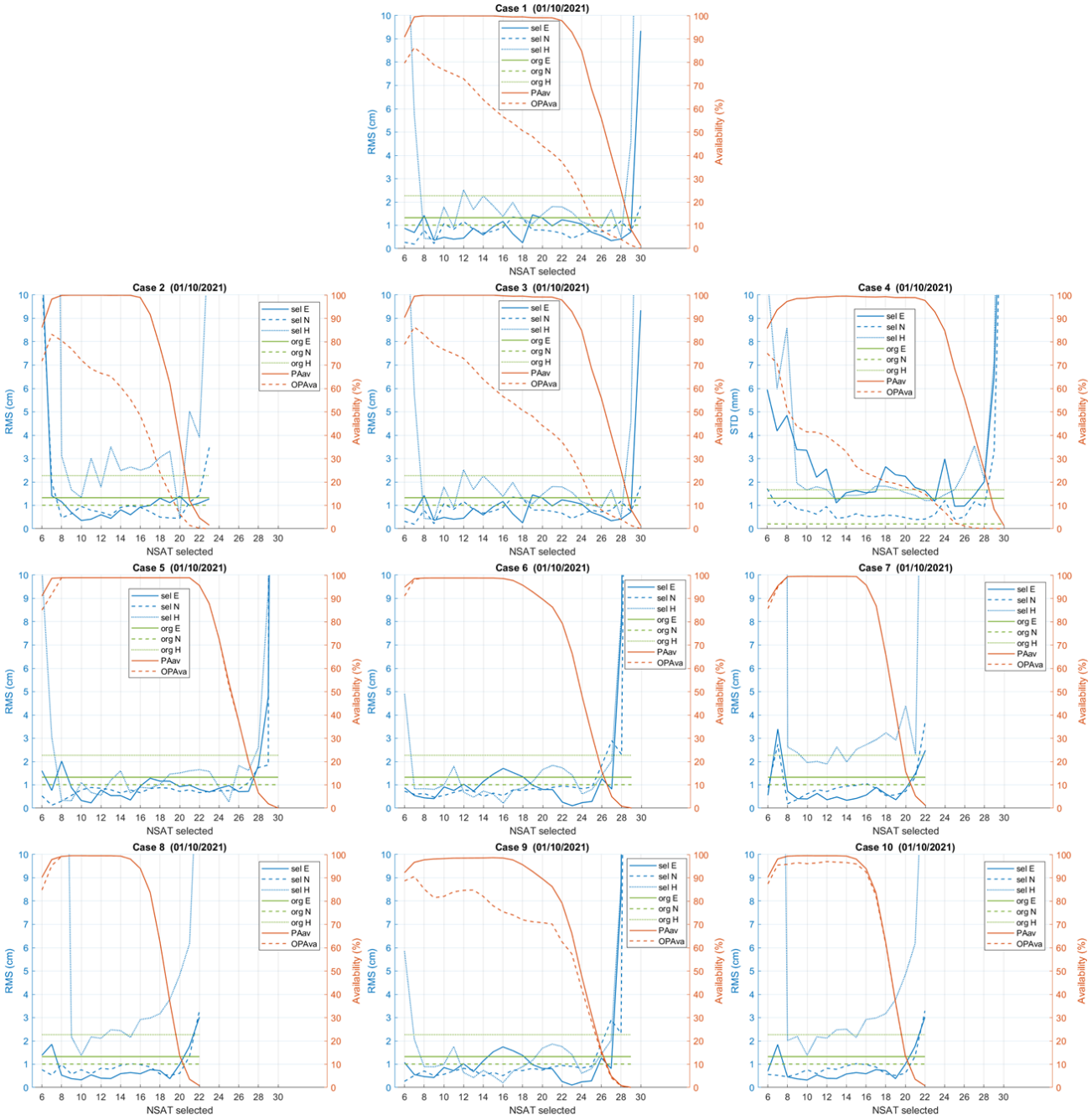

Figure B.0.23 Positioning accuracy in Easting, Northing, and Hight using the original PPP and the selected satellites from the ten selection cases. In addition, the availability of positioning and optimal positioning of the selected satellites is presented. The positioning is based on 24 hours GNSS data collected over NGB2 on 1st October 2021.

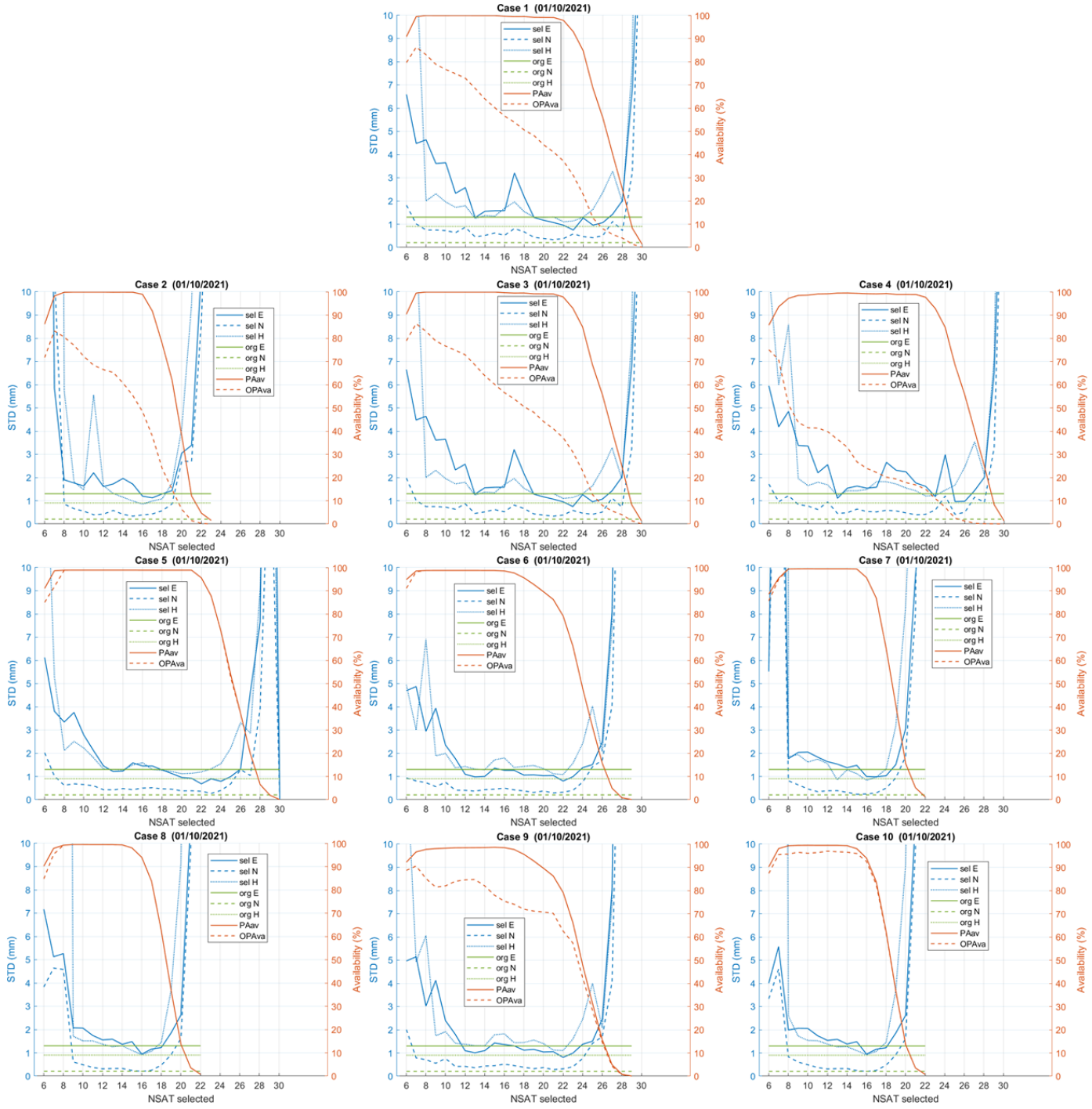

Figure B.0.24 Positioning precision in Easting, Northing, and Hight using the original PPP and the selected satellites from the ten selection cases. In addition, the availability of positioning and optimal positioning of the selected satellites is presented. The positioning is based on 24 hours GNSS data collected over NGB2 on 1st October 2021.